CAVITATION EROSION OF MATERIALS

C . J HEATHCOCK

A thesis presented in fulfilment of the
requirements for the degree of Doctor
of Philosophy

UNIVERSITY OF CAPE TOWN
1980

SYNOPSIS

This investigation was undertaken to find the optimum hydraulic fluids and materials for combating cavitation erosion in hydraulic mining machinery operating on 5:95 oil-in-water emulsions, Controlled cavitation was generated in the laboratory in a vibratory cavitation apparatus employing the stationery specimen system. The influence of separation distance between the drill tip and specimen and of varying medium temperature on cavitation erosion were also investigated but were of secondary importance to the studies on materials and emulsions,

The evaluation of the influence of a number of commercial metal cutting coolants and specific hydraulic emulsions oncavitation erosion,showed that those emulsions with a high mineral oil content suppress erosion the most, This phenomenon is considered to be either the result of a reduction in nucleation of highly damaging surface cavities due to the elimination of surface nuclei by an oil film, or to damping of cavity collapse due to the high dissolved gas content of oil-in-water emulsions,

A large number of commercial grade alloys and polymers have been investigated, The alloys ranged from single phase, face centered cubic nickel alloys to complex, multi-phase, cobalt based alloys while the polymeric materials were all linear and crystalline. The modes of erosion and mechanisms of erosion resistance were studied in detail by optical microscopy, scanning and transmission electron microscopy and X-ray diffractometry. The fractographic studies on the alloys revealed, in particular, the role played by second phase particles and other surface features such as protruding grain boundaries and surface steps created by dislocation movement, twinning and phase transformations, Furthermore, X-ray diffractometry coupled with theoretical considerations and the findings of previous investigations indicated the fundamental importance of phase transitions in contributing towards the erosion resistance of alloys,

Cobalt based Stellite alloys, nickel based cemented carbides and the intermetallic alloy NiTi have exceptionally high erosion resistance, The Stellites have a high yield stress and also undergo an awe phase transition which results in a high work hardening rate and high strain to fracture, NiTi similarly undergoes a phase transformation which allows absorption of seven per cent reversible strain and also results in a high work hardening rate. The erosion resistance of nickel based tungsten carbides is, in turn, attributable to the very high yield stress of these materials,

Ultra high molecular weight polyethylene and nylons have relatively high erosion resistances, Their exceptional performances are due to a high strain to fracture and high yield strength respectively. On the other hand low tensile strength polytetrafluoroethylene has a very poor resistance to erosion.

This work has identified various material properties which are required for erosion resistance, These are : (a) a high yield stress, (b) a high work hardening rate and (c) a high strain to fracture,

ACKNOWLEDGEMENTS

I wish to thank all those who assisted me in the research work reported in this thesis,

In particular I am very grateful to Professor A Ball for his help during the research project.

I am also very grateful to Gay Perez for her invaluable assistance. I also wish to thank Mr N Dreze and Mr B Greeves for their advice and help with the construction of the equipment and photographic work respectively,

I am thankful to Dr Semmelink and Mr M Sketch of the Central Acoustics Laboratory, University of Cape Town, for their assistance throughout my research,

The financial support of The Chamber of Mines of South Africa and the co-operation of Sandvik AB of Sweden and Deloro Stellite of England, in supplying test samples, are gratefully acknowledged,

ACKNOWLEDGEMENTS

I wish to thank all those who assisted me in the research work reported in this thesis,

In particular I am very grateful to Professor A Ball for his help during the research project,

I am also very grateful to Gay Perez for her invaluable assistance, I also wish to thank Mr N Dreze and Mr B Greeves for their advice and help with the construction of the equipment and photographic work respectively,

I am thankful to Dr Semmelink and Mr M Sketch of the Central Acoustics Laboratory, University of Cape Town, for their assistance throughout my research,

The financial support of The Chamber of Mines of South Africa and the co-operation of Sandvik AB of Sweden and Deloro Stellite of England, in supplying test samples, are gratefully acknowledged,

LIST OF SYMBOLS AND ABBREVIATIONS

α = Thermal Expansion Coefficient.

ε = Engineering Strain.

ε_{binder} = Strain in Binder of Cemented Carbides.

ε_{f} = Engineering Strain to Fracture.

ε_{u} = Engineering Strain to Plastic Instability.

$\varepsilon_{ultimate}$ = True Strain Corresponding to σ Ultimate (for Fig. 3.1 only).

γ_{mo} = Interfacial Energy between Metal and Oil.

γ_{mw} = Interfacial Energy between Metal and Water.

γ_{ow} = Interfacial Energy between Oil and Water.

ν = Poisson's Ratio.

σ_{binder} = Stress in Binder of Cemented Carbides.

σ_{p} = Proof Stress.

σ_{u} = Ultimate Tensile Strength.

$\sigma_{ultimate}$ = True Ultimate Tensile Strength.

σ_{y} = Yield Stress.

B = Universal Gas Constant.

BCC = Body Centered Cubic.

C.V.L. = Cumulative Volume Loss.

d_{crit} = Critical Separation Distance between Ultrasonic Drill Horn and Specimen.

E = Young's Modulus.

$\dot{E}$ = Steady State Erosion Rate.

EDAX = Energy Dispersive Analysis of X-Rays Attachment to SEM.

FCC = Face Centered Cubic.

G = Shear Modulus.

ΔG = Free Energy Change.

HCP = Hexagonal Close Packed.

I_r = Ratio of Intensities of HCP (101) and FCC (200) XRD Peaks of Stellites.

kHz = kilo Hertz.

M_d = Maximum Temperature at which Martensite can be Stress Induced.

M_s = Temperature of start of Martensite Reaction.

m = Mass.

n = Work Hardening Exponent

P_a = Ambient Pressure.

P_G = Pressure of Non-condensable Gas within a Cavity.

P_v = Pressure of Vapour within a Cavity.

P_{max} = Maximum Pressure at Cavity Wall Developed by a Collapsing Cavity.

PTFE = Polytetrafluoroethylene.

R = Radius of Cavity.

R_m = Maximum Radius of Cavity Prior to Collapse.

R_n = Resilience Number.

S = Surface Tension.

SE = Strain Energy to Fracture.

SEM = Scanning Electron Microscopy.

t_o = Incubation Time.

T = Temperature.

TEM = Transmission Electron Microscopy.

T_G = Glass Transition Temperature.

UHDPE = Ultra High Density Polyethylene.

UR = Hobb's Ultimate Resilience.

V.H. (H.V.) = Vickers Hardness.

XRD = X-Ray Diffractometry.

CONTENTS

CHAPTER ONE

GENERAL INTRODUCTION

As operational pressures are increased in hydraulic systems the design engineer is confronted with cavitation erosion as a serious limitation, Fig, 1,1, taken from reference 1, summarizes the various engineering aspects of this problem as seen by the designer, The design and materials selection process is based on fundamental research and screening (evaluative) tests. At this stage no satisfactory model cavitation test has been developed although there have been attempts to do so in the past (2), For existing systems cavitation erosion problems can be reduced by protection methods, operational limitations and, if very serious, by redesign, Most research done on the problem of cavitation erosion has been on the fundamental processes of cavity growth and collapse, environmental influences, mechanisms of erosion and on evaluation of the erosion resistances of materials. The findings of these investigations are summarized in a number of comprehensive review articles (Refs.1.3 to 8)

In recent years considerable effort has been concentrated on developing machines for use in the South African gold mines, to increase the efficiency of the industry (9), The confined working areas at the ore face (stope width of about 1 metre) and the very high rock strengths have required the development of a number of unique hydraulically powered machines, High costs and the pollution associated with pipe bursts preclude the use of conventional mineral oils as the hydraulic fluid and the only viable alternatives are water based fluids, such as dilute five per cent oil-in-water emulsions,

Although there are a number of advantages of using emulsions, such as lower compressibility which results in greater machine stiffness, there are also several disadvantages (10), The most serious of these is the increase in cavitation erosion of hydraulic system components, The efficiency of hydraulic machines operating on water based fluids is very dependent on small tolerances and thus cavitation erosion of pump components, such as, valves, impellers and casings severly limits the trouble free operating time of hydraulic mining machinery. Moreover damaged components (see Fig, 1.2) need to be replaced and because of the adverse conditions in the stope areas repair work is both difficult and time consuming, The net result is considerable down-time of machines,

Although a number of cavitation related problems in machines developed for gold mining have been reduced by design changes and improved materials selection (11), the operating times to failure of hydraulic system components, particularly valves, is still short and thus remains a limiting factor in the mechanisation

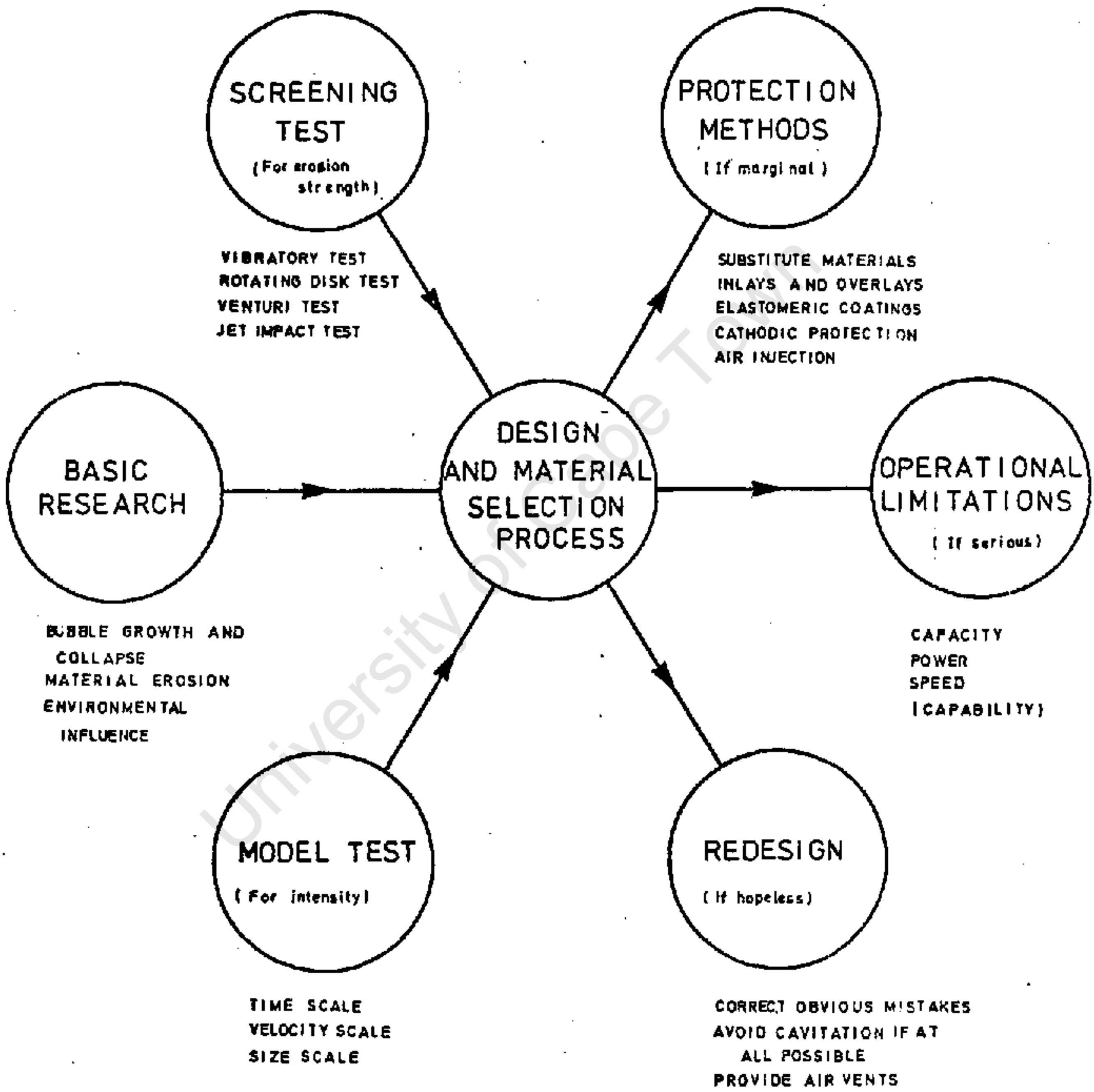

Fig. 1.1 The Engineering Aspects of Cavitation Erosion (Ref.1)

programme. It is difficult to eliminate cavitation in fluid powered machinery and since the cause cannot be removed the effect must be minimised by the use of the optimum hydraulic fluids and materials. This study was, therefore undertaken to evaluate a range of alloys and polymers for erosion resistance and to compare the effects of various dilute oil-in-water emulsions on cavitation erosion.

With regard to the dilute emulsions it has been known for some time that commercial metal cutting coolants are also excellent hydraulic fluids (10). As dilute emulsions assumed greater importance in this new role, several oil companies developed specific emulsions for use as hydraulic fluids which include a number of fully synthetic formulations (as opposed to emulsifiable oils based on mineral oil). A range of commercial emulsifiable oils was evaluated in this study to determine which emulsion or group of emulsions suppressed cavitation the most and also to gain an understanding of the mechanisms responsible for any reduction in cavitation damage.

Fig. 1.2 Cavitation Erosion Damage on an Hydraulic System Control Valve (Courtesy of The Chamber of Mines of South Africa).

A number of previous investigations have attempted to develop a means of predicting the performance of materials when exposed to an erosive environment and these are discussed in more detail later. The most convenient criteria for predicting erosion resistance are the readily available mechanical properties of materials,but as yet no reliable predicting property or combination of properties has been found. Good correlations have often been obtained with small groups of materials, but if a large range of materials is considered there is no single property or combination of properties which relates directly or otherwise to erosion resistance. More recently investigators (6, 8, 12) have realised that erosion is controlled by material microstructure and not necessarily by bulk mechanical properties.

Therefore the emphasis in the present work has been on further developing the present understanding of the microstructural control of erosion resistance. The findings obtained from erosion tests, fractographic studies and structural studies have provided a sound basis for material selection and also serve as a guide for the improvement of existing materials and for the development of more erosion resistant materials.

In this dissertation the fundamental concepts of cavity dynamics and the existing knowledge on the erosion of materials by cavitation are reviewed. The equipment and experimental techniques employed in this work are described. The results of the vibratory cavitation tests and of the fractographic and structural studies are presented and discussed. On the basis of the findings of the work on materials a list of properties,considered to determine the erosion resistances of materials,is presented.

CHAPTER TWO

CAVITATION DYNAMICS

Cavitation is a liquid phenomenon and, in general, embraces any process involving appearance and disappearance of cavities in a liquid. The present study is mainly concerned with the unstable growth and collapse of gas bubbles in a variable pressure field. This pressure field may be generated in either a flow system, for example, hydraulic machinery,or in a vibrating system, for example, a diesel engine.

The phenomenon of cavitation transforms the relatively low energy density of a pressure field into the high energy density characteristic of the neighbourhood and interior of a collapsing cavity. Since it concentrates energy into very small volumes, cavitation is able to produce effects such as the erosion of solids.

A detailed discussion on the dynamics of cavities is beyond the scope of this thesis and this chapter, therefore, simply covers some fundamental concepts of cavitation dynamics. Also the influence of various fluid parameters on cavitation erosion is briefly discussed.

2.1 CAVITATION NUCLEI, CAVITY GROWTH AND COLLAPSE

When cavities form in a liquid, localized rupturing occurs in the fluid body. This occurs when the liquid is subjected to a tensile stress which should be equal to the theoretical tensile strength of the liquid. In practice, however, cavities form at stresses well below the theoretical strength, generally corresponding to a pressure approximately equal to the vapour pressure of the liquid (13). This anomaly is due to the presence of nuclei in ordinary liquids which serve as initiating sites for rupture.

The simplest form of cavitation nucleus is a free gas bubble. But a free gas bubble in theory is not a stable nucleus since either gas diffuses into the bubble causing it to rise to the surface and vent,or surface tension forces cause gas to diffuse out of the liquid with the result that the nucleus decreases in size and eventually disappears. However, stable nuclei do exist and various forms of such nuclei have been proposed (14,15,16) :

(a) gas pocket in a crevice
(b) gas bubble with an organic skin
(c) hydrophobic impurities.

Unstable cavity growth occurs when a fluid body containing a nucleus is subjected to a reduction in pressure. The approximate conditions for growth can be derived from an analysis of the static equilibrium conditions for a spherical nucleus. At equilibrium the partial pressures of the gas (P_g) and vapour (P_v) within the nucleus must be balanced by the ambient pressure (P_a) and surface-tension pressure (2S/R) at the nucleus-liquid interface. Thus :

$$P_a + 2S/R \;=\; P_v + P_g \qquad \dots\dots\dots\dots \qquad 2.1$$

If the gas in the nucleus behaves as an ideal one then :

$$P_g \;=\; 3\,B\,m\,T/4\pi\,R^3 \qquad \dots\dots\dots\dots \qquad 2.2$$

where B = Universal gas constant
m = mass of the gas
T = temperature
R = bubble radius

For constant temperature :

$$P_g \;=\; C/R^3$$

where C = constant

By substituting for P_g in equation 2.1 and rearranging we obtain :

$$P_a - P_v \;=\; 2S/R - C/R^3 \qquad \dots\dots\dots\dots \qquad 2.3$$

This equation is plotted in Fig. 2.1 for two nucleus sizes, the upper curve being for the larger nucleus. The pressure adjacent to the bubble has a minimum value which is below the vapour pressure of the liquid. As long as the ambient pressure is above this minimum, the nucleus is stable and tends to reach an equilibrium radius corresponding to the ambient pressure. If, however, the pressure drops below the critical value, the bubble becomes unstable and grows without bound. Note that for a smaller nucleus size lower pressures are required. Since nuclei of different sizes undergo unstable growth at different liquid tensions, the characteristics of cavitation nuclei are very important.

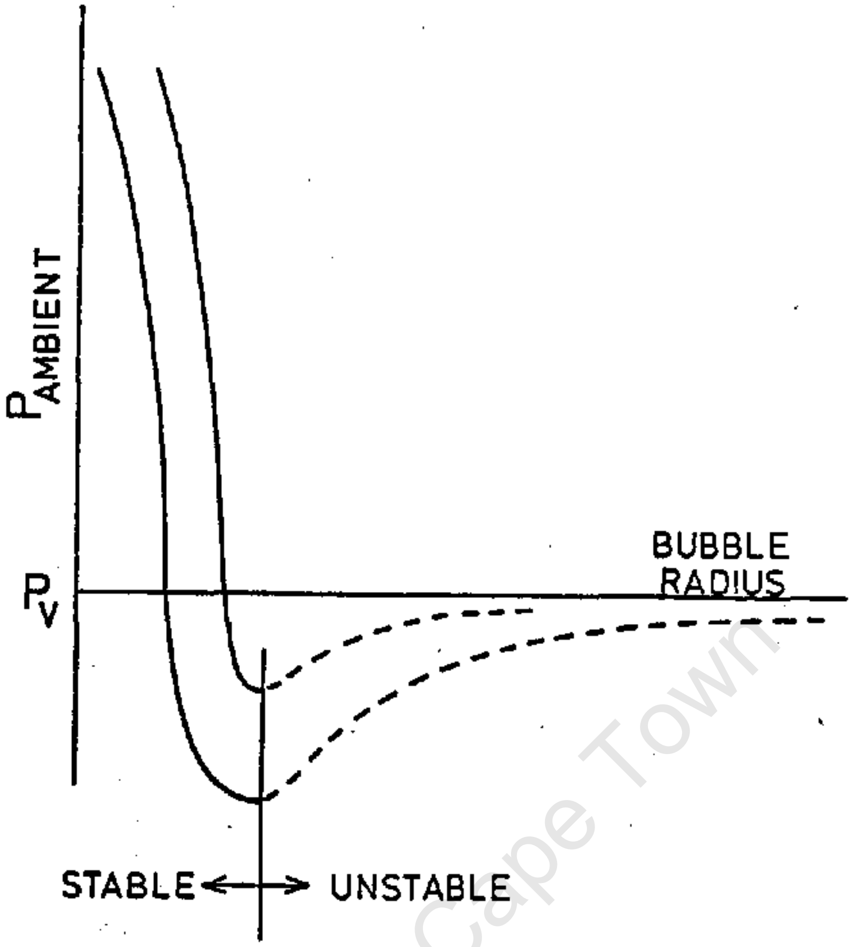

Fig. 2.1 Plots of the Conditions for Static Equilibrium of Cavitation Bubble Nuclei. The Upper Curve is for a Bubble with a Larger Radius.

Cavity collapse occurs when the ambient pressure in a cavitation zone increases again to more than the pressure within the cavities. Rayleigh (17)derived an equation for the pressures developed in the liquid adjacent to a collapsing cavity. He considered the ideal case of a spherical cavity, without gaseous contents in a static, non-viscous and incompressible liquid and obtained the approximate equation :

$$P_{max} = P_a/6{,}35\ (R_m/R)^3 \qquad \ldots\ldots\ldots\ldots\ldots \quad 2.4$$

where R_m = Maximum cavity radius

Since the cavity is assumed to be empty this equation yields infinite P_{max} for 11-).0. But, in the practical, non ideal case, the cavity contains non-condensable gas which limits the collapse pressures to a finite value.

Considerable effort has been made over the years since Rayleigh's analysis of cavity collapse to refine the equations describing cavitation processes. The findings of the various numerical analyses are reviewed by Knapp, Daily and Hammit (18)and Flynn (19).

Using equation 2.4 Rayleigh estimated that near complete collapse, that is, when the cavity radius is 1/20 of the initial, maximum radius, P_{max} would be approximately 130MPa (assuming P latm -0,1MPa). More recent estimates of the collapse pressure, in which allowances were made for the cavity contents and liquid compressibility, range from 20MPa to 400MPa (18). Other investigators have obtained collapse pressure in excess of 1000MPa by a photoelasticity technique (20),a transducer technique (21)and by a pressure bar technique (22). But despite these findings probably the best indication yet of the stresses produced by cavitation is the fact that high strength alloys of yield stress of about 1000MPa are damaged by cavitation which means that collapse pressures at the material surface must be higher than 1000MPa. Furthermore Hickling and Plesset (23)showed by numerical analysis that the pressure wave, emitted by a cavity, is attenuated as a function of 1/R. Therefore the collapse centre must be within one cavity diameter of a solid boundary to have any effect on this surface.

2.2 EFFECTS OF VARIOUS FLUID PARAMETERS ON CAVITY COLLAPSE

A number of fluid parameters influence cavitation processes including fluid compressibility, liquid vapour pressure, viscosity, surface tension, temperature of fluid and free and dissolved gas contents. The effects of these parameters on cavity growth and collapse are discussed briefly in the following section.

2.2.1 Compressibility of the Fluid

Rayleigh in his analysis of cavity collapse ignored the effect of liquid compressibility. This parameter has an important influence on cavity collapse but it is also very difficult to treat mathematically. In qualitative terms, however, this property results in the storage of collapse energy in the bulk of the liquid and thus the greater the liquid compressibility, the lower the erosion rate.

2.2.2 Liquid Vapour Pressure

An increase in liquid vapour pressure results in an increase in cavitation since the pressure of gas within a nucleus will be higher and therefore the liquid pressure reduction (tension) required to initiate cavity growth is smaller, that is, cavitation occurs at higher ambient pressure. As far as cavity collapse is concerned the effect of a high vapour pressure is probably not as significant as that of the presence of non-condensable gas. This is because the formation of vapour is a relatively slow process compared with cavity growth and the little vapour formed would have a negligible effect on the subsequent collapse process (at 20°C).

2.2.3 Viscosity

The influence of viscosity is small compared with that of compressibility and gas content and only large variations in this parameter have a significant effect on cavitation. Moreover the action of viscosity is dependent not only on the specific viscosity but also on the rate of shear. Therefore viscous effects are greatest during the early stages of growth and final stages of collapse when the wall velocity is high. Poritsky (24) studied the influence of viscosity and he found appreciable effects of this parameter in retarding both growth and collapse but only for liquids with high viscosity values (that is, much higher than water, p = lcst).

2.2.4 Surface Tension

Surface tension forces act in one way only, that is, to close any cavities formed in a liquid. Hence during the growth cycle the wall velocity will be reduced while during collapse the velocity will be high for large surface tension forces. Also surface tension forces tend to reduce the maximum size of cavities. The effect of this parameter is greatest for small cavities.

2.2.5 Temperature of Cavitating Fluid

The influence of temperature is well known although not completely understood. Temperature effects in vibratory cavitation have been widely studied and, in general, investigators have found that a maximum in erosion occurs at 40 C to 50 C for constant atmospheric pressure (25 , 26 , 27 , 28). The explanation for the reduction in erosion at temperatures above 50 C is generally accepted as being due to the increased vapour pressure of the test liquid. At low temperatures the decrease in erosion has been attributed to an increase in dissolved gas content.

2.2.6 Free and Dissolved Gas Content

The gas content of a liquid can have either an adverse effect or a beneficial effect on cavitation processes. On the one hand, a high free gas content may increase the concentration of free gas bubble nuclei and thus enhance cavitation, while a high dissolved gas content may promote gaseous cavitation or rectified diffusion* which results in the growth of subcritical nuclei to the critical size necessary for unstable, vaporous cavity growth. On the other hand compression of non-condensable gas within a cavity during the collapse cycle, results in damping of the collapse pressure. Part of the collapse energy is used up in compressing the gaseous contents of the cavity and part in raising its temperature, thus the energy available for erosion is reduced and the mechanical attack of adjacent materials is less severe.

---

* *Rectified diffusion is a process whereby the gas content of stable, pulsating bubbles, in an acoustic field of sufficient pressure, slowly increases (further discussed in Chapter 6). Gaseous cavitation is* simply *the transport of gas across a liquid/bubble interface in* an *over-saturated liquid, which results in cavity growth.*

CHAPTER THREE

MATERIALS AND CAVITATION EROSION - A REVIEW

The problem of erosion of machine components by cavitation can be reduced in three ways: by redesign, by limiting machine operating parameters such as capacity, power and speed or by selection of the optimum materials for affected components. Considerable effort has been expended on the problem of erosion of materials and in finding a suitable means of predicting material life in practical circumstances.

This chapter reviews research carried out in an attempt to alleviate these problems. Efforts to correlate mechanical properties. with erosion resistance as well as the attempts to develop erosion predicting equations are discussed. Also the findings of the more recent studies on the microstructural aspects of erosion of various metals and alloys are described.

3.1 EVALUATION OF MATERIALS - PAST RESEARCH

Erosion of materials by cavitation was first identified and investigated by W. Wagenbach. The erosion occurred in a turbine in a hydroelectric works,and Wagenbach recorded the findings of his investigation in an article published in 1907 (29). The earliest comparative cavitation erosion tests were carried out in the 1920's. The test materials were attached to a turbine runner in a power plant and left for 3i years prior to removal and inspection. The long time intervals involved,and also the number of variables in a power plant turbine, made this method of materials testing unsatisfactory. However, the advent of accelerated cavitation testing systems,viz. the venturi system, the rotating disc device and the vibratory device have made extensive laboratory investigations possible.

Two such studies were carried out between 1934 and 1936 by J.M. Mousson (30)and S. Logan Kerr (31). These two investigators tested most of the materials available at that time which were suitable for use in hydraulic machinery. These studies involved comparative erosion tests, and attempted to identify simple correlations between erosion resistance and conventional mechanical properties. Later Rheingans (32) carried out further screening(evaluative)tests on materials including the first on polymeric overlays. He also looked into the correlation between hardness and erosion resistance.

In the ensuing 30 years, numerous investigations were undertaken. These include contributions by Garcia and Mammit(33), Young and Johnston (34),Lichtman (35), Gould (36),Hobbs and Laird (37,38) and Vaidya and Preece (39). Many of these investigations covered, not only the evaluation of materials, but also extensive studies into the effect of material properties and combinations of properties on erosion resistance. In the most recent investigations (36 , 39 , 40) the modes of deformation and of material removal from metals and alloys were studied, mainly, by means of scanning electron microscopy.

3.2 THE PREDICTION OF MATERIAL PERFORMANCE

In practice the design engineer requires some parameter which he can use to specify materials for components of systems prone to cavitation erosion. Therefore considerable effort has been made to find a correlation between a material property or a combination of material properties and erosion resistance. In general good correlations are obtained for alloys with a common base metal and, of the simple mechanical properties, the best correlations have been found with hardness, yield strength and tensile strength (32,37,38). However erosion resistance - mechanical property relationships for a wide variety of alloys were always found to be poor.

Several investigators have proposed various energy based parameters as erosion resistance controlling properties such as Hobbs' ultimate resilience (UR) (41) and strain energy to fracture (SE) (421. Ultimate resilience approximately represents the elastic energy absorbed up to fracture in tension if failure is in the brittle mode and is represented diagrammatically in Fig. 3.1 . Strain energy to fracture is given by the area below the stress/ strain curve.

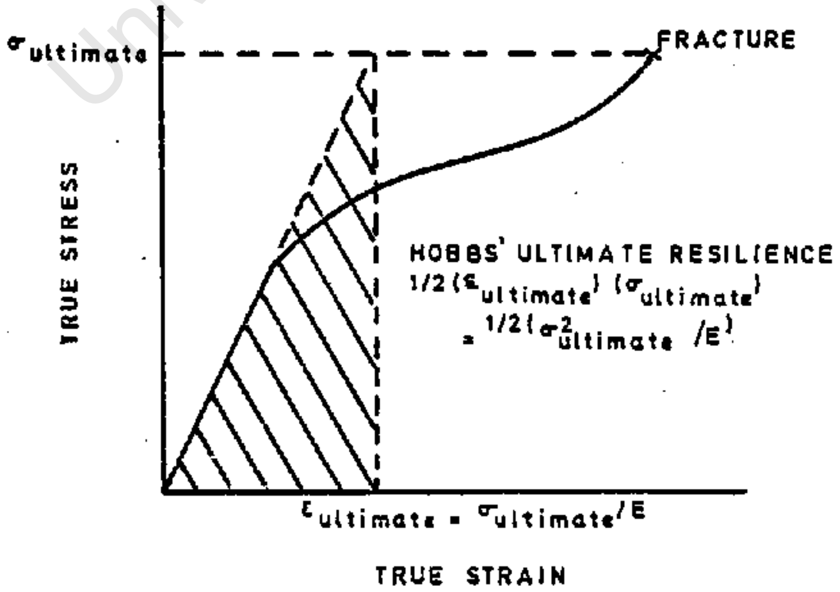

Fig. 3.1 Hobbs' Ultimate Resilience (from Ref. 33)

Initially satisfactory correlations based on SE, were obtained by Thiruvengadam (2, 42) and Hammit et al (43) for small groups of materials, but, subsequently Hobbs (41), Wood et al (44) and Heymann (45) obtained very poor correlations with SE. In contrast Hobbs' ultimate resilience has been used as a correlating parameter in many comprehensive investigations involving data from numerous facilities and covering a wide variety of alloys (41,45, 46). This property was proposed by Hobbs (41) when he noted that a material can absorb energy through elastic deformation, plastic deformation and/or fracture. Therefore he compared the proof resilience or elastic resilience $\{½\}(ø_p)^2/E\}$, ultimate resilience ($½ø_u/E$) and strain energy to fracture $\{ø +2/3(ø_u - ø_p)\}e_f$ with erosion data for 28 alloys. The best fit was obtained with ultimate resilience.

One limitation of this concept of ultimate resilience is the assumption that all materials fail in a brittle manner. Hammit (7) claims this is consistent with numerous metallographic examinations of cavitation damage. But in the present investigation, and as will be pointed out later, most materials were found to fail by a ductile mechanism!

The relation between combinations of properties and exponential functions of properties and erosion resistance have also been investigated. Tichler et al (47) found, for six copper-nickel alloys and six steels, an empirical relation between resistance against uniform material removal (R_e) and the true ultimate tensile strength of the form $R_e=Aø_u^{2.3}$. Rao et al (43) found, for a small group of alloys, good empirical agreement between erosion resistance and the product of either strain energy or ultimate resilience and hardness.

Similar correlations have been obtained with polymeric materials. Lichtman (35) found some agreement between erosion resistance and tensile strength and also erosion resistance and rebound resilience (a measure of the energy reflection and absorption on impact). Lichtman et al (49) found ultimate elongation to be an important parameter from the performance of nylon in cavitation tests, In addition a number of investigators have found relationships between drop impact and cavitation erosion and the material parameters, shore hardness and notch impact strength (50, 51).

In all relationships involving a wide variety of materials a high degree of scatter is observed,and therefore, efforts to predict erosion resistance on the basis of material properties alone have met with limited success. This has prompted the development of several erosion prediction equations and models which take into account both environmental and material parameters (2 , 45, 46). However the theories and equations developed,either remain to be confirmed in practice,or are too specific in their application for use as general predicting equations.

While investigators continue their efforts to find a reliable theoretical or empirical model for predicting erosion of materials,a new approach, which considers the problem more from the material microstructure point of view, has gained momentum in recent years and is discussed in the following section.

3.3 THE MICROSTRUCTURAL APPROACH TO THE EROSION OF MATERIALS

An engineering approach has been adopted in most investigations in the past and few studies have been conducted on the role of material microstructure in determining erosion modes and resistance mechanisms. Nevertheless the work done so far has explained many of the apparent discrepancies in relationships between erosion resistance and bulk mechanical properties. This materials science approach has emphasized that a knowledge of microstructural behaviour is an essential complement to a knowledge of the macro-response of materials. In the following sections the research work done on erosion mechanisms is discussed. This is followed by a review of the findings of investigations into the modes of erosion of various materials. The majority of this latter work has been carried out by Preece and coworkers.

3.3.1 The Search for the Mechanism of Cavitation Erosion

A number of theories on the mechanism of cavitation damage have been proposed, namely, accelerated corrosion, localised melting and mechanical stressing. Subsequent work (52 , 53 , 54) has shown that the mechanical stressing mechanism is the predominant cause of damage. This mechanism involves, accumulation of fatigue damage followed by work hardening and ultimately fracture. Atthough corrosion has been shown to play a role in cavitation erosion (55), the corrosion component depends very much on factors such as intensity of erosion, nature of fluid and material corrosion resistance. For example, in vibratory cavitation, corrosion plays a negligible part in the damage mechanism since the intensity of erosion is high,but in flow cavitation,intensities are lower and hence corrosion will play a greater part in the processes of material removal. As regards the localized melting mechanism,Vyas and Preece (54) have observed dislocations by TEM and surface slip lines in eroded aluminium, and therefore this mechanism can be disregarded since these defects would be removed by surface temperatures corresponding to the melting point of aluminium.

The mechanical stressing theory was proved in the 1960's by X-ray analysis of eroded nickel, titanium, brass and AISI 4340 steel (52, 53).Lines in the X-ray patterns became broadened after exposure to cavitation of only a few seconds indicating the occurrence of plastic deformation. More resistant materials, such as vanadium, molybdenum and tungsten also underwent plastic deformation except that longer exposures - of several minutes to several hours, to cavitation were required before plastic deformation was observed. The presence of plastic deformation in the earliest stages of erosion led investigators to believe that fatigue, work hardening and subsequent fracture was the mechanism of cavitation erosion. However transmission electron microscopy (TEM) studies of aluminium and 304 stainless steel after exposure to cavitation have revealed completely different structures to those produced by rolling or fatigue. Cold rolling or fatigue of aluminium produces a dislocation cell structure (56 , 57) while cavitation, results in a structure similar to that produced by shock loading (54, 581. The predominant microstructural features of the latter deformation modes are a uniform array of heavily jogged dislocations with an associated high density of point defect clusters and dislocation loops.

The fatigue of stainless steel produces a dislocation cell substructure (5g, 60) while shock loading (which is similar to cavitation loading) induces a structure composed of twins and twin fault bundles with interspersed E and a^{1} martensite (61). The similarities in microstructure between that of shock loaded stainless steel and that of eroded stainless steel was confirmed in the present study. Erosion therefore does not occur by fatigue per se, and the "fatigue like"striations on the eroded surfaces of Al-4%Cu and ferritic stainless steels (62, 63) are the consequence of intermittent crack growth and arrest due to the high frequency,cyclic nature of cavitation loading.

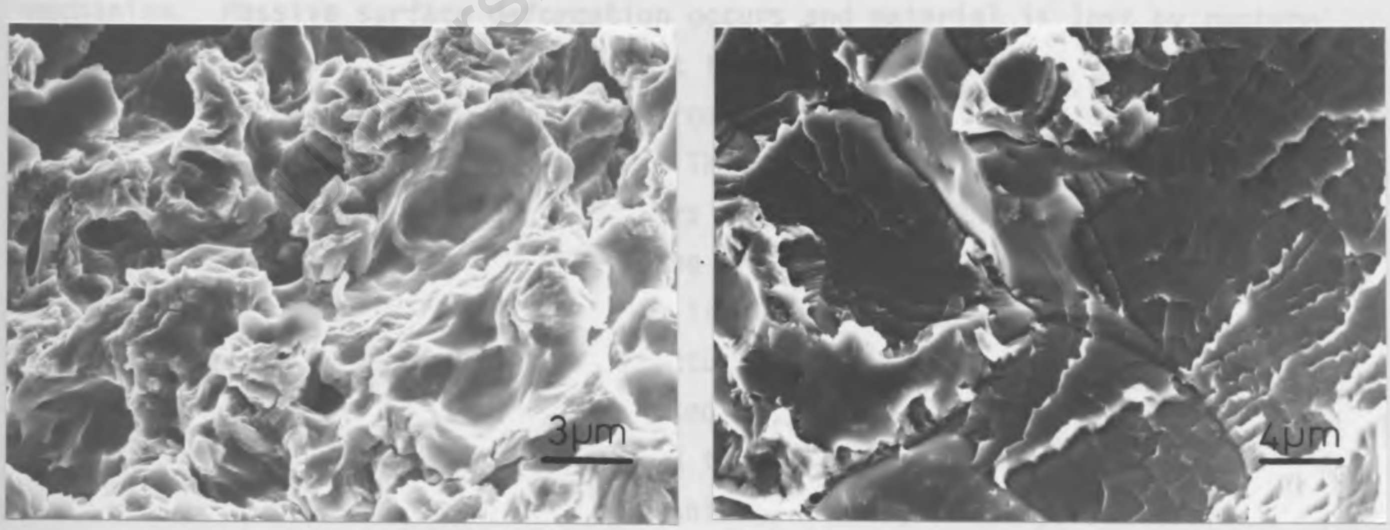

(a) (b)

Fig. 3.2 The Two Main Modes of Cavitation Erosion (a) ductile and (b) brittle (Ref. 63)

More recent fractographic studies on the erosion of a variety of materials have revealed that the erosion modes of individual materials tend to be unique (12 , 39 , 63 , 64). However, there are two principle modes of erosion,namely, the ductile and brittle modes. Individual erosion modes are simply variations of these two general modes of fracture which are represented by the fracture surfaces in the micrographs in Fig. 3.2. Differences in crystal structure, material microstructure and mechanisms of plastic deformation influence the fracture mode and the existing knowledge on the modes of erosion of a number of materials is reviewed in the following sections. The discussion considers the erosion of pure metals, alloys and polymers. In some cases the mode of liquid droplet impact erosion of materials is described (when the mode of cavitation erosion has not been investigated). One can assume some similarity between droplet impact and cavitation erosion since liquid microjets are known to occur in cavitation (65, 66),

3.3.2 Modes of Erosion of Materials

3.3.2.1 Pure Metals

Several face centered cubic metals have been investigated including nickel (52,64), aluminium (12, 64) and copper (64). These metals have a high stacking fault energy (S.F.E,) which favours dislocation cross-slip and plastic flow and thus these metals have a ductile mode of erosion. At an early stage grain boundaries and slip lines are prominent but they play no part in the failure mechanism. Massive surface deformation occurs and material is lost by rupture of asperities and lips which build up at the edges of surface craters.

Body centered cubic metals differ from face centered cubic metals in that they are highly strain rate sensitive. The cavitation erosion of pure iron has been studied by a number of investigators (12, 40, 67). It has been found that the strain rates in cavitation induce the ductile to brittle transition in this metal. The fracture mode, therefore, is a combination of both ductile and brittle modes. The ductile mode of fracture occurs by formation of twins, delineation of grain boundaries and subsequent ductile loss of the asperities at these surface defects. On the other hand the brittle mode of fracture, which is the predominant mechanism occurs by cleavage nucleated at grain boundaries and grain-twin boundary intersections.

Hexagonal close packed metals vary in their mode of erosion. For example zinc fails in a brittle manner (12,52 ,67) while cobalt fails in a ductile manner (67). Zinc is crystallographically anisotropic (axial ratio /a=1,856 cf. 1,633 for ideal close packing) and easy dislocation movement occurs only on the basal plane. Cleavage also occurs quite easily on the basal plane. The competition between these two fracture mechanisms results in zinc undergoing a ductile to brittle transition which is sensitive to strain rate and temperature. Thus on exposure to the high strain rates of cavitation the metal fails in a brittle manner.

Cobalt, on the other hand, has an almost ideal c/a axial ratio. It has a number of slip and twin systems (six of each) and when subjected to cavitation is able to deform in a ductile manner. Preece et al (67) reported that the steady state erosion rate after the incubation period of pure cobalt is an order of magnitude lower than that of pure iron. These investigators attribute this lower erosion rate to the fine network of twins, of 0,01 to 0,1um in width, which form on exposure to cavitation.

This completes the summary of the work done on erosion of pure metals. The existing knowledge on the erosion of alloys both single and multi-phase will now be considered.

3.3.2.2 Copper and Nickel Based Alloys

High SFE,copper-nickel single phase alloys erode in a similar manner to pure nickel and copper as described in the previous section (62). Copper-zinc alloys have a different mode of erosion and this can be ascribed to the lower SFE of these alloys (62) . The low SFE prevents recombination of partials necessary for cross-slip and thus only planar slip occurs. This results in less dislocation interaction and grain and twin boundaries are the major barriers to dislocation movement. A dislocation pile-up at a grain or twin boundary generates sufficient stress to overcome the shear stress required for cross-slip. Thus multi-slip, necessary for surface distortion, occurs and protrusions of material at grain and twin boundaries develop which are subsequently lost by ductile rupture.

The mode of erosion of copper based aluminium bronzes has also been studied (68). The annealed structure of these alloys consists of islands of primary solid solution phase (a) enveloped by a +y_2 eutectic. Heat treatment, as in steels, transforms the alloys to a martensitic type structure. These alloys erode by preferential removal of the soft aphase followed by loss of y_2 particles. The lowest erosion rates are obtained when the structure is martensitic with the a phase finely distributed amongst the martensite laths.

3.3.2.3 Aluminium Alloys

Vaidya and Preece (3g) investigated the modes of erosion of binary, and quartenary aluminium alloys,namely Al-Cu, Al-Mg and Al-Zn-Mg-Cu. These alloys provide an interesting example of how alloying elements, hardening mechanisms and heat treatment can alter the erosion mechanism. In the early stages of cavitation the mode of deformation in all the alloys is very similar to that of pure FCC metals. In the 'soft', low solute content alloys (Al-1%Cu in all conditions, Al-1%Mg as quenched and Al-2%Cu over-aged) the mechanism remains identical to that of the pure,face centered cubic metals at all stages of the erosion process. The asperities, formed at the edges of voids and craters, are removed by ductile shearing of the metal.

The higher solute content alloys, Al-4%Cu in the as-quenched or peak-hardened condition,fail in a completely different manner. After the initial stage of surface deformation,material is removed by random brittle pit formation.

The failure mechanism of as-quenched or peak-hardened Al-2%Cu and over-aged Al-4%Cu is a mixture of the above two mechanisms. As the strength of the alloy increases the failure mechanism gradually becomes less ductile and more by random pitting. Finally the Al-9%Mg and Al-Zn-Mg-Cu alloys lose material by undergoing fine,ductile type failure with some fatigue-type deformation occurring at the base of individual craters.Vaidya and Preece (39) explain the observed erosion resistances of the Al-alloys as follows : The mode of material removal in the Al-alloys is determined by the ability of each alloy to absorb cavitation energy which, in turn, is a function of microstructure. The low solute content alloys have high SFE's, low critical resolved shear stress and few impediments to dislocation motion. Therefore dislocation generation and movement is unhindered and is manifested by gross surface distortion and a low erosion resistance. On the other hand the high solute content alloys have a relatively greater density of dislocation sources in the form of fine 0 precipitates. The initiation of slip of these dislocations absorbs some of the cavitation energy in the early stages of erosion, but the high density of 8 phase particles restricts the mean free path of these dislocations and thus only small plastic strains are possible. This results in high stress concentrations and subsequent initiation of random pits in the surface regions of these alloys.

3.3.2.4 Ferrous Alloys

The erosion of carbon steels after a variety of heat treatments, namely, normalising, quenching and tempering and spheroidizing has been studied by Wade and Preece (40). The ferrite phase is always removed first followed by loss of carbide particles when there is insufficient supporting ferrite matrix. Thus the ferrite phase controls the erosion of steels and an improvement in erosion resistance is only gained by changing the ferrite to martensite (see Fig. 3.3).

Austenitic stainless steels,being low SFE, face centered cubic alloys erode in a manner similar to that of the low SFE,Cu-Zn alloys as described above (69, 70,71). Material piled up at grain and twin boundaries is lost by ductile fracture. Austenitic stainless steels and austenitic manganese steels have higher resistances than is expected from their strength properties (72, 69) and this has been connected to the metastable nature of these alloys and the ue+ø1 stress induced transformation. These alloys have been investigated in the present study and the findings are discussed in detail in a later chapter.

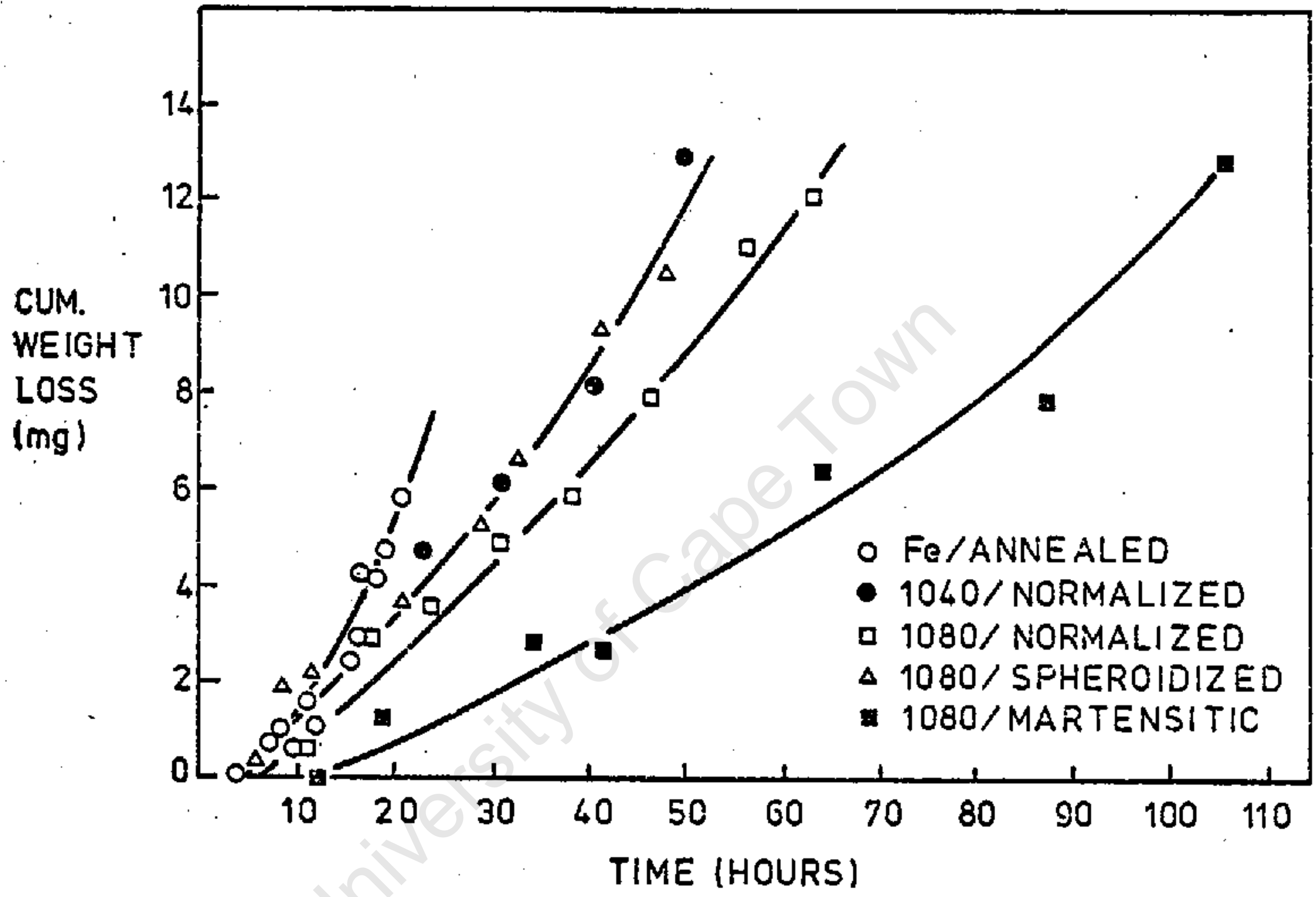

Fig. 3.3 The Erosion Curves of Various Steels (Ref. 40)

3.3.2.5 Cobalt Alloys

The fracture mechanisms occurring in Stellite alloys are of interest since these are amongst the most erosion resistant alloys available. The microstructures of these alloys consist of various carbides embedded in a cobalt rich solid solution matrix (73). An investigation by Marriott and Rowden (74) into the drop impact erosion of Stellite 6B revealed that erosion occurs in four stages : (a) Slip deformation and work hardening of the matrix (b) cracking at interfaces between carbide particles and matrix phase (c) intrusion formation at slip lines and (d) material removal by intersection of transgranular cracks and dislodging of carbide particles. Young and Johnston (75) also found that cracking of subsurface carbides occurred in this alloy during cavitation erosion in liquid sodium.

There is considerable controversy over the reasons for the exceptional erosion resistance of Stellite alloys. It has been attributed to the absorption of the erosion energy by the FCC-HCP phase transformation (76), to the planar slip mode due to the low SFE of cobalt which delays fatigue crack nucleation (72), the extremely fine microstructure as a result of twinning (8) and the high strain energy to fracture of the HCP allotrope of cobalt (77). The erosion of various Stellites has been investigated in the present study and the erosion and resistance mechanisms are discussed more fully in a later chapter.

3.3.2.6 Polymers

Most research conducted on cavitation or drop impact erosion of polymeric materials has been on coatings or overlays on metal substrates. But a few polymers such as polyethylene, polyvinyl chloride, various glass reinforced laminates, styrene-acrylonitrile and nylon have been tested as structural materials (32,35,49,50,51). Also the majority of the work done on fracture mechanisms has been on samples damaged by drop impact erosion (78, 79, 80). Hard, glassy polymers like PMMA (Perspex) were found to fracture in a 'brittle' manner. While erosion of 'soft' polymers and elastomers, such as, natural rubber, neoprene, nylon and PVC occurred by,either a tearing mode,or a mixture of both brittle and tearing fracture modes.

Chatten and Thiruvengadam (81) noted that the frequency of the applied stress is of greater importance in viscoelastic materials than for metals. If the unloading cycle is shorter than the relaxation time of the polymer, then it fails in a brittle manner while at lower frequencies the cavitation is absorbed in three ways : (a)elastically (b) partly dissipated or (c) is conducted away as heat. Subsequently polymer failure occurs by tearing as a result of accumulated strain.

Since the fracture mechanisms occurring during cavitation have not been investigated it is unknown whether these mechanisms above apply to this form of erosion. Furthermore, little is known about the influence of such polymer parameters as crystallinity, molecular weight, cross linking, intermolecular forces and chain geometry on the erosion modes and resistances. Again a number of polymers were tested in the present work and the erosion modes investigated. These are discussed in a later chapter.

CHAPTER FOUR

EXPERIMENTAL APPARATUS AND TECHNIQUES

A number of systems have been developed for conducting accelerated cavitation research. These include venturi systems, rotating disc devices and vibratory systems. The venturi system, while simulating in service conditions of flow induced cavitation, tends to be bulky and produces a low intensity of cavitation which thus requires long test periods. The rotating disc device closely simulates conditions in turbo-machines and pumps and produces higher rates of damage than the venturi system. However, the flow pattern in this device tends to be very complex compared with that of the venturi flow system. The vibratory device has the advantage of being compact, easily set up, and it produces rapid results. Also the intensity of erosion is easily controlled. This system has the disadvantage that the mode of cavitation formation is representative of only those systems in which the cavitation is produced by a vibrating surface (for example, diesel engine cylinder liners). In spite of this the vibratory apparatus is one of the most convenient methods of carrying out cavitation erosion research in the laboratory and this system was chosen for the present research programme.

This chapter describes the design and development of the vibratory equipment, the specimen preparation techniques and the method of conducting cavitation tests. In addition the instruments used to examine cavitation damage in materials are described.

4.1 VIBRATORY CAVITATION EQUIPMENT

4.1.1 Ultrasonic Drill Rigs

Two identical testing rigs were constructed using commercial ultrasonic drilling machines. These drills were supplied by KLN Ultraschall Gesellschaft of Germany. The high frequency generators of these KLN systems are able to supply a total output signal of 300 watts in the frequency range 18,5 to 22 kHz. This signal is converted to mechanical energy by Lead-Zirconate–Titanate ceramic transducers clamped under compression onto the mechanical element of the drilling system. The mechanical portion of the drill incorporates an exponential velocity transformer or 'horn' fabricated from Monel 400 alloy which amplifies the oscillations produced by the piezoelectric transducers by a factor of approximately 3,5 (see appendix 4.1).

It was decided to use the stationery specimen mounting method as adopted by Preece (54,84 rather than the vibrating specimen as recommended by the ASTM standard method G32-72. The latter is unsatisfactory for two reasons .-

(a) the vibrating action of the drill subjects the test piece to longitudinal stresses which can cause fatigue failure of the specimen. Also it is a fundamental requirement of the test that the specimens experience only stresses generated by the action of cavitation and not by any other means, (b) it is impossible to test low strength polymers or brittle ceramic materials by this method.

A rig was designed in which the specimen was mounted below the drill tip in such a way as to allow easy removal and replacement of the test piece. The rig consisted of a vertical drill stand mounted on slide bars permitting easy vertical movement of the drill (see Fig. 4.1). A specimen mounting platform was attached to the base of the drill stand. This was devised to allow the removal (for weight loss measurement) and subsequent replacement of the specimen in a constant position below the drill tip (Fig. 4.2(a)). Within the mounting platform, the specimen was located in a recessed holder which was, in turn, positioned by a slide assembly (see Fig. 4.2(b)).

Two different specimen geometries were used in this study : rectangular (14mm x 5,5mm) test pieces in the oil-water emulsions work and 12mm diameter x 3mm thick discs in the materials investigation. In each case the specimens were insulated from the metal holders by a PTFE lining in the recesses. Specimen orientation was ensured, either, simply by the test piece shape (rectangular specimen) being suitably marked,or by a locating pin in the recess for the disc specimens. A complementary notch in the latter test piece ensured constant orientation during a test.

In certain cases, for example, the cemented carbides, specimen geometry and dimensions demanded modifications of these mounting systems. The cemented carbide specimens were approximately 10mm in diameter by 5mm thick and therefore were mounted by first clamping in a stainless steel collar which, in turn was mounted in a holder having an insulated recess the same size as the collar.

The method of clamping the specimens in place varied with specimen geometry. The rectangular specimens were clamped by separate side clamps while the disc specimens were held down by a bar clamp having a tapered hole in the centre. Again the test pieces were insulated from these clamps.

The separation distance between the drill tip and specimen was set by means of a modified micrometer attached to one of the vertical slide bars. The distance was set as follows : Firstly the drill tip was carefully lowered onto the specimen and the 'height' of the lower cross-bar read off the micrometer. The predetermined separation distance of 0,35mm was subtracted from this reading and then the micrometer was reset at the new distance. The drill was then clamped in this position.

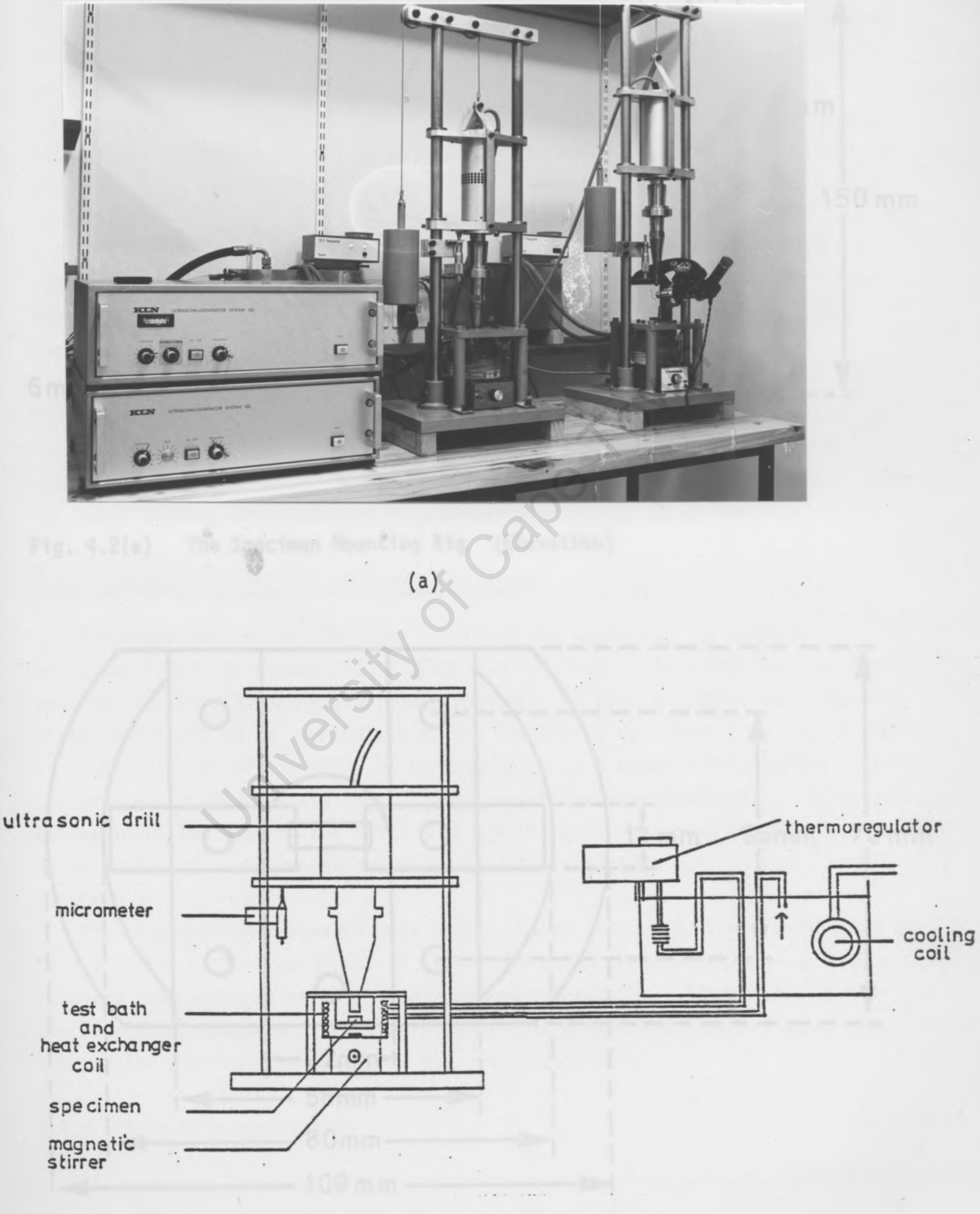

Fig. 4.1 The Vibratory Cavitation Erosion Test Apparatus

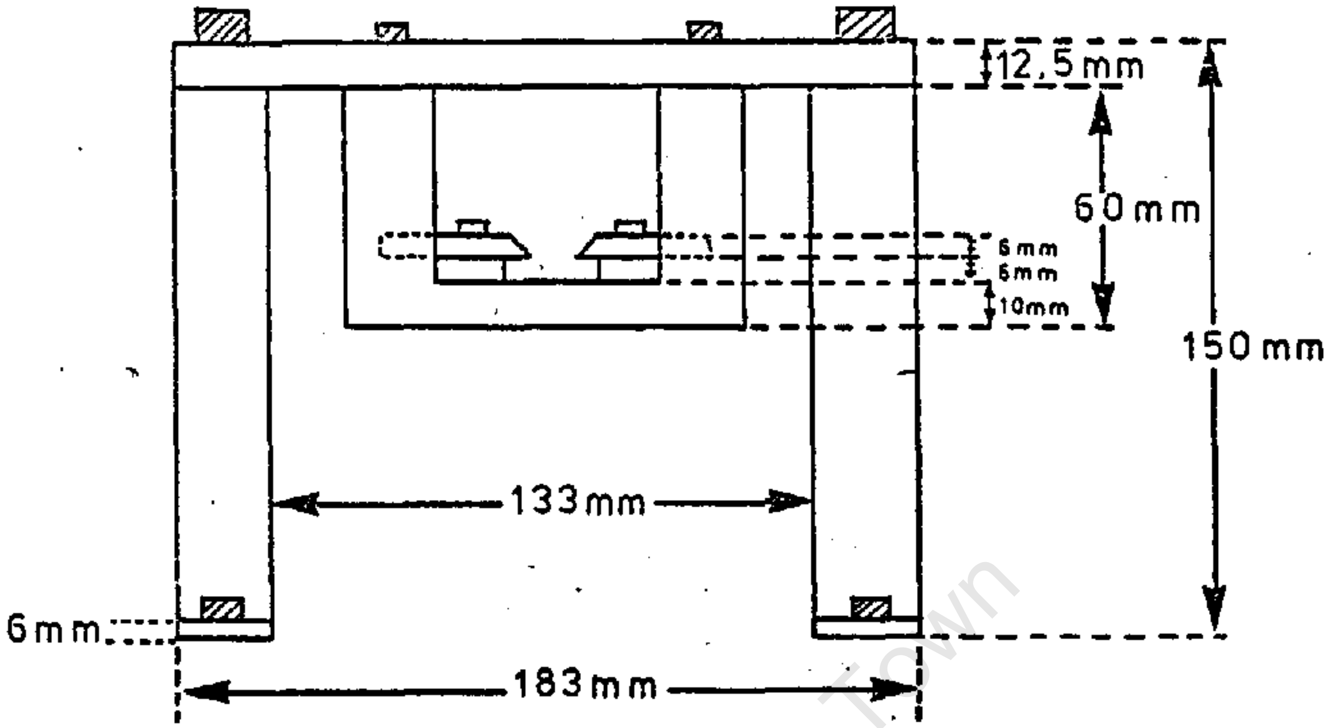

Fig. 4.2(a) The Specimen Mounting Rig (Elevation)

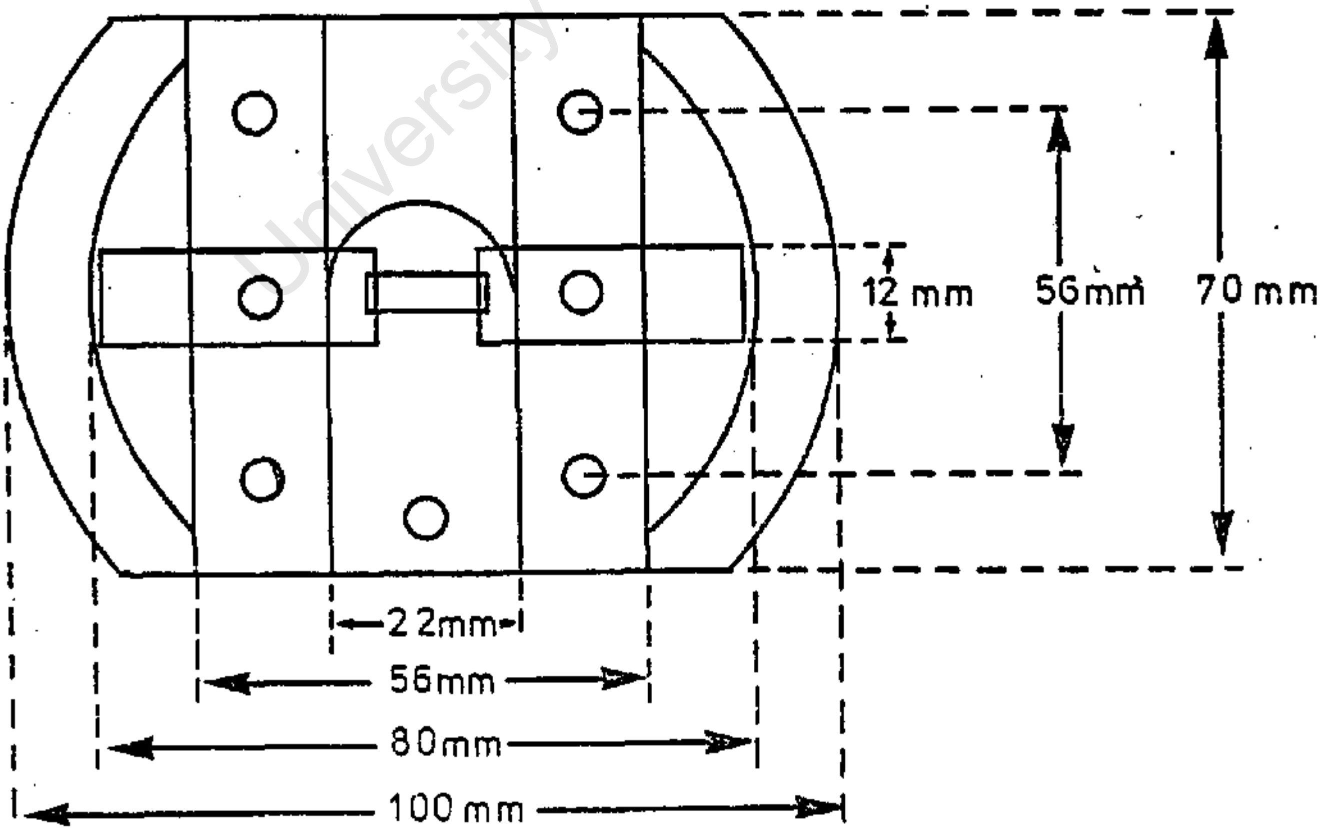

Fig. 4.2(b) The Specimen Holder Slide Assembly (Plan)

The temperature of the drill horn was found to increase to approximately 80 °C after one hour of running time,causing the horn to expand by 0,1 to 0,15mm. Therefore the machines were warmed up for one and a half hours before each test to ensure that the separation distance did not change thereafter. Furthermore, the separation distance was checked after each hour and adjustments made if necessary.

Tips for insertion into the end of the drill horns were fabricated from a titanium alloy (Ti 318A). This material was found to be suitable as it had good acoustic properties, a high erosion resistance and a low density. The last of these properties being most important since the drills were designed to take only a 2-3g end tool or tip (see appendix 4.1). This alloy, therefore, permitted a reasonable tip size without changing the resonant frequency of the drill horn. The tips were tightened in the horn with a torque wrench to 8N.m to prevent the end thread of the horn from being damaged.

During the course of a test the tips were eroded and thus after each run the tips were refaced. The small weight change caused by three of four facings was insufficient to cause a significant change in vibratory amplitude. However, after extensive erosion a slight reduction in amplitude did occur, in which case, either the power setting was increased slightly or the tip was discarded.

4.1.2 Measurement of the Vibratory Amplitude

The magnitude of the vibratory amplitude was calibrated by means of a reflected light microscope with a graduated eyepiece. The microscope was fitted onto the specimen mounting platform premanently to enable intermittent checks of the amplitude to be carried out during the course of a test (see Fig. 4.1(a)).

The amplitude of the drill is kept constant by a compensating system built into the generator. The voltage input to the transducer is automatically increased or decreased as the load on the drill horn tip changes. Nevertheless it was necessary to determine by some independent means that the amplitude did, in fact, remain constant during a test.

The amplitude measurements were made on point sources of light reflecting off facets on the tip. When the drill was in operation these point sources became extended into lines which were then measured against the calibrated graticule of the microscope eyepiece. The precision of this method was found to be within ±3um of the amplitude selected for the cavitation tests.

4.1.3 Frequency Measurement

The resonant frequency of the mechanical system of the ultrasonic drills was ±20kHz. This parameter was measured with a PM6603 counter. The drills were run at 25°C over a period of ±5 hours whilst monitoring the frequency. The individual resonance frequencies of the two drills were found to be 20,4kHz and 20,7kHz respectively and the maximum change during the five hours was 200 Hz. This is caused by the temperature increase of the drill horn, which is compensated for by the automatic frequency control.

4.1.4 Temperature Control System

The temperature of the test medium was controlled at a predetermined temperature during the course of a test. This was accomplished by circulating precooled or heated water through a glass heat exchanger coil immersed in the test bath while simultaneously agitating the contents of the bath with a magnetic stirrer.

The temperature of the circulating water was controlled in a twelve litre reservoir by the complementary action of a thermoregulator and cooling coil. This system (see Fig. 4.1) allowed tests to be carried out at any constant temperature between 5°C and 70°C.

4.2 SPECIMEN PREPARATION

The project involved a study of the effects of equipment and test liquid parameters on cavitation erosion and it was decided to use pure iron as a standard material. This material, however, was only available in the form of 5mm diameter x 150mm rods and the method of preparing specimens of a standard grain size was as follows :- the pure iron rod was cut into 3 sections 47mm, 47mm and 56mm and annealed in vacuo for one hour to remove the cold work from swaging. These rod sections were, in turn, rolled down to a flat bar section, 2,2mm thick by 5,5mm wide and then cut into 14mm lengths. After a further vacuum anneal at 650 C for one hour the specimens were pre-ground on 800 grit SiC paper and finally polished with 3um and 1um diamond paste. This method of preparation yielded a grain size of ASTM No. 4 which corresponds to an average grain diameter of 90um.

For the materials evaluation tests the 12mm diameter by 3mm thick discs were machined from sample rods. A notch was filed at a point on the circumference using a simple jig and the specimens were given any necessary heat treatment. The polishing procedure for the majority of materials was the same as that for the pure iron specimens, that is, all test pieces were ground and then polished to a 1um finish. The cemented carbides were too hard to pregrind and thus were first skimmed with a diamond impregnated wheel prior to the final polish.

4.3 CAVITATION TEST PROCEDURE AND CONDITIONS

The ultrasonic drills were warmed up for 1½ hours with a new or refaced tip in the end of the drill horn and fresh liquid, either distilled water or an oil-water emulsion, in the test bath at the required temperature. A pre-polished specimen was weighed on a chemical balance accurate to ±0,1mg and then mounted in the cavitation rig. After setting the separation distance with the modified micrometer, the specimen was immersed in the test liquid and the drill adjusted to resonance. After a suitable time interval, depending on the type of material, the drill was stopped and the specimen removed. The test piece was washed in alcohol, dried thoroughly and then re-weighed (in the oil-water emulsions tests the specimens were also washed in ether to remove any residual oil). The test piece was then replaced in the rig and the test restarted.

The test times varied from five to forty hours depending on the erosion resistance of the material. In the short tests the specimens were weighed at hourly intervals while in the longer tests weight loss checks were made at 2 or 5 hour intervals.

The conditions of testing varied according to the particular set of experiments. In the case of the oil-water emulsions study, the following conditions were employed :-

Amplitude	70um
Sep. distance	0,4mm
Medium	5‰ or 10% oil-in-water emulsions
Bulk temperature	45 C
Material	Pure Iron (grain size ASTM No.4), 1um polish
Test time	5 hours

A separation distance of 0,4mm was used in these tests since at the commencement of this part of the project the drills were not warmed up. In fact the distance was set at 0,5mm at the start of a test but due to the expansion of the horn during the first hour the gap decreased to 0,4mm and remained so throughout the rest of the test run.

For the materials evaluation tests the parameters were :-

Amplitude	76um
Sep. distance	0,35mm
Medium	Deionized water
Bulk temperature	25°C
Test times	various

4.4 TECHNIQUES OF STUDYING EROSION MECHANISMS, MICROSTRUCTURE AND STRUCTURAL CHANGES

For all microstructural investigations of materials a Reichert "MeF2" Universal Camera Microscope having a Normarski interference attachment was used. Other facilities on the microscope employed in this work include steep-oblique,bright ground,incident-light illumination (pseudo-relief) and dark ground, incident-light illumination. Also the diamond pyramid micro hardness tester was used to determine the hardnesses of different phases in certain materials.

The modes of erosion of materials were studied by means of a Cambridge S180 scanning electron microscope equipped with an energy dispersive analysis of X-rays (EDAX) attachment. All specimens were gold-palladium coated prior to examination to obtain the highest quality images possible.

A limited amount of transmission electron microscopy (TEM) was done on 304 stainless steel to investigate the stress induced phase transformation that occurs during erosion of this material. Specimens were prepared from 0,25mm sheet specimens which had been eroded for various times. 3mm disc samples were taken from the eroded area and thinned from the non-eroded back surface since the region of interest was the area immediately below the eroded surface.

Electropolishing was done in a Bainbridge unithin foil thinning unit. This unit employs the jetting technique with alternating polarity and yields foils with a central hole surrounded by electron transparent material. The polishing conditions were 65 volts at room temperature in 80:20 acetic acid/ Perchloric acid electrolyte.

Thinning from one side only was accomplished by manually controlling the polarity so that the back surface of the specimen was anodic for the majority of the thinning time. Occasionally the polarity was reversed to obtain a light polish on the eroded surface as well. The thin foils were examined in both a Philips EM300 TEM at 100kV and a high voltage microscope at an accelerating voltage of 200kV. Structural features were studied in the bright field mode while selected area diffraction patterns were recorded for identification of the various phases.

The crystallographic structures of materials and the occurrence of phase transformations were studied by X-ray diffractometry. The instrument employed for this study was a Philips X-ray generator with a parafocusing goniometer/ detector system. Cu-Ka radiation was used with a mono-chromator to eliminate reflections from K6 radiation. Specimens were investigated in the polished and eroded condition.

CHAPTER FIVE

THE INFLUENCE OF VARYING SEPARATION DISTANCE AND BULK TEMPERATURE OF THE TEST MEDIUM

Several equipment parameters and liquid properties affect the intensity of vibratory cavitation erosion. Equipment parameters which affect erosion include: the vibratory amplitude, frequency and the separation distance between drill tip and test piece. The properties or states of the test fluid which influence cavitation are: temperature, type of fluid, density, viscosity, gas content, compressibility and presence of solid impurities. Of these various parameters, the following were investigated in this study:

(i) drill tip to test piece separation distance, d
(ii) temperature of the test fluid
(iii) gas content
(iv) presence of solid impurities.

The effect of adding impurities to a test bath of (distilled water), such as, suspended solids from a mine service water or pure kaolin,failed to produce any significant change in the erosion rate of pure iron(compared with that in distilled water.) Also aerating the fluid (that is, distilled water saturated with air) during the course of a test did not affect the erosion rate of pure iron compared with that in distilled water at equilibrium gas content. These two parameters will not, therefore, be considered any further. The following section presents and discusses the results of the work on the first two of the abovementioned parameters,viz., the effects of separation distance and temperature of the test fluid.

5.1 RESULTS AND DISCUSSION

5.1.1 Effect of Varying Separation Distance

The effect of this parameter was investigated by monitoring the erosion of pure iron in distilled water as a function of the distance between drill tip and specimen. The results of these tests are shown in Fig. 5.1. The graph indicates that maximum erosion occurs when the distance between test piece and drill tip is approximately 0,35mm (hence the 'standard' separation distance of 0,35mm used in all subsequent work).

As mentioned in the previous chapter, the drill was warmed up for one and a half hours prior to a cavitation test to ensure that the horn did not change length due to thermal expansion during the course of a test. Vyas and Preece (21) investigated this variable by measuring the stress beneath the vibrating tip by means of a transducer technique and also by monitoring the weight loss of aluminium samples as a function of separation distance. In contrast to the above result they found a maximum in erosion (cumulative weight loss) for d = 0,5mm. Singer and Harvey (28)also studied the influence of separation distance for aluminium and copper and found maxima in erosion, as measured by weight loss, at 0,89mm and 0,51 mm respective}y.

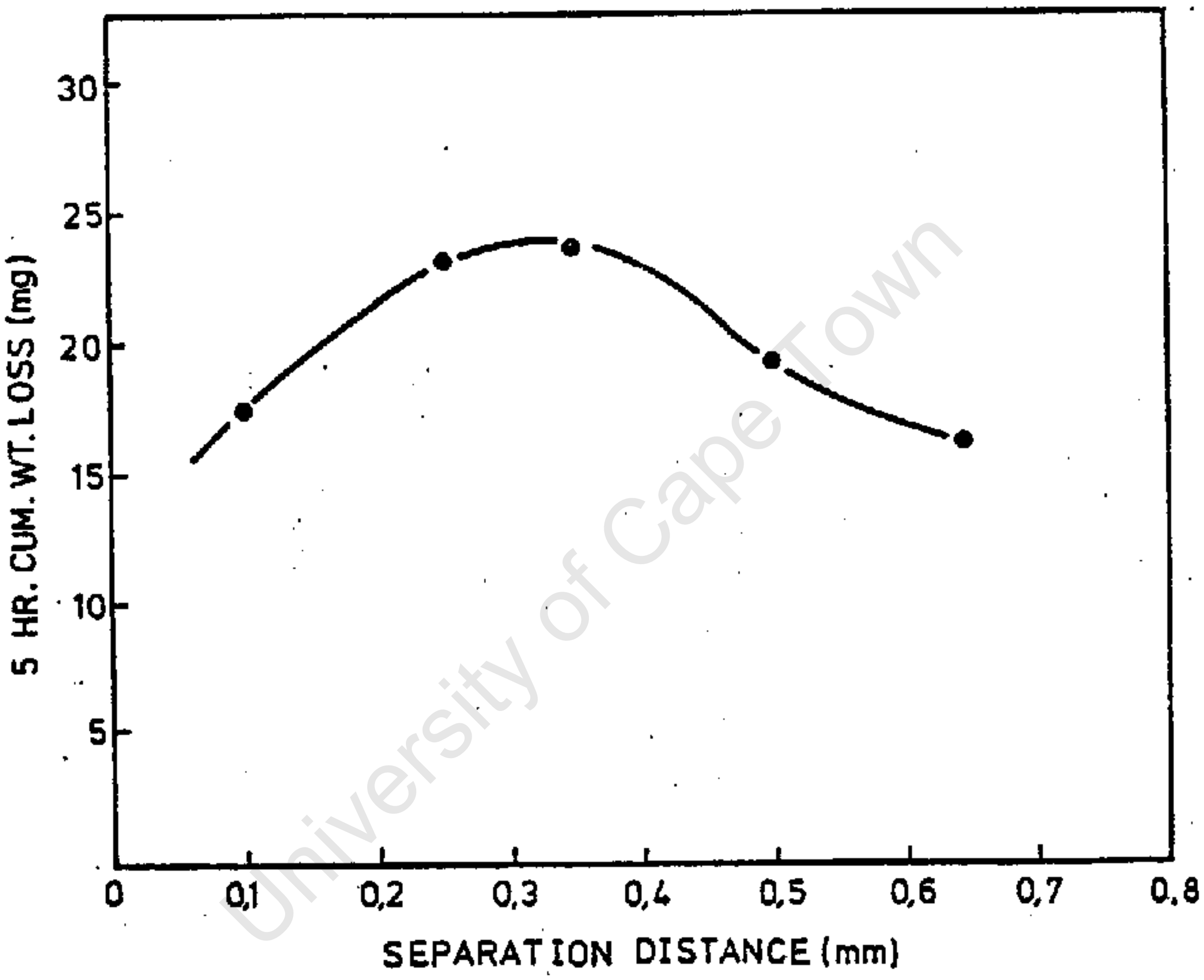

Fig. 5.1 The Effect of Separation Distance on the Erosion of Pure Iron

Vyas and Preece (21) interpreted the separation distance phenomenon as being the result of two opposing effects: the pressure change in the liquid in the cavitation zone is inversely related to the separation distance and since this pressure change determines the intensity of cavitation, the stress measured by the transducer increases for decreasing d. On the other hand for very small separation distances, the number of nuclei decreases and also the volume of liquid into which cavities can grow is reduced, thus the cavitation intensity decreases. The net result' is a maximum in erosion at a critical separation distance (dcrit).

It is agreed that the decrease in erosion for $d>d_{crit}$ is due to the decrease in acoustic pressure amplitude. However, it is considered unlikely that a decrease in the number of nuclei is responsible for the decrease in erosion for distances less than d_{crit}. This is because nuclei of the order of 5um in size, which is very much less than the minimum separation distance studied by Vyas and Preece, can initiate vibratory cavitation (85). The separation distance would have to be much less than 0,1 mm before the concentration of nuclei of critical size , in the fluid between tip and specimen, was affected. On the other hand it is agreed that a small separation distance will restrict the maximum size to which cavities can grow, which in turn, results in a decrease in erosion.

In addition to these effects it is proposed that the temperature of the fluid in the zone between specimen and vibrating tip plays a part in reducing erosion for separation distances less than d_{crit}. The temperature of the fluid in the gap probably increases to more than 50 C as d is decreased below distances of 0,5mm. This rise in temperature will cause an increase in the vapour content of the cavities which, in turn, will cushion their collapse and hence reduce erosion.

5.1.2 The Effect of Varying Bulk Temperature

The results obtained on the influence of the temperature are shown in Fig. 5.2. The temperature effect was investigated in both distilled water and three 5% oil-in-water emulsions and the emulsion curve in Fig. 5.2 is representative of the results obtained in these three emulsions. A maximum in erosion occurs for a bulk temperature of 35 C in both distilled water and the emulsions.

This result agrees with the findings of Singer and Harvey(28) but is a little different from the 40 C to 50 C found by a number of other investigators (25, 26,27,86). Hobbs (87) ascribed the discrepancy in findings to the differences in test methods since in his apparatus the film was continuously changed during a test (86) while in the apparatus used in the present work and in that used by Singer and Harvey the film between the tip and specimen was 'static' during the course of a cavitation test. Although the temperature of the film was not measured in this study, Singer and Harvey did carry out such a check by inserting thermocouples in a dummy specimen. Interestingly they found that the temperature of the film was no more than 4 C over the bulk temperature. Thus the true temperature at which maximum erosion occurs is more likely to be about 40 C. This will apply to the results of the present work as well.

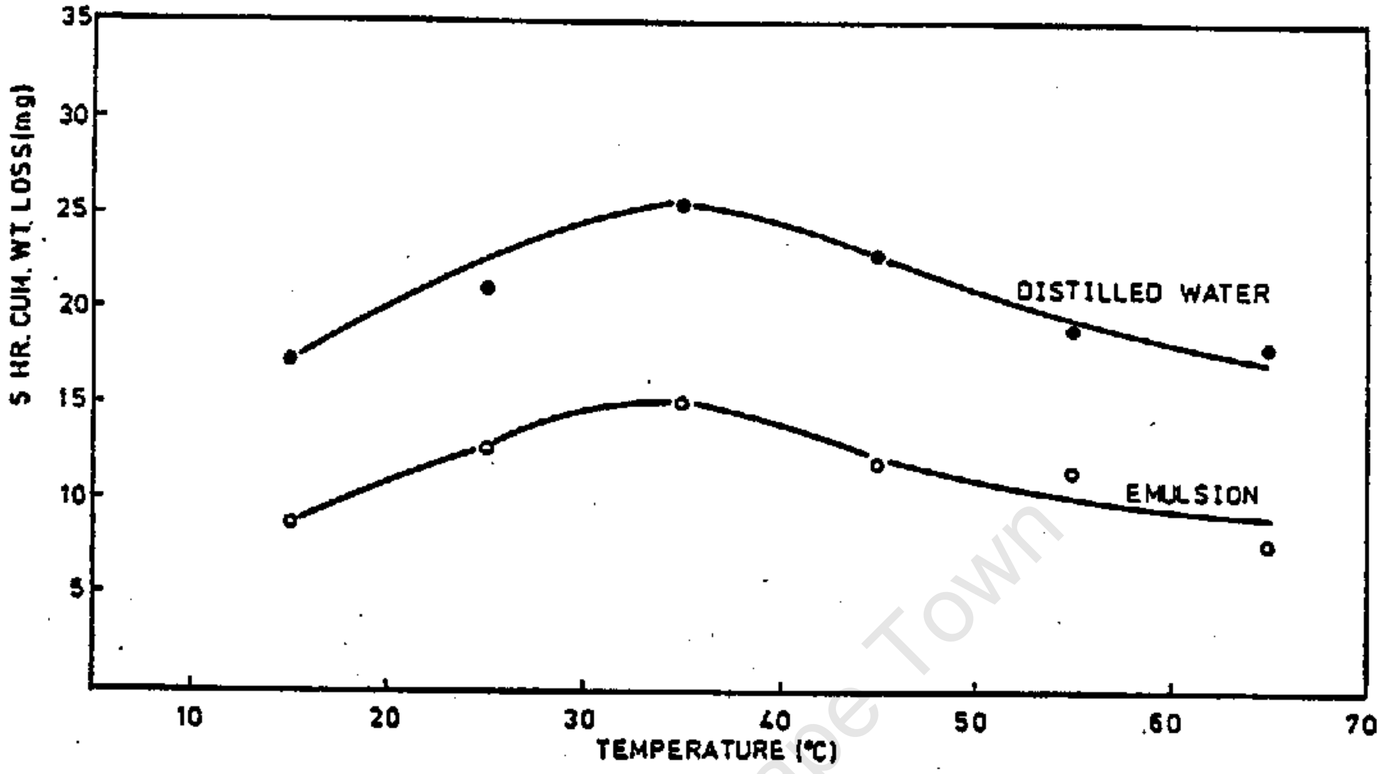

Fig. 5.2 The Effect of Medium Temperature on the Cavitation Erosion of Pure Iron

Singer and Harvey also carried out tests with a moving specimen apparatus and found that the temperature corresponding to maximum erosion was about the same as that for the stationery specimen rig. Thus there is still some doubt about the precise temperature at which maximum erosion occurs and whether it is affected by variations in the test method.

As mentioned earlier the explanation for the reduction in erosion at temperatures greater than about 45 C is generally accepted as being due to the increased vapour pressure of the test liquid. This results in an increased cavity vapour content which, in turn, leads to cushioning of cavity collapse and a reduction in erosion. But the explanation for the decrease in erosion at temperatures below 45 C is less well established. It has been proposed that the increased solubility of gas at low temperatures leads to a higher gas content in the cavities which again results in increased damping of the collapse pressures. However, there are several arguments against this theory.

Hobbs and Laird (25) investigated the temperature effect at two constant gas contents, namely, 5ml/1 and 11ml/1 and found that the higher gas content resulted in a slightly lower rate of erosion at low temperatures (28mg/hr cf.

32mg/hr at 15°C). Hickling (88), in following up this finding, suggested that the increase in the gas content of water as the temperature decreases from 30°C to 0°C (about 40%) is insufficient to cause the observed decrease in erosion. In addition, he pointed out that at lower temperatures the rate of diffusion of gases is reduced and would offset any improvement derived from a higher dissolved gas content.

Alternative mechanisms have been proposed. Leith (89)has suggested that the increased viscosity and surface tension at low temperatures were the reasons for the decreased erosion. Hickling (88)proposed a mechanism of ice formation within collapsing cavities while Plesset(27)proposed that chemical activity might be an important factor. 'These latter explanations, however, have gained even less support than the former.

A further effect which will contribute to the decrease in erosion rates at low temperatures is the reduction in liquid vapour pressure (P_V). The decrease in P_V for a temperature reduction from 40°C to 10°C is only about 10kPa and therefore, as in the case of the gas content, viscosity and surface tension, the effect of vapour pressure is likely to be small. However, it appears that the decrease in erosion at low temperatures is not controlled by any one parameter, but is the consequence of the combined effect of small changes in a number of fluid properties.

Furthermore it was observed that in distilled water corrosion of test pieces increased significantly for temperatures greater than 40°C. But it was also noticed that in the oil-in-water emulsions tests no corrosion occurred at high temperatures yet the trends in the two media are identical. This evidence tends to eliminate any possible influence of corrosion on the temperature effect.

5.2 CONCLUSIONS

This work on the influence of the separation distance and of the bulk test fluid temperature on cavitation erosion has shown that:

(i) A maximum in erosion of pure iron occurs for a separation distance of 0,35mm.

(ii) Maximum erosion of pure iron occurs at a bulk test fluid temperature of 40°C in both distilled water and 5:95 oil-in-water emulsions.

CHAPTER SIX

EVALUATION OF OIL-WATER EMULSIONS

The use of water based emulsions as hydraulic fluids in equipment employed in the confines of a mine has many advantages. Originally emulsions were used because of their fire resistance and the coal mining industry, in particular, has been using emulsions for a number of years(10). Present efforts to mechanise gold mining in South Africa requires considerable application of hydraulic power and 5:95 water based emulsions are being used extensively in this programme. In this case economic factors have dictated the use of these fluids rather than their fire resistance. The elimination of the pollution problem associated with failure of hydraulic pipe lines is another factor but is of secondary importance.

Emulsions are generally considered to be the dispersion of one liquid in another with which it is immiscible. An emulsion consists of three phases known as the internal phase, external phase and the interphase. The internal phase is the dispersed phase and the external phase the matrix, while the interphase is the emulsifier that binds the external and internal phases.

There are three common types of water based emulsions, namely, water-glycols (40% to 50%) water, invert water-in-oil emulsions (40% water, 60% oil) and dilute oil-in-water emulsions (5% oil,95% water). The former two are very similar to mineral oils in terms of properties and can, therefore, be used without difficulty in existing hydraulic machinery. But, in spite of a high water content, they cost about twice as much as mineral oil. The 5:95 dilute emulsions are far cheaper than mineral oil but have disadvantages in that they have poor lubricating and corrosion inhibition properties and also low resistance to cavitation.

A limited amount of work has been done to evaluate the influence of water based emulsions on cavitation erosion. The National Coal Board of the United Kingdom has compared the erosion rates of various materials in each of the above-mentioned emulsions with that in distilled water and a mineral oil (9q. It appears, however, that a comparative evaluation of a range of oil-in-water emulsions has not been carried out as yet. This investigation was, therefore, undertaken to establish whether the emulsion type affects cavitation erosion, and if so, to determine the causes of any such trend. This chapter describes the findings of this work and also presents tentative explanations for the influence of oil-in-water emulsions on cavitation.

6.1 RESULTS AND DISCUSSION

Dilute oil-in-water emulsions were originally developed as machine cutting fluids. But it has been found that these fluids can also be employed as hydraulic media. The subsequent increasing use of these media in hydraulic machinery has resulted in several oil companies developing emulsifiable oils specifically for use as hydraulic fluids. In this present investigation a number of conventional cutting fluids plus a range of specific hydraulic emulsions were tested to ascertainwhethererosion could be reduced by use of a particular emulsion or group of emulsions. The commercial names of the various emulsifiable oils may not be published and thus the emulsions have been labelled as oils A to V.

The conditions of the cavitation tests carried out in the oil-in-water emulsions have been described in an earlier chapter. Pure iron was used as the 'standard' material throughout these tests. A number of control tests were carried out in pure distilled water for comparative purposes and also to determine the degree of experimental scatter in these tests.

The range of emulsions were tested in two concentrations, namely, 5% and 10% or 5:95 and 10:90 oil to water. Figs. 6.1 and 6.2 are histograms showing the relative cumulative' weight losses obtained from pure iron cavitated in the emulsions for five hours. Included in the 5:95 histogram is the result of a mineral hydraulic oil (Oil A) while the average distilled water result appears in both histograms. The 5:95 emulsion tests were all done in duplicate but the 10:90 tests only once each. The scatter in the 10:90 emulsions is expected to be of the same order as that in the 5:95 emulsions, that is,on average, 4,8% of the mean.

The histograms show the following: (a) little cavitation erosion occurs in pure mineral hydraulic oil (b) all emulsions suppress cavitation erosion in comparison with distilled water (c) some emulsions suppress erosion more than others and (d) there is some change in order when the oil concentration in the emulsions is doubled.

The virtual elimination of erosion in mineral oils was first reported by Rheingans (32) who eroded materials in a mineral seal oil and a transformer oil. Later Hobbs (91) tested two hydraulic oils and found they reduced erosion considerably in comparison with water. Kenny et al (90)obtained similar results to that of Hobbs and also found that invert emulsions were as effective as mineral oils in suppressing cavitation damage.

The low incidence of cavitation damage in mineral oil is the result of a combination of factors. In comparison with water, mineral oils have:

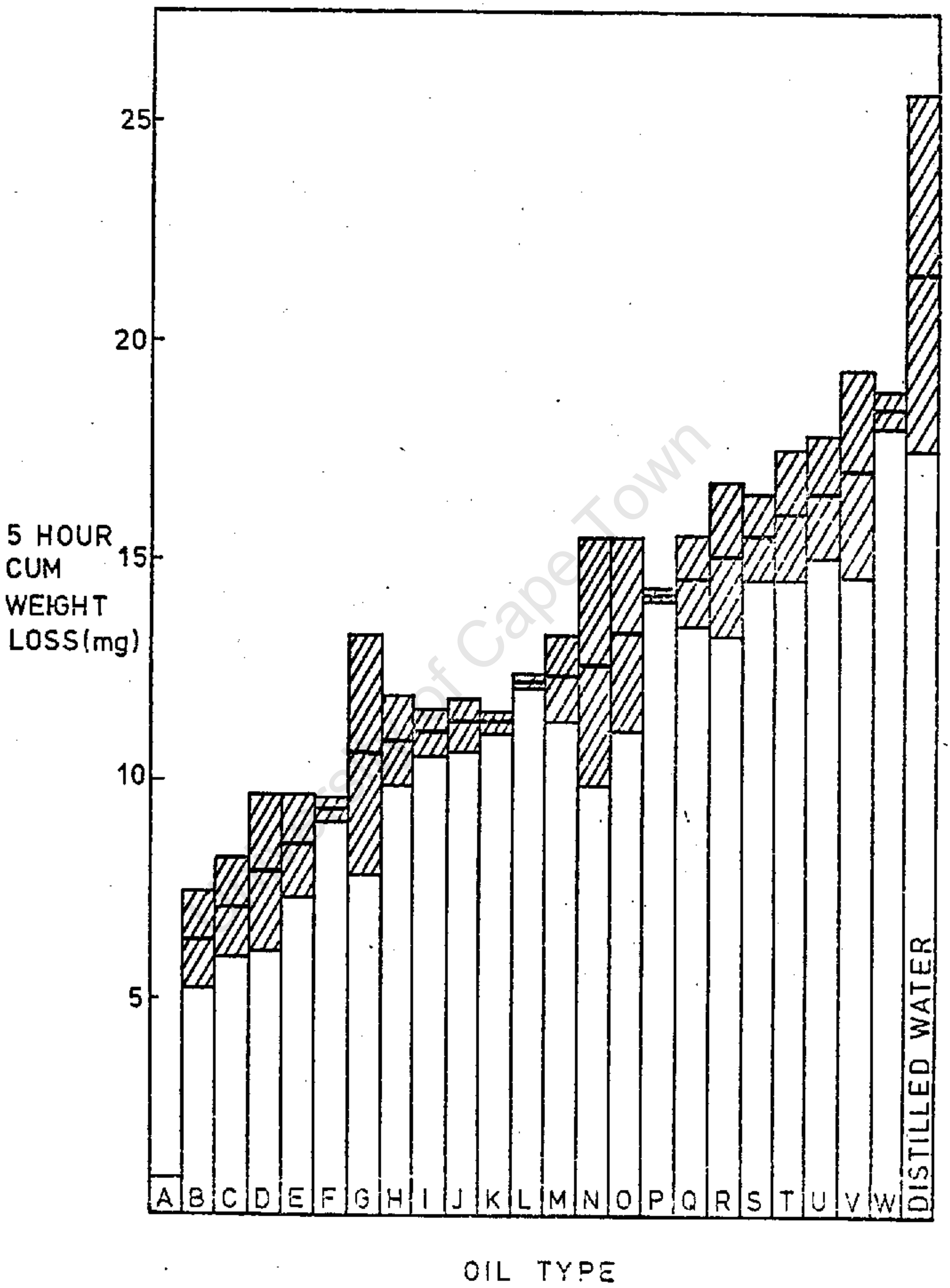

Fig. 6.1 The Relative Performances of the 5:95 Emulsions

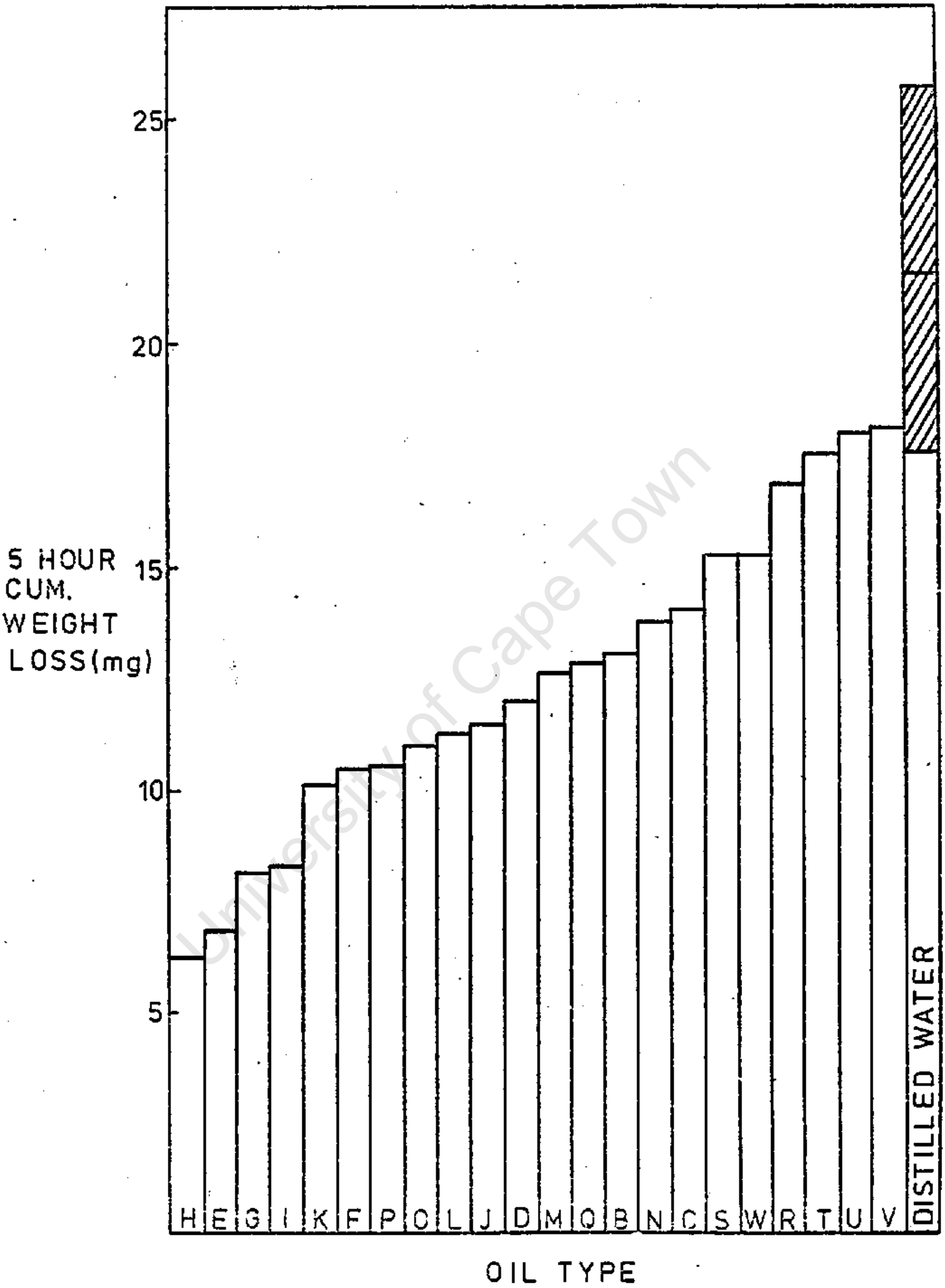

Fig. 6.2   The Relative Performances of the 10:90 Emulsions

(i) A lower vapour pressure
(ii) A higher dissolved air content (about 5 times that of water)
(iii) A higher viscosity (-30 times that of water)
(iv) Lower bulk surface tension.

The dominant parameters in reducing cavitation damage would be the low vapour pressure, high viscosity and high dissolved air content. A lower vapour pressure means a greater drop in pressure is required to initiate vaporous cavitation, while if unstable cavitation does develop then the high viscosity exerts considerable drag on the moving cavity wall and slows down the processes of growth and collapse. The high dissolved air content results in cushioning of cavity collapse. The net result is a negligible erosive potential of cavitation in mineral oil.

The performance of the oil-in-water emulsions is more important to this investigation and the trend in the histograms will now be discussed.

6.1.1 Emulsion Properly - Cavitation Erosion Relationships

The trend in emulsion performance must be the result of changes in one or more of the physical properties of these fluids. Thus common fluid parameters known to affect the dynamics of cavitation were investigated, namely, kinematic viscosity, density, bulk surface tension, mineral oil content (oil droplet size) and dissolved air content. Since water is the continuous phase in 5:95 emulsions their kinematic viscosity is very close to that of water. Values obtained from the oil companies showed that viscosities varied between 0,72 and about 1,20 centistokes in the 5:95 emulsions and as expected the viscosities of the 10:90 emulsions were not much different (0,77 to 1,37). Moreover the viscosity of the original emulsifiable oil has no influence on the emulsion viscosity. Similarly the densities of the emulsions were found to be much the same as that of water. Also the compressibilities and vapour pressures of these fluids are equivalent to that of water (92).

On the other hand the bulk surface tensions of the emulsions (as measured by the drop weight method(93)) were found to be about half that of water (72,4 dynes/cm), the majority of the values being between 30 and 40 dynes/cm. However, no correlation could be found between this parameter and the cavitation erosion data of the emulsions. But oil droplet size, which is a function of the ratio of the mineral oil and emulsifier contents, did show some correlation with the performance of the oil-in-water emulsions. There is also evidence that the dissolved air content, which is about two and a half times that of water, may influence cavitation in these water based fluids.

6.1.2 The Effects of Mineral Oil Content and Oil-droplet Size on Emulsion Performance

The majority of emulsions are based on mineral oil. Addition of an emulsifier renders a mineral oil 'soluble' in water by breaking up the bulk oil and forming an interfacial layer around oil droplets thereby linking the internal oil phase to the external water phase. *Consequently the size of oil droplets is dependent on the ratio of the concentrations of emulsifier and mineral oil base*.* For a high mineral oil content (80-90%) the emulsion is milky in appearance which corresponds to a droplet size of about 2 to 5um. When the oil content is a little lower, namely, 50 to 70% the emulsion is rather less milky and has a droplet size of the order of 0,5um. For an oil content of less than 50% the emulsion is clear and the droplet size approximately 0,05um,while a few of the emulsifiable oils are fully synthetic (that is, not based on mineral oil) and form true, clear solutions with water.

Fig. 6.3(a) and (b) are plots of cumulative weight loss versus mineral oil content of the 5:95 and 10:90 emulsions. In each case the best fit line and the correlation coefficient as determined by regression analysis are given. The correlation is more satisfactory in the 5:95 emulsions than in the 10:90 emulsions, the coefficients of correlation being 0,84 and 0,74 respectively. Note that Emulsion F yielded an exceptionally low result for a synthetic formulation and was therefore left out of the regression analysis.

The high experimental scatter obtained in these tests is due to the use of pure iron as the test material. It is now realized that pure iron was a poor choice as a standard test material and that a stable austenitic stainless steel would have been more satisfactory. Pure iron was found to erode partly by a ductile mode and partly by a brittle intergranular mode. This has been reported before by Preece et al (67) and Erdman-Jeznitzer and Louis (12). The complex erosion mechanism is a consequence of the high strain rate of vibratory cavitation

* *The emulsifier and mineral oil base make up the majority of an emulsifiable oil (90 to 95%) and thus the mineral oil content can be written as:*

$$V_o = 1 - V_e$$

where V_o = *volume of mineral oil*
and V_e = *volume of emulsifier*

Therefore, the droplet size of the emulsion can be considered proportional to the mineral oil content.

** *Note that the oil contents of the emulsions have been plotted and not the oil contents of the emulsifiable oils prior to dilution. For example, in Emulsion B the oil content of the emulsifiable oil is 90%. If 5mls of this oil are mixed with 95mls of water then the oil content of the emulsion is 5% x 0,9 = 4,5%. The synthetic emulsions do not contain any mineral oil and are therefore plotted against zero oil content in Fig. 6.3 (a) and (b).*

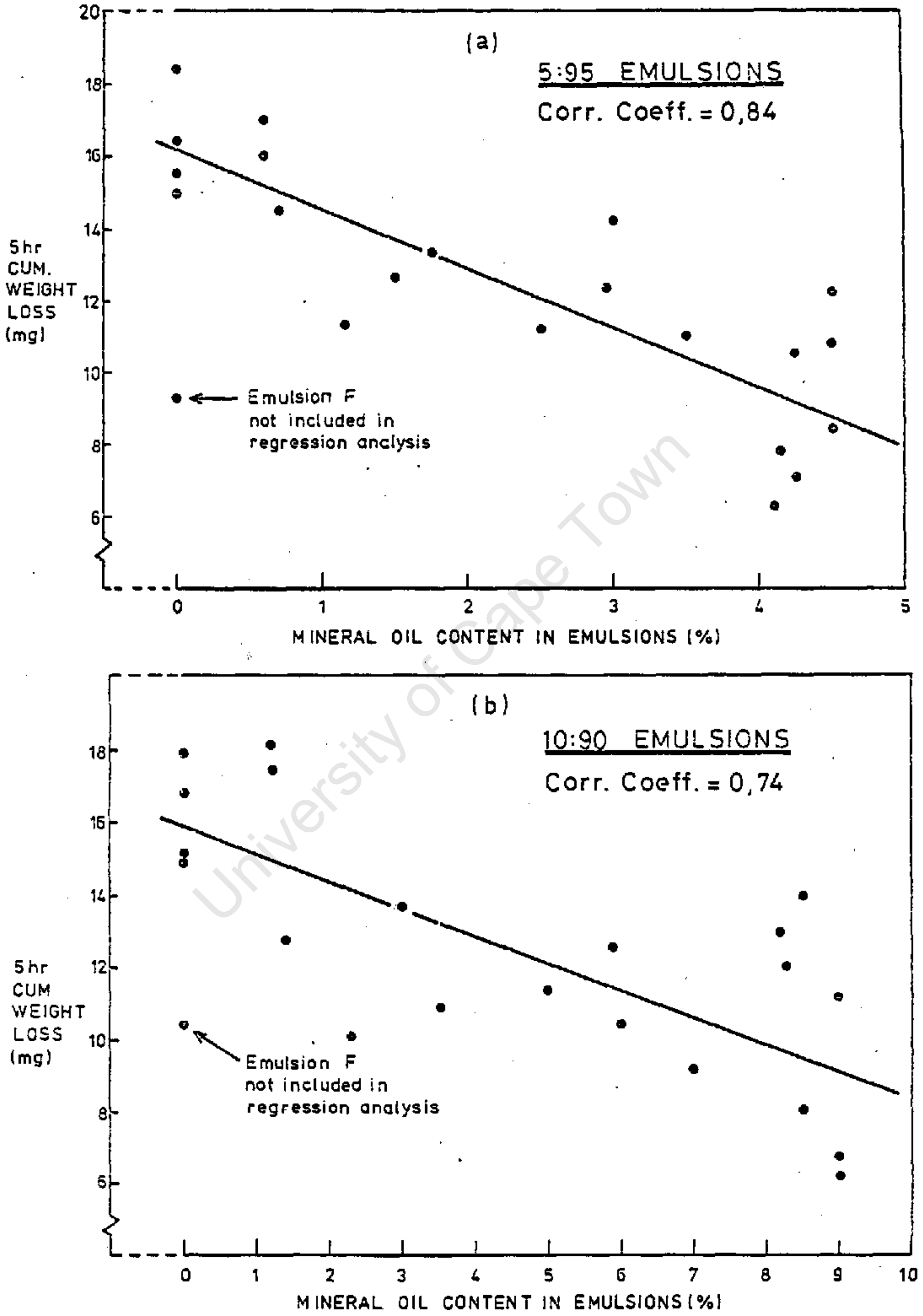

Fig. 6.3 The Relationship Between Erosion Weight Loss and Emulsion Mineral Oil Content.

which appears to correspond to the ductile to brittle transition in this metal. Moreover the proportion of brittle fracture occurring in any one sample is random since it depends on the number of favourable sites in the cavitation zone from which brittle crack propagation can occur. As a result the experimental scatter, when using pure iron as the test material, tends to be high.

The oil droplet size effect was subject to some doubt since the emulsions, being from numerous different sources, varied in base oil type and emulsifier type. It was decided, therefore, to confirm these results by carrying out erosion tests in emulsions representing the three oil droplet size groups, that is, opaque, semi-opaque and clear, but formulated from the same emulsifier and base oil type. Furthermore a hardened,low alloy steel was used as the material in these tests, instead of pure iron, to reduce experimental scatter. The results of these tests are given in Fig. 6.4. The trend in this graph clearly confirms the correlation found between the erosion data and oil contents of the emulsions tested previously.

Further evidence of the influence of oil content/droplet size on the cavitation erosion of pure iron can be found in the damaged surfaces of the test specimens. The proportion of brittle fracture decreases as the oilcontent of the emulsions increases. Figs. 6.5(a) to (d) are scanning electron micrographs of representative areas of eroded surfaces of pure iron specimens after exposure to cavitation in distilled water and the three main types of emulsions respectively. The reduction in brittle cleavage is an indication of a decrease in the strain rate of the impinging cavitation.

The influence of oil content and resulting oil droplet size on erosion could be the consequence of two possible effects. One mechanism is based on the ability of the oil phase to wet the metal specimen thereby eliminating surface nuclei. These surface nuclei are probably of the form suggested by Harvey (14) namely, gas pockets in crevices. If these pockets entrapped in surface cracks could be removed, the nucleation of highly erosive cavities at the specimen surface would be reduced. Such a mechanism could be related to the oil content and oil droplet size of the emulsions.

As the oil content of the emulsion is increased (and the emulsifier content reduced) the oil droplet size increases. This change in droplet size is, effectively, due to a reduction in the interfacial energy between the oil and water phases. According to wetting theory the ability of the oil phase to wet the metal test piece is controlled by the relative interfacial energies between oil and water, yow , metal and oil, ymo' and metal and water, ymw (See Fig. 6.6.)

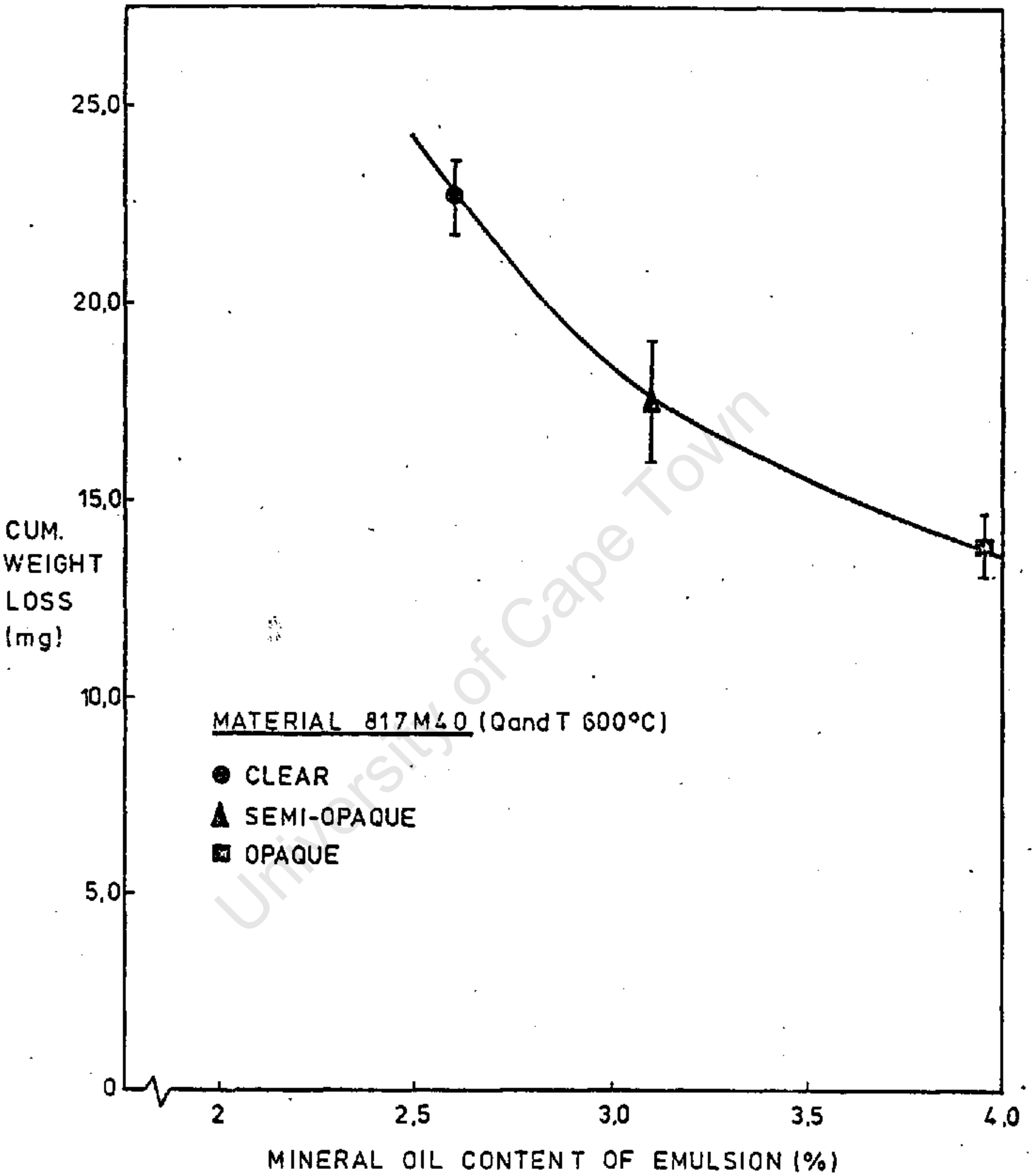

Fig. 6.4 The Relationship between Erosion Weight Loss and Oil Content for Emulsions of Constant Base Oil and Emulsifier Type.

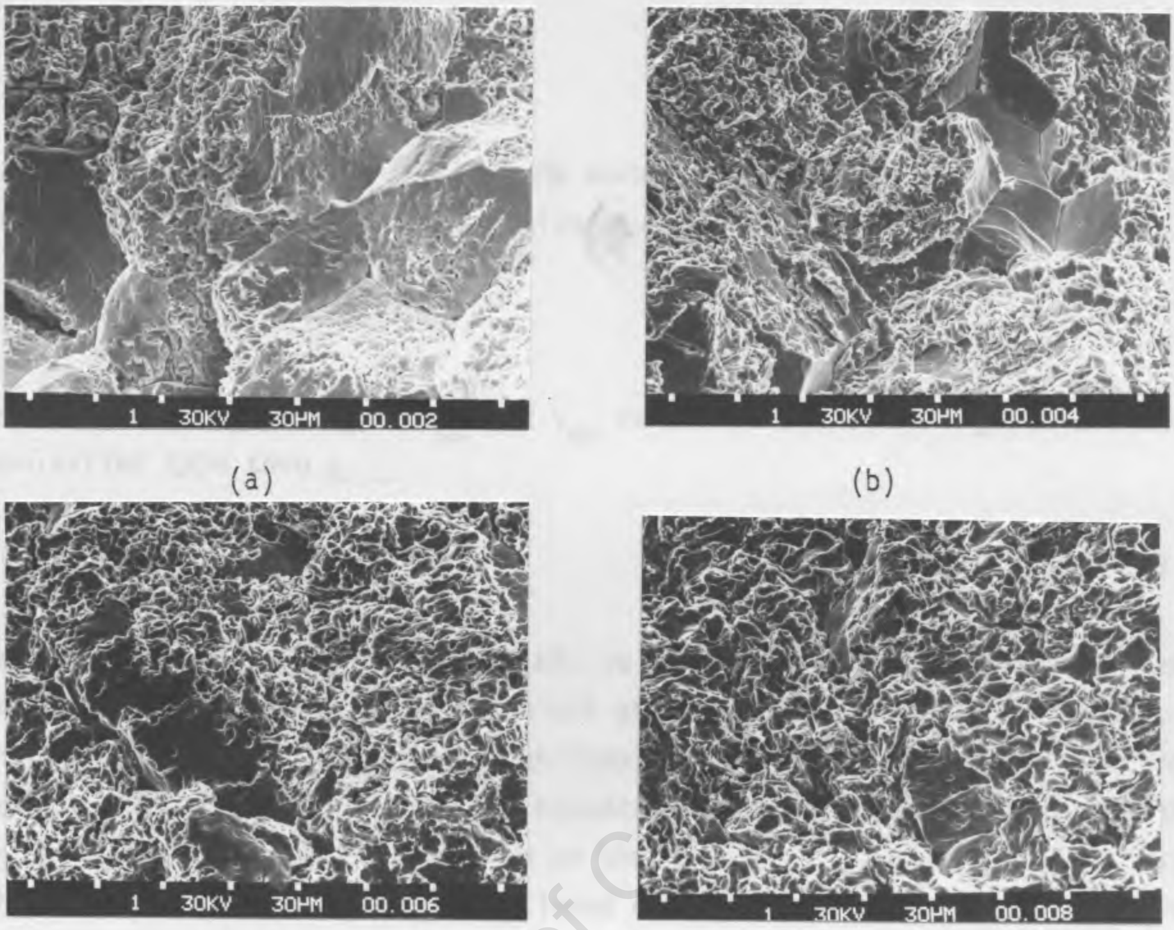

(a) (b) (c) (d)

Fig. 6.5 The Eroded Surface of Pure Iron in (a) Water (b) Clear Emulsion (Oil Content, 50%) (c) Semi-opaque Emulsion (Oil Content, 50-70%) (d) Opaque Emulsion (Oil Content, 80-90%)

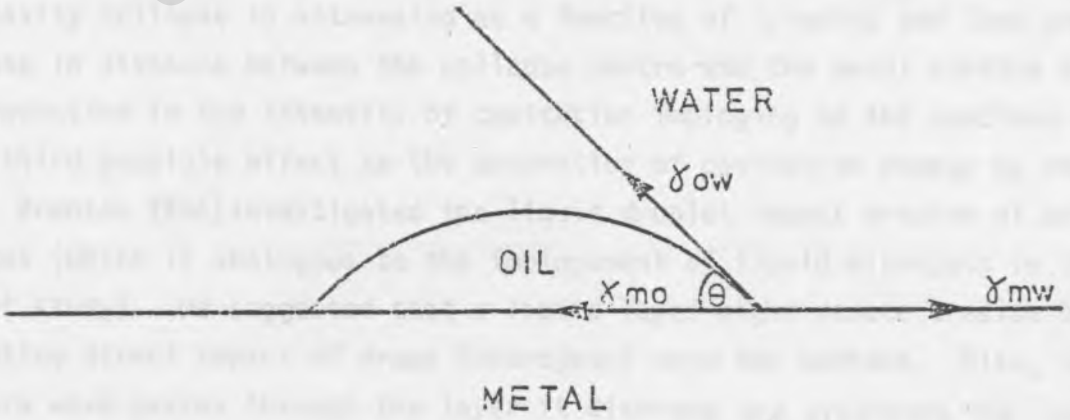

Fig. 6.6 Interfacial Energies in a Three-Component System

At equilibrium these energies are related by the equation:

$$\gamma_{mw} = \gamma_{mo} + \gamma_{ow} \cos\theta \qquad \text{.............} \quad 6.1$$

Wetting ability is equivalent to the work per unit area W, required to break the oil-metal interface which is given by (18):

$$W = \gamma_{mw} + \gamma_{ow} - \gamma_{mo} \qquad \text{.............} \quad 6.2$$

Assuming that the energies γ_{mw} and γ_{mo} remain constant for a given oil and emulsifier type then :

$$W = \gamma_{ow} + \text{constant} \qquad \text{.............} \quad 6.3$$

In other words the ability of the oil to wet the metal is directly related to the interfacial energy between the oil and water. Since y_{OW} is, in turn, directly related to the oil content/droplet size the degree of wetting that occurs is proportional to the oil content and it is proposed that the high oil content emulsions form a thin film on the surface of the test pieces. Note that the bulk surface tension mentioned earlier is not a measure of the interfacial energy between the oil droplets and metal. Therefore the lack of any correlation between this parameter and erosion does not contradict the above theory.

The presence of an oil film could reduce erosion in three ways: The most significant effect as mentioned earlier, would be the elimination of highly erosive surface cavities since the oil layer would prevent Harvey type nuclei from operating at the specimen surface. In addition the distance between the closest cavities and the metal surface will be increased. The pressure front from cavity collapse is attenuated as a function of 1/radius and thus any small increase in distance between the collapse centre and the metal surface will result in a reduction in the intensity of cavitation impinging on the specimen surface.

A third possible effect is the absorption of cavitation energy by the oil film. Brunton (93a)investigated the liquid droplet impact erosion of wetted surfaces (which is analogous to the impingement of liquid microjets in the present study). He suggested that a liquid layer might reduce erosion by preventing direct impact of drops (microjets) onto the surface. Also, as the pressure wave passes through the layer it diverges, and providing the layer thickness is much greater than the diameter of the droplet, attenuation of the pressure wave occurs and it varies as the square of the layer thickness.

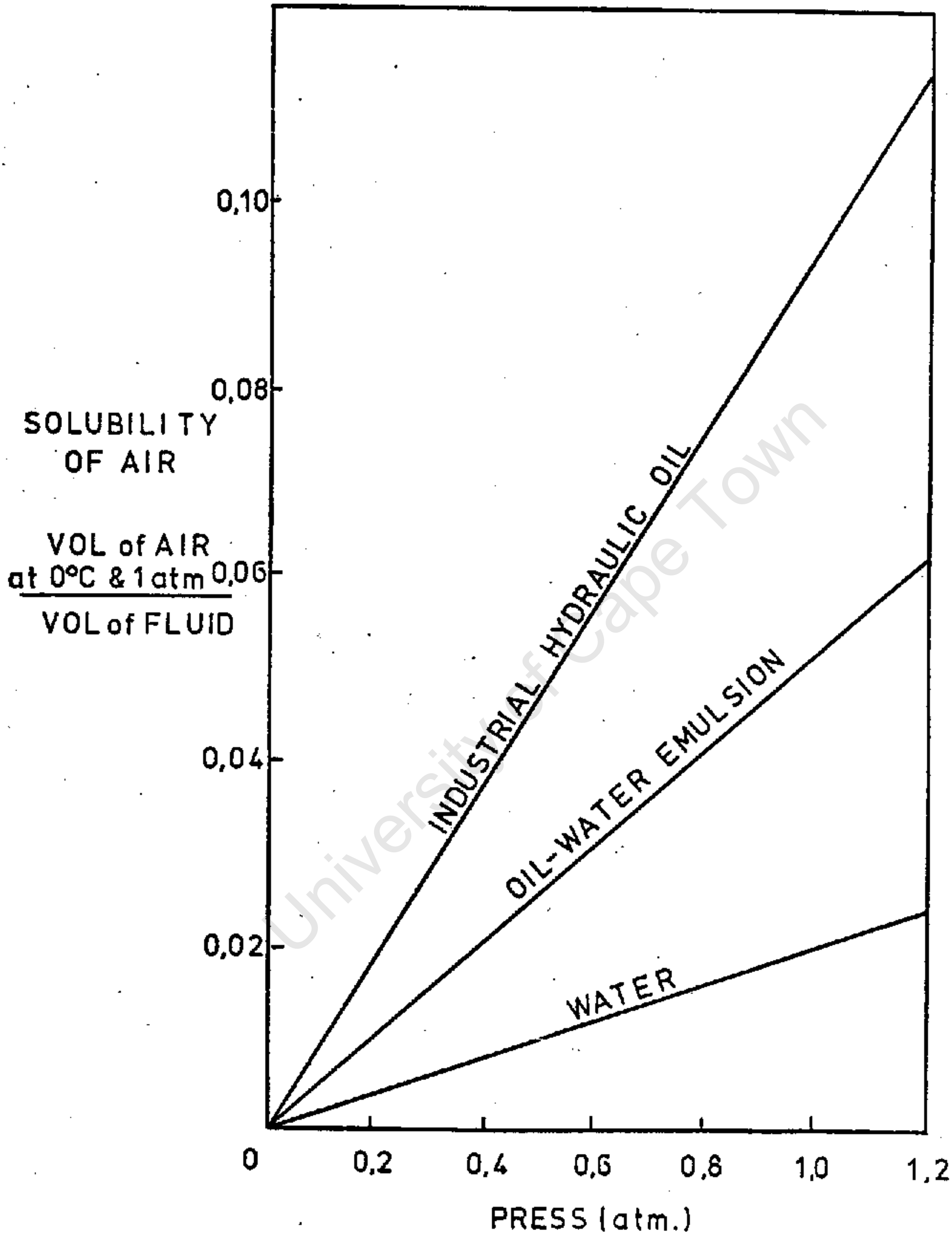

Fig. 6.7 The Solubility of Air in Three Common Hydraulic Fluids

Therefore he points out that for erosion protection by a liquid film the important characteristic is not the absolute layer thickness but the thickness of the layer relative to the size of the impacting droplet (microjet).

There is another probable mechanism which could explain the generally lower erosion rates observed in oil-water emulsions and possibly the trend in emulsion performance as well. This involves the air content of the emulsions. Fig. 6.7 is a graph taken from ref. 93b showing the relative solubilities of air in distilled water, an oil-water emulsion and a mineral hydraulic oil. Clearly at 1atm. pressure the amount of dissolved air in an oil-water emulsion is more than two and half times that in distilled water. This higher dissolved air content could have an important influence on vibratory cavitation erosion.

The diffusion of dissolved air across the cavity wall during growth and collapse of a cavity was investigated by Epstein and Plesset (94). They found the process to be too slow (at room temperature) to appreciably affect the contents of the cavity and thus the collapse pressures. However, in an oscillating acoustic pressure field, some gas bubbles are of subcritical size, which in a field of sufficient intensity, undergo radial oscillations. During the expansion cycle the pressure in the bubbles is reduced sufficiently to induce diffusion of gases from the liquid into the bubbles through the expanded surface. During compression the reverse occurs but through a reduced surface area and the result is a net transport of gas into the bubbles. This phenomenon, known as rectified diffusion, causes the bubbles to grow. When the cavities reach critical nucleus size they undergo vaporous growth and on collapse the non-condensable gas introduced by rectified diffusion cushions the collapse process and thus assists in suppressing erosion.

Since oil-in-water emulsions have dissolved air contents two and a half times higher than distilled water, it can be expected that erosion rates in these fluids should be lower as a consequence of rectified diffusion and greater cushioning of collapse pressures. Furthermore it is proposed that the dissolved air contents of the emulsions may be dependent on mineral oil content, that is, the higher the oil content the higher the concentration of dissolved air. If this is the case then the mechanism described above could play a role in determining the trend in the performance of the emulsions. However, at this stage there is no evidence to substantiate this suggestion and further investigation of this problem is required. Initially the total gas contents of the emulsions could be measured by means of a van Slyke gas content apparatus to establish whether any relationship exists between the mineral oil and dissolved air contents.

6.2 CONCLUSIONS

This work on emulsifiable oils has shown that oil-in-water emulsions, in general, suppress cavitation damage. Moreover within the group of emulsions the ability to reduce erosion varies and appears to be directly related to the mineral oil content of the emulsifiable oils. The trend in the performance of the various emulsions may be due to either or both of the following effects:

(i) The ability to form a thin oil film on the surface of the metal sample which is related to the y_{ow} interfacial energy and the oil content of the emulsifiable oil.

(ii) The dissolved air content of oil-in-water emulsions is two and a half times higher than that of water which results in cushioning of cavity collapse and hence a reduction in erosion. Also the dissolved air content might be directly related to the mineral oil content of the emulsions.

CHAPTER SEVEN

EVALUATION OF MATERIALS

Although the operating life of hydraulic systems components can be increased by improved design, the judicious choice of materials is of great importance. Incorrect selection of materials often reduces the effectiveness of improved design and therefore considerable research has been carried out over the last five years under practical circumstances in the South African Gold Mining industry to determine the optimum materials for use in hydraulic mining machinery (11).

A laboratory evaluation of materials was conducted as a complementary study to the practical investigation within the mining industry. The materials selected for erosion testing were, therefore, those which have either been used, are being used at present or which have potential for use in erosive environments in hydraulic mining equipment. These materials include: Stellite alloys, cemented carbides, a range of stainless steels, low alloy steels, nickel alloys, cast irons and several polymers.

Material microstructures, cavitation induced phase transformations and fracture mechanisms were elucidated by the various techniques of optical microscopy, scanning and transmission electron microscopy (SEM and TEM) and X-ray diffractometry (XRD). In addition an energy dispersive analysis of X-rays (EDAX) system attached to the SEM was used to identify phases in the Stellite alloys.

This chapter presents and discusses the results obtained from the vibratory cavitation tests as well as subsequent information obtained from fractographic and microstructural studies. Furthermore, the microstructural requirements of an alloy having maximum erosion resistance are proposed.

7.1 RESULTS AND DISCUSSION

In total 48 different alloys and polymers were tested in this project under the test conditions described in an earlier chapter. The materials, together with their compositions and heat treatments are listed in Appendix 7.1 - Tables A to D while the results of the erosion tests are summarized in Fig. 7.1. The erosion curves (cumulative volume loss vs. time) of the materials are presented in Appendix 7.2. Most of the alloys have erosion curves showing an incubation period followed by a constant rate of weight loss zone. This was the general form of curve found by Hobbs and Laird (37)and is illustrated in Fig. 7.2(a). Some polymers did not exhibit an incubation period while a few alloys never attained a steady state period even on prolonged testing and thus some of the curves are of the type in Fig. 7.2(b)&(c).

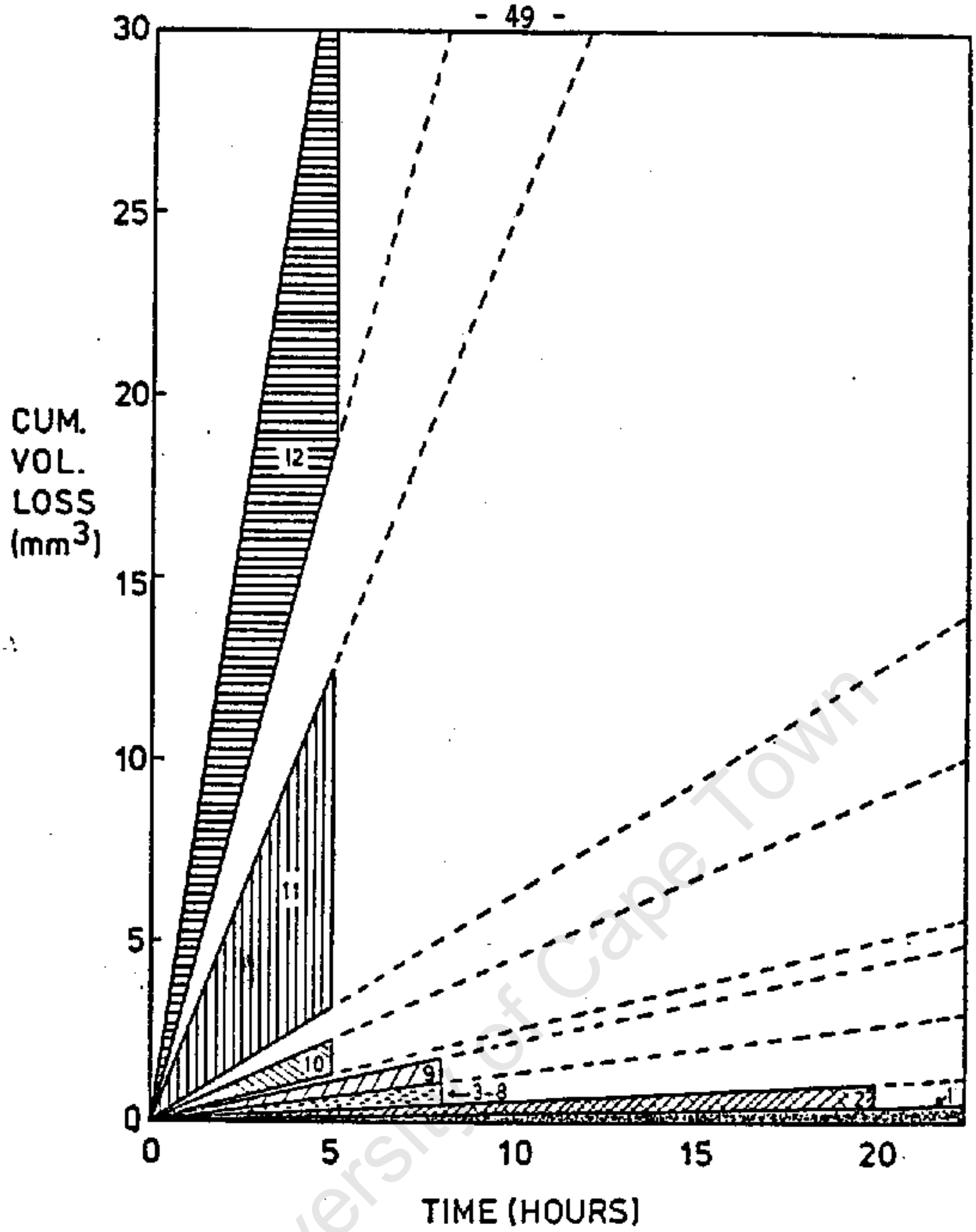

GROUP 1

Stellite 3
WC/Ni:8LC
WC/Ni:8MC
Stellite 20
Stellite 4
NiTi

GROUP 2

Stellite 6
Stellite 8
Stellite 2006
Flurodur
TiC/WC/Ni:CN02

GROUP 3

817M40 (200°C)
DIN 4112 (200°C)
DIN 4112 (300°C)
DIN 4112 (400°C)
WC/Co:CG60

GROUP 4

Nylon 6,6
Nylatron GSM
Cast Iron:CB24
WC/Co Lab Grd A
817M40 (300°C)

GROUP 5

WC/Co:CT65
DIN 4112 (500°C)
817M40 (400°C)
Cast Iron:TB18
WC/Co Lab Grd C

GROUP 6

WC/Co:CG35
Alloy 3040
835M30 (200°C)
Alloy C
817M40 (500°C)

GROUP 7

431S29 (400°C)
431S29 (200°C)
WC/Co:CG20
835M30 (300°C)
Hadfield's Steel

GROUP 8

835M30 (400°C)
DIN 4112 (600°C)
WC/Co:40C
431S29 (300°C)
AISI 304

GROUP 9

835M30 (500°C)
WC/Co:CT30
Polyacetal
817M40 (600°C)
835M30 (600°C)

GROUP 10

431S29 (500°C)
431S29 (600°C)
3Cr12Ni (900°C)
AISI 316
Incalloy 825

GROUP 11

Monel 400
3CR12 (900°C)
Cast Iron SG80
PTFE
AISI 409

GROUP 12

PTFE + 15% glass
PTFE + 60% bronze
PTFE + Carbon + Graphite
PTFE + 25% glass
AISI 430
PTFE + 25% carbon

Fig. 7.1 A Summary of the Cavitation Erosion Curves of the Materials Tested in this Study.

There are numerous parameters upon which erosion resistance may be based, These include incubation time (t_o), cumulative weight or volume loss, (CWL, CVL), rate of weight or volume loss in the steady state zone (E) and time to reach maximum erosion rate (t_{max}) To obtain,a true assessment of material performance it is necessary to consider more than one of these parameters since an evaluation based on a simple parameter such as cumulative volume loss can be misleading. Therefore in this thesis the materials have been graded according to the total cumulative volume loss,but at the same time,the incubation time and the erosion rate after the acceleration stage have been considered as well. The incubation time is defined, in this study, as that time when the slope of the cumulative volume loss vs. time curve deviates from the average slope of the initial low erosion rate period. This definition is depicted in Fig. 7.2 for the various erosion curve forms obtained in this work. Furthermore when the value of t_o is clearly between two points then the midpoint value is taken as the incubation time. Fig. 7.2 also illustrates the method of determining E. The values of CVL, t_o and E for all the materials are listed in Table 7.1. In most cases the materials were tested only once,but for the few that were tested twice or more, an indication of the experimental scatter is given. The error, -A was calculated as follows:

$$\bar{\delta}(\%) = 1/\bar{x} \sum_{i=1}^{n} |\bar{x}-x_i|/n \quad x100$$

where $\bar{x}$ = average total CVL

x_i = CVL of 1st, 2nd, ...,nth test

n = number of tests conducted

In other words $\bar{\delta}$ is the mean deviation expressed as a percentage of the average CVL. The average scatter for all materials tested in duplicate, or more often, was ±8,8%.

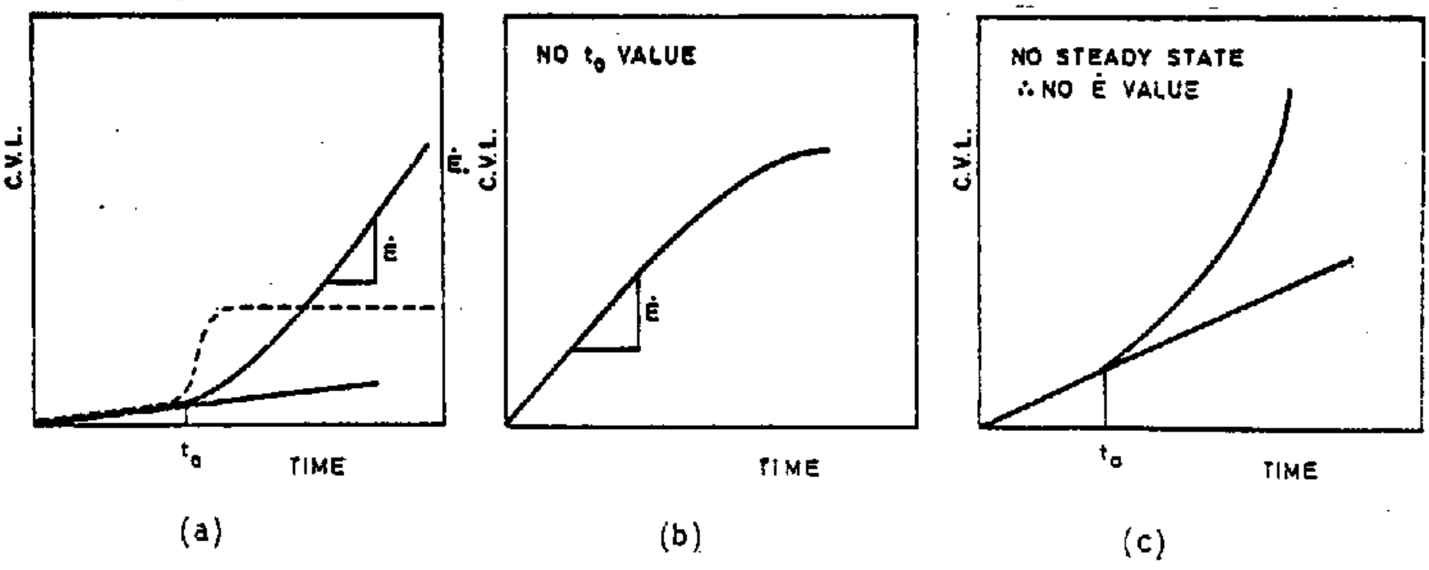

Fig. 7.2 The Various Forms of Erosion Curves Obtained in this Study

TABLE 7.1

MATERIALS - ORDER OF PERFORMANCE

MATERIAL	C,V.L, (mm³)				t_o (HRS)	AVERAGE $\dot{E}$ (mm³/hr)	V.H.**	R_n †	±$\bar{\delta}$ †† (%)
	40 HRS	20 HRS	7 HRS	5 HRS					
Stellite 3	0,53	0,14	0,02	0,01	12,5	0,022	531	106	1,89
WC/Ni:8LC	0,52	0,19	0,05	0,01	7,5	0,015	1478	108	7,7
WC/Ni:8MC	0,72	0,34	0,11	0,03	5,0	0,021	1246	113	9,72
Stellite 20	0,93	0,35	0,03	0,01	7,5	0,030	610	106	
Stellite 4	1,00	0,39	0,03	0,02	7,5	0,031	501	94	
NiTi	1,12	0,23	0,02	0,01	12,5	0,048	200	35	17,4
Stellite 6	1,15	0,40	0,04	0,02	7,5	0,037	399	80	
Stellite 8	1,24	0,43	0,02	0,01	7,5	0,040	335	78	
Stellite 2006	1,94	0,87	0,17	0,08	5,0	0,054	440	90	
Flurodur	-	0,94	0,28	0,20	0	0,055	-	48	
TiC/WC/Ni:CN02	-	1,13	0,30	0,18	2	0,064	1710	109	0,88
817M40 (200°C)	-	1,17	0,10	0,05	7	0,092	604	108	
DIN 4112 (200°C)	-	1,26	0,23	0,10	4	0,079	636	103	
DIN 4112 (300°C)	-	-	0,35	0,19	3	0,086	577	96	
DIN 4112 (400°C)	-	-	0,38	0,21	3	0,068	531	89	
WC/Co:CG60	-	-	0,38	0,21	3	0,074	1048	94	2,6
Nylon 6,6*	-	3,60	0,05	0	6	0,290	-	89	
Nylatron GSM*	-	4,14	0,43	0,07	4	NSS	-	84	11,6
Cast Iron:CB24	-	-	0,46	0,23	3,5	0,124	873	103	
WC/Co:Lab Grd A	-	-	0,47	0,28	3	0,100	933	88	10,6
817M40 (300°C)	-	-	0,51	0,28	3	0,115	529	98	
WC/Co:CT65	-	-	0,52	0,27	3	0,115	933	106	2,88
DIN 4112 (500°C)	-	-	0,52	0,34	2,5	0,100	463	90	
817M40 (400°C)	-	-	0,59	0,34	3	0,128	469	96	
Cast Iron:TB18	-	-	0,60	0,38	2,5	0,120	688	93	
WC/Co:Lab Grd C	-	-	0,62	0,38	2,5	0,122	835	95	8,7
WC/Co:CG35	-	-	0,66	0,45	1	0,101	1267	111	
Alloy 3040	-	-	0,68	0,42	2	0,140	388	79	
835M30 (200°C)	-	-	0,69	0,42	3	0,131	502	100	
Alloy C	-	-	0,72	0,36	3	0,200	229	55	
817M40 (500°C)	-	-	0,78	0,38	2	0,163	400	88	
431S29 (400°C)	-	-	0,78	0,43	2	0,166	423	75	
431S29 (200°C)	-	-	0,82	0,47	2	0,173	427	76	

TABLE 7.1 con't ...

MATERIAL	C.V.L. (mm³) 40 HRS	20 HRS	7 HRS	5 HRS	t_o (HRS)	AVERAGE $\dot{E}$ (mm³/hr)	V.H.**	R_n †	$\pm\bar{\delta}$ †† (%)
WC/Co:CG20	-	-	0,82	0,55	1	0,134	1452	107	
835M30 (300°C)	-	-	0,83	0,51	2	0,166	419	89	
Hadfield's Steel	-	-	0,86	0,48	2	0,188	181	33	12,2
835M30 (400°C)	-	-	0,87	0,54	2	0,182	396	91	
DIN 4112 (600°C)	-	-	0,96	0,56	2	0,200	330	68	
WC/Co:40C	-	-	0,96	0,62	1	0,171	1033	110	
431S29 (300°C)	-	-	1,04	0,61	2	0,205	406	80	
AISI 304	-	-	1,10	0,70	2	0,215	194	48	
835M30 (500°C)	-	-	1,19	0,68	2	0,243	355	84	
WC/Co:CT30	-	-	1,23	0,82	1	0,205	1168	103	
Polyacetal	-	-	1,23	0,49	3	0,318	-	77	14,6
817M40 (600°C)	-	-	1,55	1,03	2	0,280	328	79	7,9
835M30 (600°C)	-	-	1,76	1,07	2	0,348	277	71	6,25
431S29 (500°C)	-	-	1,77	1,04	2	0,358	325	74	
431S29 (600°C)	-	-	2,48	1,51	2	0,486	262	70	
3 CR12Ni (900°)	-	-	-	1,72	2	NSS	266	70	
AISI 316	-	-	-	1,95	2	0,520	194	53	17,9
Incalloy 825	-	-	-	2,25	2	0,577	186	49	
Monel 400	-	-	-	3,41	1	0,815	159	38	
3 CR12 (900°C)	-	-	-	4,17	2	NSS	167	43	
Cast Iron SG80	-	-	-	6,79	1	1,82	160	52	
PTFE	-	-	-	10,6	0	2,2	-	36	
AISI 409	-	-	-	12,5	1	NSS	129	38	
PTFE + 15% glass	-	-	-	16,1	0	4,0	-	30	
PTFE + 60% bronze	-	-	-	27,2	0	7,0	-	33	
PTFE + Carbon + Graphite	-	-	-	28,5	0	6,5	-	38	
PTFE + 25% glass	-	-	-	36,1	0	10,0	-	28	
AISI 430	-	-	-	37,2	1	8,3	180	40	
PTFE + 25% carbon	-	-	-	42,2	0	12,0	-	37	
							Average Scatter ±8,8		

* *Figures approximate only - samples absorbed water during test - corrected against a control.*

** *V.H. = Vicker's Hardness*

†† $\pm\bar{\delta}$ = *Experimental Scatter (see text)*

† R_n = *Resilience Number*

NSS = *No steady state ∴ no* $\dot{E}$

The relationships between two mechanical properties and the erosion test data were investigated. One of the properties considered was hardness. This property being simple and readily obtainable is a most convenient parameter for use as a criterion for erosion resistance. However, attempts in the past, to correlate erosion resistance with hardness have not resulted in relationships sufficiently reliable for use in materials selection and machine design. The relation between erosion and hardness obtained in the present work also showed considerable scatter (Fig. 7.3). In particular a few alloys (in the lower left hand corner) show a large deviation from the average trend and the reasons for the exceptional resistances of these few alloys are given in the following discussion. It is important to appreciate that hardness can be used as a criterion for erosion resistance. But it is essential that the engineer, who bases material selection on hardness, simultaneously has a knowledge of the influence of material microstructure on erosion resistance in order to understand the significance of exceptional material performance whether favourable or unfavourable.

Another property considered was a parameter designated resilience number (R_n), which is directly related to material hardness. This is an arbitrary number corresponding to the rebound height of a hardened steel hammer dropped from a constant height onto the surface of a test piece. It is a dynamic measure of a material's relative ability to absorb and reflect the energy of impact.

A Shore Scleroscope was used to obtain these values of resilience number. Note that these values are not equal to the Shore hardness of the material, since this latter test requires that a diamond tipped hammer of standard dimensions be used and not the hardened steel hammer employed in the resilience tests. The resilience number test is similar to the ADL rebound ball test described in ref.95, a modified version of which was used by Lichtman(35) in his work on erosion of polymeric overlays. The similarity between the action of an impacting jet or spherical shock wave and that of the impacting hammer in this simple dynamic test prompted the investigation of this parameter. The relationship between resilience number and cumulative volume loss for the whole range of materials (see Fig. 7.4) shows a trend of decreasing erosion for increasing resilience (see also Table 7.1). Since R_n and hardness are directly related, the same materials show a deviation from the general trend.

The two extreme modes of erosion, namely, ductile and brittle have been described in an earlier chapter. It was also pointed out that individual materials often have unique erosion modes and the existing knowledge on the erosion modes of individual materials has. been reviewed. In the following sections the mechanisms of resistance and the modes of erosion of the materials investigated in the present study are discussed. The response of materials is explained in terms of mechanical

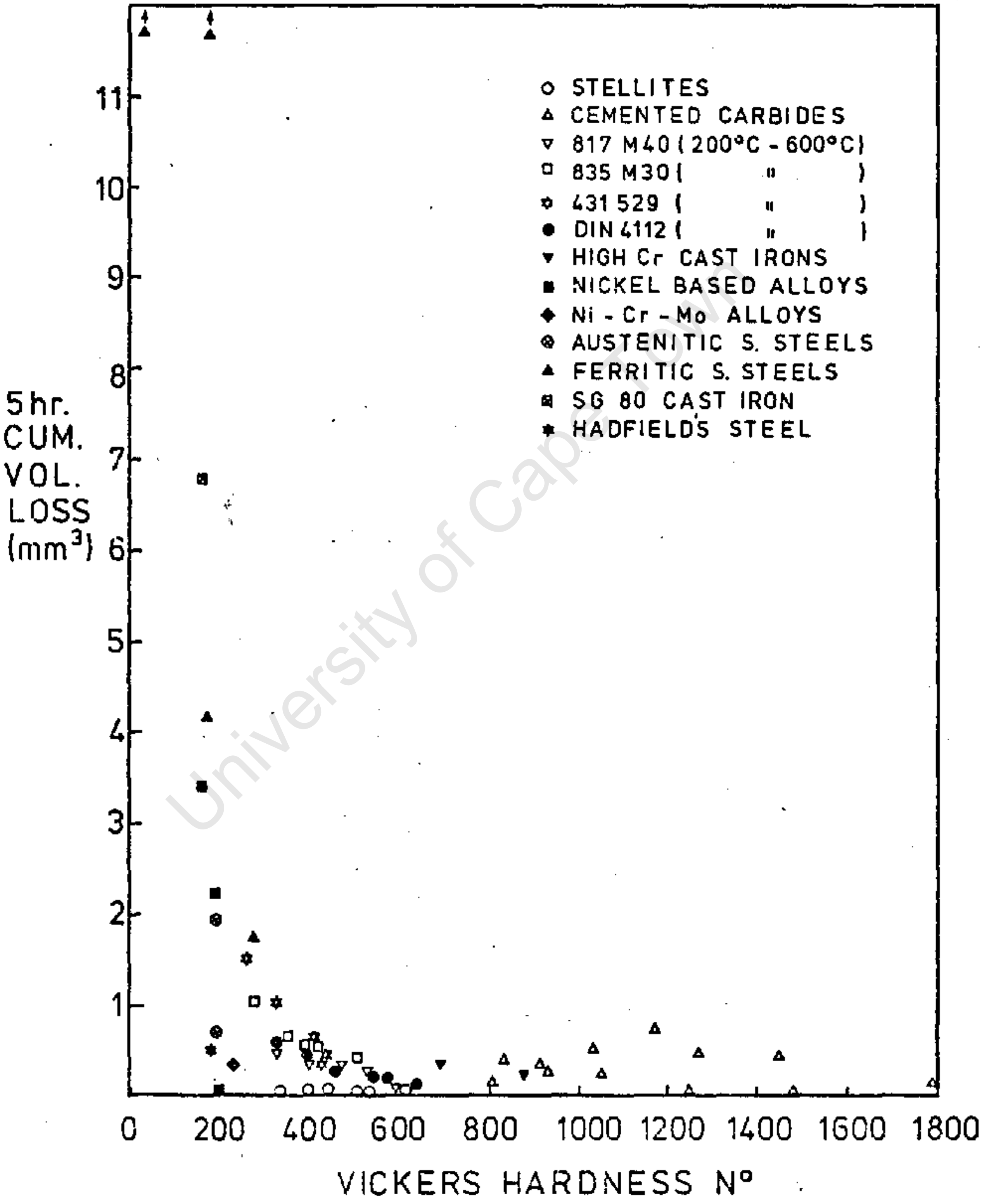

Fig. 7.3 Erosion Volume Loss vs. Hardness.

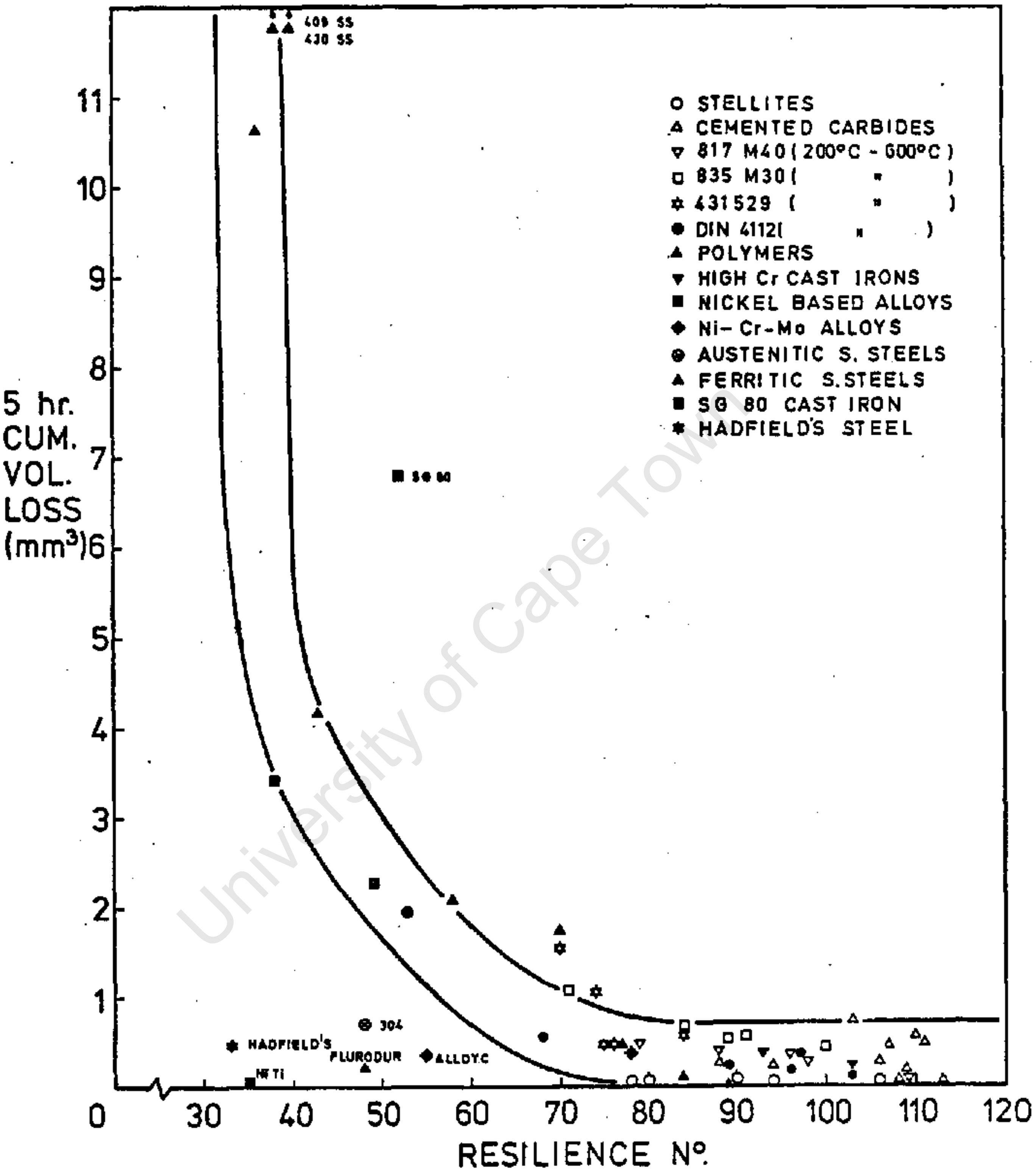

Fig. 7.4 Erosion Volume Loss vs. Resilience No..

properties and microstructure. The materials are dealt with in groups based on the major compositional element/s, that is, low alloy steels, stainless steels, cast irons, nickel alloys, cemented carbides, cobalt based Stellites and polymers.

7.1.1 Low Alloy Steels

Two low alloys steels have been tested, namely, 817M40 (or EN24) and 835M30 (or EN30B). Several specimens of each steel were quenched from -840 C and tempered at five different temperatures between 200 C and 600 C, in increments of 100 C. Thus the samples were all martensitic but with varying hardnesses according to the tempering temperature (see Fig. 7.5).

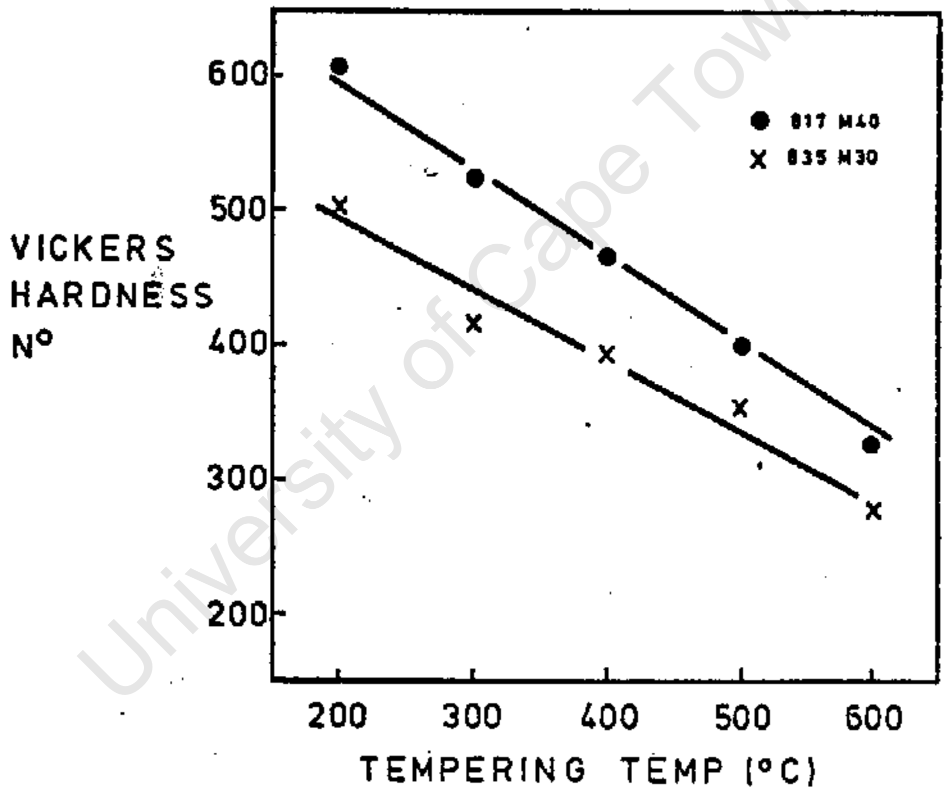

Fig. 7.5 Hardness vs. Tempering Temperature for 817M40 and 835M30 Steels

In general the 817M40 samples have superior erosion resistance to the 835M30 samples which may be ascribed to the higher hardnesses of the former samples. Hardness is a good indication of erosion resistance in this case, since the alloys are structurally identical. This is reflected in a plot of erosion resistance (CVL) vs. hardness (Fig. 7.6). Note that the 817M40 Q&T 200 C is considerably more resistant than the specimens tempered at higher temperatures. In particular, the incubation time of this sample is more than twice that of the 300 C to 600 0 samples (see Table 7.2).

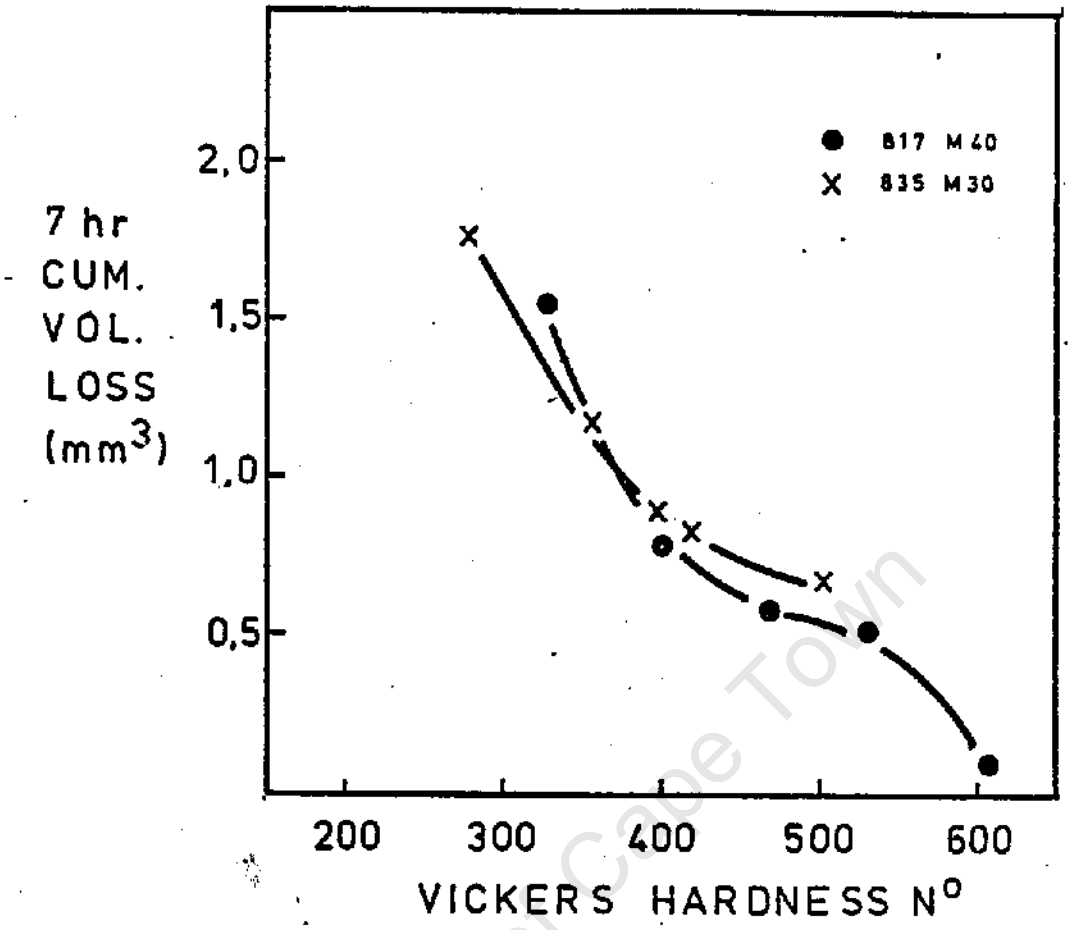

Fig. 7.6 Erosion vs. Hardness No. for 817M40 and 835M30 Steels

TABLE 7.2

Alloy	Main alloying elements			Tempering Temp. $^{\circ}C$	CVL 7 hrs.	t_o hrs	$\dot{E}$ mm³/hr	V.H.	R_n
	C	Cr	Ni						
817M40	0,43	1,05	1,48	200	0,10	7	0,092	604	108
				300	0,51	3	0,115	529	98
				400	0,59	3	0,128	469	96
				500	0,78	2	0,163	400	88
				600	1,55	2	0,280	328	79
835M30	0,32	1,12	3,96	200	0,69	3	0,131	502	100
				300	0,83	2	0,166	419	89
				400	0,87	2	0,182	396	91
				500	1,19	2	0,243	355	84
				600	1,76	2	0,348	277	71

The fracture surfaces of these martensitic steels are all similar and the erosion mode becomes more ductile in character with increasing tempering temperature. Figs. 7.7(a) and (b) show the eroded surfaces of 817M40 and 835M30 both Q & T at 400 C in the early stages of erosion while Figs. 7.8(a) to (e) show the severely eroded surfaces of the 817M40 samples over the range of tempering temperatures. Figs. 7.7(a) and (b) show that erosion is initiated by 'blistering' at the edges of martensite plates followed by material removal by ductile rupture. This early stage mode of erosion is in contrast to that described by Wade and Preece (40) who reported that erosion occurred initially by brittle pitting and grain boundary cracking in a martensitic AISI 1080 plain carbon steel.

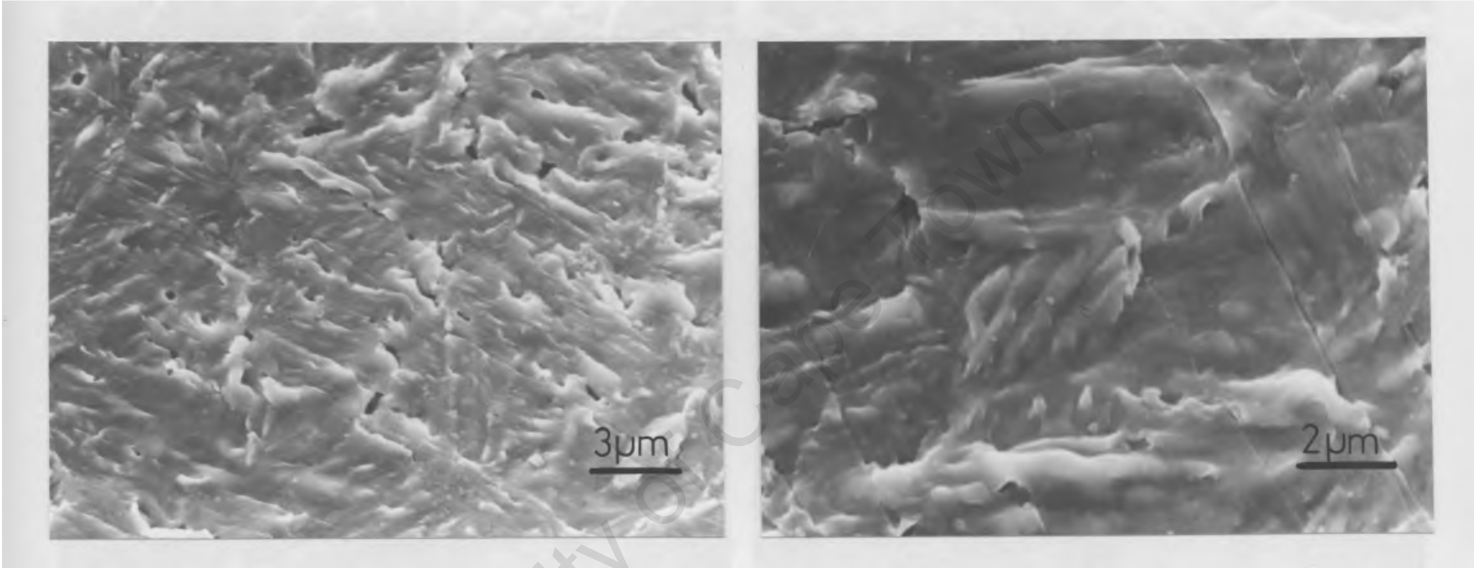

(a) 817M40 (4000x) (b) 835M30 (6400x)

Fig.7.7 The Erosion Mechanisms of 817M40 and 835M30

The 'ductile' nature of the erosion of these alloys is surprising considering the high hardnesses of the test samples and also the strain rate sensitivity of steels in general. Note that in vibratory cavitation the strain rate is high enough to produce the ductile to brittle transition (DBT) in pure iron (see chapter 6). However alloying, in particular, additions of nickel and also the heat treatment of steels reduces the DBT temperature by more than 40 C (96). Alloying is, presumably, also the explanation for the different early stage erosion mechanisms observed by Wade and Preece in 1080 steel. A further factor which will contribute to the erosion mode in these alloy steels is the fine microstructural dimensions of the martensite phase. This structure has a greater toughness compared with the equilibrium microstructure.

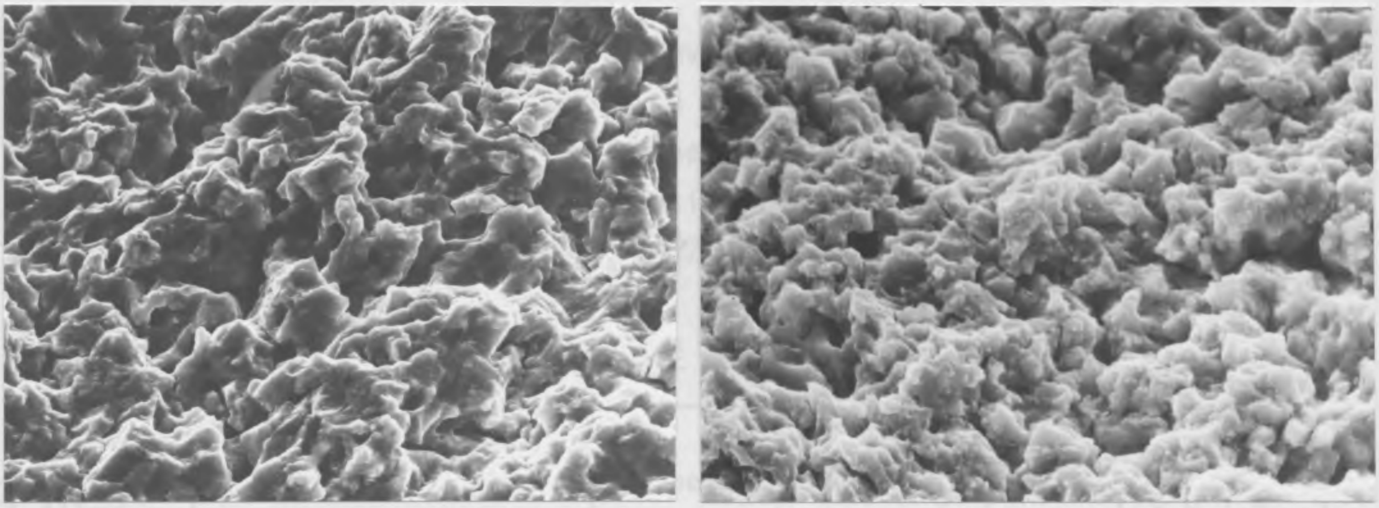

(a) 200°C (b) 300°C

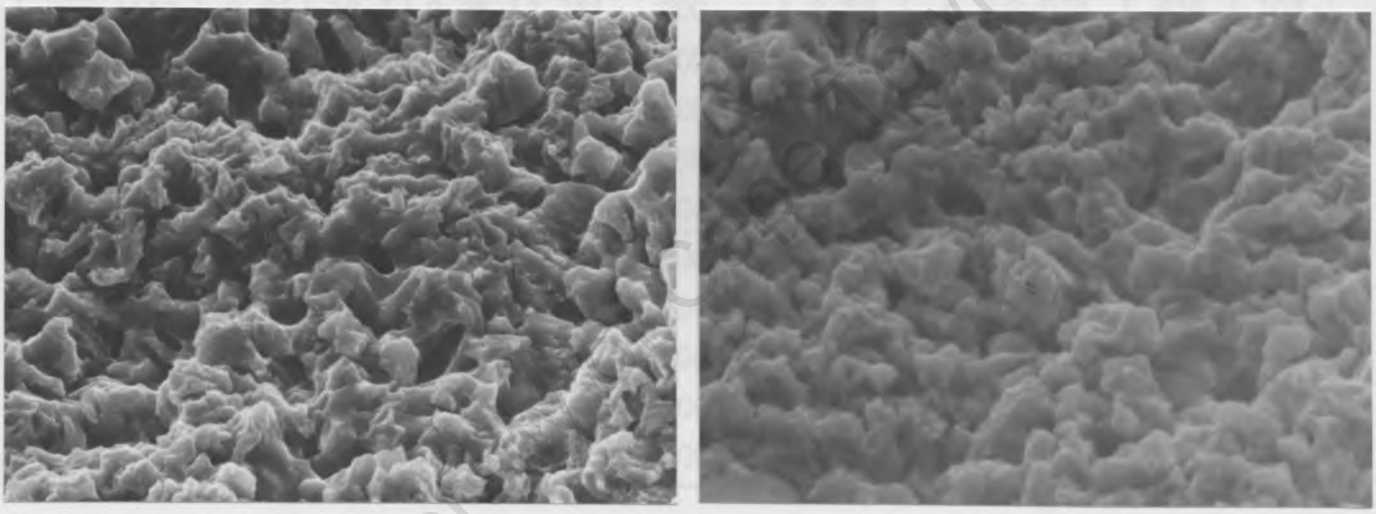

(c) 400°C (d) 500°C

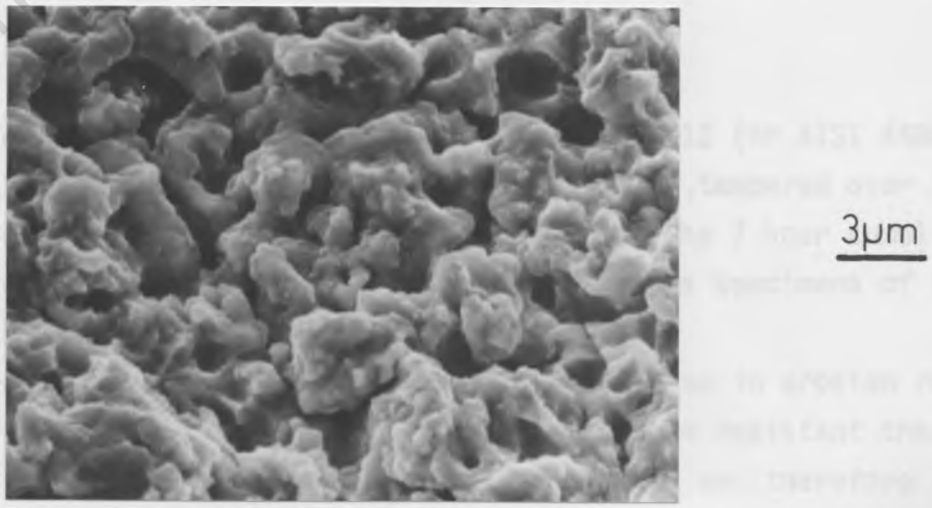

(e) 600°C

Fig. 7.8 Eroded Surfaces of the 817M40 Specimens. Note that the Mode of Erosion Becomes More Ductile with Increasing Tempering Temperature (All 4000 x Magnification)

7.1.2 Stainless Steels

A number of stainless steels were investigated,namely, two austenitic, four ferritic and two martensitic steels. In addition an austenitic manganese steel (Hadfield's steel) was tested and has been included in this section for convenience. The compositions, Vickers hardness, resilience numbers and erosion data of these alloys are listed in Table 7.3, 7.4 and 7.5 below.

TABLE 7.3

Alloy	Main alloying elements				Tempering	CVL	t_o	$\dot{E}$	V.H.	R_n
	C	Cr	Ni	Mo	Temp °C	7 hrs	hrs	mm³/hr		
DIN 4112	0,91	18,5	0,25	1,15	200	0,23	4	0,079	636	103
					300	0,35	3	0,086	577	96
					400	0,38	3	0,068	531	89
					500	0,52	2,5	0,100	463	90
					600	0,96	2	0,200	330	68
431S29	0,11	15,6	2,34	-	200	0,82	2	0,173	427	76
					300	1,04	2	0,205	406	80
					400	0,78	2	0,166	423	75
					500	1,77	2	0,358	325	74
					600	2,48	2	0,486	262	70

7.1.2.1 Martensitic Stainless Steels

The martensitic high alloy steels evaluated were DIN 4112 (or AISI 440B), and BS 431S29 (or AISI 431).Again five samples of each alloy,tempered over a range of temperatures,were tested.The relationship between the 7 hour cumulative volume loss and Vickers hardness number for the various specimens of the two alloys are plotted in Fig. 7.9.

The DIN 4112 results show the expected monotonic decrease in erosion resistance with decreasing hardness.In addition,this alloy is more resistant than the 431529 steel.This is understandable since the carbon content and therefore the hardness of the samples of the former alloy are much greater than that of the latter (see Table 7.3).The 431S29 samples,although they follow the expected trend,do show an anomaly.The specimen tempered at 400 °C has a similar resistance to the specimen tempered at 200 °C.This discrepancy is due to

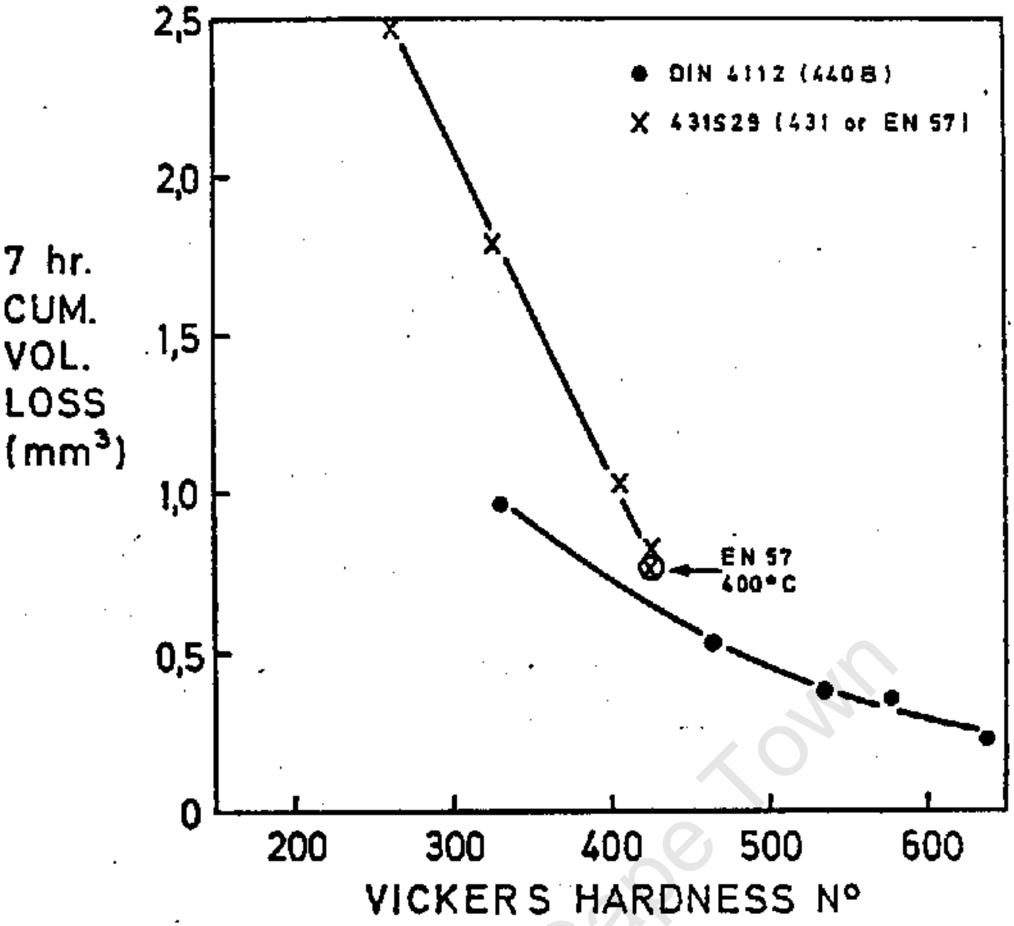

Fig.7.9 Erosion Volume Loss vs. Hardness.

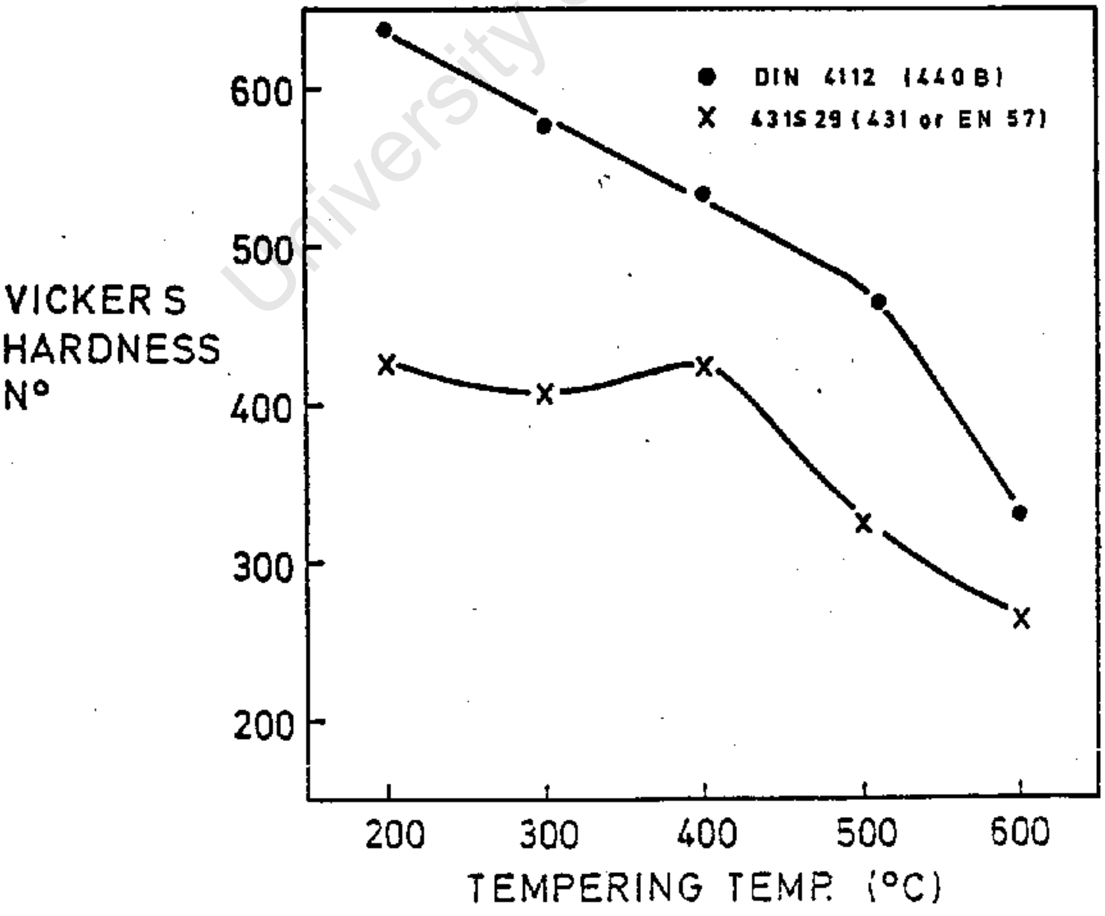

Fig.7.10 Hardness vs. tempering temperature.

secondary hardening which is reflected in the relationship between Vickers hardness No. and tempering temperature in Fig. 7.10. This form of hardening results from the precipitation of alloy carbides when sufficient thermal energy becomes available for diffusion of substitutional elements in the lattice. In general, however, the two alloys fit in with the overall trend of materials performance i.e. they fall within the average band of materials in Figs. 7.3 and 7.4.

The microstructures of DIN 4112 and 431S29 in the heat treated condition are shown in Figs. 7.11(a)&(b). The effect of the different carbon contents is clear from the size and number of chrome carbides present in the respective samples. Fig. 7.11(c)-(f) show the erosion mechanisms of these alloys which in the martensitic phase is much the same as that of the heat treated low alloy steels discussed in the previous section. As regards the chrome carbides, in 431S29 they do not seem to play any significant role in the erosion of this alloy, but in DIN 4112 the carbides are obviously more resistant to cavitation than the martensite matrix as shown by Fig. 7.11(e). However, these large carbide particles also have a detrimental effect in terms of erosion initiation (as is the case in the Stellite alloys). The carbides and martensitic matrix differ in elastic properties. There ore when the alloy is stressed, as in a cavitating liquid, the matrix and carbide phases undergo different strains, and in order to relieve the elastic mismatch, cracking occurs or is promoted at the carbide-matrix interface. This mechanism was often observed in the present materials investigation and will be mentioned again in the discussion below. The micrographs in Fig. 7.11(e)&(f) show clearly that cracking and removal of material occurs at the carbide-matrix interface. The detrimental effect of carbide may explain the difference in incubation times for the samples of DIN 4112 and 817M40 both tempered at 200 °C; the 817M40 sample has a much longer incubation period than the DIN 4112 sample in spite of the former alloy having the higher hardness (see Tables 7.2 & 7.3).

7.1.2.2 Austenitic Stainless Steels and (Hadfield's) Manganese Steel

Of these alloys the manganese steel is the most resistant followed by AISI 304 and then AISI 316 stainless steels. Both AISI 304 and, particularly, Hadfield's steel have much higher resistances than expected on the basis of their mechanical properties (hardness and resilience number - see Table 7.4), and therefore deviate from the average curves in Fig. 7.3 and 7.4.

Figs. 7.12(a)-(f) reveal the mechanisms of erosion of these alloys. Material removal is initiated at and propagated from the slip and/or twin boundary steps at the surface and at grain boundaries, although in Hadfield's steel pitting also occurs in between the shear features. The overall erosion mode is one of ductile fracture as indicated by the micrograph in Fig. 7.12(d).

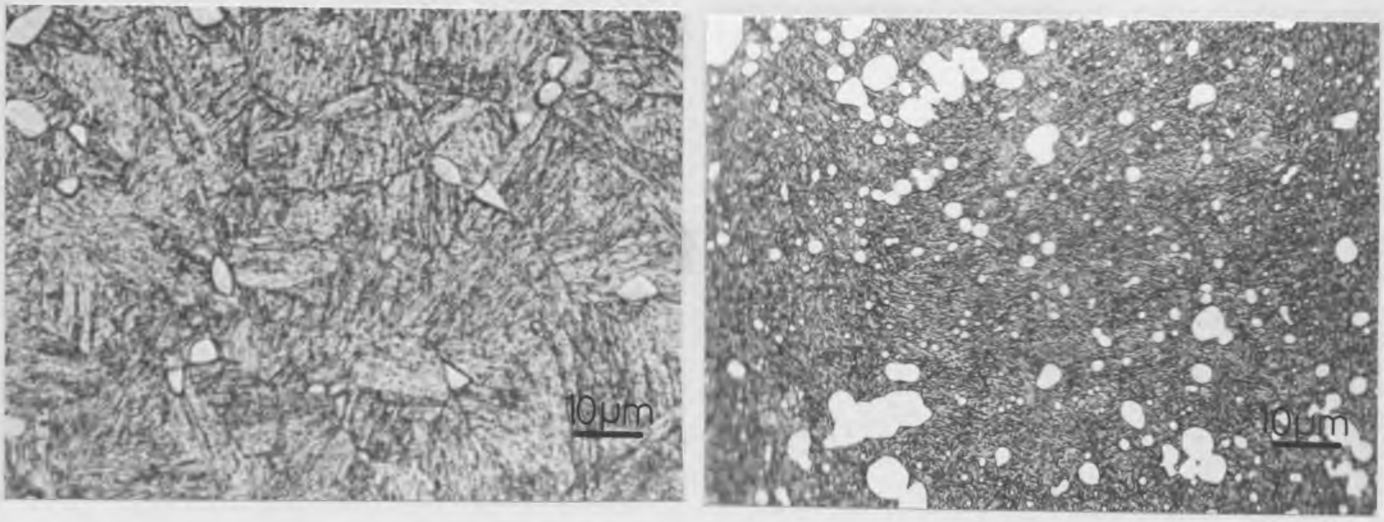

(a) Microstructure 431S29

(b) Microstructure DIN 4112.

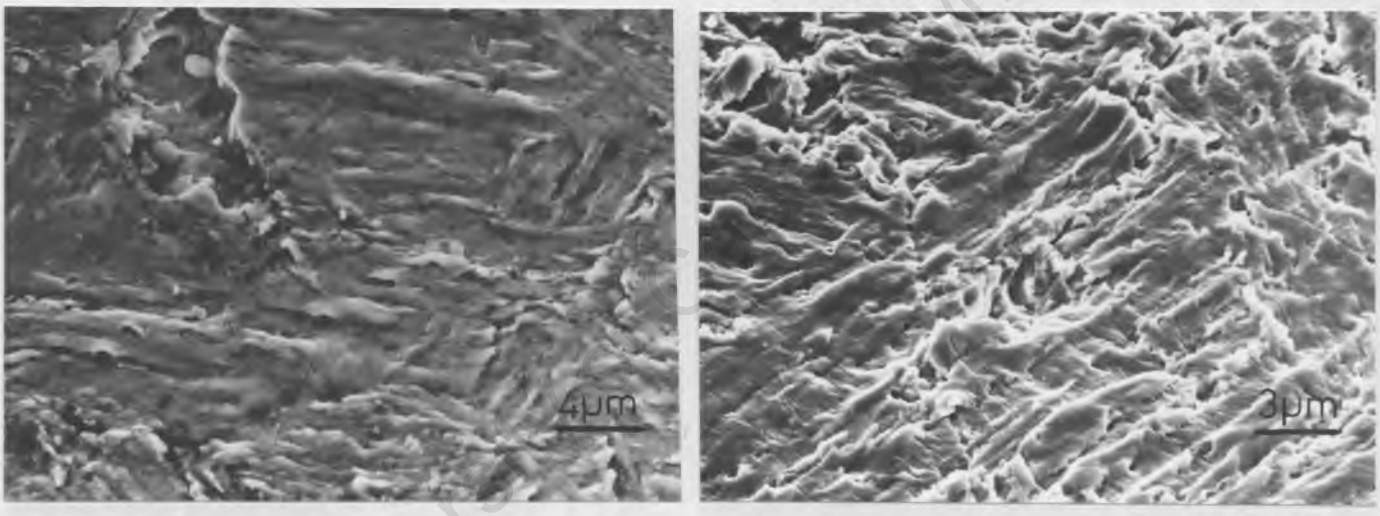

(c) Damage near edge of eroded area in 431S29 (2700x)

(d) Same as (c) different area (4000x)

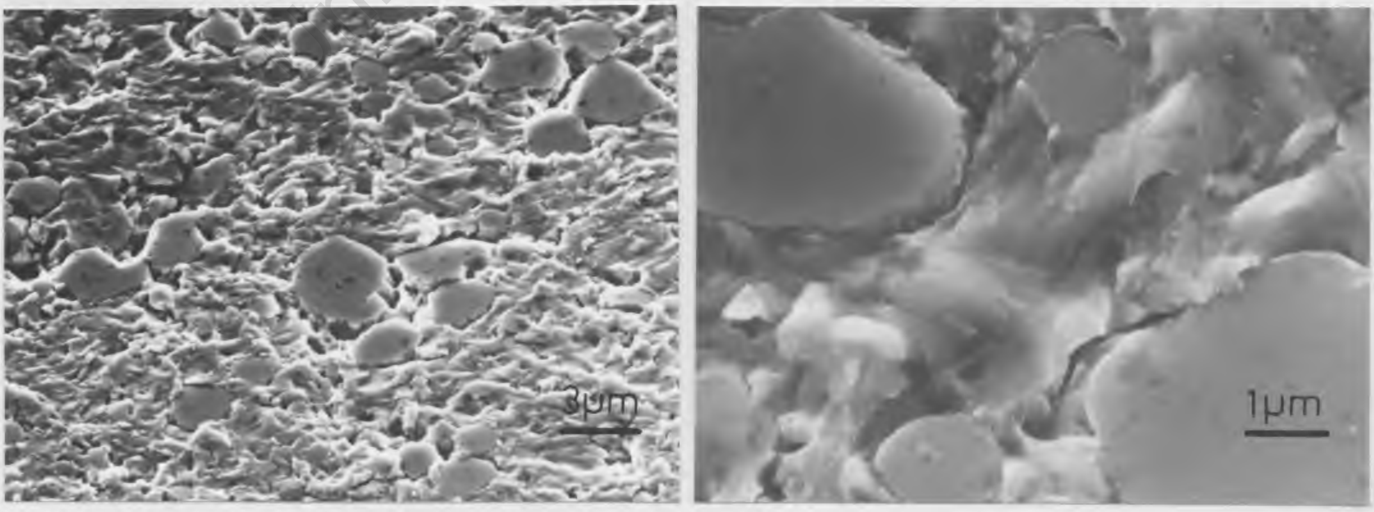

(e) Damage near edge of eroded area of DIN 4112 (4000x)

(f) Cracking at the carbide matrix interface in DIN 4112 (13600x)

Fig. 7.11 Microstructures and eroded surfaces of the martensitic stainless steels.

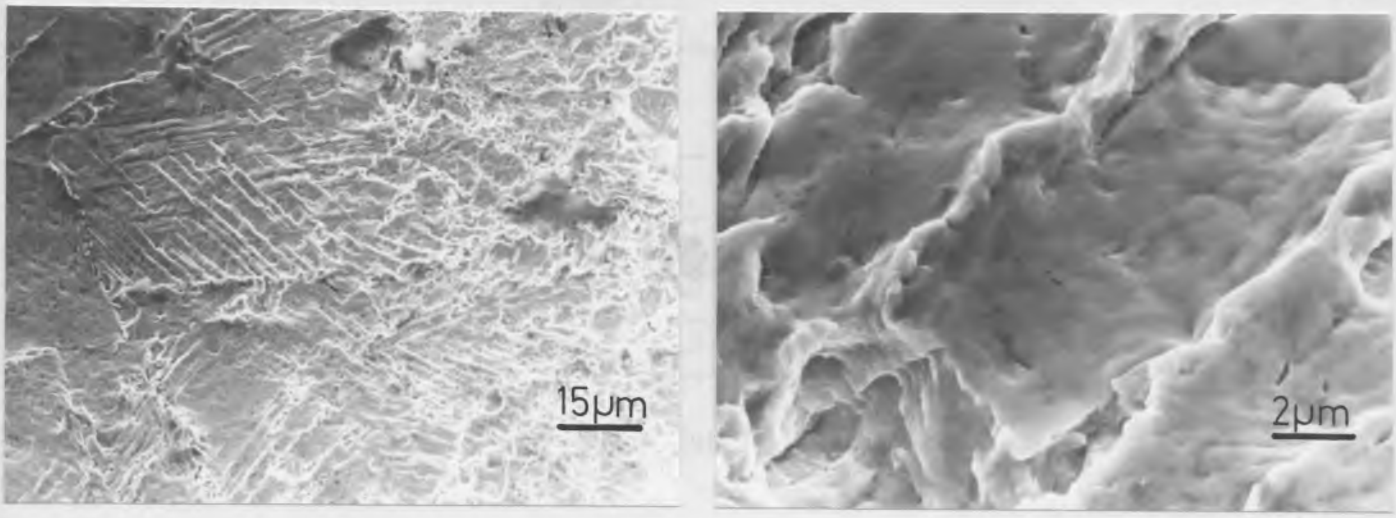

(a) Damage near edge of eroded area of AISI 304 (700x).

(b) Erosion initiation at protruding slip/twin boundary of AISI 304 (5400x).

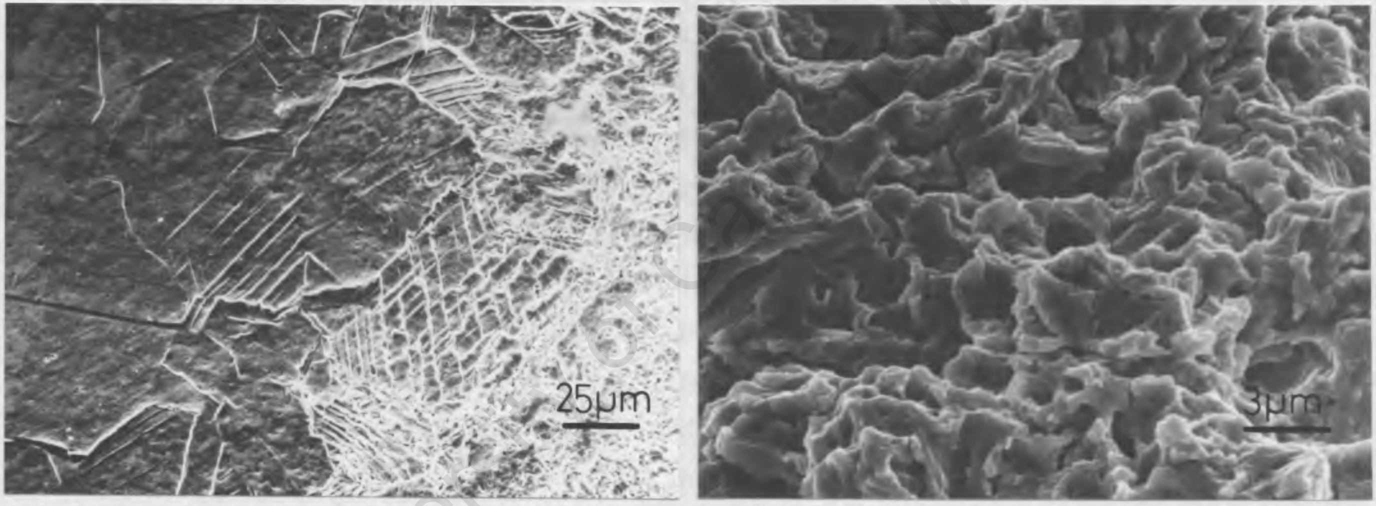

(c) Damage near edge of eroded area of AISI 316 (400x)

(d) Advanced erosion in AISI 316 (4000 x)

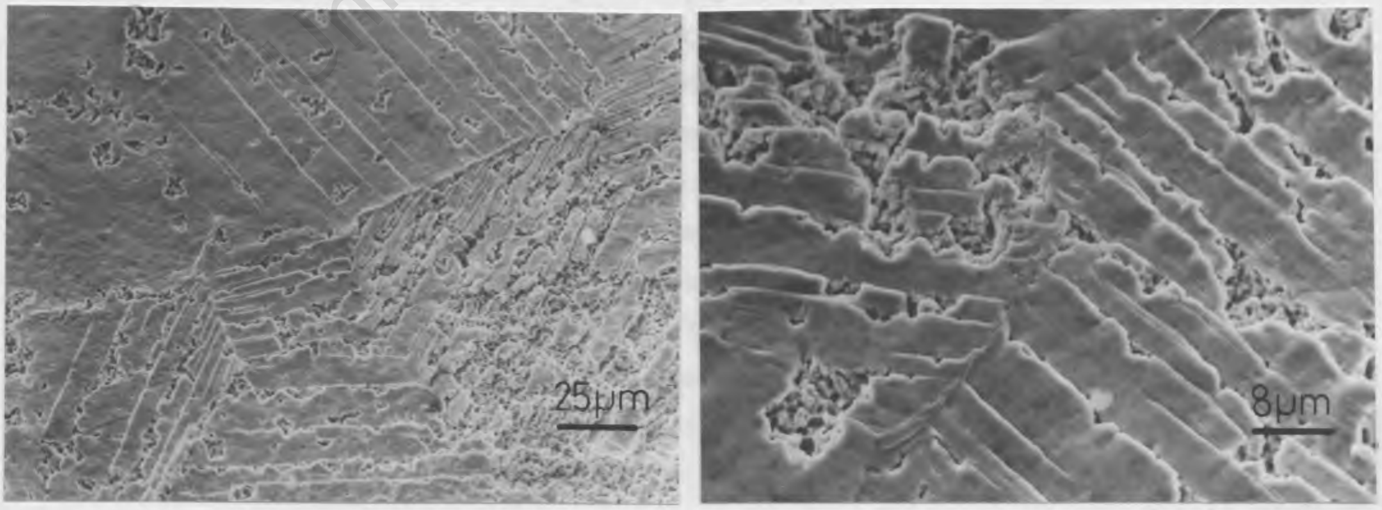

(e) Damage near edge of eroded area of Hadfield's Steel (400x)

(f) Same as (e) - higher magnification (1360x)

Fig. 7.12 Modes of erosion of Austenitic Steels.

TABLE 7.4

Alloy	Main alloying elements					CVL 5 hrs	t_o hrs	$\dot{E}$ mm /hr	V.H.	R_n	M_s^* °C	$M_{d30}^{*\dagger}$ °C
	C	Cr	Ni	Mo	Mn							
AISI 304	0,08	18,2	8,4	-		0,70	2	0,215	194	48	-44,5	35,65
AISI 316	0,06	16,5	10,4	2,02	-	1,95	2	0,520	194	53	-149	-2,14
Hadfield's	0,84	-	-	-	13,9	0,48	2	0,188	181	33	-358,7	-3,67

†M_{d30} This corresponds to the temperature at which 50% martensite forms for a true strain of 0,30.

* Approximate temperatures.

AISI 304 has a higher resistance than expected from its strength properties and moreover it is more resistant than AISI 316 which has very similar properties to AISI 304 (see Table 7.4). This effect is undoubtedly related to the y-austenite to a martensite shear transformation which occurs in the former alloy. Figs. 7.13 and 7.14 are XRD traces revealing the structures of 304 and 316 before and after exposure to cavitation for five hours. Very little material is transformed in AISI 316, whereas a considerable reaction occurs in AISI 304. This is in accordance with the M_s and M_d temperatures (listed in Table 7.4) which, in turn, are a function of alloying element content. The M_s and M_{d30} temperatures were calculated from equations developed by Pickering (97).

Examination by transmission electron microscopy of thin foils taken from regions just below the eroded surface of AISI 304 revealed the mechanism of nucleation of martensite (see Fig. 7.15(a)-(d)). Uneroded AISI 304 (annealed) has a very low dislocation density but contains a number of stacking faults. On exposure to cavitation the dislocation density increases rapidly in some areas (Fig. 7.15(a)).while in other regions less dislocations form and deformation twinning predominates (Fig.7.15. (b)). a' martensite is nucleated at twin intersection points (Fig.7.15 (b)) and eventually, in highly deformed areas, a complex structure develops of twins plus interspersed a' martensite (Fig.7.15 (c) & (d)). These structures are very similar to those found by Moin & Murr (61) in shockloaded 304 stainless steel. The morphology and structure of this martensitic transformation in Fe-Cr-Ni alloys has also been studied by Lecroisey & Pineau (98)

The formation of martensite increases the work hardening rate of AISI 304 resulting in high ultimate stress levels while maintaining good uniform elongation (98). Both these mechanical properties are important in withstanding cavitation erosion and this is discussed in a later section. It is interesting that

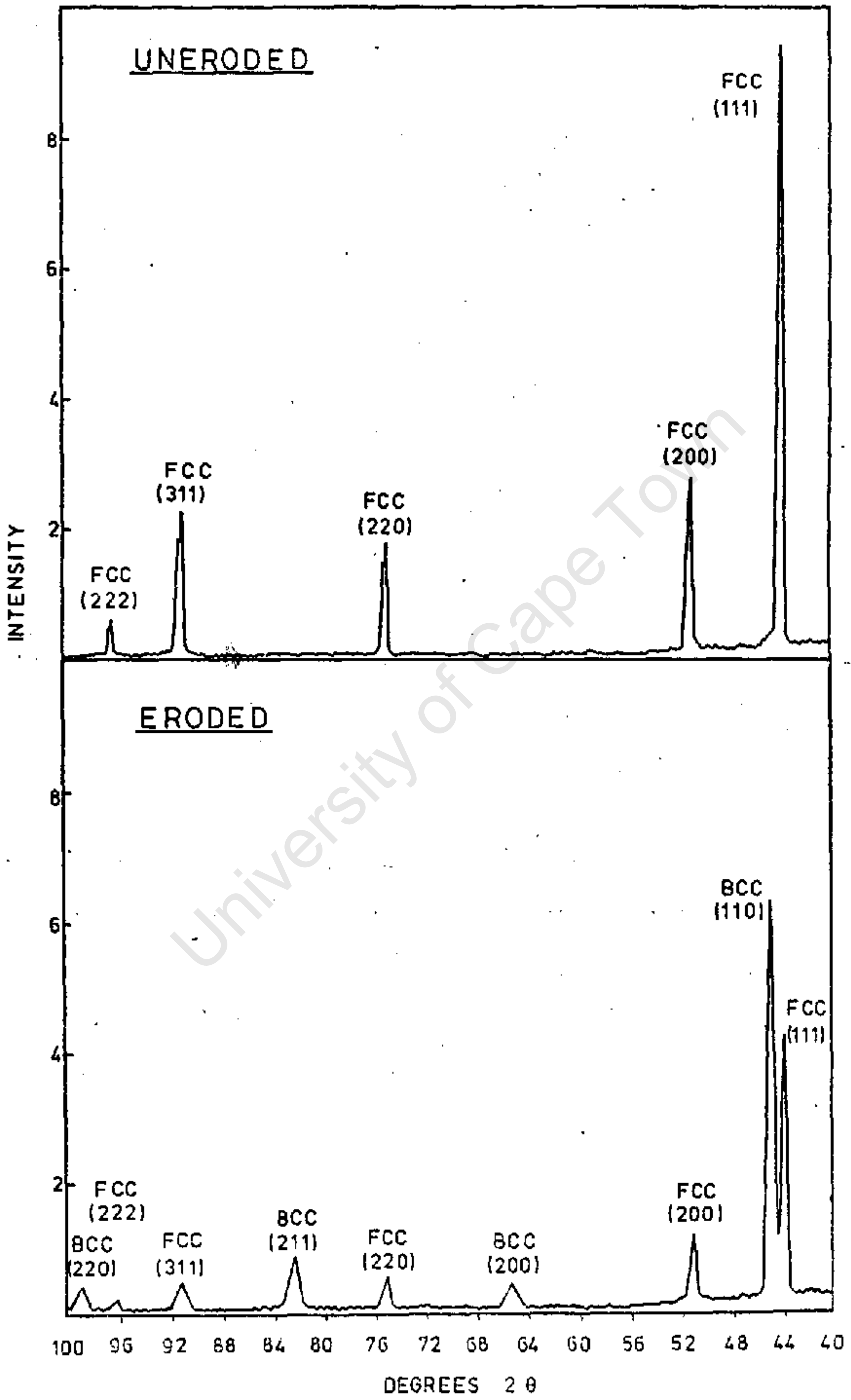

Fig. 7.13 The stress induced $\gamma \rightarrow \alpha'$ transformation in AISI 304.

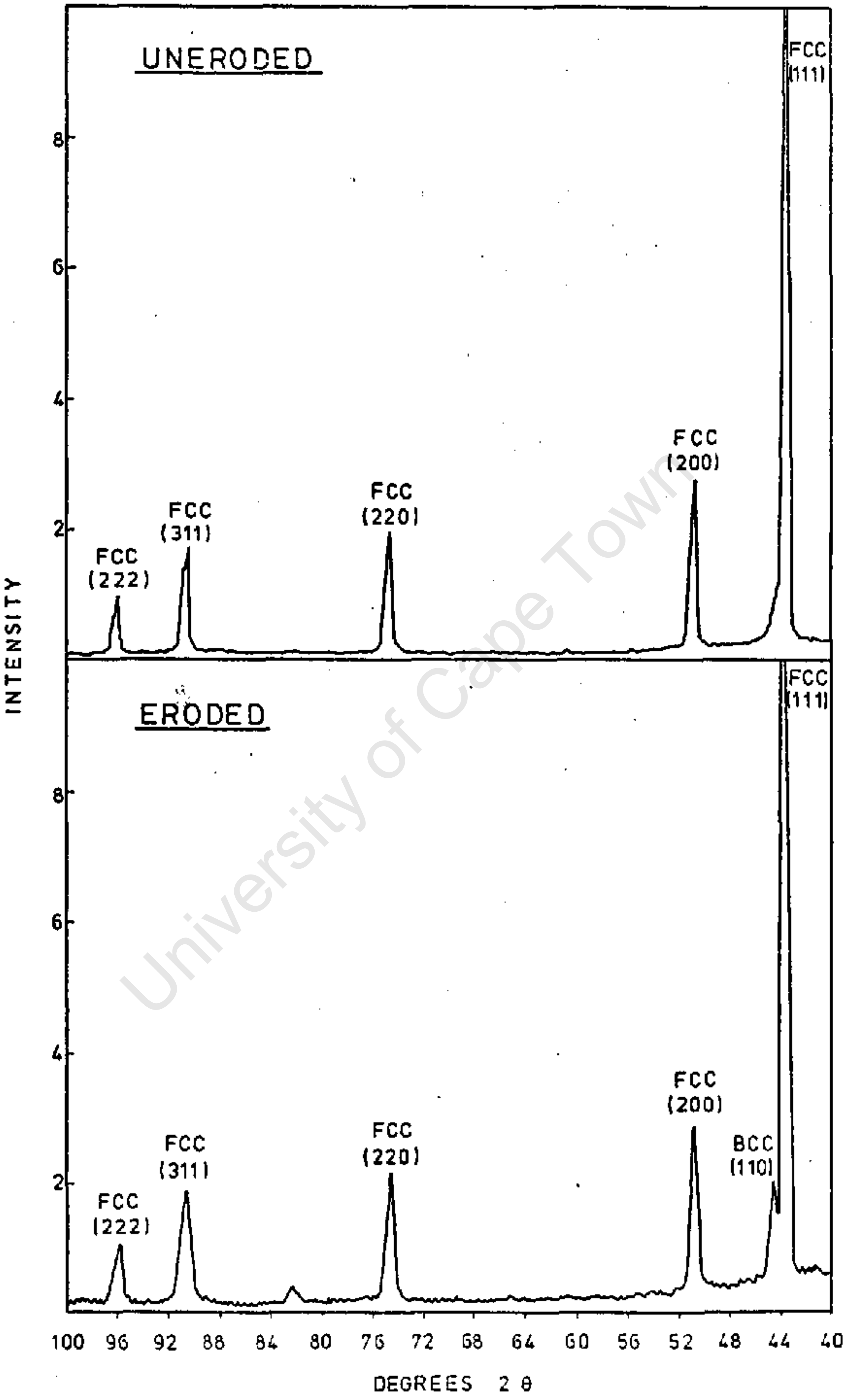

Fig. 7.14 The structure of AISI 316 before and after erosion.

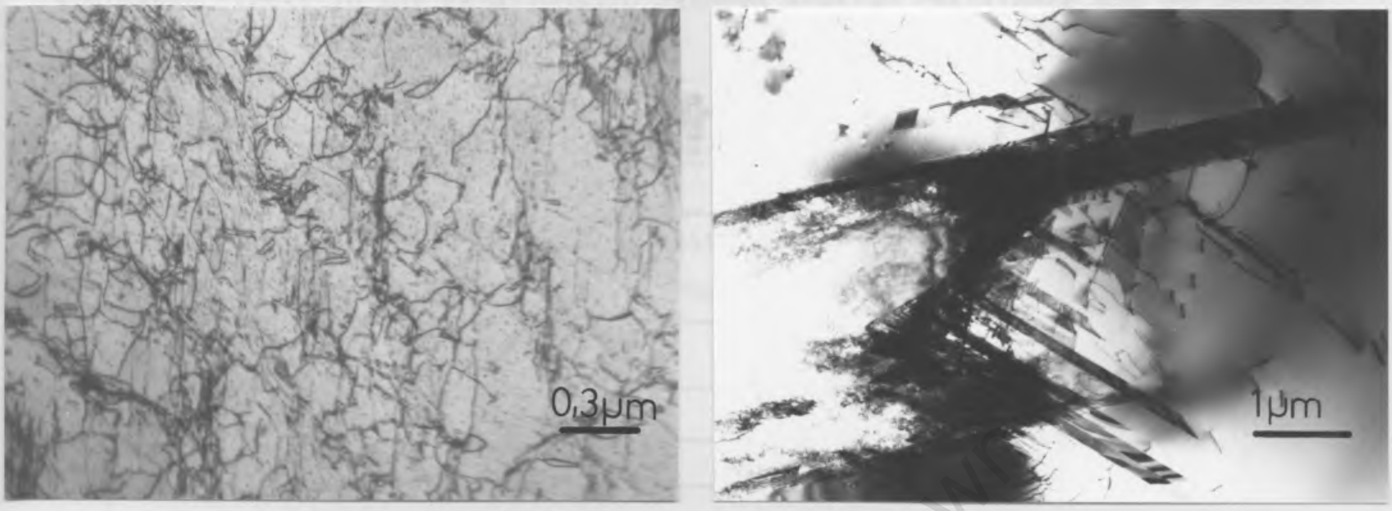

(a) Dislocation density after exposure to cavitation (35000x)

(b) Cavitation induced twins and the nucleation of martensite at twin intersections (12800x)

(c) Highly deformed area showing density of twins and martensite (12800x)

(d) Heavily deformed area showing high density of martensite (32000x)

Fig. 7.15 Transmission electron micrographs of AISI 304 showing nucleation of cavitation induced martensite.

AISI 301, which has the highest rate of work hardening of the austenitic stainless steels, had the highest resistance of the 300 series steels tested by Woodford (72). Dr Woodford discounts (I think wrongly!) the trend shown by the stainless steels in the relationship between erosion resistance and percentage phase transformation (see Table 7.5).

TABLE 7.5

Steel	Total Phase Transformed	50 Hr Wt. Loss (gm)
301	93	0,063
304	83	0,070
303	66	0,099

In addition to the action of the second phase in providing obstacles to dislocation motion, resulting in a high work hardening rate, the transformation can be expected to absorb a small amount of shear strain without any associated work hardening. Furthermore if the rat' reaction is reversible, and there is some evidence that this may be the case (99),this would be *an* important mechanism of strain absorption without work hardening. This subject is considered in more detail in section 7.2.

Hadfield's austenitic manganese steel, has a different resistance mechanism. This alloy, like AISI 316 is stable and does not transform to any great extent as shown in the XRD data of Fig. 7.16. Also the little martensite that forms is c martensite rather than a' martensite. Again this agrees with the calculated M_s and M_d temperatures in Table 7.4. While the order of cavitation erosion resistance between Hadfield's steel and AISI 304, obtained in this study, agrees with that reported by Bogachev and Mints (59)the transformation characteristics do not since these authors found the transformation reaction y÷e+a to go virtually to completion (85%). Roberts (100)on the other hand, found,on hammering Hadfield's steel that a small amount of c martensite formed,accompanied by the development of fine twins and dense tangles of dislocations.

The superior performance of Hadfield's steel can be ascribed to its high rate of work hardening, which is higher than that of AISI 304 (n=0,6 cf. n=0,44 for c>0,08%). Numerous theories have been proposed in the past for the mechanism of work hardening in Hadfield's steel including stacking fault - dislocation interactions, and fine twinning (IN) More recently, however, Dastur and Leslie (102) discounted the stacking fault theory since these defects are not commonly observed in Hadfield's steel due to a high SFE (20-40mJ/m^2 cf. 19mJ/m^2 for AISI 304). On

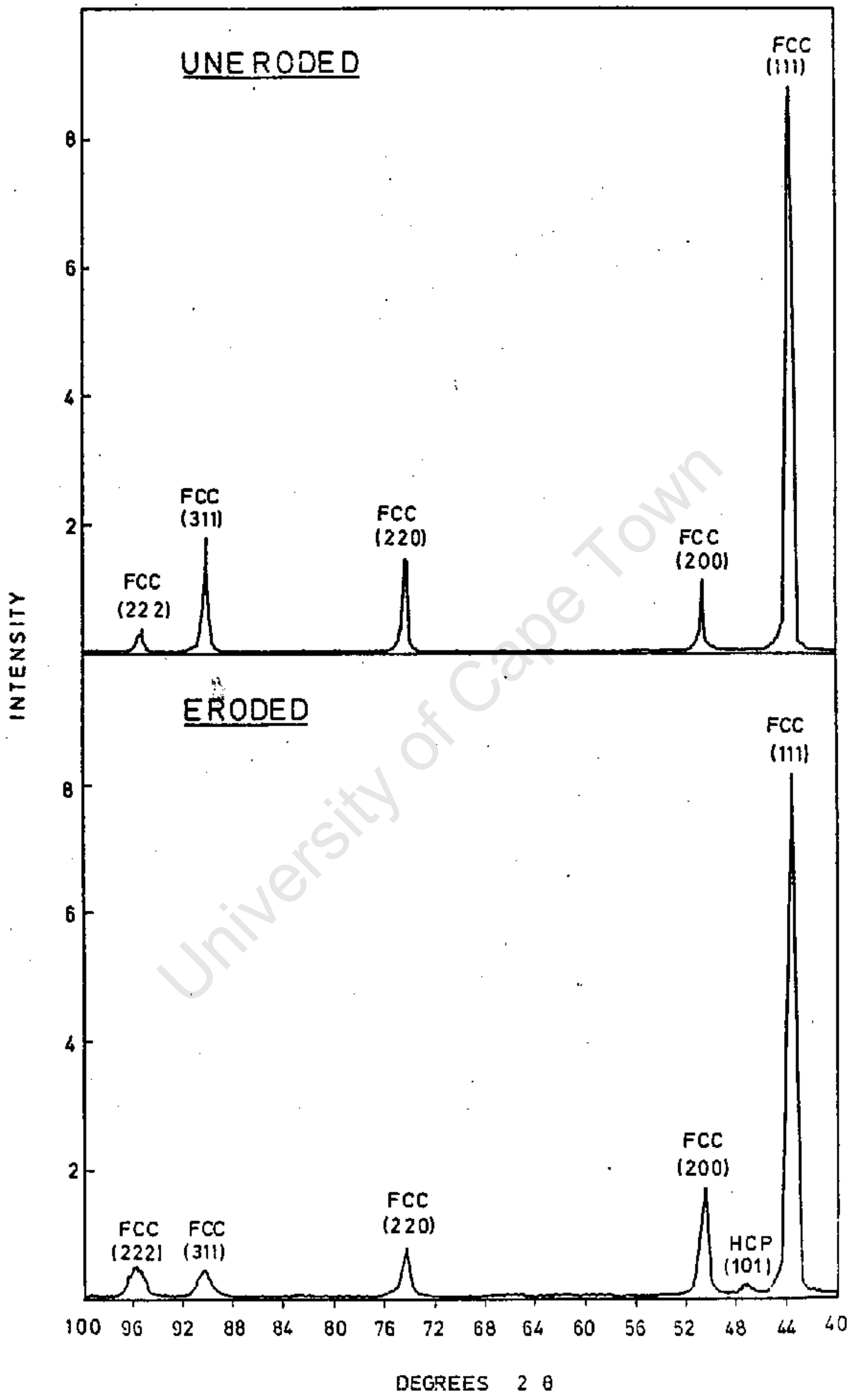

Fig. 7.16 The structure of Hadfields Steel before and after erosion.

the other hand, the twinning theory is, in part correct,but it does not hold for high temperature deformation when the work hardening rate remains high. Dastur & Leslie have proposed, instead, that dynamic strain ageing is the main cause of the unique hardening. This occurs by Mn-C couples (not carbides) aligning themselves in the strain fields of dislocations thereby continuously stabilizing these defects in the lattice.

7.1.2.3 Ferritic Stainless Steels

In contrast to the other stainless steels the standard ferritic alloys AISI 409 and 430, have very poor erosion resistance. In fact, they rank as the two worst alloys tested in this project. The development alloys 3CR12* and 3CR12Ni-rich performed rather better than the conventional AISI standard ferritic steels (see Table 7.6).

TABLE 7.6

Alloy	Main Alloying elements			CVL 5 hrs	t_o Hrs	$\dot{E}$ mm /hr	V.H.	R_n	FF†
	C	Cr	Ni						
430	0,14	16,35		37,2	1	8,3	180	40	
409	0,03	11,42	0,31	12,5	1	NSS††	129	38	11,72
3CR12	0,02	11,14	0,42	4,17	2	NSS	167	43	11,52
3CR12Ni	0,03	11,49	1,31	1,72	2	NSS	266	70	9,13

† Ferrite factor
†† No steady state

The poor erosion resistance of these alloys is attributable to the strain rate and notch sensitivity of BCC metals. The high strain rates produced by cavitation result in rapid brittle fracture along transgranular (AISI 430) or both transgranular and intergranular (AISI 409) paths (see Figs. 7.17(a)-(d)). Note that the lower the chrome content the less severe is the fracture mechanism (pure iron could be included in this series as a ferritic with no chromium - it shows a combined ductile - brittle mechanism). The presence of chromium is not entirely the cause of the Notch sensitivity of these steels, rather it is the synergic effect of chromium and a critical concentration of interstitial carbon and nitrogen, particularly for chromium levels above 15-18% (103).

The two development alloys 3CR12 and 3CR12Ni-rich are very similar to AISI 409 in composition. However, there are small differences in the alloying element

---

** South African Patent Application SA 78/4764*

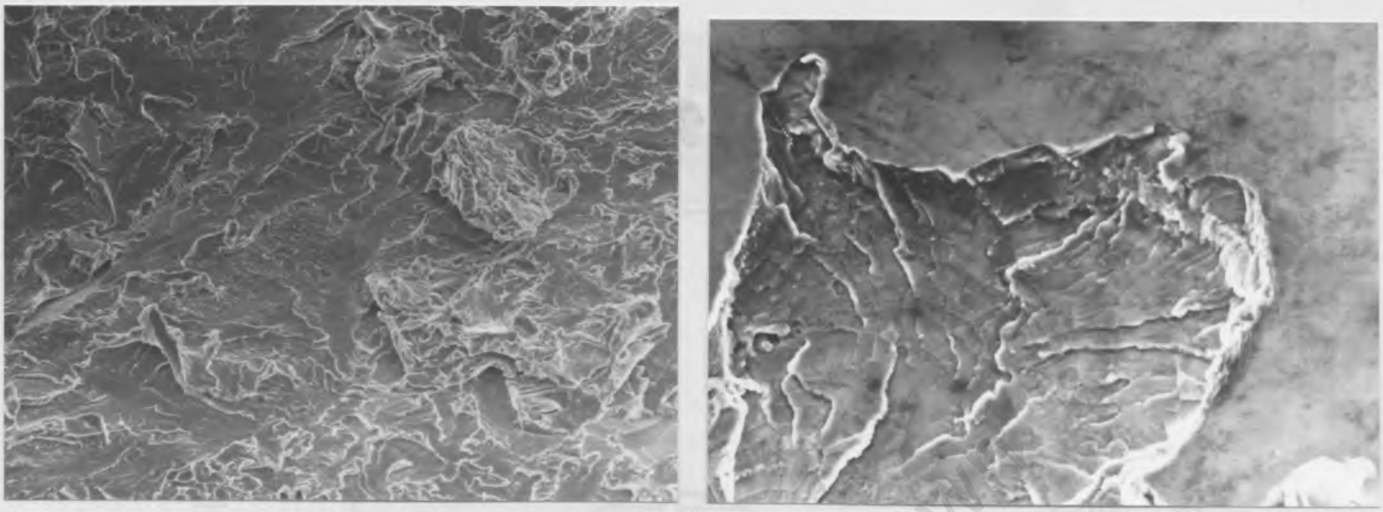

(a) General brittle failure in AISI 430 (400x)

(b) Damage near edge of eroded area of AISI 430 (1360x)

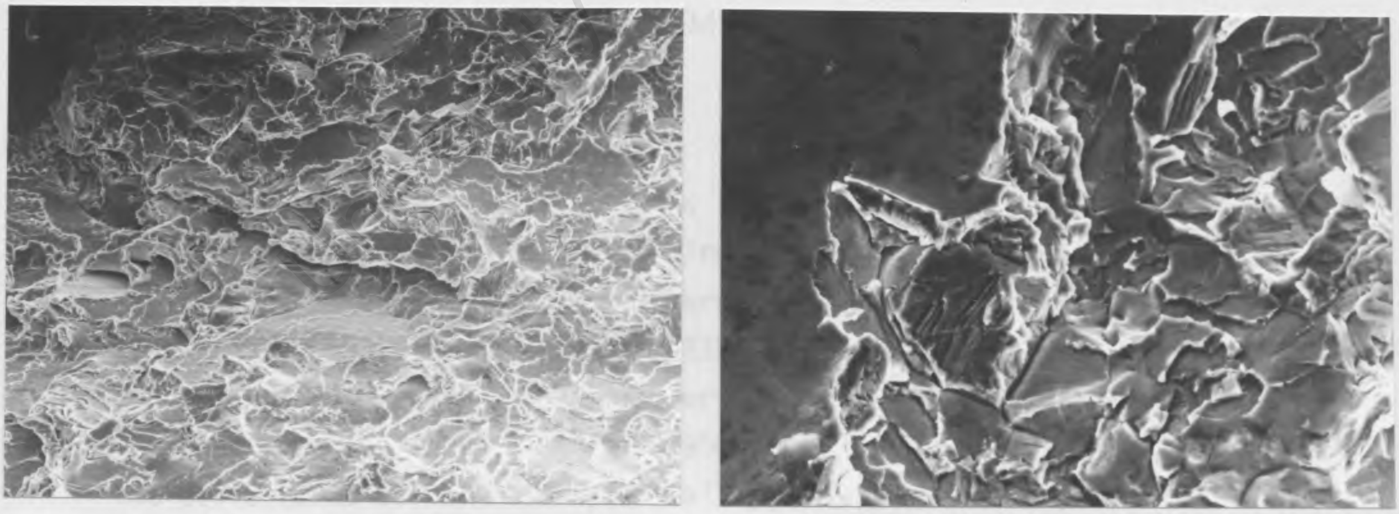

(c) General failure in AISI 409 (400x)

(d) Damage near edge of eroded area of AISI 409.Note partial intergranular failure (1360x)

Fig.7.17 Eroded Surfaces of Ferritic Stainless Steels.

contents which are sufficient to alter the a+y loop (see Fig. 7.18) such that by normalising at 800-900 C the structures of these development alloys become a fine mixture of a-ferrite and æ-martensite.

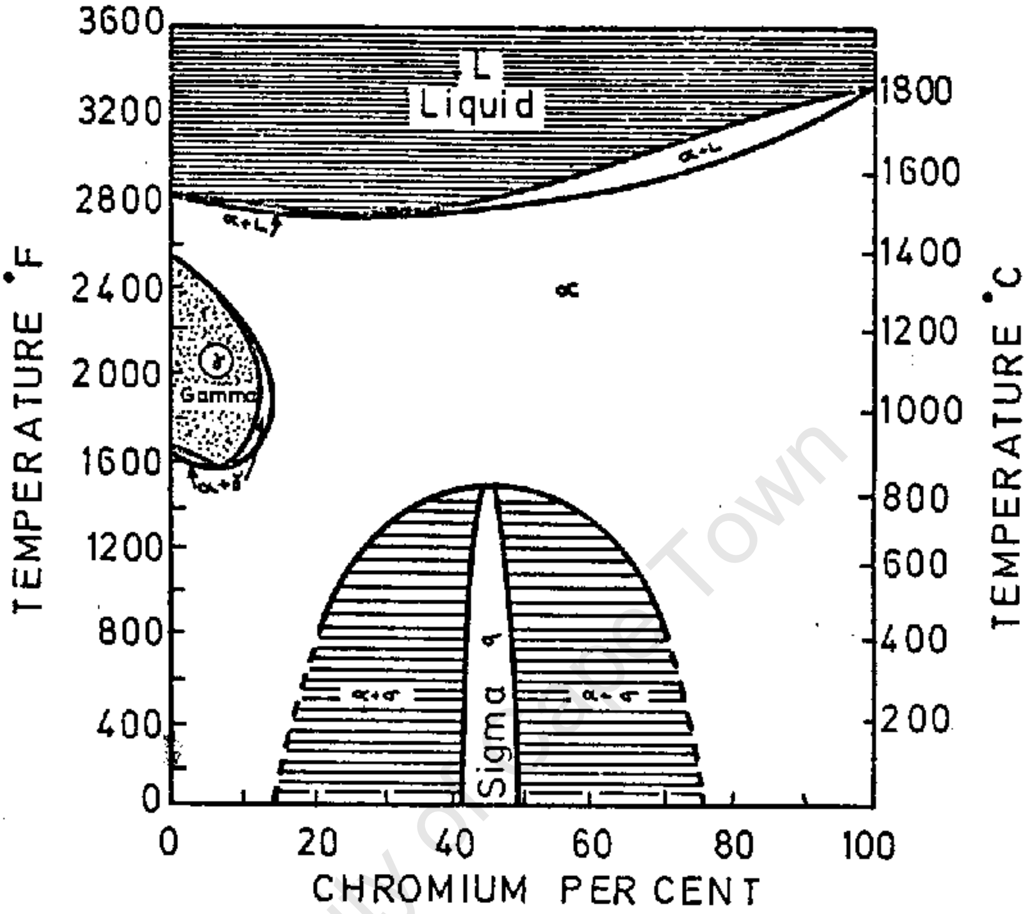

Fig. 7. 18 Fe-Cr Phase Diagram

The ratio of the a and a' phase contents is controlled by the ferrite factor (104)of the alloys, a lower factor leading to a greater proportion of martensite (see Table 7.6). On the basis of the ferrite factors, the difference between the erosion results for AISI 409 and 3CR12 would appear to be larger than expected. This is probably the result of the former alloy being in the warm worked condition rather than in the optimum normalised (900 C) condition.

The performance of the development alloys can be altered by normalising at different temperatures to obtain various structures from warmworked(as received) to duplex (normalised at 900 C). Fig. 7.19 shows how the erosion resistance of the alloys vary with these different heat treatments. Initially the erosion increases as the deformed structure recrystallizes to form single phase ferrite. At higher temperatures the structure becomes duplex and the presence of 'ductile' martensite leads to a reduction in erosion.

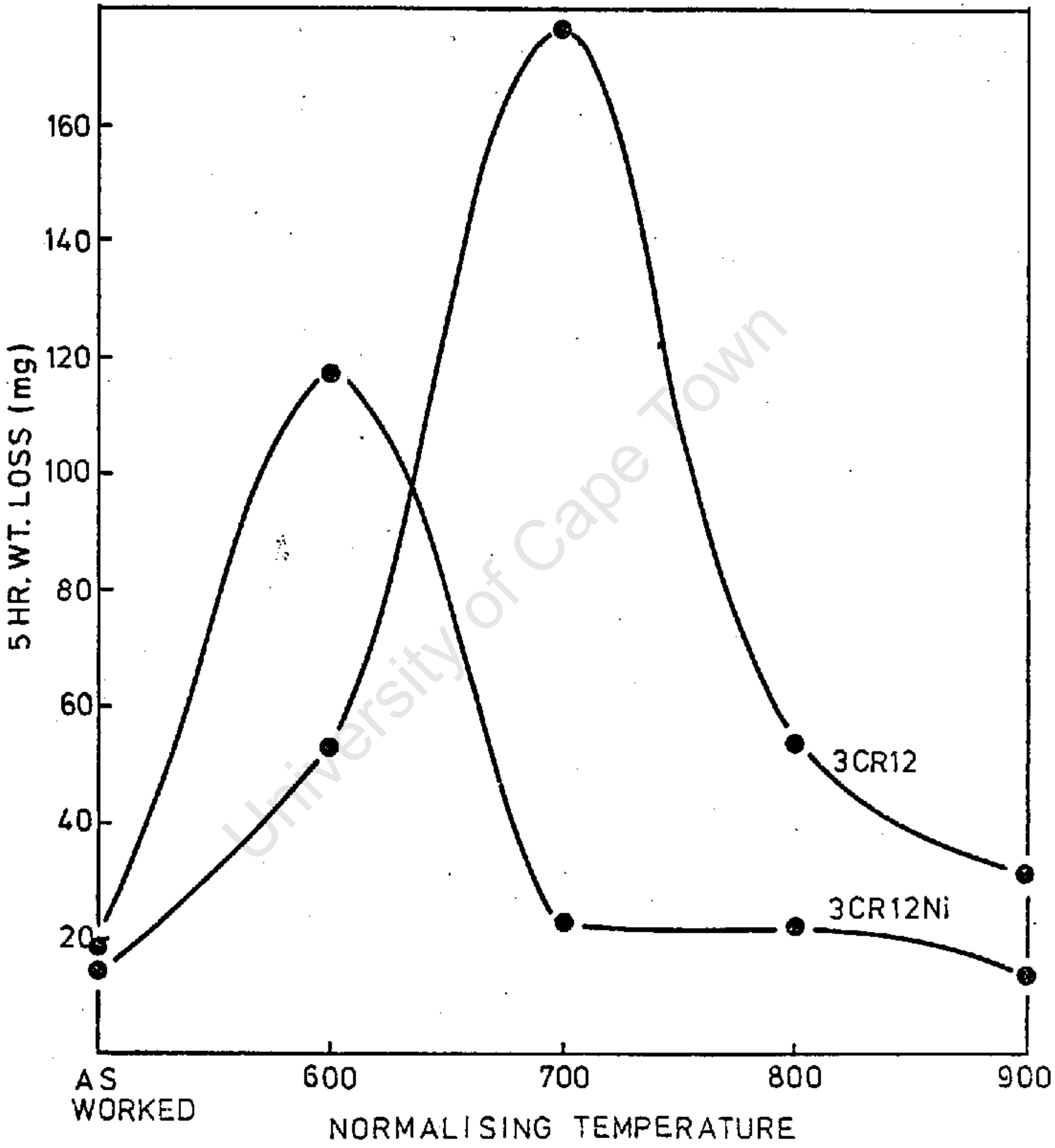

Fig.7.19 The erosion resistance of 12% chromium Ferritic Steels as a function of heat treatment.

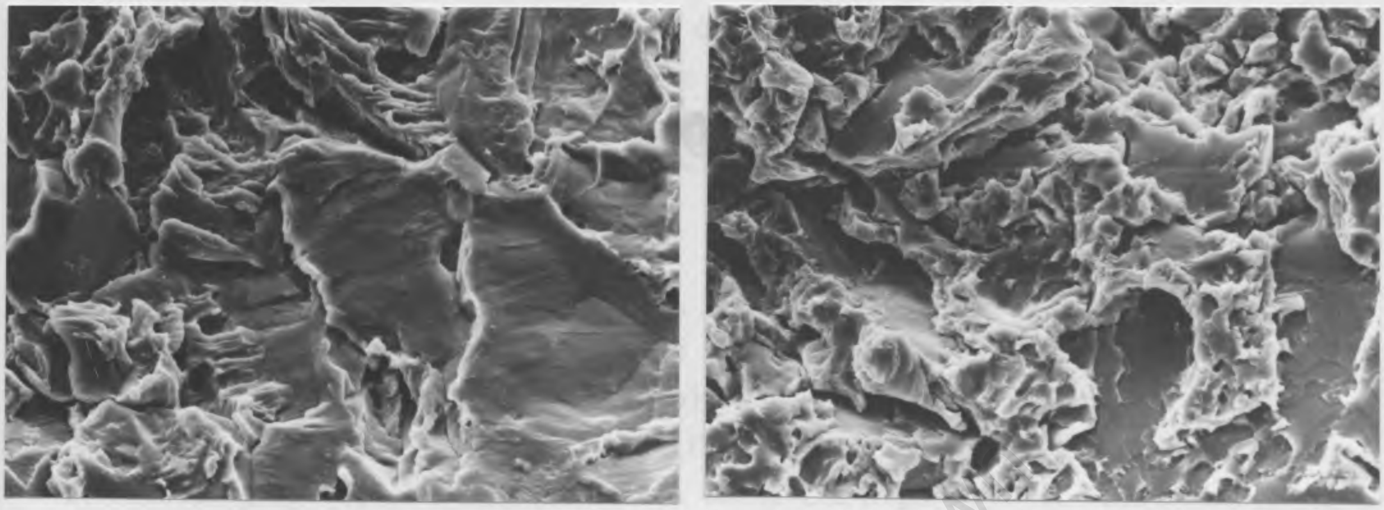

(a) 3CR12 normalised at 700^{o}C - fully ferritic.

(b) 3CR12 normalised at 900^{o}C - duplex.

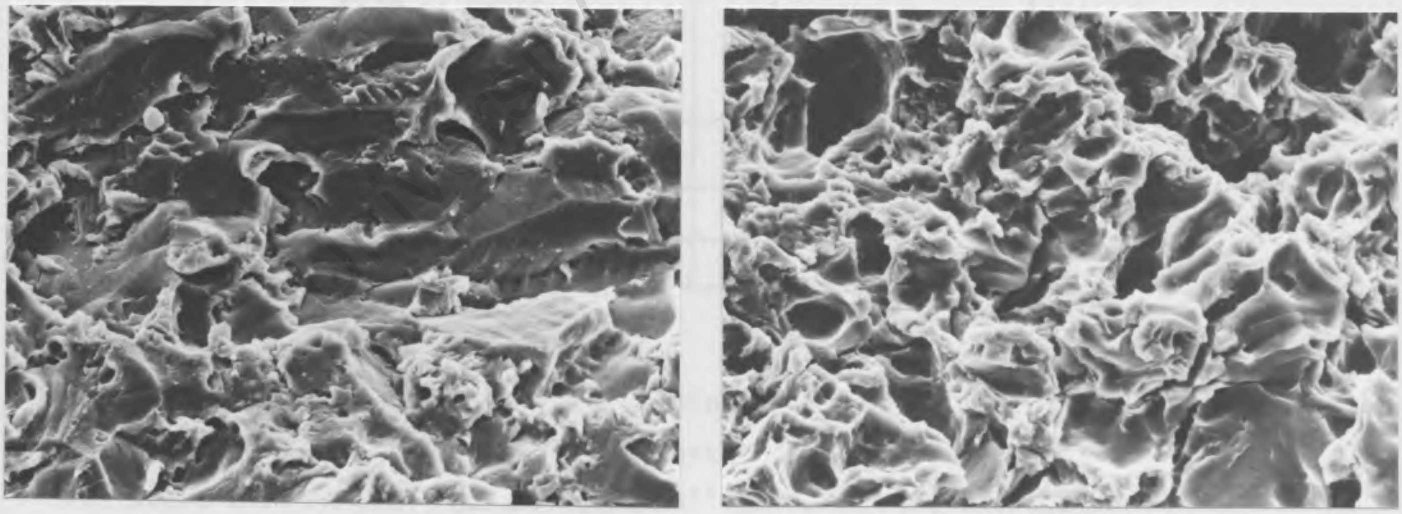

(c) 3CR12Ni normalised at 600^{o}C - fully ferritic.

(d) 3CR12Ni normalised at 900^{o}C - duplex.

Fig. 7.20 Eroded surfaces of 3CR12 and 3CR12Ni in the single phase and the duplex phase condition.(Magnification all 2000x)

The presence of martensite phase was verified by SEM fractographic studies and Fig. 7.20(a)-(d) show the eroded surfaces of 3CR12 and 3CR12Ni-rich in the single phase condition (700 C and 600 C respectively) and in the duplex phase condition (900 C for both). The duplex phase a+a' structure results in partially ductile and partially brittle fracture as indicated in the micrographs. This work illustrates the strong control microstructure has on the mode and rates of erosion.

7.1.3 Cast Irons

Three cast irons were investigated, namely, a nodular cast iron (SG 80) and two high chromium cast irons (CB 24 and TB 18). The latter two alloys have high hardnesses compared with SG 80 (see Table 7.7). Moreover the structures of these alloys differ considerably as shown in Fig. 7.21(a), (c) & (e). SG 80 is comprised of nodular graphite in a ferrite matrix while the high chromium materials consist, in the case of TB 18,of a complex mixture of chrome carbides, a eutectic phase and'solid solution phase while CB 24, with the higher chromium content, consists of a large number of fine chrome carbide particles (ti6um) in a solid solution matrix.

TABLE 7.7

Alloy	Main Alloying elements				CVL 5 hrs	t_o hrs	$\dot{E}$ mm³/hr	V.H.	R_n
	C	Si	Cr	Mo					
SG 80	3,48	2,62			6,79	1	1,82	160	52
CB 24	3,0		23,2		0,23	3,5	0,124	873	103
TB 18	2,21		12,8	1,34	0,38	2,5	0,120	688	93

The erosion resistances of these alloys follow the hardness and resilience values. CB 24 is a little more resistant than TB 18 while both are much more resistant than SG 80. The two former alloys follow the average trend in Fig.. 7.4 while SG 80 deviates to the high side, that is, it has a lower erosion resistance than one would expect from its resilience number. Furthermore, considering the difference in hardness between CB 24 and TB 18 one would expect a greater difference in erosion resistance. This discrepancy is considered to be due to microstructural differences. In CB 24 the chrome carbides provide initiating sites for erosion as a result of cracking at the matrix-carbide interface as discussed in an earlier section (see Fig. 7.21(f)). On the other hand, in TB 18 cast iron the acicular phase is preferentially removed while the while the darker islands of eutectic are more resistant (see Fig. 7.21(d)).

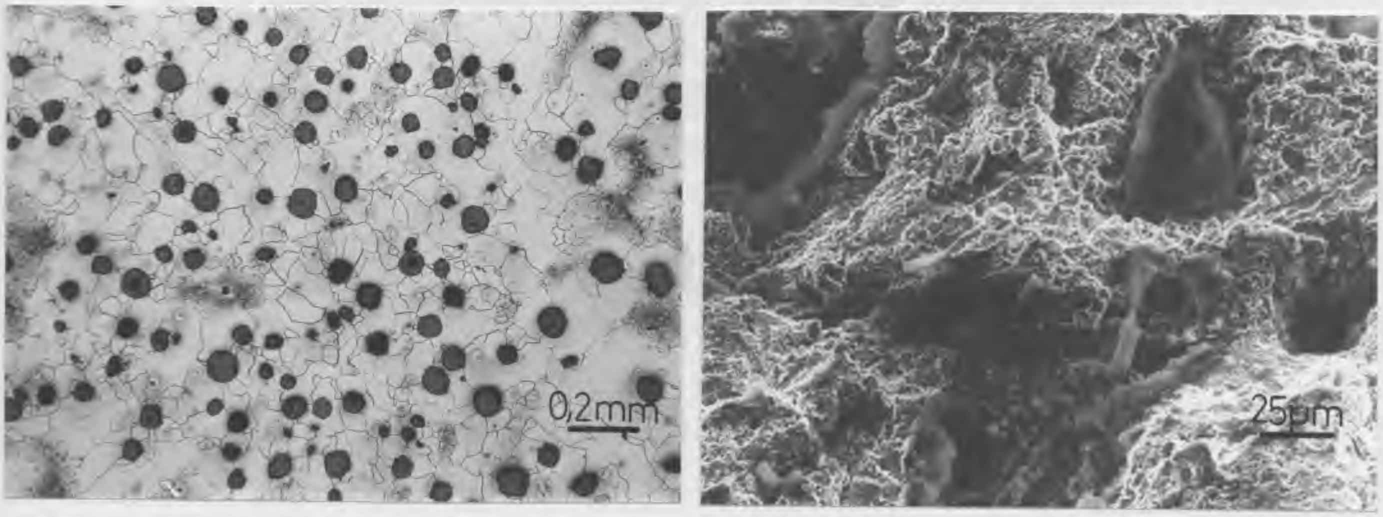

(a) Microstructure of SG80.

(b) Eroded surface of SG80 (400x)

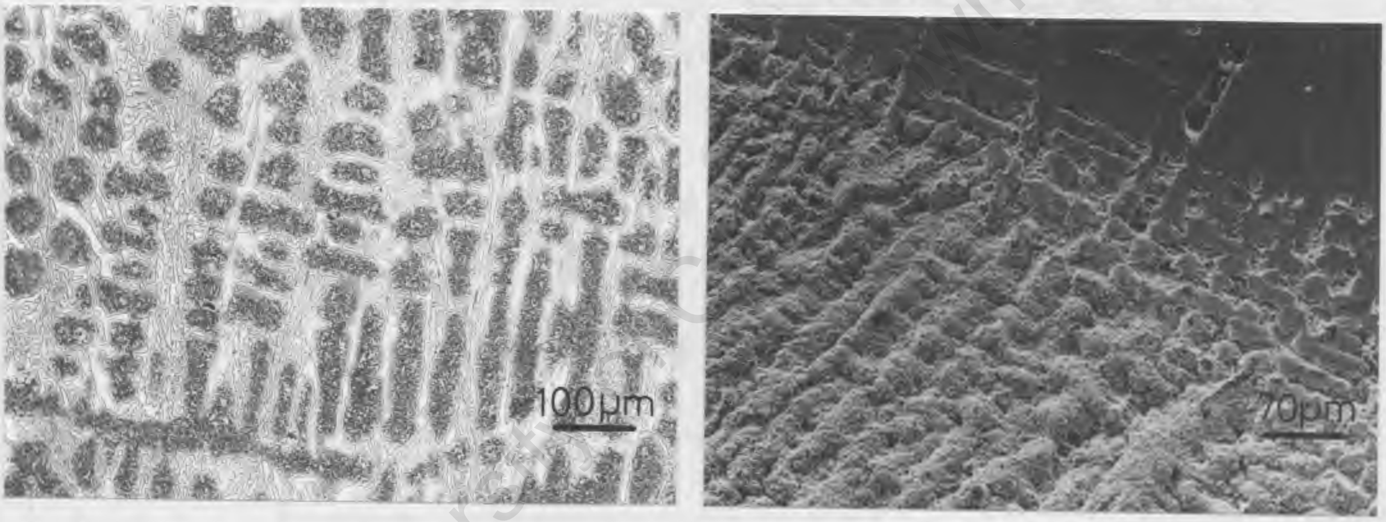

(c) Microstructure of TB18

(d) Damage near edge of eroded area of TB18 (140x).

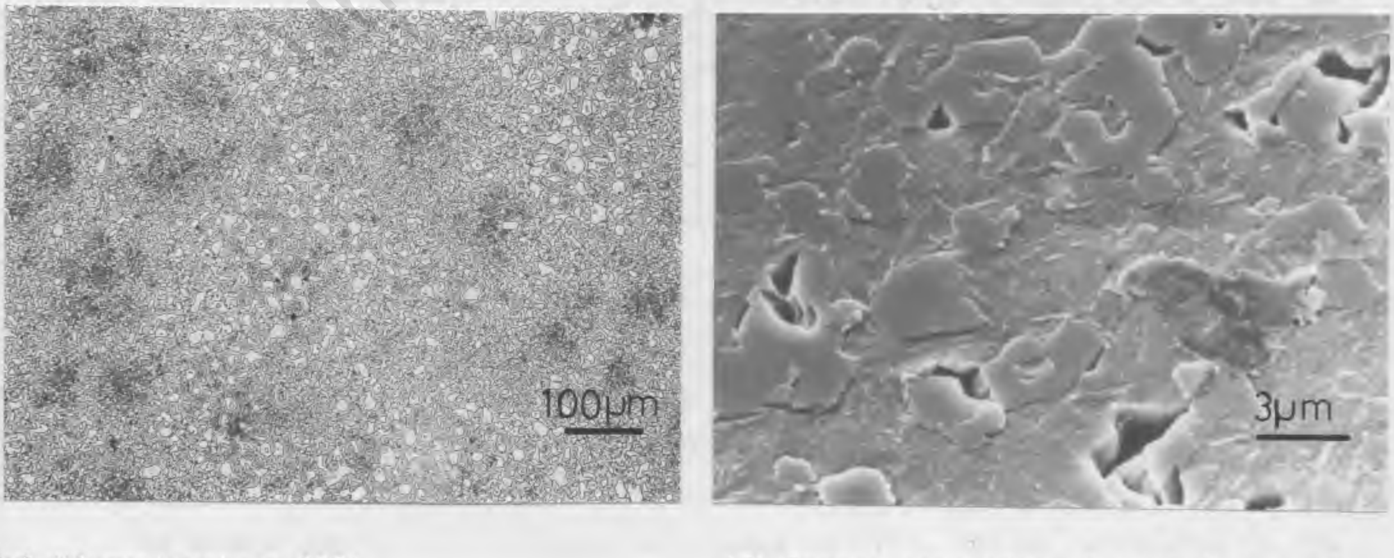

(e) Microstructure CB24

(f) Damage near edge of eroded area of CB24 (4000x).

Fig.7.21 Microstructures and modes of erosion of cast irons.

SG 80, as expected, erodes by initial loss of the graphite nodules followed by brittle failure of the ferrite matrix (see Fig. 7.21(b)). In addition severe corrosion occurs during erosion of this alloy and corrosion products lining the recesses of removed nodules can be seen in Fig. 7.21(b). This reaction is assisted by the presence of graphite,since the ferrite matrix is anodic with respect to the carbon nodules. The preferential removal of the graphite nodules simplifies the degradation of the ferrite matrix,since the pits are ideal initiating sites and from a very early stage in the erosion process matrix material is rapidly removed. These 'weak sites' result in SG 80 having a lower erosion resistance than expected from its resilience number value.

7.1.4 Nickel Based Alloys

This group includes the alloys: NiTi, Monel 400, Incalloy 825, Alloy C and Alloy 3040. The nickel-titanium intermetallic alloy, NiTi, has a very high resistance to erosion which agrees with the findings of Bard (105).The as cast Ni-Cr-Mo alloys, Alloy 3040 and Alloy C, are somewhat less resistant than NiTi while the wrought Ni-Cu alloy, Monel 400 and the wrought Ni-Fe-Cr alloy, Incalloy 825 are the least erosion resistant alloys of the group.

TABLE 7. 8

Alloy	Main alloying elements							CVL 5 hrs	t_o hrs	$\dot{E}$ mm^3/hr	V.H.	R_n
	C	Ni	Cr	Mo	Cu	Fe	Ti					
NiTi		53,5					45,3	0,01	12,5	0,048	200	35
Incalloy 825		41,0	20,8		2,13	31,8		2,25	2	0,577	186	49
Monel 400		66,6			31,9			3,41	1	0,815	159	38
Alloy C	0,1	52,9	17,0	17,0		6,0	W5,0	0,36	3	0,200	229	55
Alloy 3040	1,28	47,7	34,0	10,0		3,0	Nb3,0	0,42	2	0,140	388	79

The intemetallic alloy NiTi has a long incubation time, approximately 12,5 hours. In addition the erosion rate after t_o is considerably less than that for other alloys having a comparable hardness (eg. 316 stainless steel, E = 0,520). Furthermore, NiTi has a very low resilience and its erosion/resilience relation shows a considerable deviation from the average trend in Fig. 7.4 .

The exceptionally high erosion resistance of NiTi, can be attributed to the occurrence of a martensitic transformation in this material. If this alloy is deformed at temperatures close to the M_s* temperature approximately 7% reversible

---

* *Temp. at which martensite reaction starts*

strain can be accommodated by processes associated with the martensitic transformation (106).Moreover if the test temperature is between the A_f* and M_d* temperatures (see Fig. 7.22), then the transformation is fully reversible.

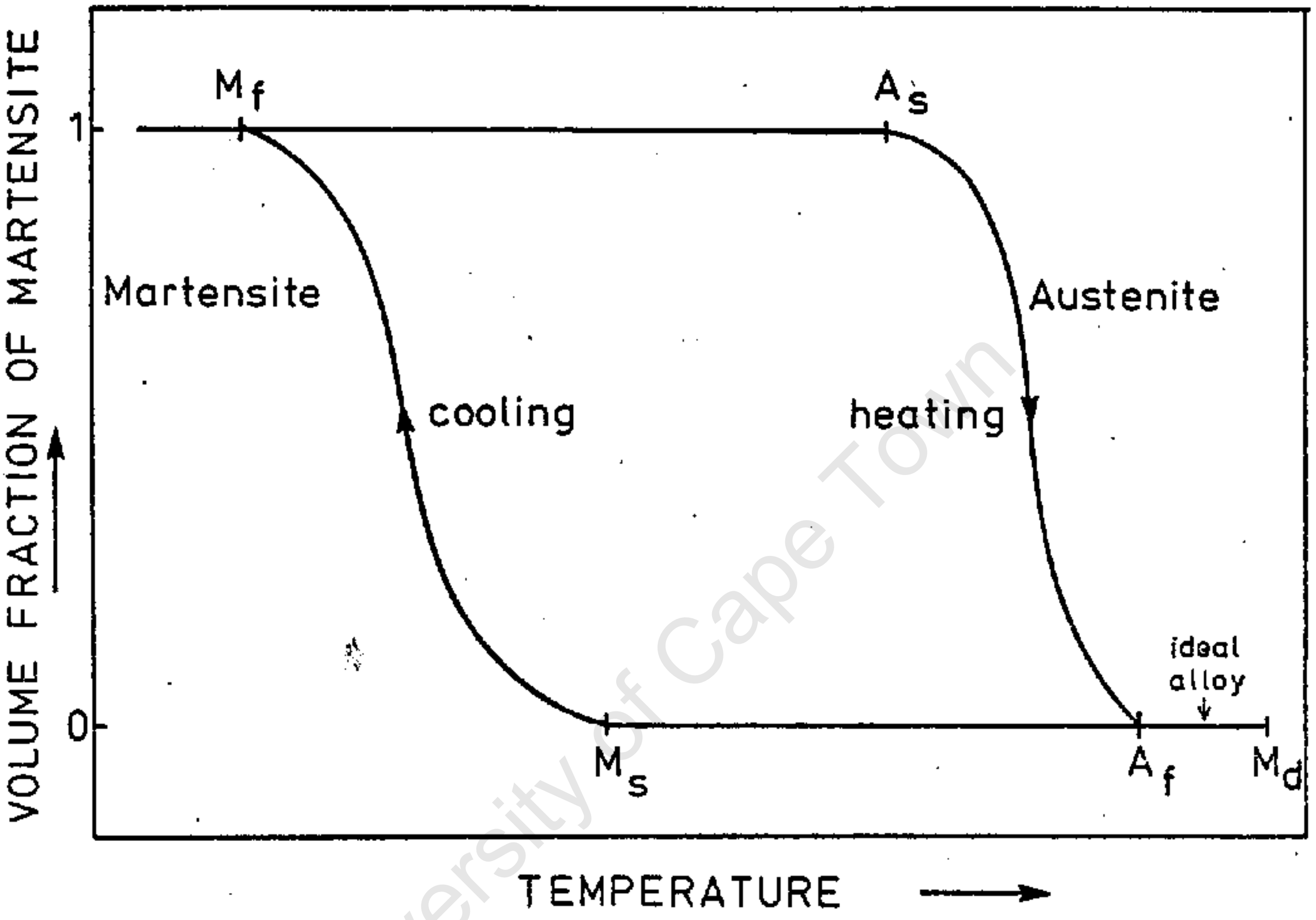

Fig. 7.22 Phase Transition Hysteresis in NiTi (Ref. 106)

The M_s temperature of the alloy studied in this work was approximately 200 ^{0}C and hence it was martensitic at room temperature. The erosion resistance of this material can be attributed to the accommodation of strain by a combination of: (i) growth of martensite phase, (ii) stress induced growth of one martensite orientation at the expense of an adjacent, unfavourably orientated one, (iii) a stress induced reorientation of martensite and (iv) a stress induced twin boundary migration within a martensite variant (106). The important implications of strain absorption are discussed in section 7.2.

Although this sample has an exceptionally high resistance it is not the optimum alloy. A NiTi alloy with maximum erosion resistance would clearly be one

---

*A_i. *Temp. at which the reversion to Austenite is complete*

*M_d *Max. Temp. at which the martensite reaction can be induced by deformation.*

which transforms reversibly at the temperature of deformation. This alloy would have an M_d temperature just above room temperature or the test temperature and therefore an A_f temperature a little below the test temperature (see Fig. 7.22).

The cast alloys,Alloy3040 and Alloy C are complex Ni-Cr-Mo alloys. Both contain a small amount of iron and, in addition, alloy C contains 5% tungsten while Alloy3040 has 3% niobium. Alloy C has about 1/10 of the carbon content of Alloy 3040.

As regards erosion performance,Alloy 3040 has a resistance expected for a material of its hardness (see Fig. 7.3). On the other hand Alloy C, which has a hardness half that of alloy 3040, not only has a slightly longer t_o than Alloy 3040, but also has an E rate not much greater than that of its counterpart (see Table 7.8). Moreover the volume loss/resilience relationship for Alloy C deviates from the average trend in Fig. 7.4. The microstructures and cavitation fracture surfaces of the alloys are shown in Fig. 7.23(a)-(d). The relative performances of these alloys can be explained in terms of microstructures and fracture mechanisms.

Alloy 3040has a high carbide content, mainly Cr_7C_3 and Mo_6C carbides plus a small amount of niobium carbide, which increases the bulk hardness. At the same time, however, these carbides provide a large number of sites for initiation of erosion. Fig. 7.24a) clearly shows that cracking occurs at the interface between the carbides and the nickel rich solid solution matrix due to the elastic mismatch between carbide phase and matrix. Moreover within the matrix, which has a eutectic type structure, erosion is initiated at, and propagates rapidly from interlamellar interfaces.

Alloy C, on the other hand, has a much lower carbide content and, although the fractography studies (Fig. 7.23(b)) show that the carbide phase is still preferentially eroded, overall there are fewer erosion nucleating sites compared with Allay 3040. This explains the longer incubation time of Alloy C. However,, later in the erosion history the lack of carbides is a disadvantage as indicated by the slightly higher steady state erosion rate at $t>t_o$. After the incubation time the fine carbide microstructure in Alloy 3040 is beneficial in retarding crack growth, plastic deformation and ductile rupture. The relationship between these alloys is analagous to that between Stellite 8 (0,27%C) and the other high carbide content Stellites (see section 7.1.6)

These nickel based alloys have a high SFE (probably n.60mJ/m^2) and therefore do not benefit from a phase transition induced improvement in mechanical properties. The exceptional resistance of Alloy C (considering its mechanical properties) is thought to be due to solid solution hardening which results in a high critical resolved shear stress for dislocation motion. Alloy C and Alloy 3040 contain equal amounts of alloying elements but in the latter alloy a high proportion of chromium, molybdenum and niobium will be tied up as carbides and thus the nickel

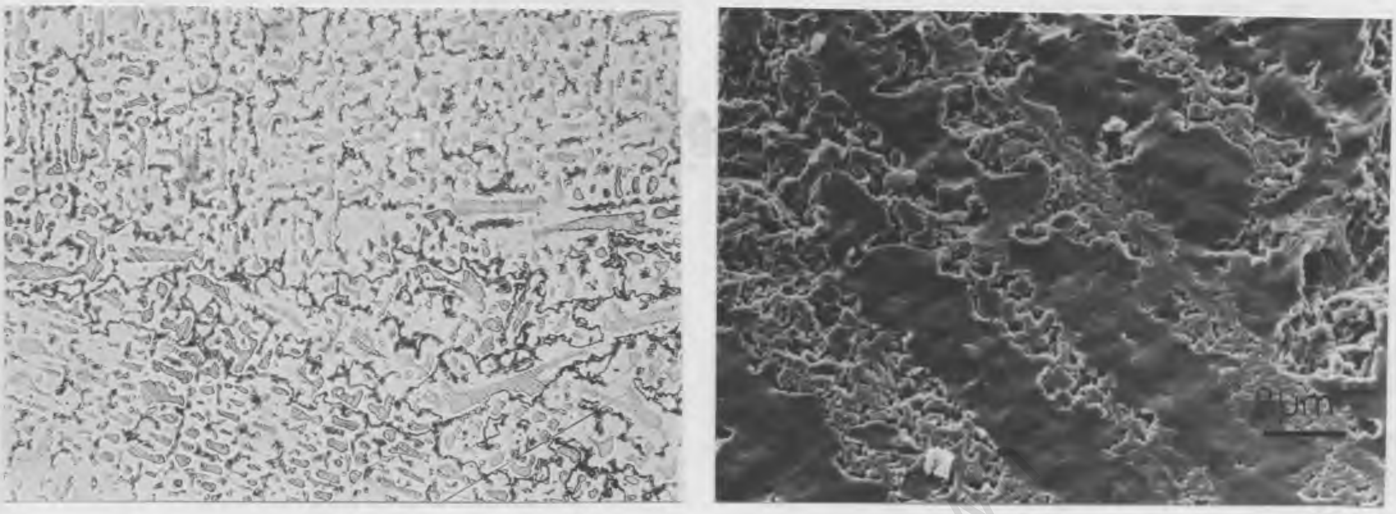

(a) Microstructure of Alloy C

(b) Mode of erosion of Alloy C (1360x)

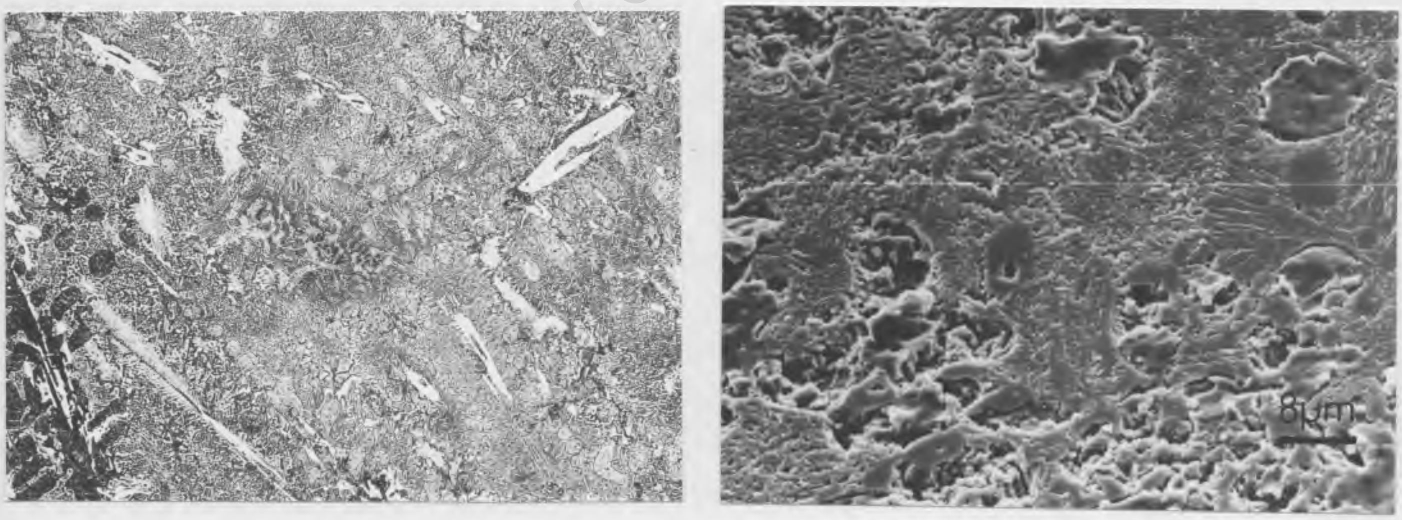

(c) Microstructure of Alloy 3040

(d) Mode of erosion of Alloy 3040 (1600x)

Fig. 7.23 Microstructures and modes of erosion of Ni-Cr-Mo cast alloys.

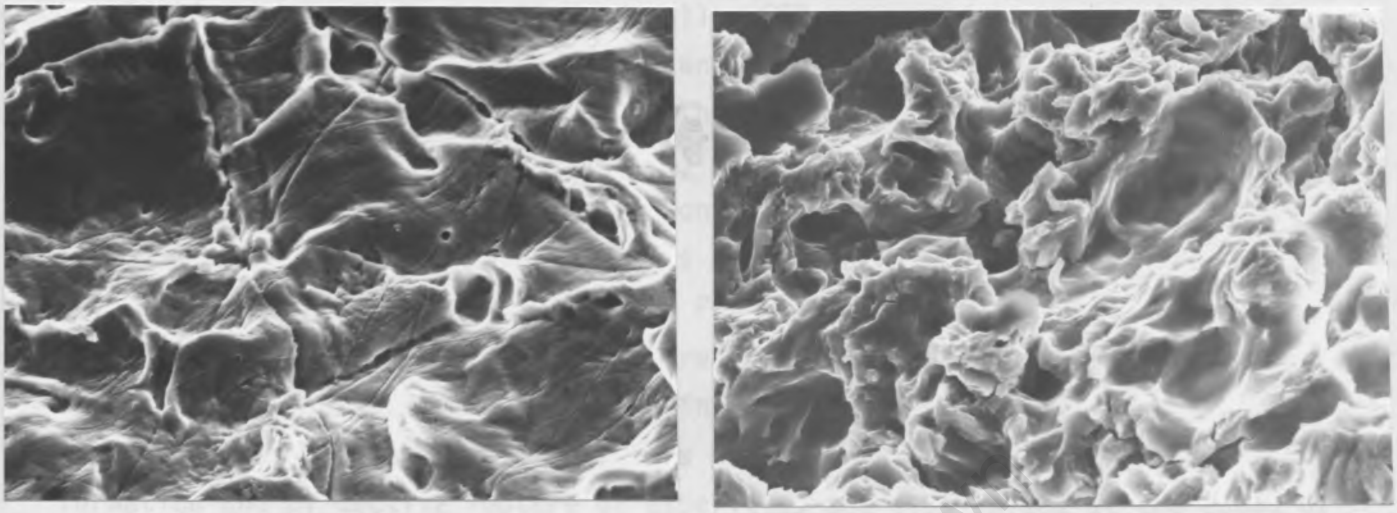

(a) Damage at edge of eroded area of Monel 400.

(b) General damage of Monel 400.

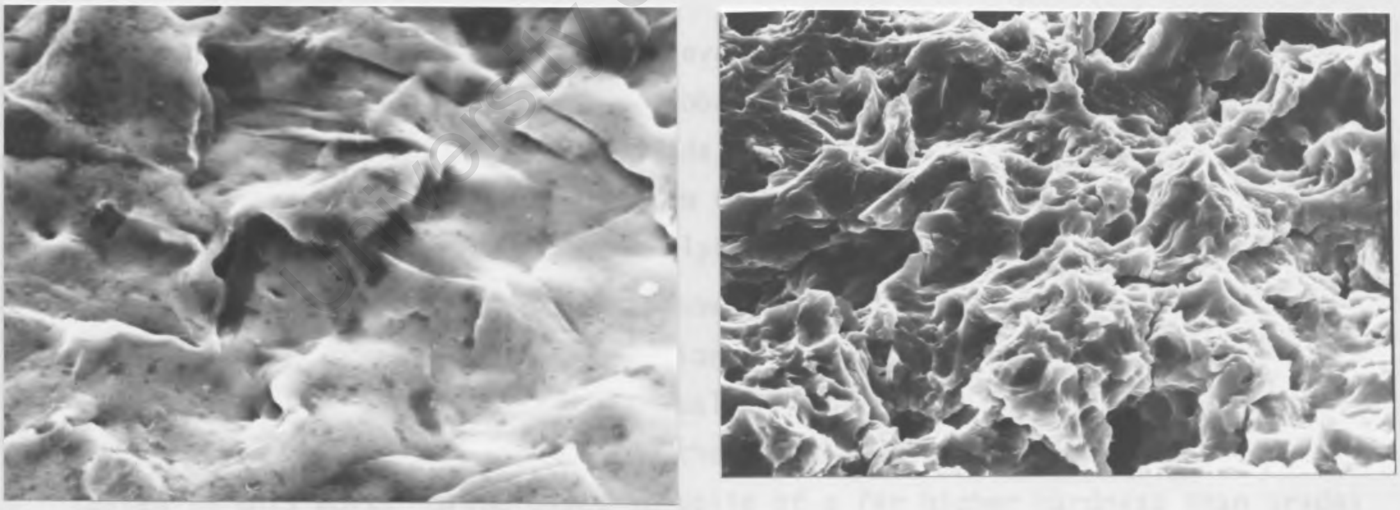

(c) Damage at edge of eroded area of Incalloy 825.

(d) General damage of Incalloy 825.

Fig. 7.24 Modes of erosion of the Monel 400 and Incalloy 825. (All 4000x) rich matrix of Alloy C can be expected to have a higher hardness than the same phase in Alloy 3040.

The remaining two nickel based wrought alloys, namely, the Ni-Cu alloy, Monel 400 and the Ni-Fe-Cr alloy, Incalloy 825 responded to cavitation in the manner_ typical of high stacking fault energy, single phase, face centered cubic metals (Chapter 3, Section 3.3.2.2). This mode of erosion has been reported by other investigators (62 , 64 , 12) and is now faily well understood. The high SFE results in easy dislocation cross-slip and plastic deformation. Hence highly ductile deformation occurs during erosion of these materials.

The fracture surfaces are shown in Figs. 7.24(a)-(d). The micrographs of regions near the edges of the eroded areas illustrate the massive deformation which occurs in the early stages of erosion in these materials. Furthermore the micrographs of the heavily eroded areas show that material loss occurs by crater formation and by ductile rupture of asperities and lips formed at the edges of these craters.

The slightly higher erosion resistance of Incalloy 825 is expected since this material has the higher concentration of alloying elements. Greater solid solution hardening results in a slightly higher bulk hardness and thus a moderately better erosion resistance than Monel 400.

7.1.5 Cemented Carbides

A range of cemented carbides was evaluated for resistance to cavitation erosion. Two binder metals, namely, cobalt and nickel were investigated and in all the samples, except one, the carbide phase was tungsten carbide. The exception was grade CNO2 which contained titanium carbide. This particular sample also contained lesser amounts of chrome, molybdenum and tungsten carbides.

The erosion results (Table 7.9), show that the two nickel based tungsten carbide samples have much higher erosion resistances than either the titanium carbide/nickel based sample or the cobalt based samples. In fact the two former cemented carbides are amongst the most erosion resistant materials tested in this work. Grade CNO2, in spite of a far higher hardness than grades 8LC and 8MC, is approximately three times less resistant than the WC-Ni grades. The best cobalt based sample (CG60) has a similar steady state erosion rate to grade CNO2, but the erosion resistances of these cobalt based carbides vary considerably and the worst grade has an E value of 0,20mm^3/hr. In general, the cobalt based carbides have low resistances in relation to their hardness values and they deviate from the average trend in the plot of erosion vs. hardness (Fig. 7.3). The performance of these carbides is in complete contrast to the findings of Beckwith and Marriott (107) who, in their studies on droplet impact erosion of Haynes stellite 6B and WC-10% Co cermet, found the cermet to be much more erosion resistant than the Stellite alloy.

TABLE 7.9

Alloy grade	Composition (%by wt)		Grain size µm	CVL 7 hrs	t_o hrs	$\dot{E}$ mm³/hr	V.H.	R_n
	Binder	Carbide						
8LC	5Ni	95WC	2	0,05	7,5	0,015	1478	108
8MC	9Ni	91WC	2	0,11	5,0	0,021	1246	113
CN02	10Ni	90 Complex C	2	0,30	2	0,064	1710	109
CG20	6Co	94WC	2	0,82	1	0,134	1452	107
CT30	6Co	94WC	5	1,23	1	0,205	1168	103
CG35	9,5Co	90,5WC	2	0,66	1	0,101	1267	111
4DC	9,5Co	90,5WC	5	0,96	1	0,171	1033	110
CG60	15Co	85WC	2	0,38	3	0,074	1048	94
CT65	15Co	85WC	5	0,52	3	0,115	933	106
Lab grd A	20Co	80WC	2	0,47	3	0,100	933	88
Lab grd C	25Co	75WC	2	0,62	2,5	0,122	835	95

The microstructures of the cemented carbides are shown in Figs. 25(a)-(f). Only four representative structures are shown for the cobalt based samples. Figs, 7.26(a)-(h) are SEM micrographs of the eroded surfaces of a number of the carbides revealing the mechanism of erosion of these materials. The carbide phase is much harder than the cobalt or nickel binder phases and therefore the binder is preferentially eroded followed by removal of carbide particles when there is no longer sufficient binder to retain these particles. Note that the removal of binder phase is initiated at the binder-carbide interface as shown in Fig. 7.26(e) (area marked A). Also Fig.7.26(h) shows that considerable loss of binder occurs prior to removal of the carbide particles.

Fig. 7.27 is a plot of erosion (cum. vol. loss) vs. binder content. This graph depicts the influence of binder content and grain size on the erosion resistance of these materials. Clearly the most important feature of these results is the high resistance exhibited by the two nickel based cermets. Following the good performance of the cobalt based Stellites this result was somewhat unexpected. In addition the cobalt-tungsten carbide combination has a very low interfacial energy which results in nearly perfect wetting during sintering and hence a very good adhesion in the solid state (the wetting angle of cobalt on tungsten is zero). On the other hand nickel does not wet tungsten carbide as well as cobalt and therefore the bonding between carbide grains and nickel binder is not as strong as in the case of the cobalt binder. Despite the attributes of cobalt as a binder, the cemented carbides based on this metal are much less erosion resistant than those based on nickel.

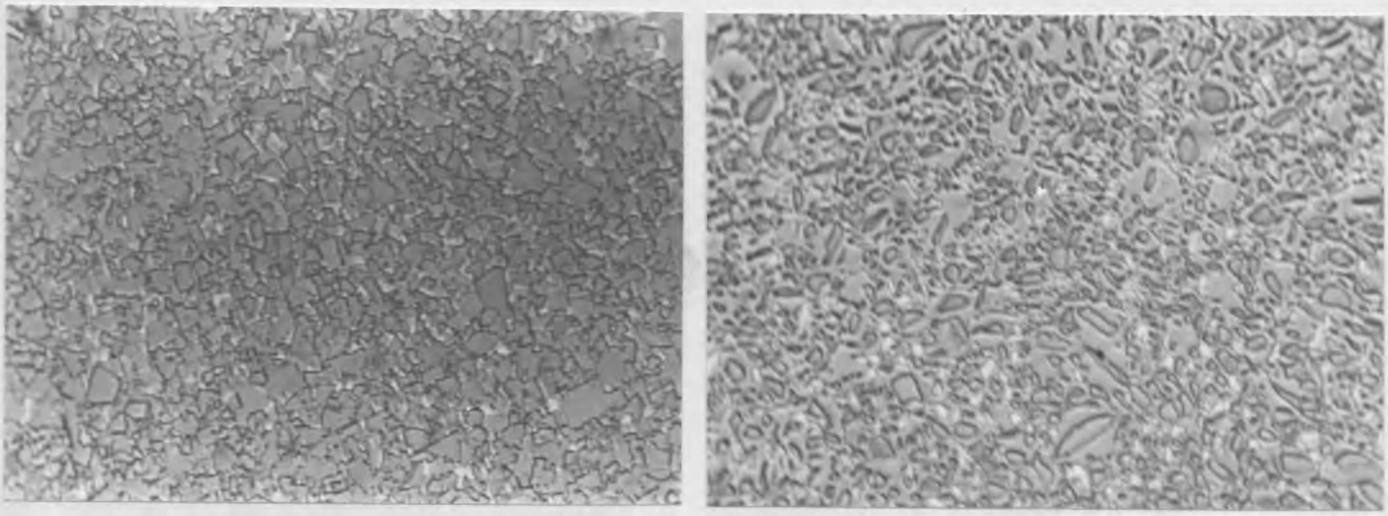

(a) WC/Ni grade 8 MC

(b) TiC/WC/Ni grade CN02

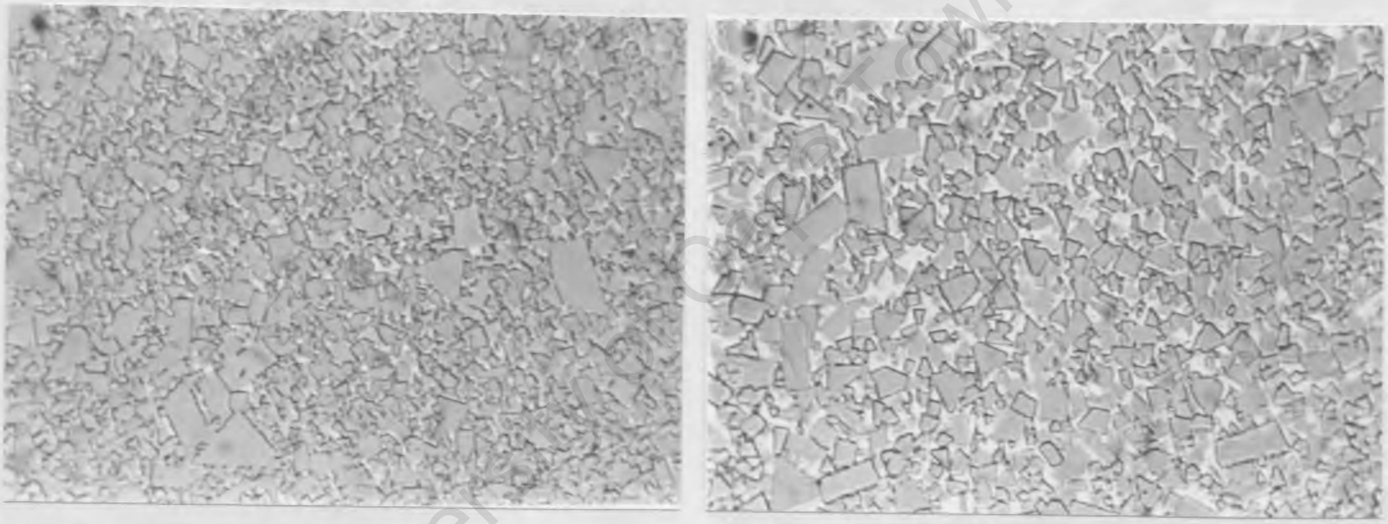

(c) WC/Co grade CG20

(d) WC/Co grade CG60.

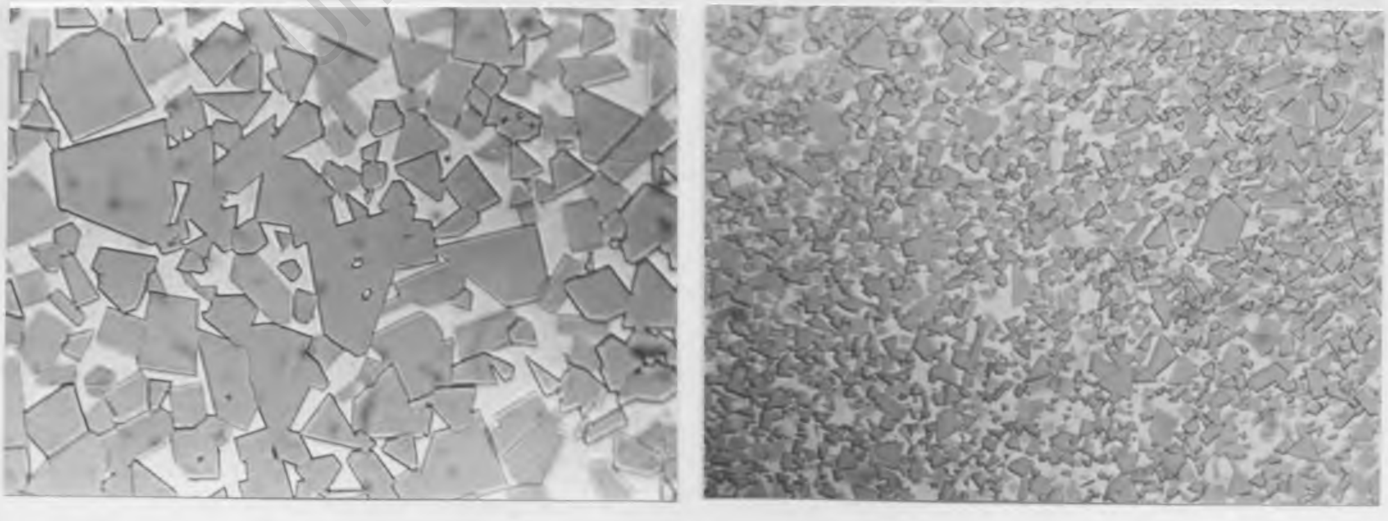

(e) WC/Co grade CT65

(f) WC/Co Lab grade A.

7μm

Fig.7.25 Microstructures of various cemented carbides.

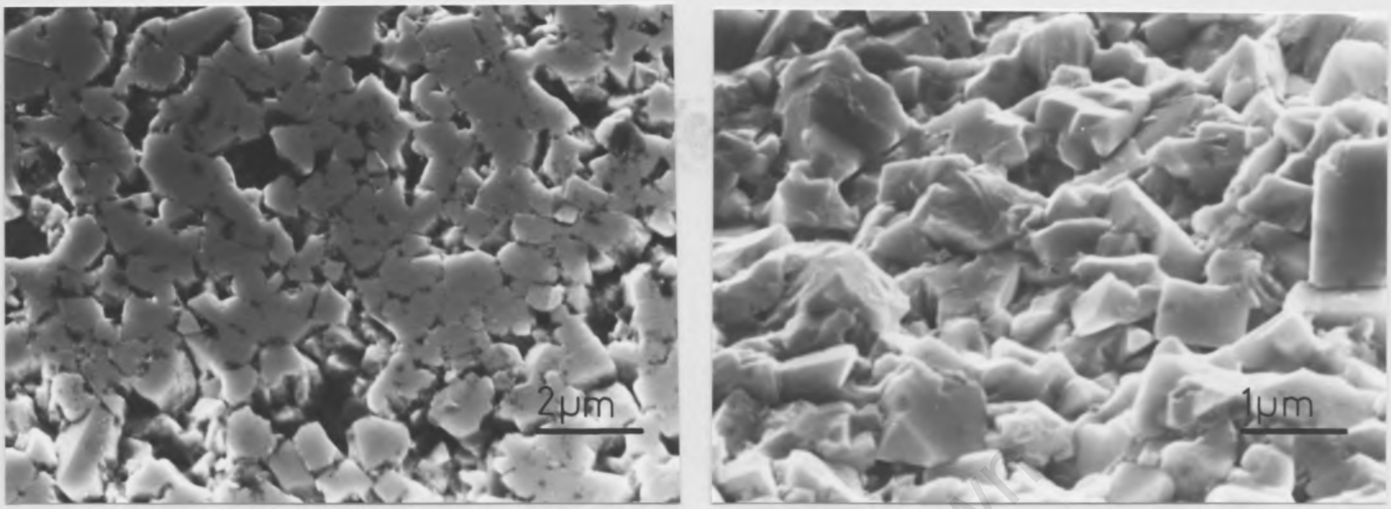

(a) Damage near edge of eroded area of grade 8LC (6800x).

(b) General damage of grade 8LC (13600x).

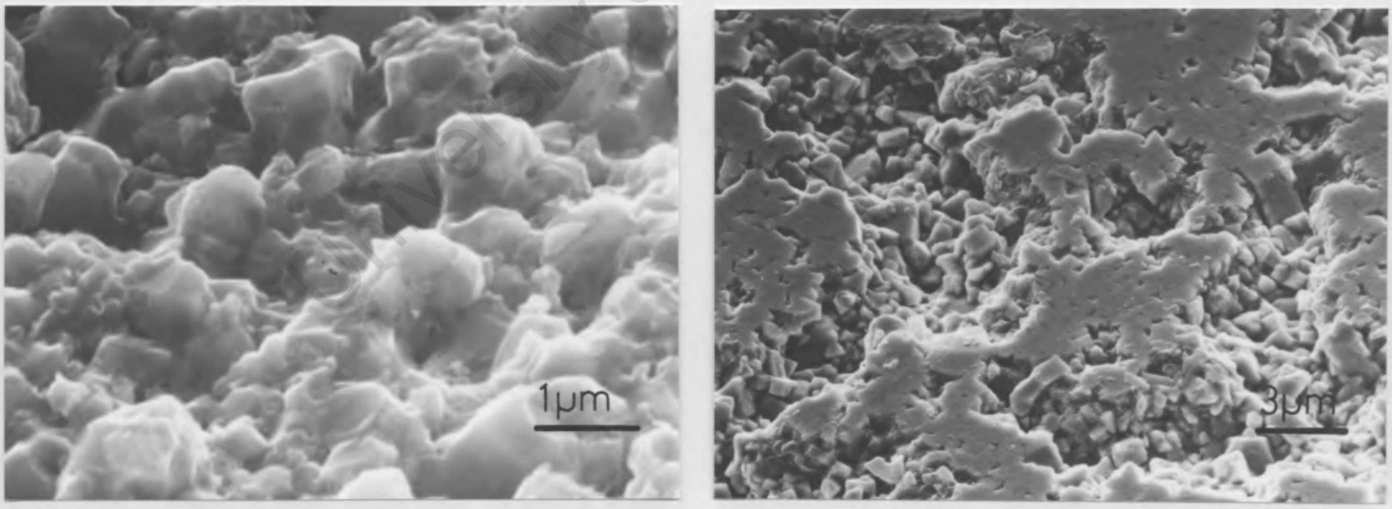

(c) General damage of grade CN02 (13600x)

(d) Damage near edge of eroded area of grade CG 20 (4000x).

Fig.7.26 Modes of erosion of cemented carbides.

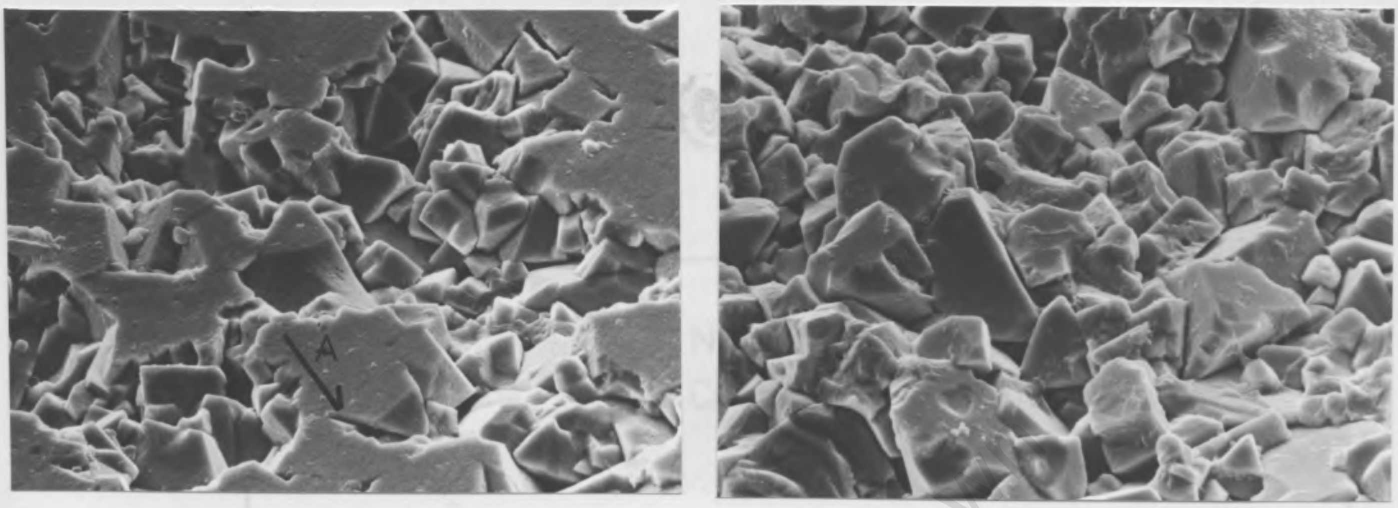

(e) Damage near edge of eroded area of grade CT30

(f)General erosion of grade CT30

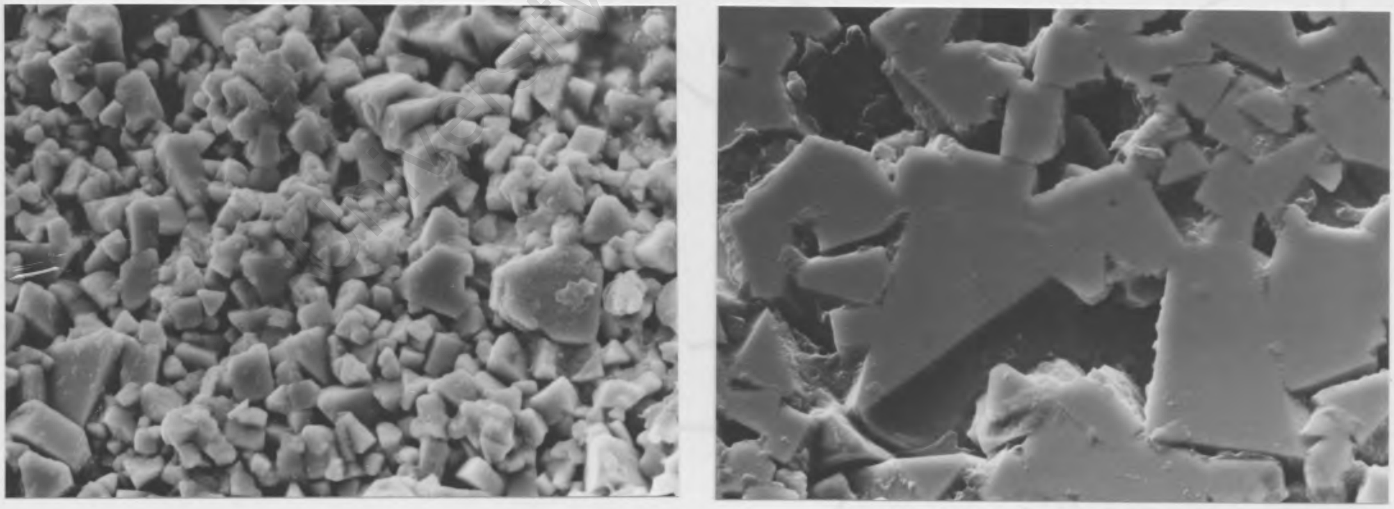

(g) Advanced erosion of grade CG 60

(h) Damage near edge of eroded area of grade CT65

Fig.7.26 Continued. (magnifications all 4000x)

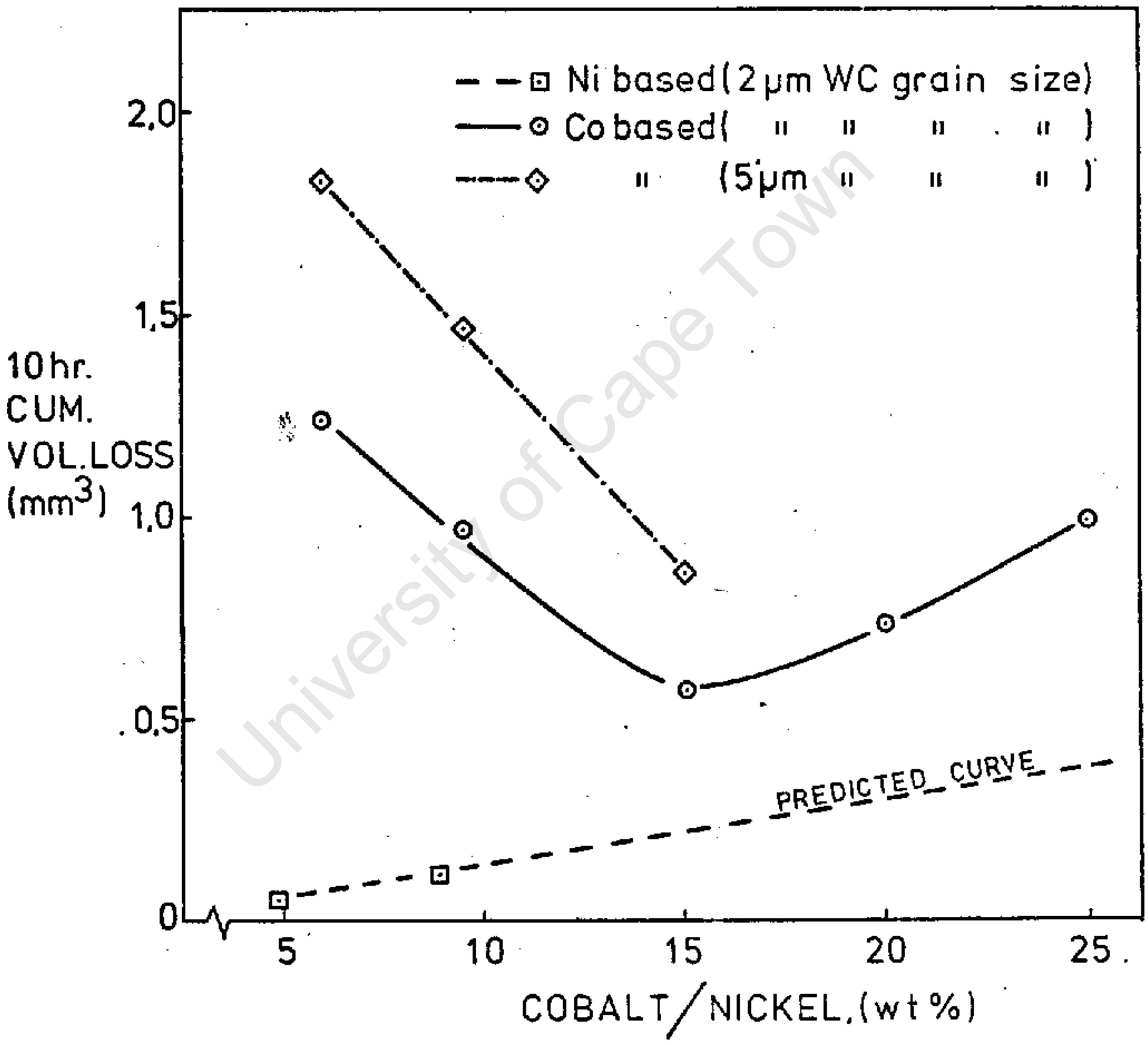

Fig.7.27 The effect of binder type,binder content and carbide particle size on the erosion resistance of cemented carbides.

The influence of the type *of binder metal* on the performance of the cemented carbides is not fully understood, but, it is proposed that the state of stress in these materials is an important factor in controlling erosion resistance. In the 'as sintered' condition residual stresses exist in the cemented carbides due to the differences in coefficients of thermal contraction (a) and also in elastic properties between the carbide phase and that of the binder. The thermal contraction coefficient of cobalt is approximately three times that of tungsten carbide (cobalt and nickel are about the same, $12 \times 10^{-6}\,^{\circ}C^{-1}$ and $13 \times 10^{-6}\,^{\circ}C^{-1}$ respectively). On cooling from high temperature, residual stresses are generated in the composites. The carbide grains are subjected to a triaxial compressive stress and the binder subjected to a triaxial tensile stress.

One can calculate the order of magnitude of the stresses in the binder phase using the model proposed by Newkirk and Sisler (108). This model considers *an* (annular) sphere of carbide phase, the centre or core of which, at high temperature contains liquid binder metal. As the system is cooled, the binder metal, having the higher a is placed under triaxial tension. Then by applying the equations developed by Timoshenko (109) for the strains in a three dimensional stress system, and assuming that the triaxial stresses are balanced by the triaxial strains and that the stresses and strains are equal along the three coordinate axes, then:

$$\varepsilon_{binder} = (\sigma_{binder}/E)(1-2\nu) \qquad \ldots\ldots\ldots\ldots\ldots\ldots\ldots\ldots\ldots\ldots\ 7.1$$

where ε_{binder} = strain in the binder phase
σ_{binder} = stress (tension) in the binder phase
E = Young's modulus of binder
ν = Poisson's ratio of binder

by rearranging equation 7.1 one obtains :

$$\sigma_{binder} = \varepsilon_{binder} E/(1-2\nu) \qquad \ldots\ldots\ldots\ldots\ldots\ldots\ldots\ldots\ldots\ldots\ 7.2$$

Using equation 7.2 and assuming that the residual strain in the binder is equal to the difference in the lattice parameter of pure nickel and the lattice parameter of the nickel phase in the cermet divided by the lattice parameter of pure nickel, Newkirk and Sisler(108) estimated that the residual stress in the nickel binder of TiC-Ni cermets was of the order of 1090MPa.

The residual stresses in the WC-Co cermets studied in this work are of much the same order as those in TiC-Ni samples, namely, 1200MPa (see Appendix 7.3). However, in the cobalt based carbides the residual stress pattern is also affected by the volumetric contraction associated with the allotropic awe transformation. This awe phase transition is well known in the WC-Co cermets (110,111). In the present study the phase change was followed by X-ray diffraction and Fig. 7.28 shows the XRD traces of WC-Co, grade CT65, before and after erosion. The samples were all partially transformed prior to the erosion test as a result of mechanical prepolishing, however, further transformation occurred during the erosion test. Sarin and Johannesson (111) report that a complete transition from FCC to HCP form induces a shear which ultimately results in a tensile strain of c6%. They also point out that in compression testing of WC-Co samples less than 10% transformation occurs prior to fracture which implies that failure starts at about 0,6% strain. In the present work it would appear from the relative intensities of the FCC (111) and HCP (101) peaks that about 50% transformation has occurred after exposure to cavitation for 10 hours.

The important characteristic of this strain accompanying the transition is that it is tensile in nature. This will lead to an increase in the tensile stresses within the cobalt binder and in fact one can estimate the increase in stress using equation 7.2. If it is assumed that the extent of transformation is about 25%, then according to Sarin and Johannesson (111) the tensile strain in the cobalt as a result of the transition will be approximately 1,5% or E_{CO}=0,015. Then by equation 7.2

$$\sigma_{Co} = 0{,}015 \times 215 \times 10^3 / 0{,}36$$

and $$\sigma_{Co} = 8958\text{MPa}$$

Although this estimate of stress is most likely far higher than the actual stresses in these materials,this calculation does indicate that very small transition induced strains can result in very high stresses in the binder phase.

The carbide phase is known to form a continuous skeleton (111,112,113)e and it is assumed that the rigidity of this skeleton is sufficient to withstand the shrinkage stresses of the matrix. (The ability to withstand deformation will be a function of carbide content and carbide grain size). Thus when the matrix undergoes a phase change,the tensile stresses are increased in the binder and the cobalt-carbide bond will be weakened. It is conceivable that in some instances actual debonding occurs between the cobalt matrix and carbide particles. The erosion mechanism described earlier indicated that the interfacial bond plays an important role in the erosion of WC-Co cemented carbides and hence any factor leading to a weakening of this bond must also result in a decrease in erosion resistance. Since the nickel based grades 8LC and 8MC do not undergo a phase change, it is reasonable to expect that they should have a higher resistance.

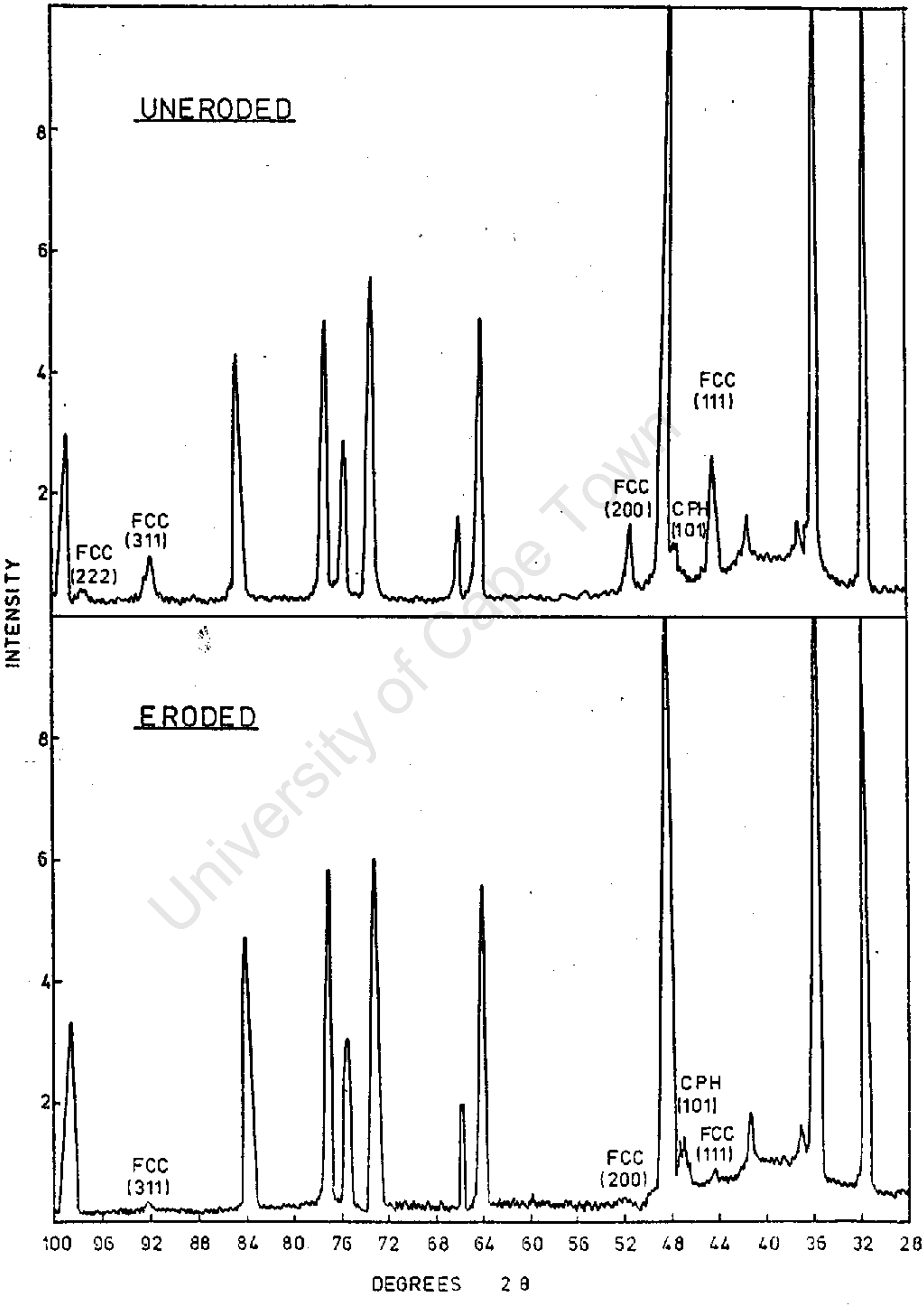

Fig.7.28 The structure of WC/Co grade CT65 before and after erosion.

The effect of binder content on the cobalt and nickel based cermets (see Fig. 7.27) can be explained in terms of the hardness of the binder phase and the influence of the phase transition. The graph shows that the 2um grain size cobalt based samples increase in erosion resistance as the binder content decreases from 25% to 15%. This is considered to be the consequence of an increase in plastic constraint and therefore hardness of the binder phase. Dawihl and Frisch (1 13)report that the microhardness of the matrix phase in WC-Co cermets increases from HV660 for 25% cobalt content up to HV825 (in a 6% cobalt content composite) (see Fig. 7.29). The increased hardness of the matrix results in an increase in erosion resistance of this phase and thus of the composite.

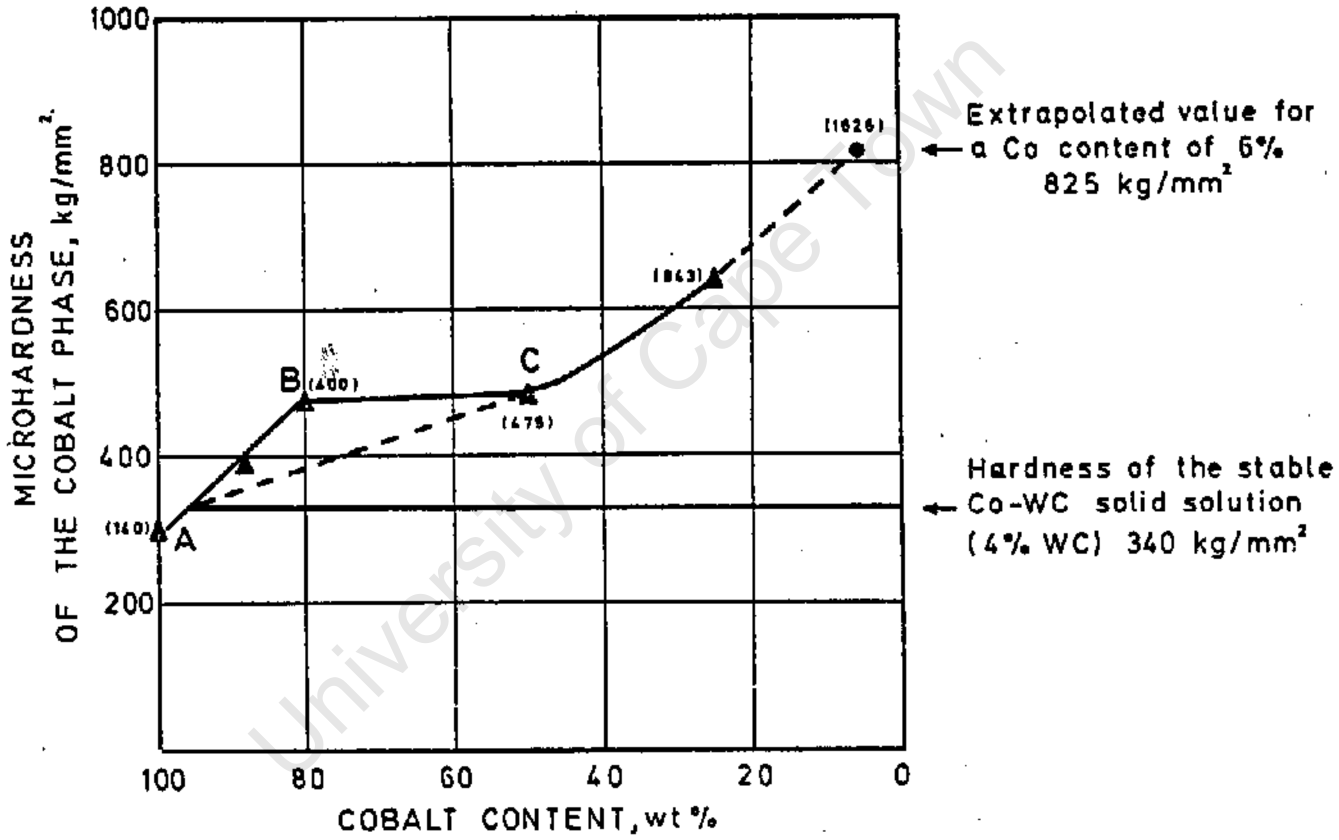

Fig. 7.29 The Hardnesses of the Binder Phase and Bulk Composite as a Function of the Binder Content in WC-Co Cermets (---●--- hardness of matrix, ——▲—— bulk hardness) (Ref.113)

of a rapid increase in the contiguity* of these composites for cobalt contents < 15% (see Fig. 7.30) (112) .

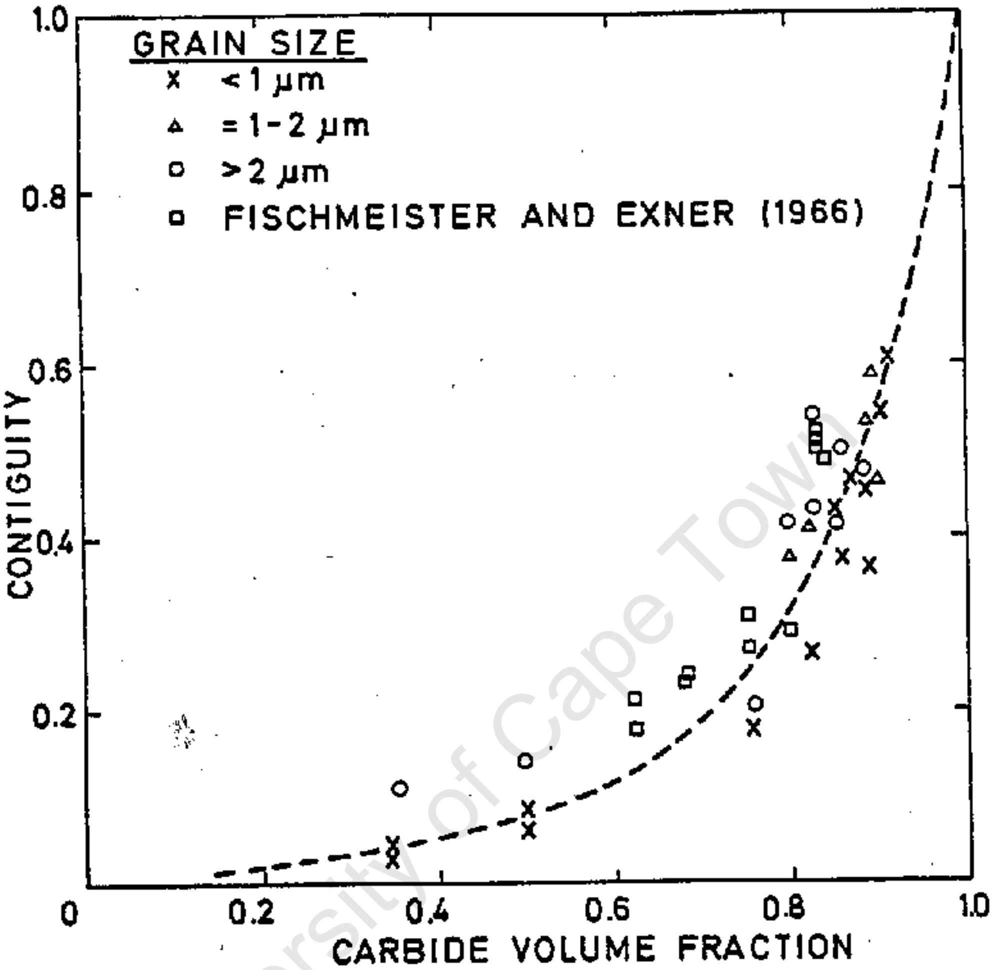

Fig. 7.30 Contiguity as a Function of Binder Content (Ref.112)

This effect, in turn, leads to a large increase in the rigidity of the carbide skeleton and the carbide phase has a greater ability to withstand the transition induced stresses. This effect further promotes cracking at the carbide - matrix interface and offsets any benefit derived from hardening of the binder due to an increase in plastic constraint. Thus the binder is removed more easily by the forces of cavitation and the erosion rates of these samples increase accordingly.

The carbide grain size also influences the erosion resistance of the cobalt based carbides (see Fig. 7.27). An increase in grain size from 2um to 51.1m results in a consistent increase in CVL for increasing carbide content (85% to 94%). The larger carbide particle size results in lower packing densities in the carbide

---

** Lee and Gurland(112)define contiguity as being that fraction of the total internal surface area of a sample which involves carbide to carbide interfaces.*

phase. The mean free path* in the binder phase is increased (112)and consequently the plastic constraint and hence hardness of the binder phase are decreased as indicated by bulk hardness values** - see Table 7.10. The decrease in hardness results in a small increase in the erosion rates of these large grain size samples.

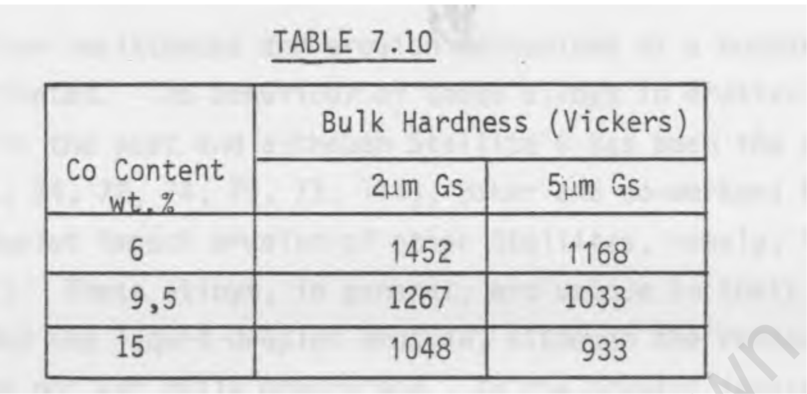

TABLE 7.10

Co Content wt.%	Bulk Hardness (Vickers)	
	2µm Gs	5µm Gs
6	1452	1168
9,5	1267	1033
15	1048	933

The lower erosion resistance of the complex carbide, grade CNO2, compared with the WC-Ni grades is also of interest. The explanation for this result may lie in the morphology and distribution of the carbide particles. The microstructure (Fig. 7.25(b)) shows that the carbides vary in shape while the mean free path length between the particles is greater than in similar tungsten carbide samples (grades 8MC or CG20). Moreover the material appears to consist of 3 phases : a grey phase incorporating darker, needle like equiaxed particles (presumably the TiC particles) plus a lighter phase which, presumably, is the Ni-Co binder. This is more obvious from the SEM micrograph (Fig. 7.31) of the uneroded surface of this material.

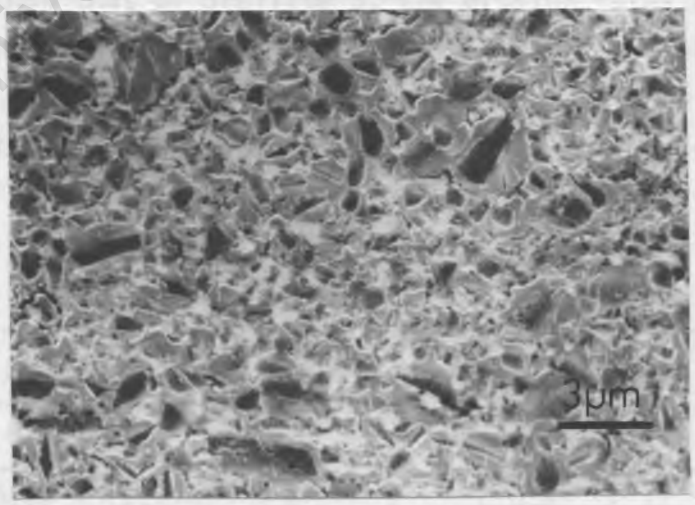

Fig. 7.31 SEM Micrograph of Uneroded Grade CNO2

** The mean free path in the binder is a function of carbide grain size, volume-fraction of binder and contiguity.*

*** Bulk hardness values are directly related to hardness of binder phase. (See fig.7.29)*

Examination of the fracture surface (see Fig. 7.26(c))also shows that the resistant carbide particles are not in intimate contact. Hence the lower erosion resistance of grade CNO2 is due partly to the lower concentration of resistant carbides and also partly to the lack of a continuous carbide skeleton.

7.1.6 Stellites

The erosion resistances and erosion mechanisms of a number of Stellite alloys have been evaluated. The behaviour of these alloys in erosive environments has been studied in the past and although Stellite 6 has been the subject of most of this work (30, 34, 72, 74, 75, 77, 114), Baker and co-workers have investigated the liquid droplet impact erosion of other Stellites, namely, Stellites 1, 4, 7, 8 and 12 (114). These alloys, in general, are unique in their ability to resist both cavitation and liquid droplet erosion, although the reasons for this high resistance are not yet fully understood. In the present investigation Stellites 3, 4, 6, 8, 20 and 2006 have been evaluated. These were selected to determine the effects of varying hardness, composition and nature of microstructure on mechanisms of erosion resistance and modes of erosion.

These Stellite alloys, as expected, constitute some of the most erosion resistant materials tested and are comparable with the two nickel based tungsten carbides and the intermetallic compound NiTi. Predictably Stellites 3 and 20 are the most erosion resistant of the group since they are of similar high macro-hardnesses. Stellite 20, however, is less resistant than Stellite 3 and the CVL figures in Table 7.11 indicate that Stellite 20 lost nearly twice as much material as Stellite 3. Also note that, although the incubation time of Stellite 20 is less than that of Stellite 3, the erosion rates after t_o are approximately the same. These results confirm again that hardness is an unreliable criterion for erosion resistance prediction, even within a group of alloys like the Stellites, since Stellite 20 has a higher hardness than Stellite 3.

TABLE 7.11

Alloy	Main alloying elements						CVL 40 hrs	t_o hrs	$\dot{E}$ mm^3/hr	V.H.	R_n
	C	Cr	W	Mo	Fe	Ni					
Stellite 3	2,61	30,2	11,9				0,53	12,5	0,022	531	106
Stellite 4	1,17	31,3	14,0		1,06	0,16	1,00	7,5	0,031	501	94
Stellite 6	1,15	24,3	5,11	0,27	3,32	1,43	1,15	7,5	0,037	399	80
Stellite 8	0,27	27,0	-	5,25	0,78	2,86	1,24	7,5	0,040	335	78
Stellite 20	2,35	33,1	16,3	-	2,22	1,38	0,93	7,5	0,030	610	106
Stellite 2006	1,40	30,3	-	6,3	19,8	7,7	1,94	5,0	0,054	440	90

The lower erosion resistance of Stellite 20 compared with Stellite 3 is considered to be due, primarily, to the differences in microstructure between the two alloys which, in turn, govern the modes of erosion (see Fig. 7.32 (a)-(d) and Fig. 7.33(a)-(d)). Stellite 3 consists of a regular dendritic structure of Cr_7C_3 and W_6C carbides in a cobalt rich solid solution matrix while Stellite 20 has a more heterogeneous structure of acicular Cr_7C_3 carbides in a fine eutectic matrix (73 , 115). The micrograph and EDAX spectra in Fig. 7.32(c) show that in Stellite 3 the carbides are removed first in the early stages of erosion although some material is also lost from the matrix phase at points where twin boundaries intersect (see Fig. 7.32(d)). However, not all the carbide phase is 'weak' since it has been observed that the acicular eutectic areas of this phase are more resistant than both the matrix and the dendritic carbides. Stellite 20, on the other hand, with its heterogeneous microstructure, has a greater number of erosion nucleation sites in the form of carbide/matrix interfaces at which erosion can be initiated (see Figs. 7.33(c) and (d)). Furthermore the Cr7C3 carbides in this alloy are considerably harder than they are in Stellite 3 as a result of the higher alloying element content(115) (DPH 1860 for Stellite 20 cf. DPH 1100 in Stellite 3). The Cr7C3 carbides in Stellite 20 have low toughness* and undergo brittle fracture. pus more carbide is lost at an earlier stage on exposure to an erosive environment compared with Stellite 3.

The differences in t_o are therefore primarily due to microstructural differences. But after t_o the surfaces of the specimens are severly deformed and surface nucleation sites have less influence on erosion of these alloys, and thus the steady state E values are much the same. Although carbides are detrimental in that they reduce t_o,it is conceivable that they can also be beneficial by acting as barriers to crack propagation at times, $t > t_o$. The higher erosion resistance of Stellite 3 compared with the other alloys must be a function of the fine, regular carbide phase in this alloy.

Stellites 4, 6 and 8 have erosion resistances nearly identical to that of Stellite 20 in spite of steadily decreasing bulk macrohardness values (see Table 7.11) These results can be explained as follows : Stellites 4 and 6 have similar compositions except for tungsten content. Figs. 7.34(a)-(d) and Fig. 7.35(a)-(c) show the microstructures and modes of erosion of the two alloys. Stellite 4 is comprised of a dendritic structure of (Cr_7C_3 , W_6C + cobalt rich solid solution) eutectic interspersed with islands of a Cr/Co rich solid solution phase. Clearly

---

* *Note that the tungsten carbide particles in the cermets discussed in the previous section do not undergo brittle fracture like the* Cr_7C_3 *particles in Stellite 20 in spite of WC having a far higher hardness (HV2000). This would indicate that tungsten carbide has a higher toughness (less notch sensitive) than chrome carbide under the high strain rate loading of cavitation.*

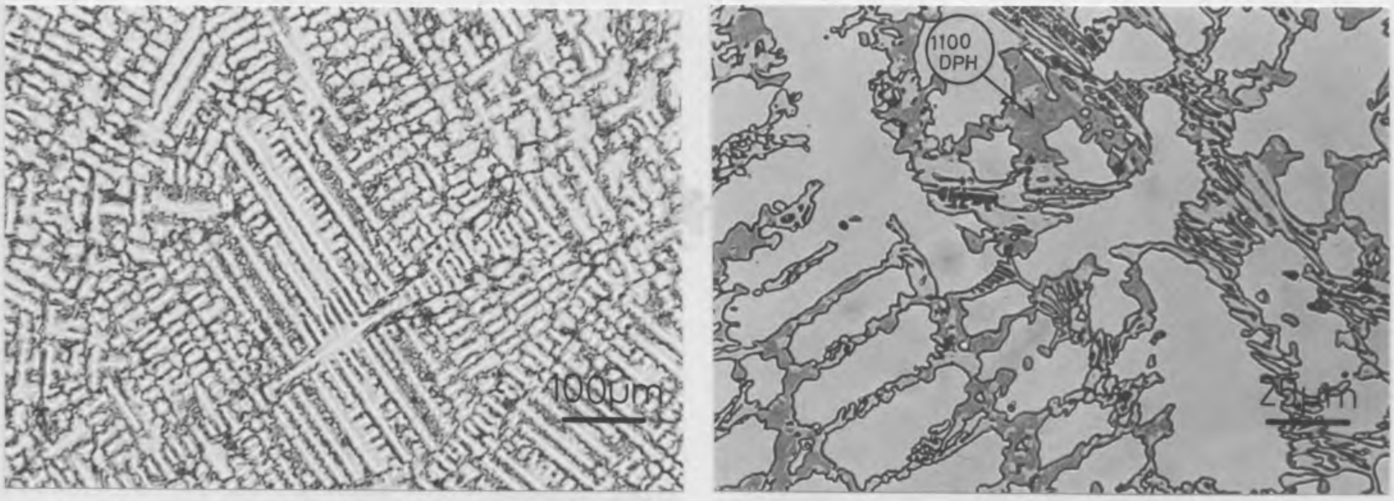

(a) Microstructure (110x)

(b) Microstructure (435x)

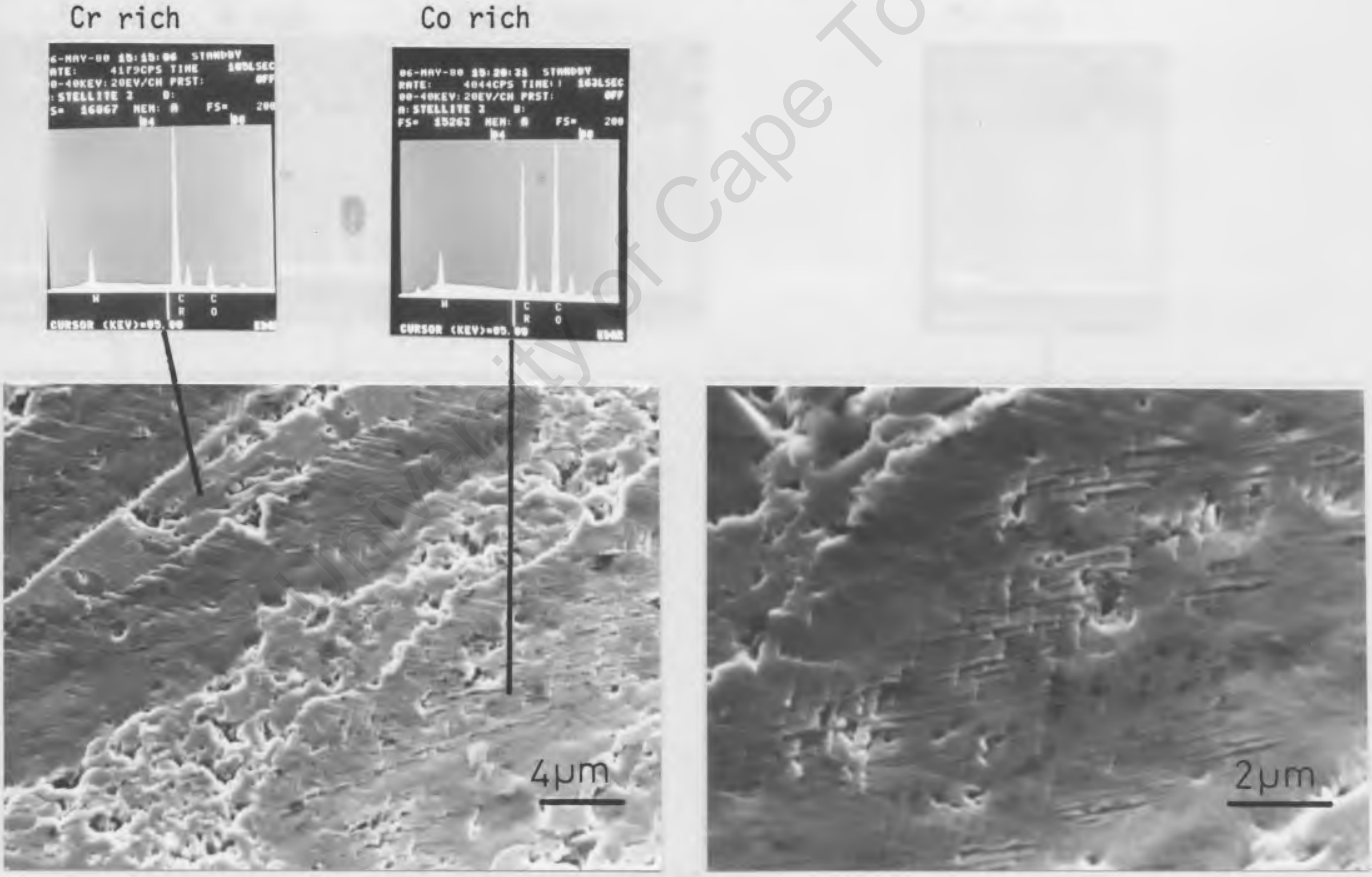

```
6-MAY-80 15:15:06  STANDBY
ATE:     4179CPS TIME    105LSEC
0-40KEV: 20EV/CH PRST:       OFF
:STELLITE 3    B:
S=  16067  MEM: A    FS=     200
W      C   C
       R   O
CURSOR (KEV)=05.00            EDX
```

```
06-MAY-80 15:20:31  STANDBY
RATE:     4044CPS TIME:  163LSEC
00-40KEV: 20EV/CH PRST:       OFF
A:STELLITE 3    B:
FS=  15263  MEM: A    FS=     200
W      C   C
       R   O
CURSOR (KEV)=05.00           EDAX
```

(c) Preferential removal of chrome carbide phase (2700x)

(d) Material loss from twin boundary intersections (6800x).

Fig.7.32 Microstructure and mode of erosion of Stellite 3.

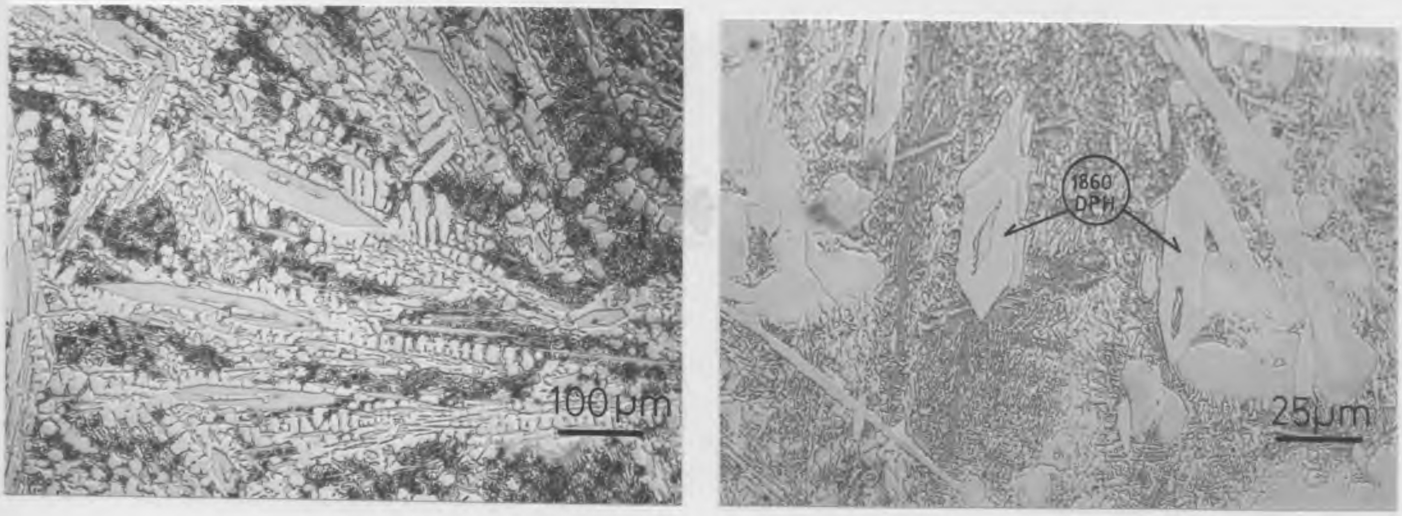

(a) Microstructure (110x)

(b) Microstructure (435x)

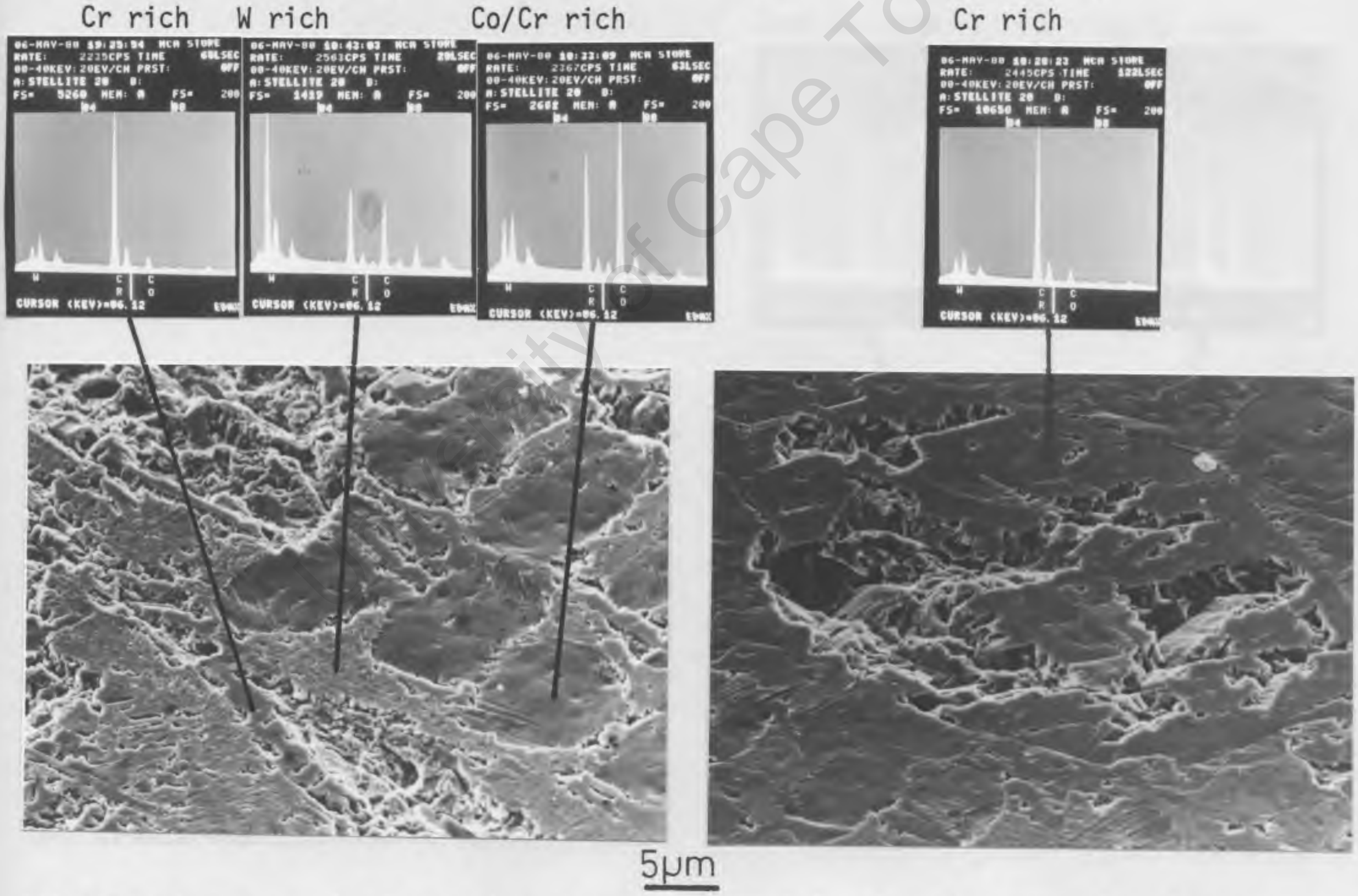

(c) Selective removal of acicular chrome carbides and cracking at the solid solution phase/eutectic interface (2000x)

(d) Selective fracture of a chrome carbide (2000x)

Fig.7.33 Microstructure and mode of erosion of Stellite 20.

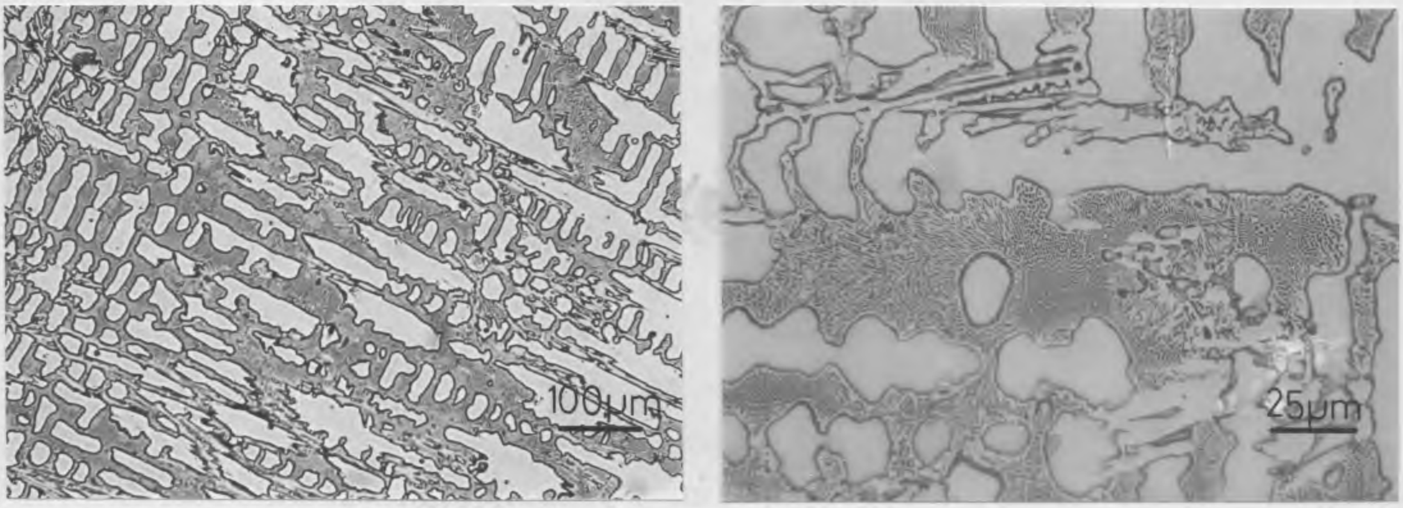

(a) Microstructure (110x)

(b) Microstructure (435x)

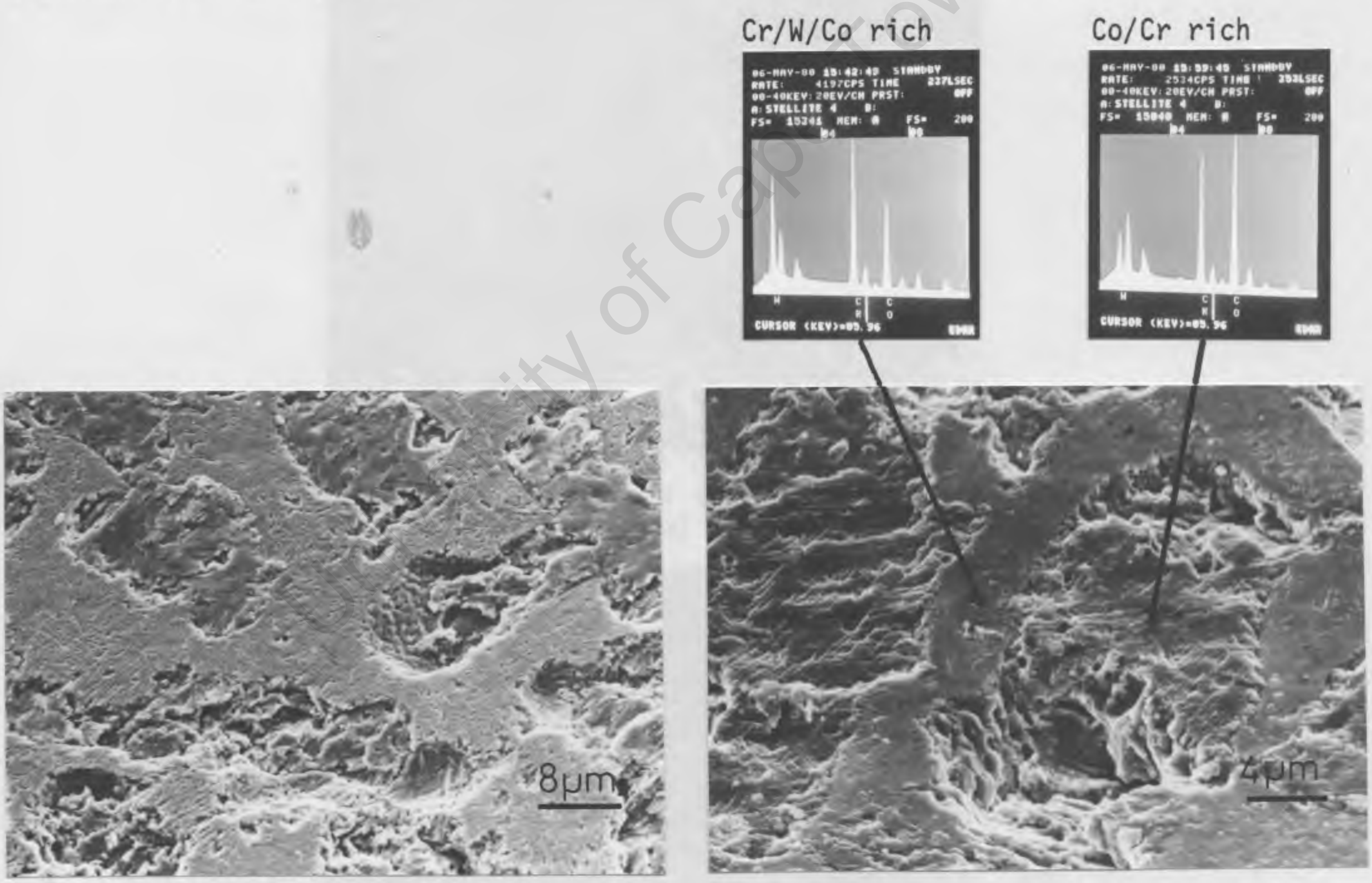

(c) Damage near edge of eroded area (1360x)

(d) Preferential removal of cobalt rich matrix phase (2700x)

Fig. 7.34 Microstructure and mode of erosion of Stellite 4.

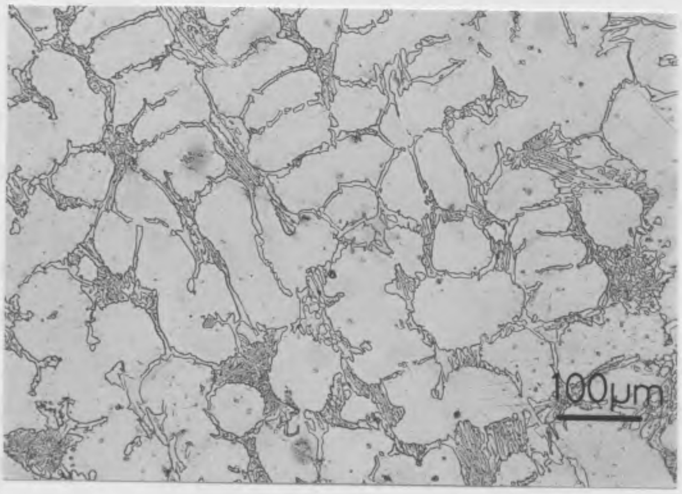

(a) Microstructure (110x)

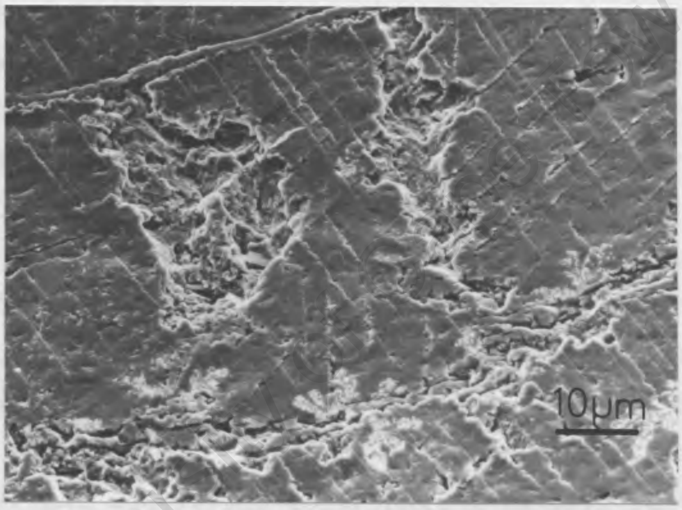

(b) Damage near edge of eroded area showing preferential removal of carbide phase (1100x)

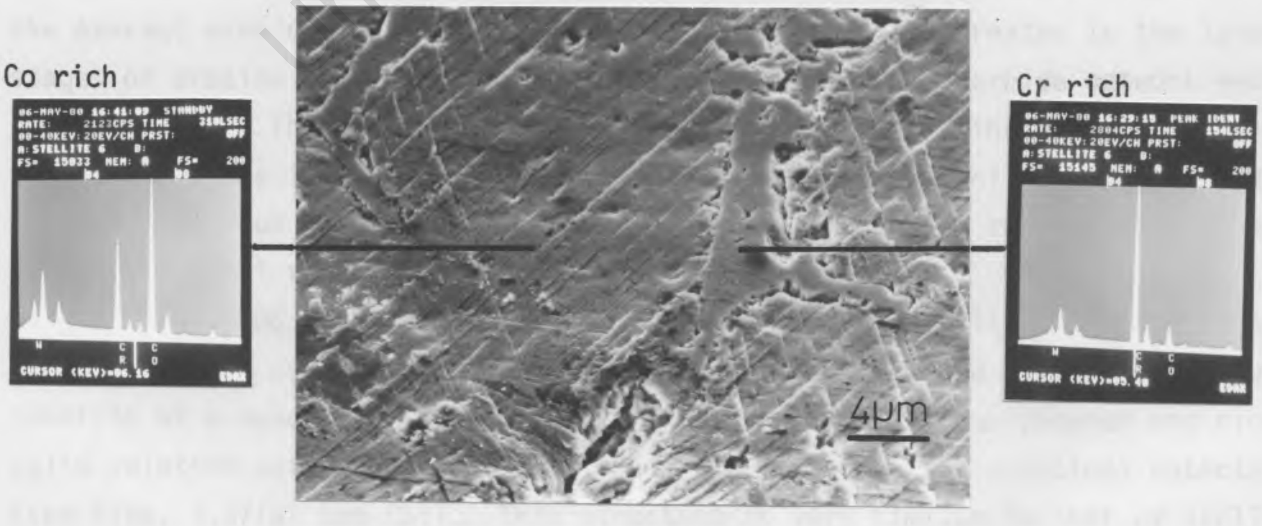

(c) Interface cracking and selective carbide removal (2700x)

Fig. 7.35 Microstructure and mode of erosion of Stellite 6.

the insular solid solution phase is removed first in the early stages of erosion while the remaining eutectic phase withstands the erosive environment (see Fig. 7.34(c) and (d)). On the other hand Stellite 6 has a similar erosion mechanism to Stellite 3 - the carbide phase is removed preferentially. Also it is less predominant in the overall microstructure (Figs. 7.35(b) and (c)). Interestingly, in spite of the differences between these alloys, their erosion resistances are much the same.

Stellite 8, in turn, is not much less erosion resistant than Stellites 4 and 6,although it has a very low carbon content (0,27%), and consequently,a lower macro-hardness than both these alloys. Its microstructure consists almost entirely of a cobalt, chrome and molybdenum rich solid solution interspersed with traces of carbide (see Fig. 7.36(a)). On exposure to cavitation extensive twinning occurs and a network of fine twin boundaries forms in the surface regions of the specimen. The alloy erodes by initial loss of carbide followed by loss of matrix material from twin boundary intersections (see Fig. 7.36(b) and (c)). Since the resistance of Stellite 8 is similar to that of alloys 4, 6 and 20 it is clear that the role played by carbides in resisting erosion is small compared with that of the cobalt rich solid solution phase.

This apparent unimportance of carbides has been reported before. Gould (76) found that the erosion of Stellite 6B is little altered whether carbides are present or absent. More recently, Antony and Silence(77) reported that the resistance of 1,0% carbon Stellite 6B is little different to that of a similar, low carbon alloy. Clearly the cobalt rich solid solution is the erosion resistant phase and the important mechanisms contributing to this resistance are discussed later in this section.

Another feature of Stellite 8 is that its erosion rate is initially less than the average erosion rates of Stellites 4, 6 and 20 but is greater in the later stages of erosion. This is probably due to the lack of a carbide network embedded in the matrix. The initial erosion rate is reduced due to the absence of nucleating sites in the form of matrix/carbide interfaces while in the more advanced stages of erosion the lack of barriers to crack propagation results in a greater rate of material removal than in Stellites 3, 4, 6 and 20.

Stellite 2006, is less resistant than Stellite 8. Stellite 2006 has higher nickel and iron contents than any of the other Stellites and the microstructure consists of a dendritic network of a chrome, cobalt, iron, molybdenum and nickel rich solid solution matrix plus (Mo_6C, Cr_3C_7 + cobalt rich solid solution) eutectic (see Figs. 7.37(a) and (b)). This structure is very similar to that of Stellite 4 and it is interesting that the erosion mechanism is also similar, that is, the matrix phase is removed before the eutectic phase in the early stages of erosion (see Figs. 7.37(c) and (d)).

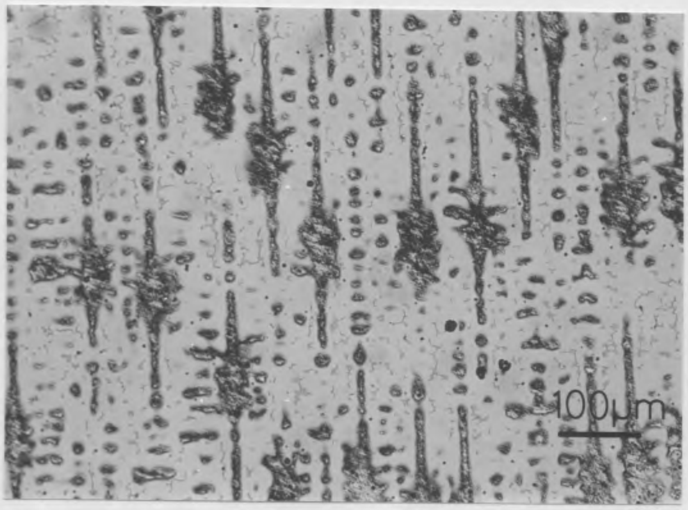

(a) Microstructure (110x)

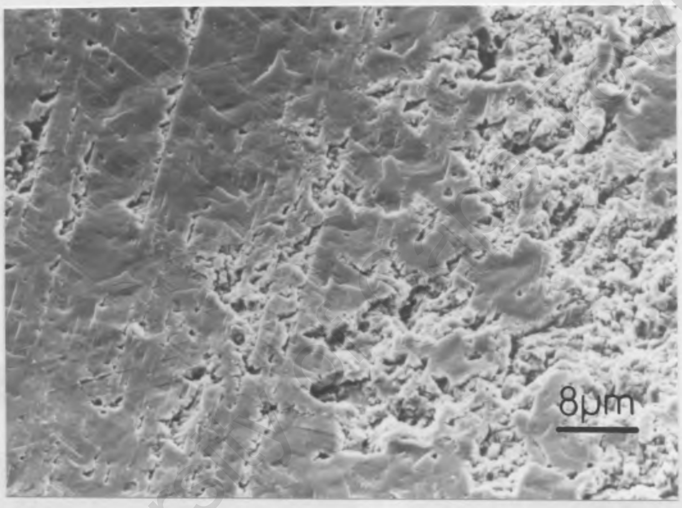

(b) Damage near edge of eroded area (1360x)

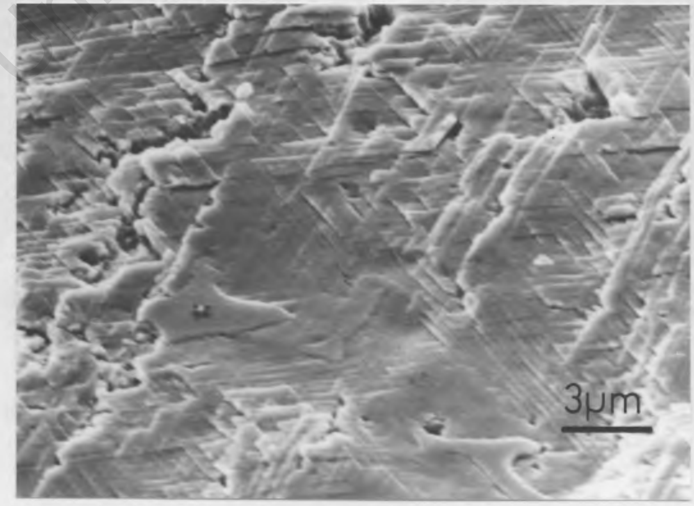

(c) Material removal at twin boundary intersections (4000x)

Fig. 7.36 Microstructure and mode of erosion of Stellite 8.

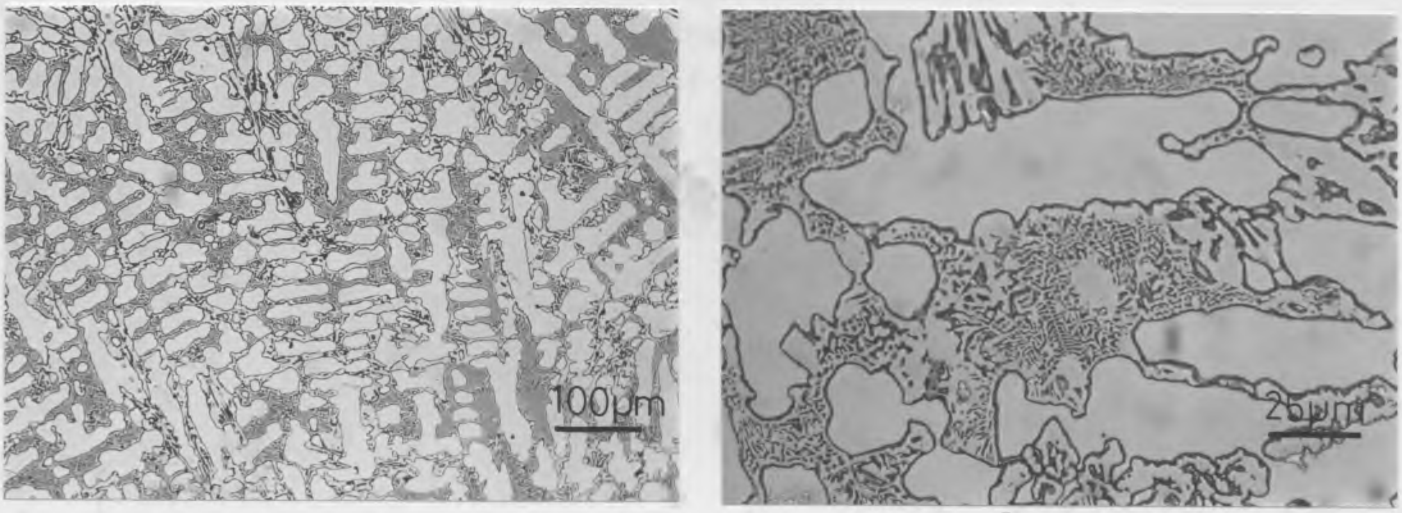

(a) Microstructure (110x)

(b) Microstructure (435x)

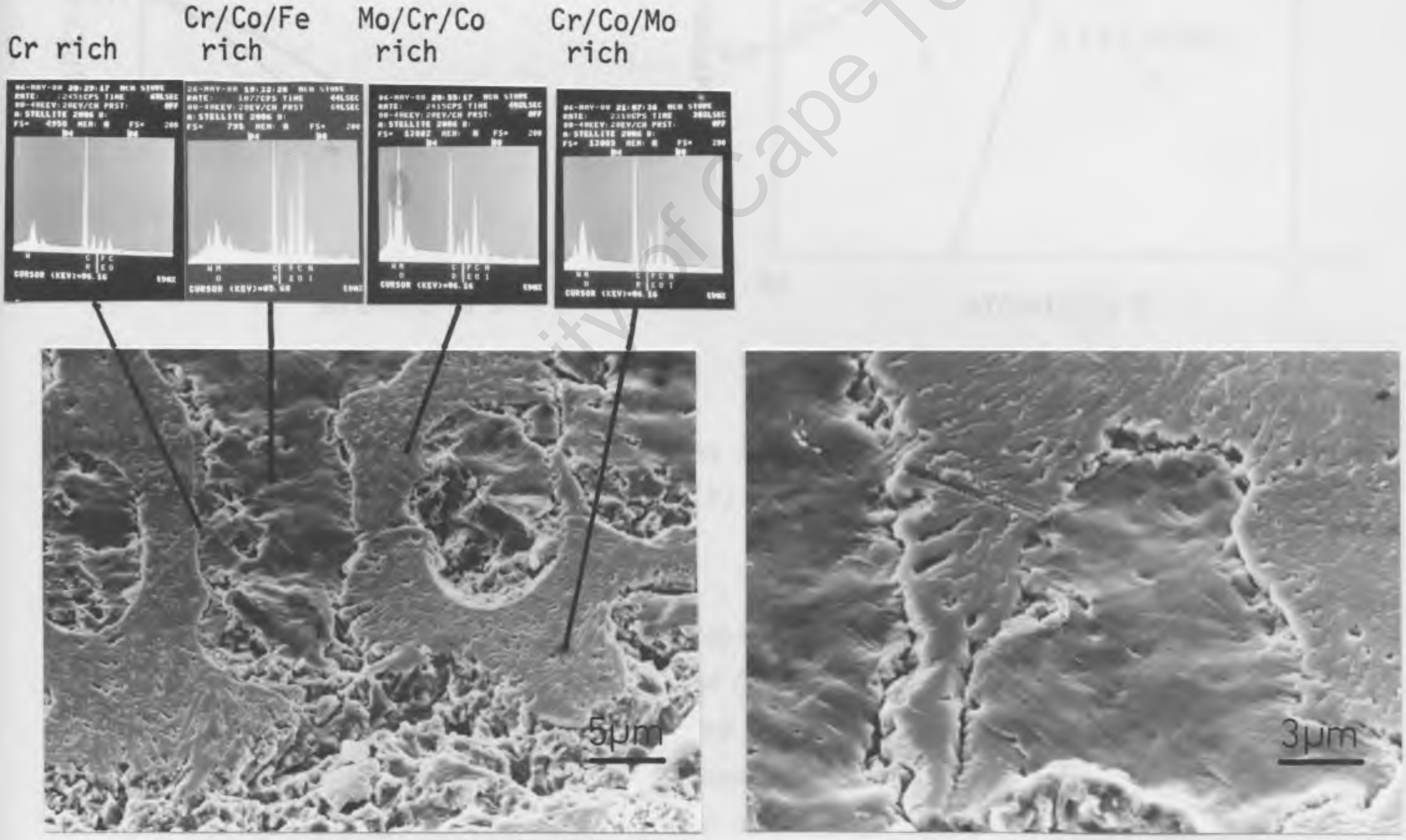

(c) Selective removal of matrix phase (2000x)

(d) Cracking at the matrix/eutectic interface (4000x)

Fig. 7.37 Microstructure and mode of erosion of Stellite 2006.

The lower erosion resistance of Stellite 2006 is in agreement with the findings of Woodford (72) and Woodford and Beattie(116)on Co-Fe alloys and can be explained as follows : additions of chromium, tungsten and molybdenum stabilize the HCP phase in cobalt alloys while additions of iron and nickel tend to stabilize the FCC structure (117)(see Fig. 7.38) which implies that these latter elements increase the stacking fault energy (SFE) of cobalt alloys.

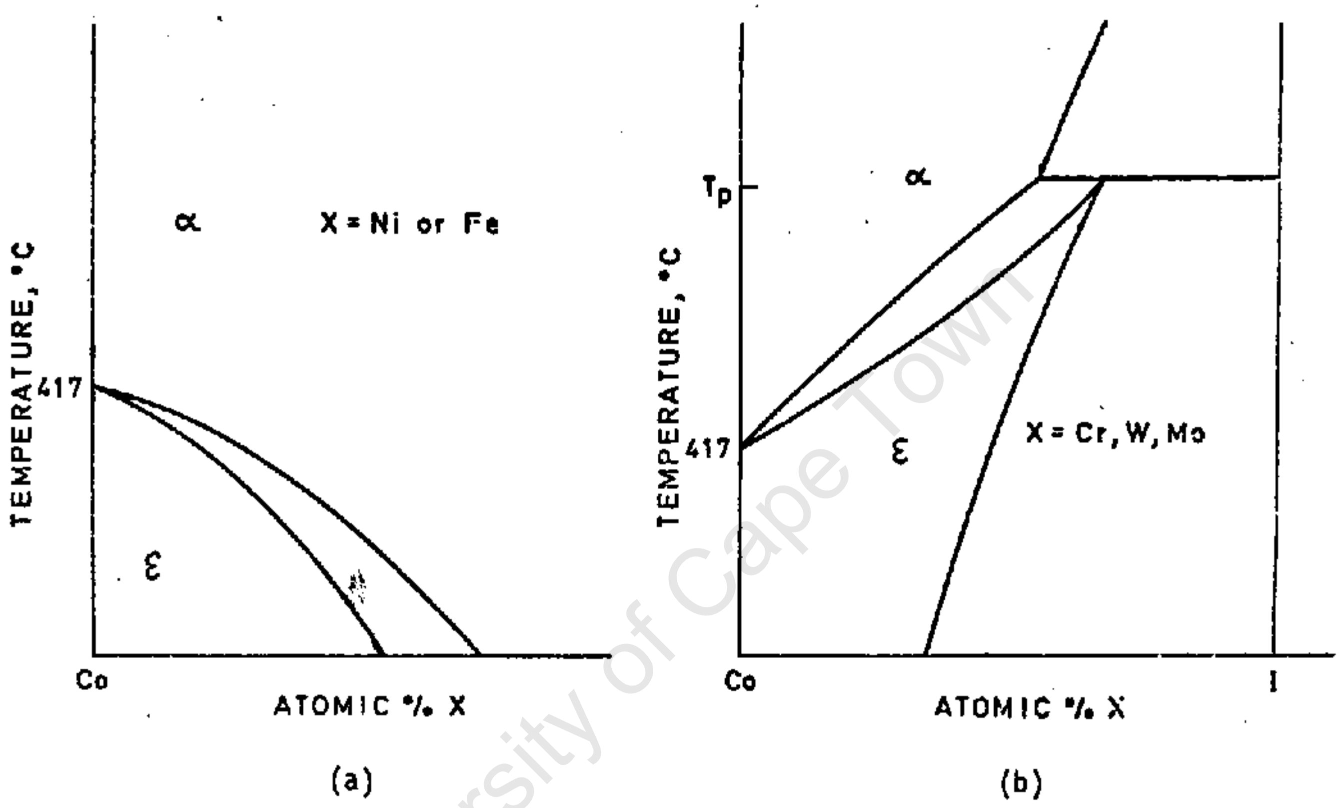

Fig. 7.38 The Effect of Various Alloying Elements on the Phase Diagram of Cobalt (a) Nickel and Iron (b) Chromium, Tungsten and Molybdenum (Ref. 117)

The effect of nickel on the SFE of cobalt alloys has been reported by Remy and Pineau (118)and Graham and Youngblood (119). In the present study, evidence of this stabilization of the FCC structure in Stellite 2006 was obtained by X-ray diffractometry (XRD). The XRD traces of Stellite 3 and Stellite 2006 after mechanical polishing but prior to erosion are shown in Figs. 7.39 and 7.40. A qualitative estimate of the relative amounts of the FCC and HCP phases are given by the ratio (119) :

$$I_r = I_{(101)_{hcp}} / I_{(200)_{fcc}}$$

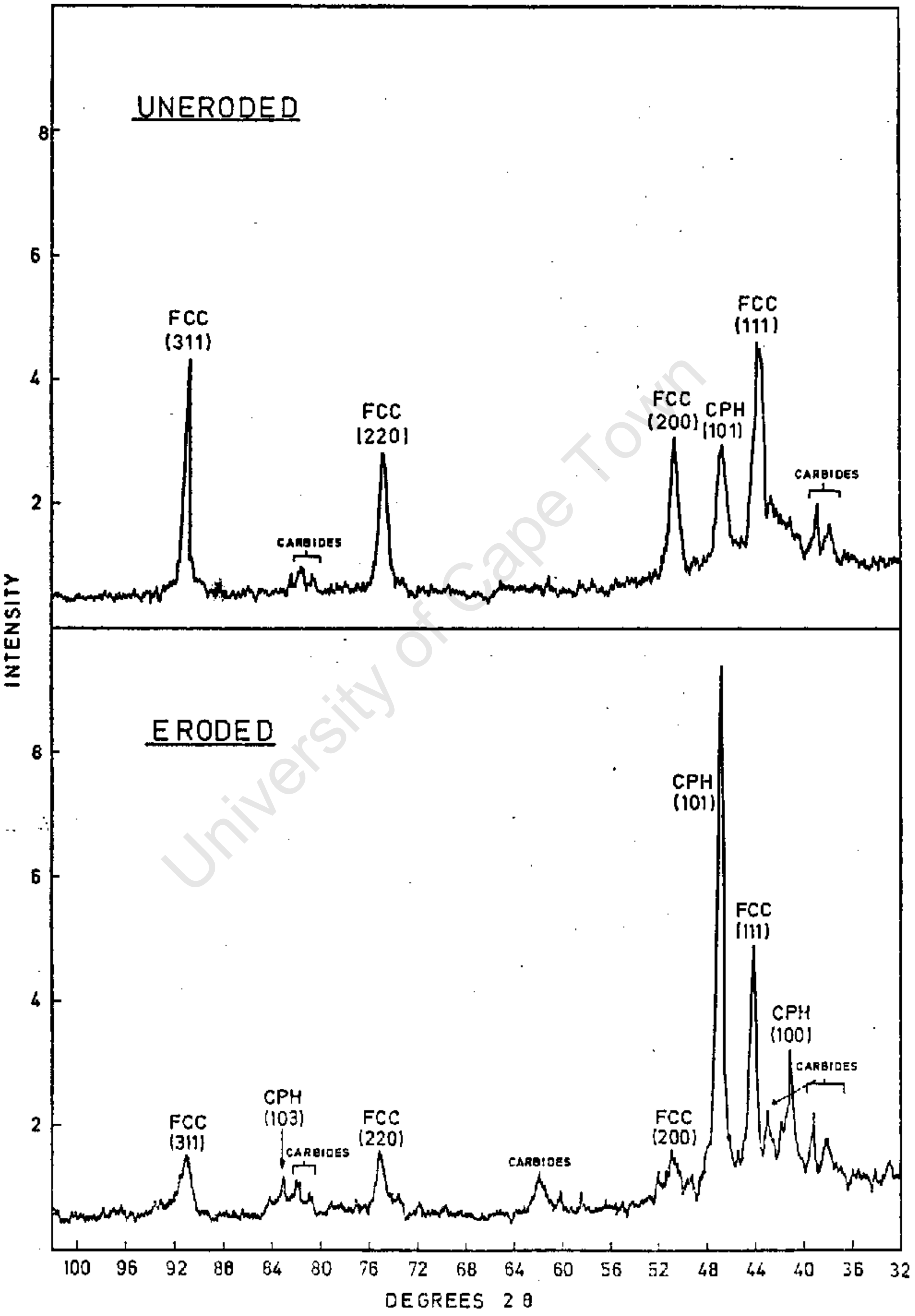

Fig. 7.39 The structure of Stellite 3 before and after erosion.

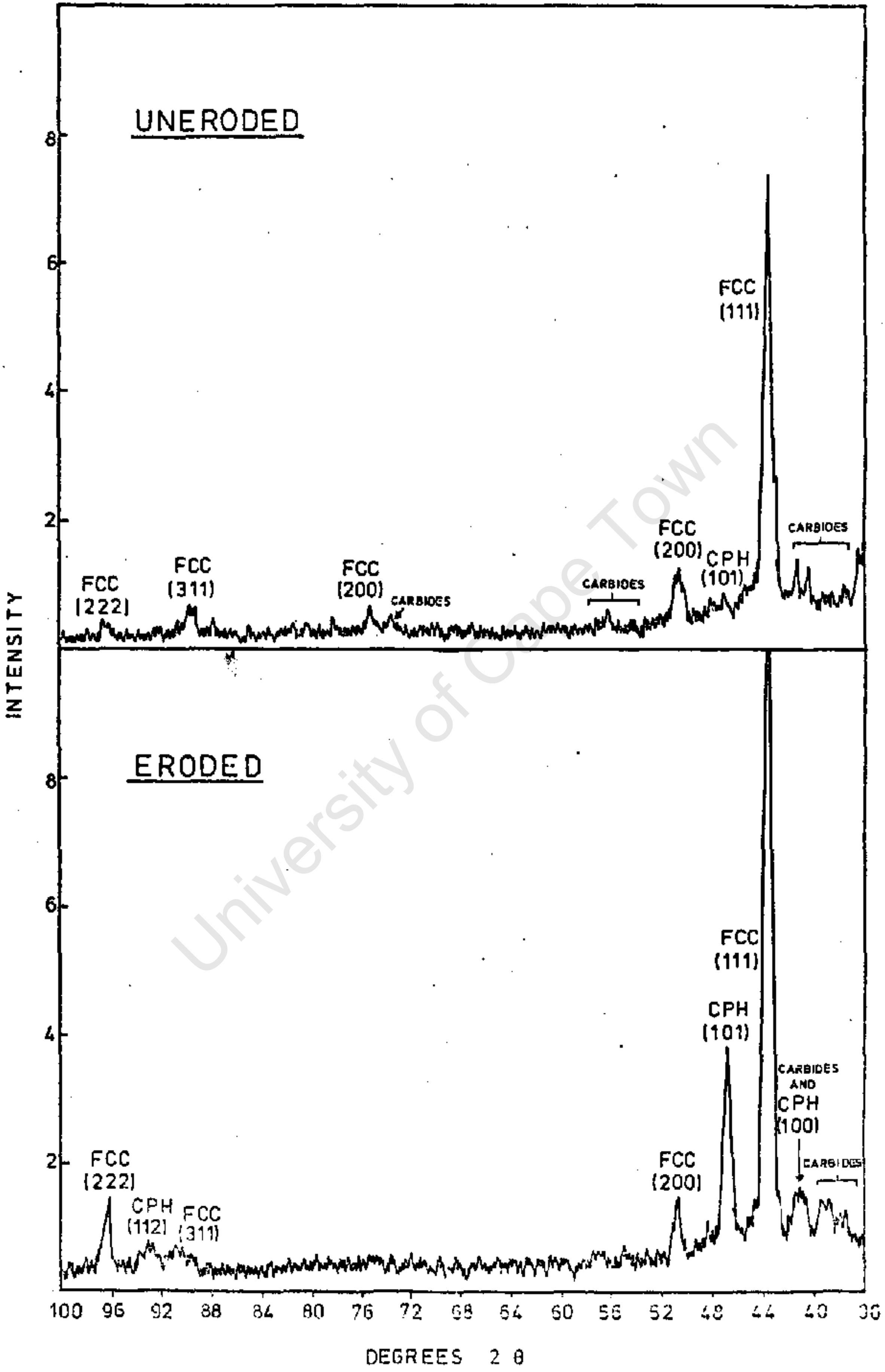

Fig.7.40 The structure of Stellite 2006 before and after erosion.

The ratios for the two alloys before and after erosion are listed in Table 7.12 which shows that during erosion less aye transformation occurs in Stellite 2006 than in Stellite 3. Note that a small amount of HCP phase is present in both alloys before erosion. This is the result of mechanical prepolishing. Also note that Stellite 2006 is less transformed than Stellite 3 at this stage as well. These results are in accordance with the compositions and expected SFE's of the respective alloys.

TABLE 7.12

Alloy	I_r Before Erosion	I_r After 40 hrs Erosion
Stellite 3	0,77	14,5
Stellite 2006	0,29	3,4

The consequence of a higher SFE, and therefore a more stable FCC phase, is a reduction in the amount of twinning and in the extent of the aye transformation. Both these microstructural changes are known to cause a rapid increase in yield strength and work hardening rate of cobalt based alloys. Hence any decrease in the ability to undergo twinning and the a÷c phase transition, will result in a decrease in erosion resistance since increases in both strength and work hardening rate are known to be beneficial in resisting erosion. That a reduction in twinning occurs in Stellite 2006 is clear from the micrograph in Fig. 7.37(d) (compare this with Stellite 4, Fig. 7.34 (d)) while proof of a reduction in the extent of transformation has already been provided by the XRD work described above.

There has been considerable controversy in the past over the precise role of the FCC to HCP allotropic transformation which occurs in the Stellites. This diffusionless transformation occurs at 417 °C in pure cobalt, the FCC form being stable at temperatures greater than 417 °C. The driving force for the transformation from the FCC to the HCP form is small, mainly due to the small free energy change involved in tnis transition (AG-4 x 10^6 J/m^3). However the SFE of pure cobalt is 20mJ/m^2 which is somewhat higher than that of the chromium, tungsten and molybdenum alloys of cobalt (-10mJ/m^2). Therefore the free energy change associated with the transformation in low SFE cobalt alloys must be greater, that is, the phase change is a thermodynamically more favoured reaction in the alloys.

Initially Gould (76) proposed that the phase transition absorbed part of the cavitation energy and in this way caused a reduction in erosion. However, Woodford (72) in a comprehensive study on Stellite 6B, austenitic stainless steels and a number of TRIP steels showed that empirically, there appears to be no direct relationship between phase transformations and erosion resistance. But since these transformable FCC alloys have a higher resistance than similar non-transformable FCC alloys, he proposed an alternative explanation for their erosion resistance in terms of their stacking fault energy and resultant planar slip mode. He concluded that the role of the phase change was incidental rather than instrumental in determining the resistance of Stellite alloys.

Antony and Silence (77) have suggested that the exceptional erosion resistance of the cobalt based alloys is due to the high strain energy to fracture of the HCP form of cobalt solid solutions. The HCP form is the product of the phase transition and hence they suggest, on the basis of the findings of Remy and Pineau(118),that the SFE should be kept low (10 - 15 mJ/m^2) to facilitate the structure change. Preece (8) , on the other hand, has proposed that the resistance of these alloys is due to the formation of a fine dispersion of second phase with the same elastic properties as the surrounding matrix. Again this indicates an incidental rather than intrumental role of the transition.

Recently Remy and Pineau(118) and also Graham and Youngblood(119) have demonstrated the influence of the presence of E-HCP platelets and mechanical twins on the mechanical properties of Co-Ni and Co-Ni-Cr-Mo alloys. The latter investigators showed that the size of individual HCP platelets is of the order of 0,01pm in width while the mechanism of platelet formation is by separation of partials on alternate {111} FCC planes (hence the orientation of the deformation lines in the SEM micrographs presented above). Graham and Youngblood also found that the yield strengths of Co-Ni alloys increased by 3 to 5 times as a result of E-HCP platelet and twin formation. They ascribed this hardening to the formation of an intersecting network of HCP platelets preventing the movement of dislocations.

Furthermore Remy and Pineau found that in Co-Ni-Cr-Mo alloys which exhibited the a-'c transition, a maximum in homogeneous elongation occurred at temperatures close to the M_d* temperature while both the transition and mechanical twinning resulted in a rapid increase in the work hardening rate. However, they demonstrated that the high elongation to failure is a result of the deformation mode being mostly by mechanical twinning and that the presence of more than 10% E-phase is detrimental to the ductility of the alloys: They also investigated the correlation between the SFE and mode of deformation in these alloys and concluded that in order to obtain the optimum mechanical properties, the SFE should be 15 to 20mJ/m^2 which corresponds to an M_d of about 25 °C.

* *m_d - maximum temperature at which* a÷E *transition can be stress induced.*

An additional mechanism which has been given some consideration in the present study is that of absorption of strain without associated work hardening by the a.E transformation. The energy absorbed in the transition (namely, AG = 4 to 8 x 10^{6} J/m^{3}) only controls the kinetics of the reaction and is of no importance in the absorption of cavitation energy, besides,the value of AG is small anyway (cf.yø transition in steels AG = 5 x 10^{8} J/m^{3}). According to Sarin and Johannesson (111) the transition (in the cobalt binder of cemented carbides and it is presumed the same applies to the Stellite alloys) involves a shear which ultimately results in a tensile strain of -6% for 100% transformation. This means that a proportion of strain induced by cavitation occurs without any associated strain hardening.

The beneficial effects of strain absorption by a phase transformation have been observed in the present work with the shape memory alloy NiTi (see section 7.1.4)

On average the extent of transformation in the Stellites is probably of the order of 50% and thus a shear strain of the order of 3% could occur without appreciable work hardening taking place. These mechanisms of resistance are discussed further in Section 7.2.

7.1.7 Polymers

Flurodur, an ultra high molecular weight polyethylene(UHMWPE), was found to have the highest erosion resistance of the polymers, followed closely by the polyamides nylon 6,6 and nylatron GSM. Polyacetal is rather less resistant than Flurodur and the nylons but is far superior to the polytetrafluoroethylene (PTFE) samples, pure and filled. These latter materials are amongst the least erosion resistant materials evaluated. Also polyacetal and the two nylons undergo incubation periods in the early stages of erosion (see Fig. 7.42 and Table 7.13).

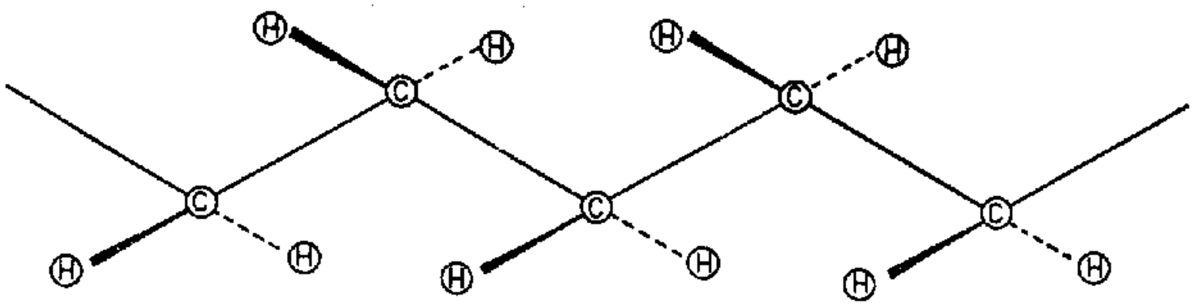

Fig. 7.41 Structure of Polyethylene

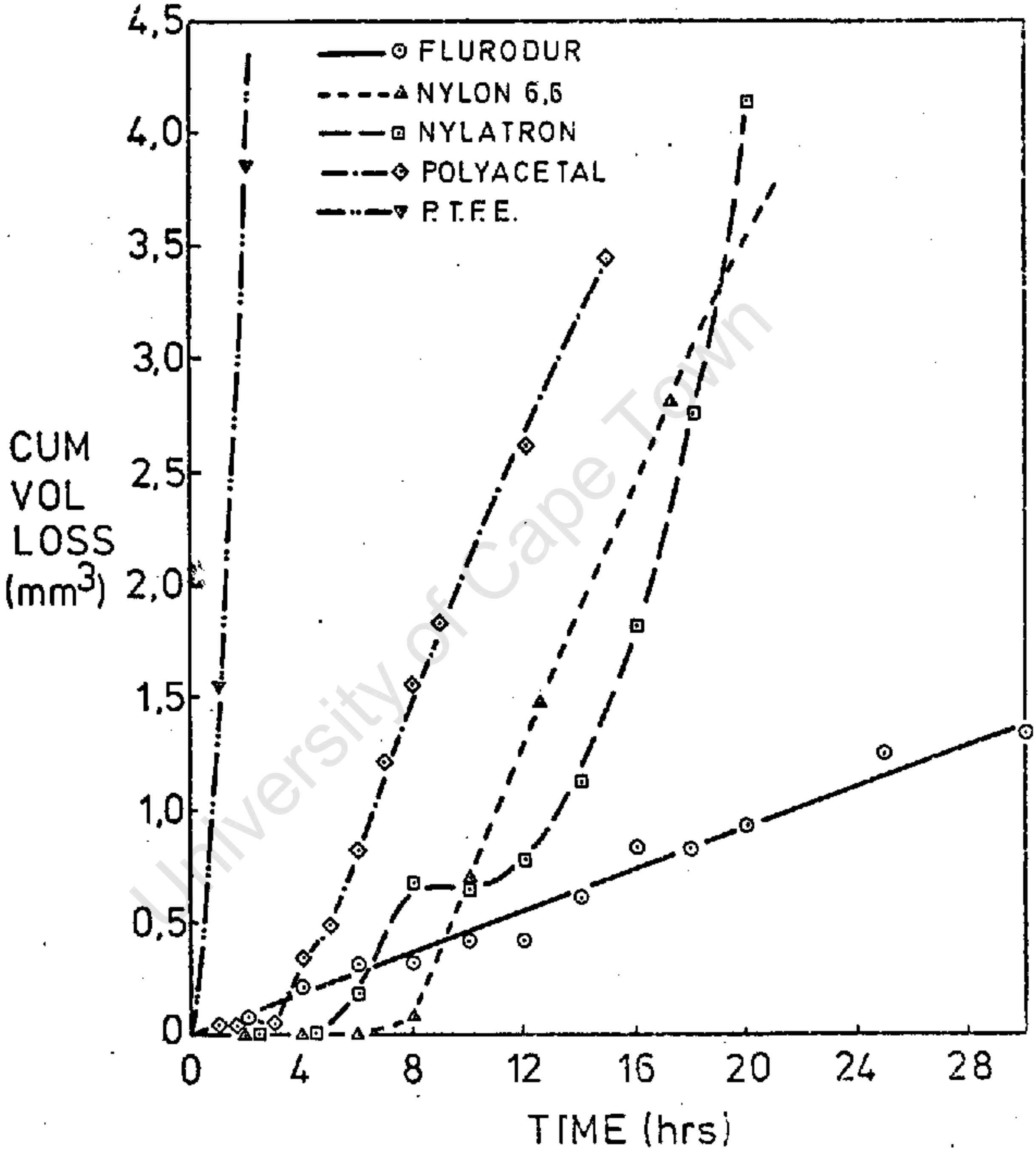

Fig. 7.42 The Erosion Curves of the Polymers

Flurodur or UHMWPE is a linear polymer of ethylene with a zig-zag configuration (see Fig. 7.41). The long chain molecules combine and form fibres of the order of microns in thickness. The ultra high molecular weight form of polyethylene has little or no side branching and thus the degree of crystallinity is very high (approximately 95%). The moderate strength of the polymer is entirely due to close molecular packing and high crystallinity. There are no secondary molecular forces between the chains, such as hydrogen bonding, although van der Waal's forces may have a small effect at the packing densities of UHMWPE.

This polymer has an exceptional erosion resistance - much higher than expected from its strength properties (resilience number). This is evident from the relationship between erosion and resilience for Flurodur which deviates from the average trend shown in Fig. 7.4. The exceptional erosion resistance of Flurodur is considered to be a consequence of its high elongation to fracture (500%) which is much greater than the other polymers (see Table 7.13).

TABLE 7.13

Polymer	CVL* 5 hrs	t_o hrs	$\dot{E}$ mm³/hr	T_G* °C	%* χstal-linity	σ_u* MPa	$\%\epsilon_f$*	R_n
Flurodur	0,20	0	0,055	-120	95	35	500	48
Nylon 6,6	0	6	0,290	20	60	80†	90**	89
Nylatron	0,07	4	NSS	-	-	80	45	84
Polyacetal	0,49	3	0,318	-73	80	70	35	77
PTFE	10,6	0	2,2	-	70	20	250	36

** approximate values*

*** This increases to about 300% when Nylon 6,6 absorbs 2,5% water.(Ref. 120)*

† The tensile strength is not much affected by the presence of H_2O - 75MPa at 2,5% water (Ref. 120)

The effect of a high ϵ_f is reflected in the fracture surface of this material (see Fig. 7.43(a) and (b)). In general, erosion occurs by scission of fibres which are, in turn, bundles of micro-fibrils. Part of a severed fibre showing limited axial splitting, exposing free fibril ends, is marked in Fig. 7.43(b). This mode of fracture is similar to that reported by Hearle (121)who called the fracture mechanism - transverse "fibrous" break. The importance of this mode of fracture becomes evident when the fracture surfaces of Nylon 6,6 and Polyacetal are considered. These two polymers have tensile strengths twice that of Flurodur and yet they are both less resistant to erosion than Flurodur.

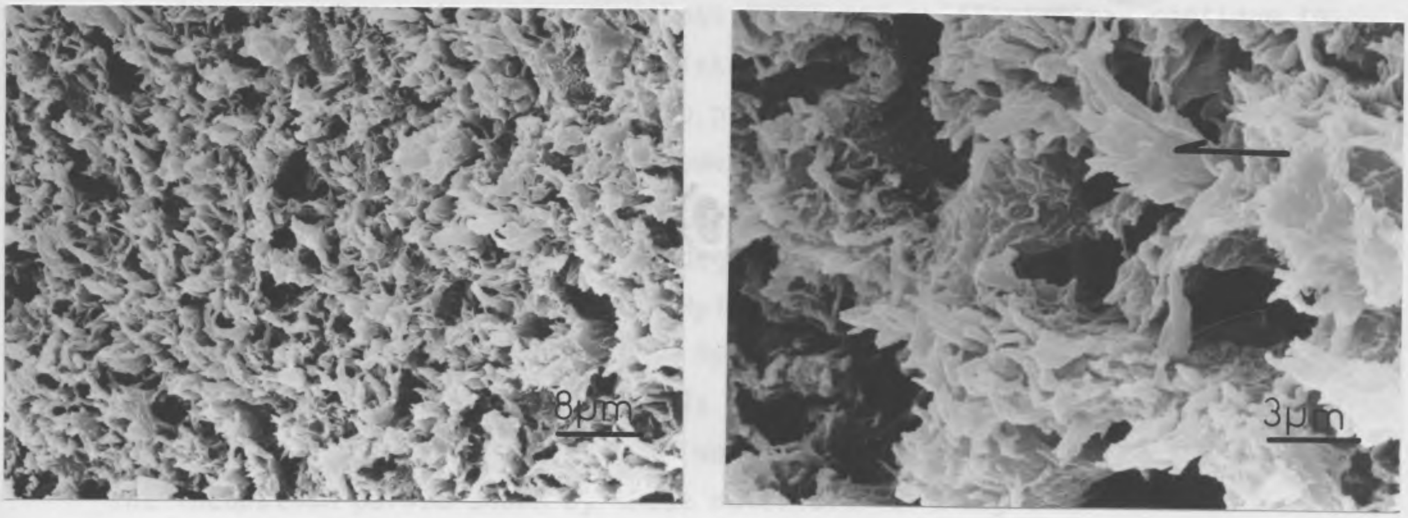

(a) (1360x) (b) (4000x)

Fig. 7.43 Erosion Mechanism of Flurodur

Nylon 6,6 and Nylatron GSM, a molybdenum disulphide (MoS_2) filled nylon (probably 6,6 or 6), are copolymers of a dicarboxylic acid and a diamine and are also linear, fibrous polymers. The molecules contain polar >C=O and >N-H groups which lead to a strong intermolecular attraction between chains through hydrogen bonds (see Fig. 7.44).

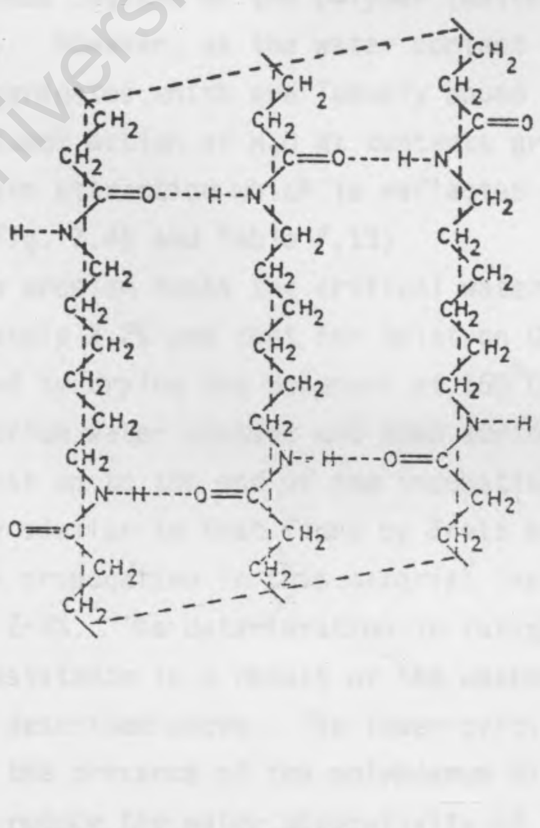

Fig. 7.44 Structure of Nylon 6,6 (Ref.122)

Nylon 6,6 is, therefore, a highly crystalline polymer. However, it also has a high glass transition temperature (about 20 °C) and on storage may continue to crystallise which is accompanied by shrinkage. The degree of crystallinity obtained on forming is very sensitive to processing conditions and may vary from 10% to 60% depending on whether the polymer was fast or slow cooled. Crystallinity can be increased to the maximum of '140% by annealing at 170 C.

As in the case of polyethylene the degree of crystallinity determines the mechanical properties of the polymers. Nylons, have, in comparison with other polymers, very high strengths, in fact, Nylon 6,6 is the strongest nylon known. However, the strengths of these materials are dependent on moisture content and the nylons have a high affinity for water.

The incubation period shown by these materials is thought to be related to the slight reduction in strength properties as a result of water absorption. Bretz et al (123)have studied the effect of moisture on the rate of fatigue crack propagation in Nylon 6,6 while Papir et al (124) investigated the influence of water on the relaxation behaviour of Nylon 6. In both investigations water was found to affect the performance of the polymers. The mechanism by which water influences the properties of the polymers was explained as follows : As the water content increases from 0,2 to 2,5% the H_2O molecules diffuse into the amorphous regions of the polymer and become tightly bound to the polyamide chains by breaking the hydrogen bonds and forming 'water bridges' between pairs of >C=0 groups. This inclusion of tightly bound water results in an improvement in the molecular packing in the amorphous regions of the polymer (which must result in a small increase in strength). However, as the water content is increased above 2,5% the H_2O molecules form aggregates which are loosely bound as bridges between >C=0 and >N-H groups. The diluent action of H_2O at contents greater than 2 to 3% causes a reduction in interchain attraction which is reflected in the mechanical properties of the polymer (see Fig. 7.45 and Table 7.13)

In the cavitation erosion tests the critical water content of Nylon 6,6 was found to be approximately 2,2% and that for Nylatron GSM about 1,1%. These critical contents were obtained by drying the polymers at 150 °C for five hours in vacuo to calculate the equilibrium water content and then adding to this the water absorbed during the erosion test up to the end of the incubation time. The critical content for Nylon 6,6 is very similar to that found by Bretz et al (123) who reported that the rate of fatigue crack propagation in this material increased rapidly for a water content greater than 2-3%. The deterioration in fatigue properties and also cavitation erosion resistance is a result of the weakening of the polymer structure by absorbed water as described above. The lower critical H_2O content of Nylatron is presumably due to the presence of the molybdenum disulphide filler, since fillers are known to reduce the water absorptivity of nylons (125).

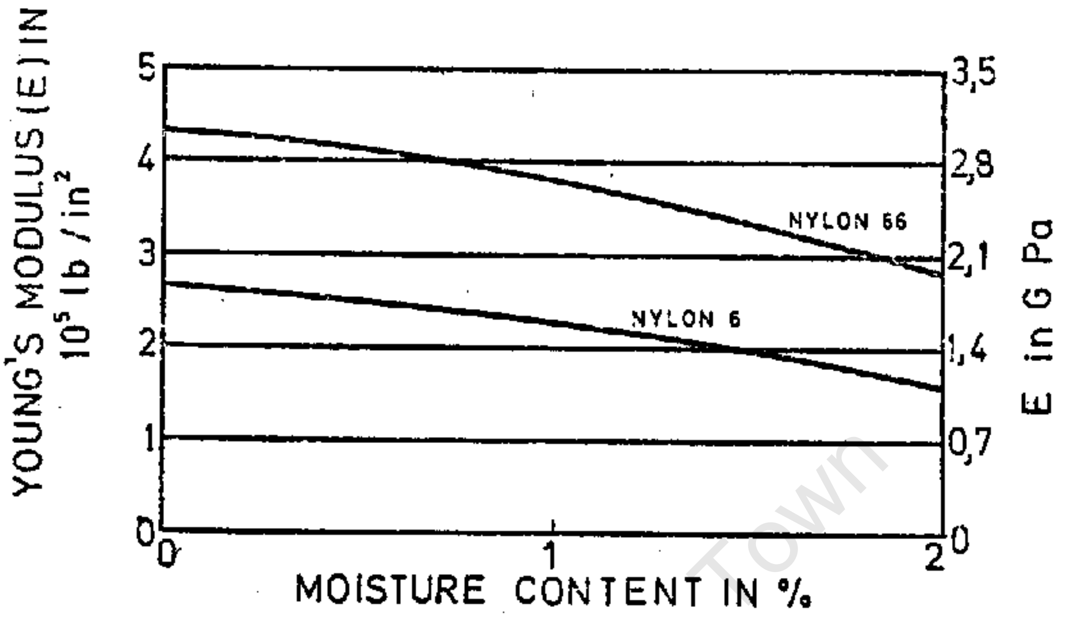

Fig. 7.45 The Effect of Moisture on the Tensile Modulus of the Nylons

Nylon 6,6, in addition to a small amount of fibrous fracture, loses materials in a brittle fashion (see Fig. 7.46(a)). A close-up view of a crack leading to formation of a chip is shown in Fig 7.46(b). Nylatron is more like Flurodur in its mode of erosion than its counterpart. Some brittle cracking is evident in Fig. 7.46(c) but the predominant failure mode is the same as that of Flurodur . Fig. 7.46(d) shows a fractured fibre and exposed fibril ends as a result of axial splitting. This difference in fracture modes between Nylon 6,6 and Nylatron is probably a further effect of the MoS_2 filler in the latter polymer.

The erosion resistances of the nylons, relative to the range of materials is good. However, within the polymer group (on the basis of Resilience No.) one would have expected the nylons to be much more resistant than Flurodur. This is considered to be due, partly, to the effect of water on these materials and also partly to the brittle fracture mode_

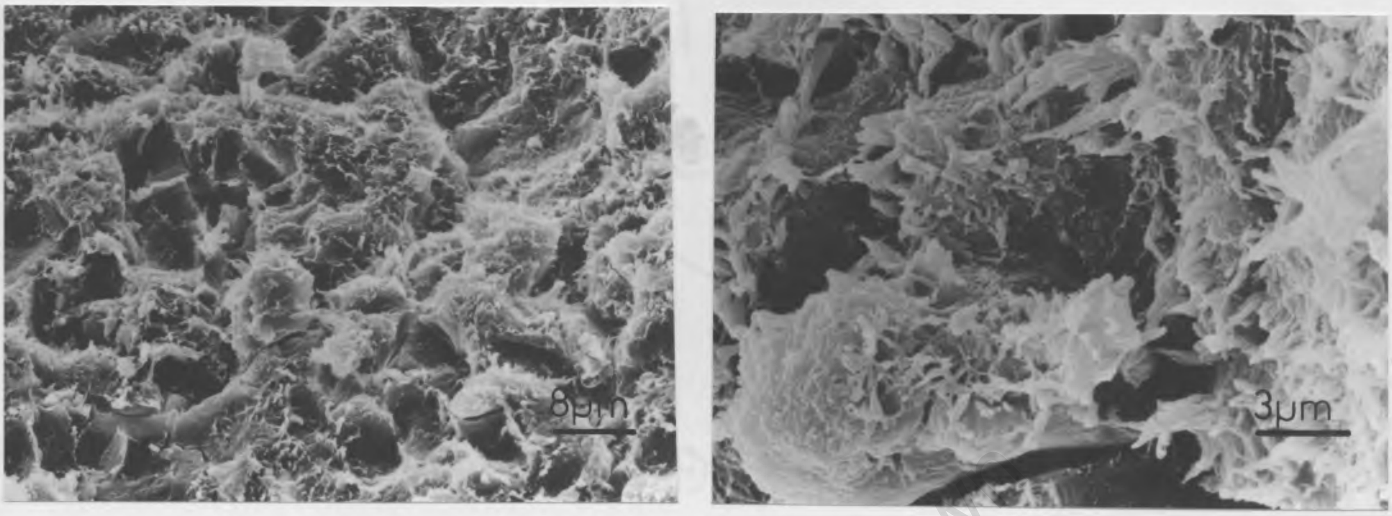

(a) General erosion of Nylon 6,6 showing brittle cracking (1360x)

(b) Chip formation in Nylon 6,6 (4000x)

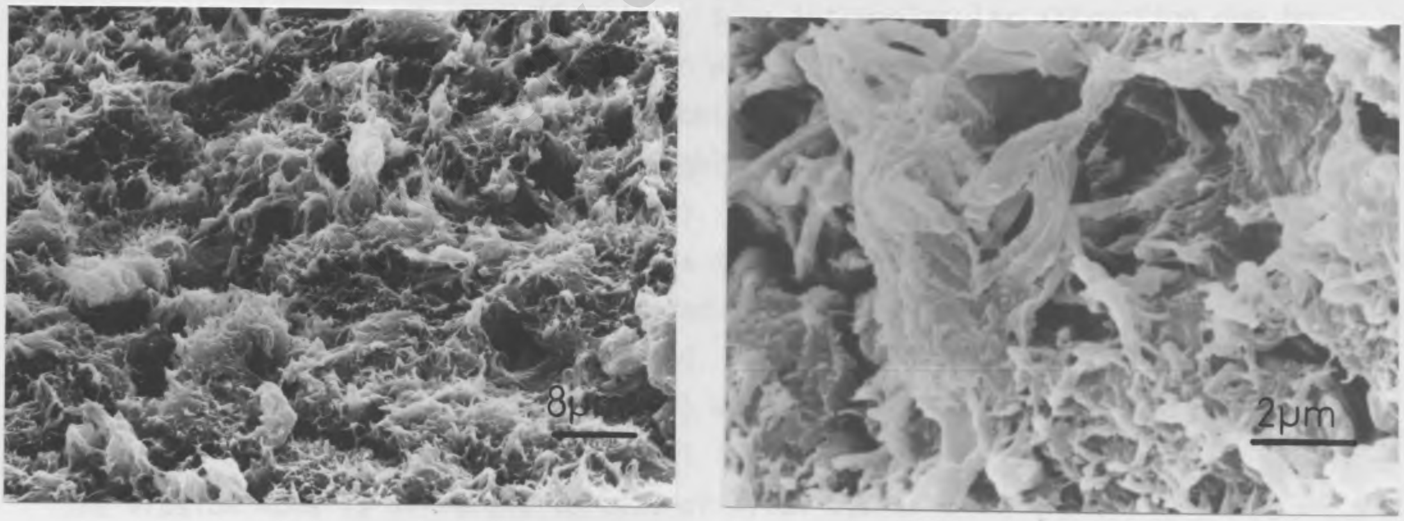

(c) General erosion of Nylatron GSM (1360x)

(d) Fractured fibril in Nylatron GSM (6800x)

Fig. 7.46 Modes of Erosion of Nylon 6,6 and Nylatron GSM.

Polyacetal ("Delrin")a homopolymer of formaldelhyde, is a linear polymer very similar in structure to polyethylene (see Fig. 7.47), the difference being that every alternate carbon atom is replaced by an oxygen atom.

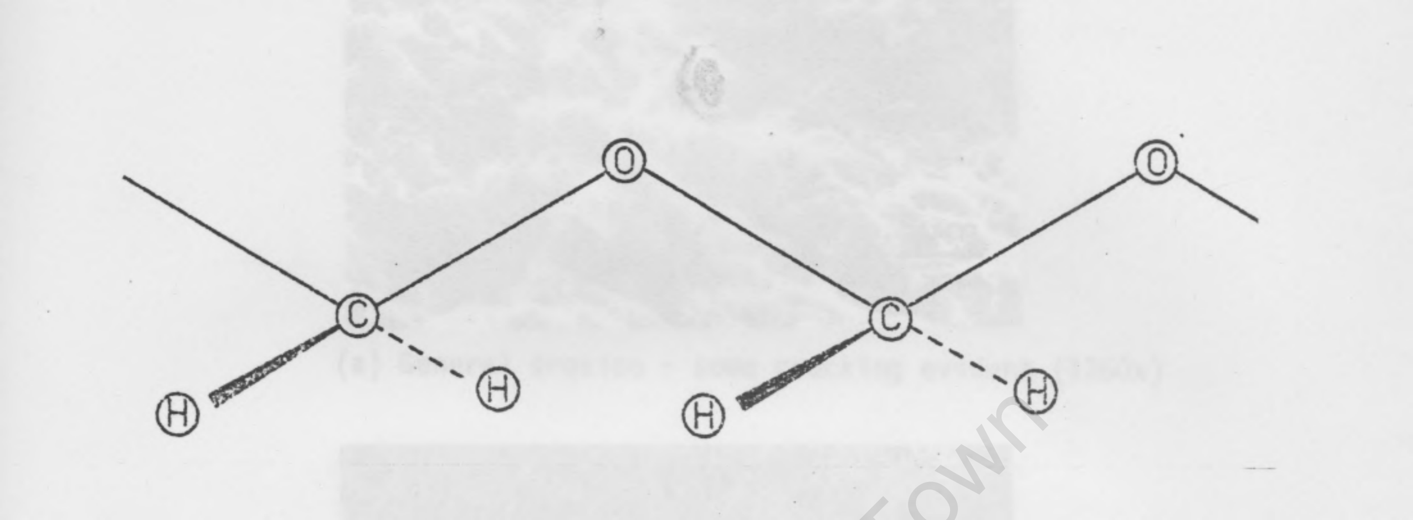

Fig. 7.47 Structure of Polyacetal 'Delrin'

The 'backbone' C-O bond in polyacetal is shorter than the C-C bond in polyethylene and hence polyacetal is a closer packed, more dense polymer with substantially higher tensile strength than Flurodur. Some intermolecular attraction due to hydrogen bonding and dipole interaction will occur,although it will be far weaker than that in the nylons. Polyacetal has a T_G of -73 ^{0}C and like the other linear polymers discussed above, is highly crystalline (capable of up to 80% crystallinity when quenched from 160 ^{0}C).

Again if strength properties were a criterion for erosion resistance, Polyacetal would be far more resistant than Flurodur. But the erosion results show the order to be quite the reverse of the expected. This is considered to be due to a low elongation to fracture (see Table 7.13) which is reflected in the mode of erosion. Figs. 7.48(a) to (c) show that material is lost in chips of 40um or more in size. The erosion mode is different to that of Nylon 6,6 in that the fracture surface does not have 'brittle facets'. Also the size of the particles lost from polyacetal are much bigger than those in Nylon 6,6 (compare Fig. 7.46(a) and Fig. 7.48(a)).

The incubation period shown by Poiyacetal is not understood. Although this polymer absorbs water (-0,5% at 30% relative humidity) the moisture content does not appear to influence the mechanical properties of the material. However it might be due to an increase in crystallinity (hence strength) through stress induced chain straightening.

(a) General erosion - some cracking evident (1360x)

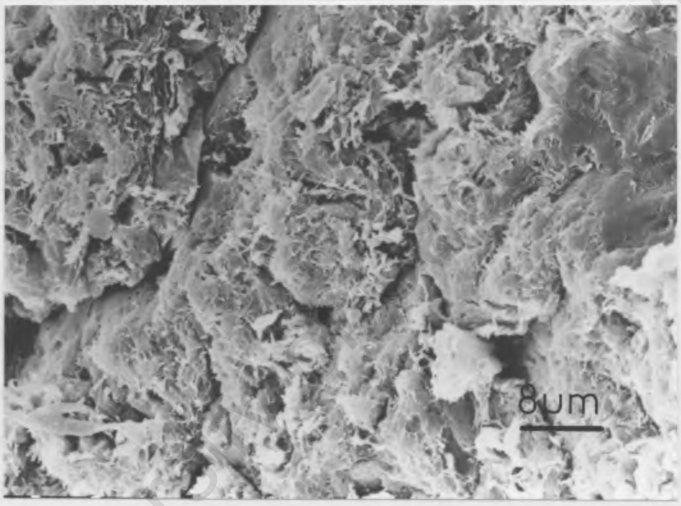

(b) Brittle cracking of eroded surface (1360x)

(c) Same as (b) (2700x)

Fig. 7.48 Mode of Erosion of Polyacetal 'Delrin'.

A further set of polymer specimens were investigated which were all based on polytetrafluroethylene (PTFE or Teflon). The PTFE is, again, a linear polymer free from any significant amount of chain branching(see Fig. 7.49).

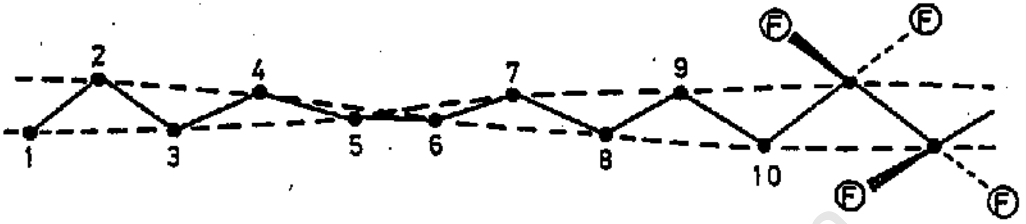

Fig. 7.49 Structure of PTFE (Ref.122)

Due to steric hindrance between the large fluorine atoms (larger than hydrogen) PTFE cannot form a planar zig-zag structure like polyethylene and instead takes up a spiral zig-zag configuration. It is capable of a high degree of crystallinity (up to 94%),but because of the high strength of the C-F bond there is little intermolecular attraction between the chains and thus the polymer does not have a high rigidity or tensile strength (resilience No.). There is a direct relationship between specific gravity and percentage crystallinity for Teflon (125), and since the pure PTFE sample tested in this work had an SG of 2,13 it should have had a crystallinity of about 50%.

The erosion results indicate that pure PTFE and PTFE plus various fillers have very poor resistance to cavitation which is attributable to the low tensile strengths and hence low resiliences of these materials ($\o_u$-20MPa).

The mechanisms of erosion of these polymers are shown in the micrographs in Fig. 7.50(a) to (d). Unlike the other polymers PTFE does not fracture in a fibrous manner and instead massive deformation occurs which results in the formation of deep holes in the surface. Moreover the detrimental influence of filler particles can be observed in Figs. 7.50(b) and (c). Material removal is initiated at the filler/polymer interface - a nucleation mechanism which has been observed so many times in this study.

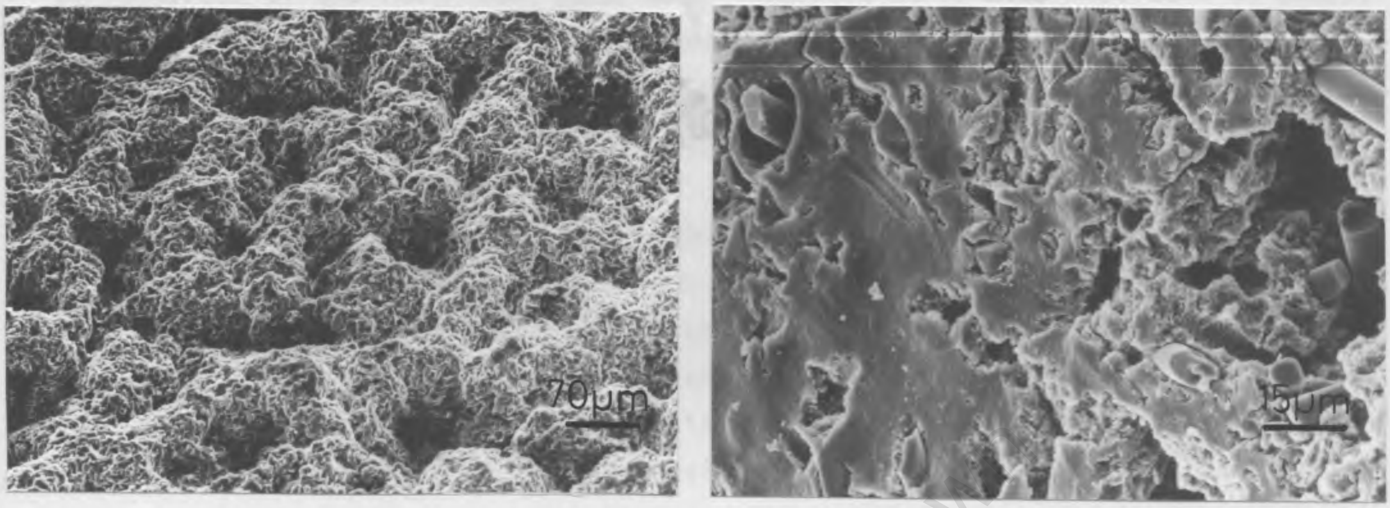

(a) General erosion of pure PTFE (140x)

(b) Nucleation of erosion at glass fibre/polymer interface (680x)

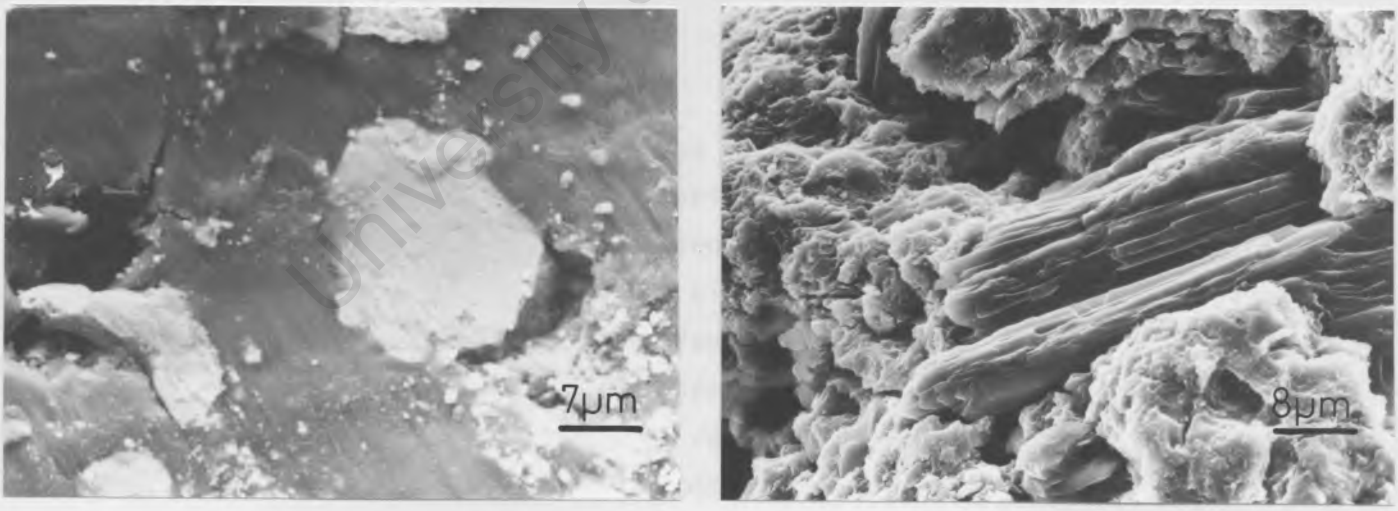

(c) Nucleation of erosion at PTFE/bronze particle interface (1600x)

(d) Graphite particle in PTFE (1360x)

Fig. 7.50 Modes of Erosion of Various PTFE Samples.

7.2 GENERAL CONSIDERATION OF EROSION RESISTANT MATERIALS

The discussion so far has been concerned with explanations of the relative performances of the individual materials. However, it is also important to assess the information gained from this work and to consider in more detail those material properties which in general lead to a high erosion resistance. Such information can be used to improve existing materials and also as a guide in the development of new, more resistant alloys and polymers.

Clearly a number of the alloys and polymers should not be used in erosive environments, namely, ferritic stainless steels, PTFE and PTFE plus various fillers, Monet 400, Incalloy 825 and 316 stainless steel. SG80 cast iron should be included in this list,but because of its good castability and low cost it will continue to be used regardless of its very low erosion resistance. Of the remaining alloys and polymers obviously those with a high resistance are important but, of particular interest are those few materials which do not conform to the relationships between erosion resistance and strength properties. An understanding of the reasons for these favourable deviations from the general trend would be of great value.

Erosion involves micro-fracture of materials and therefore those properties which relate to fracture will also determine erosion resistance. The important properties are :

1. Yield strength (ø)
2. Rate of work hardening (WHR).
3. Strain to plastic instability (a_u)

Yield strength is important since alloys do not fail by bulk material removal but rather by loss of small volumes of material from asperities or surface irregularities formed as a result of plastic deformation. Plastic deformation may occur by one or more processes, namely, planar or wavy slip of dislocations, twinning or a stress induced phase transformation. The surface defects produced by these processes include massive ductile craters with lips, protruding grain boundaries and twin and phase boundary steps. Material is readily removed from these surface lips and steps since the cross-section areas exposed to the impact pressures of cavitation are small.

Despite the many estimates of collapse pressures which have been made (see Chapter 2, section 2.1) the knowledge that high strength alloys with yield stresses of up to 1000MPa are damaged indicates that the impacting stresses are somewhat higher than 1000MPa. Erosion problems cannot be overcome by using high strength materials since they have low toughness, that is, they are sensitive to surface flaws and prone to brittle fracture. As a result these very high strength materials have limited erosion resistance and moreover they have limited practical application even if they were resistant to cavitation. Thus the engineer is compelled to use lower strength materials.

Since the formation of surface steps and irregularities is unavoidable the two properties controlling deformation, that is, the work hardening rate (WHR) and the strain to plastic instability (C_u), are also important parameters in determining erosion resistance. Moreover it can be shown that the work hardening exponent (n) is directly proportional to the true strain to instability (see Appendix 7.4), and since the work hardening rate and n are in turn directly related (according to eqn. 5 appendix 7.4) it follows that a high WHR results in a correspondingly high value of E_u. Clearly a high work hardening rate and a high strain to instability are both desirable for erosion resistance and the exceptional or anomolous resistances of alloys such as the Stellites, NiTi, 304 stainless steel and Hadfield's steel are a consequence of a high WHR. In the former three alloys a phase transformation is responsible for this high work hardening rate.

The controversial material phenomena of phase transformations have been mentioned many times in this discussion and quite obviously these structural changes play an important role in determining the erosion resistance of several alloys. A phase transition is a mechanism of producing obstacles to plastic deformation processes thereby influencing the work hardening rate and, as mentioned above, a high work hardening rate results in a high strain to instability. A phase transformation can also absorb varying amounts of strain (depending on the material) without any associated strain hardening. Clearly such a mechanism increases the number of loading cycles to fracture and therefore contributes towards the erosion resistance of a transformable material.

The extremely high erosion resistance of the Stellite alloys is a combined effect of a high yield stress, a high work hardening rate and an associated high strain to instability (of the cobalt rich solid solution phase). The mechanism responsible for the high WHR is complex and is not fully understood as yet. Work on other cobalt based alloys has shown that the stress induced improvement in mechanical properties of cobalt solid solution alloys is related to the occurrence of mechanical twinning and the a-•-E transition (118,119). In Co-Ni-Cr-Mo alloys it has been found that maximum $_{Cu}$ and WHR are obtained by ensuring that:

(a) plastic deformation proceeds mostly by twinning and
(b) not more than 10% E - HCP phase is formed.

The mechanism of resistance of NiTi is also related to a martensitic type phase transformation. This alloy can absorb 7% reversible strain with no associated work hardening through the transition and also by reorientation or growth of existing martensite. In addition, at strains greater than 7% rapid work hardening occurs. These properties are evident in the stress-strain curve of this alloy (see Fig. 7.51). Therefore, although NiTi has very low strength properties,the ability to absorb strain and the high WHR at E > 7% result in an erosion resistance equivalent to that of the Stellites.

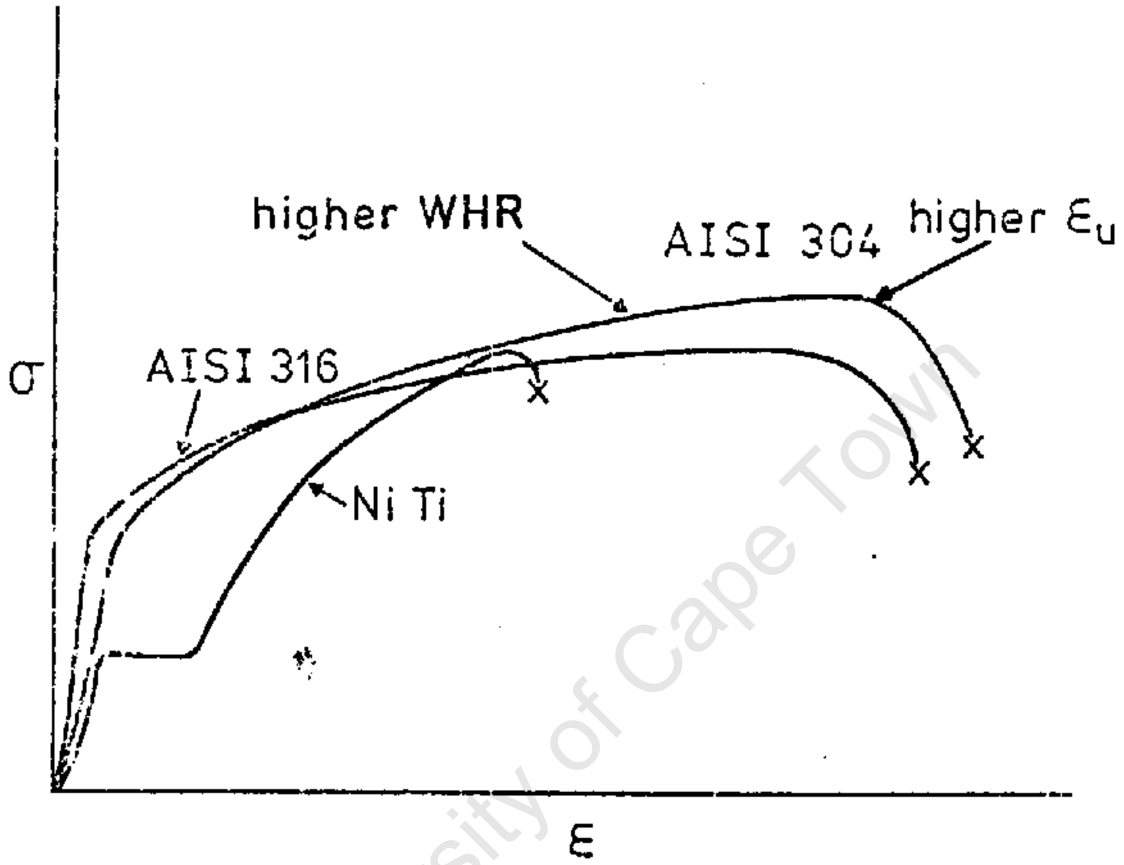

Fig. 7.51 A schematic representation of the stress-strain curves of NiTi, AISI 304 and AISI 316.

The austenitic stainless steels,AISI 304 and 316 , are another example of the effect of a phase transformation on the erosion resistance of alloys. The erosion tests showed AISI 304 to be more resistant than AISI 316. The higher resistance of the former alloy is related to the y + E + a' transition. This results in higher WHR and e_u values than AISI 316, as is evident in Fig. 7.51, and hence a better erosion resistance. Furthermore, according to Pickering (97), for metastable stainless steels,the maximum work hardening rate and maximum strain to instability are obtained by ensuring that:

(a) no martensite is present prior to straining as the presence of this transformation product increases the flow stress level relative to the work hardening rate and also decreases the optimum strain value.

(b) an optimum amount of martensite is formed at a critical stage in the straining process so that the high work-hardening rate gives rise to a high strain to plastic instability.

The anomalous erosion resistance of Hadfield's steel is also due to a high work hardening rate. However, in this case, the high WHR is not due to a phase transformation. Instead, Dastur and Leslie (102) consider it to be the result of dynamic strain ageing.

Although the mechanism of resistance is the same for all the 'anomalous' alloys, that is, a high work hardening rate, the indirect cause of this property can be one of a number of possible mechanisms. Furthermore, these mechanisms generally require a low stacking fault energy which, in turn, is a function of alloying element content. A SFE of 10 to 20 mJ/m^2 appears to be the optimum for austenitic stainless steels and cobalt based alloys.

The performance of the cobalt based tungsten carbides is also influenced by the a e phase transition except, in this case, it appears to be detrimental to the erosion resistance of these materials. The reduction in volume associated with the transition increases the tensile stress across the matrix-carbide interface which promotes debonding between the matrix and carbide phases.

In contrast the erosion resistances of alloys such as the heat treated steels, nickel based cemented carbides and the other non-transformable alloys are purely a function of the yield stresses of the homogeneous martensite, binder phases and solid solution phases respectively. The cavitation stresses exceed the yield stresses of these materials, plastic deformation occurs and material is lost by ductile fracture of twin and grain boundary surface steps and by ductile failure of lips of cratersin high SFE alloys.

In general,second phase particles cause a reduction in erosion resistance whether the material be a high strength (e.g. Stellite 20) or a low strength material (e.g. PTFE + fillers). This is due to the high interfacial stresses caused by the elastic and plastic mismatches of the dissimilar phases. Only when the carbide phase forms a very fine, intimate network, such as in Stellite 3, is the carbide phase of any benefit to the material,since in this form it retards crack propagation.

The work on polymers has shown that, as in the case of metals, no simple relation between erosion resistance and mechanical properties exists for polymeric materials. Again a knowledge of the microstructure of polymers is necessary to understand their erosion performance. Also there is the additional complication in some polymers of the influence of absorbed water on mechanical properties.

Most polymers deform in a viscoelastic manner under load and this response can be modelled by a system of springs and dashpots. The displacement (y) per unit time of viscoelastic materials is a complex combination of elastic, anelastic and viscous displacement components. Thus total viscoelastic displacement is given by:

$$\gamma_{total} = \gamma_1 + \gamma_2 + \gamma_3 \qquad \ldots\ldots\ldots \qquad 7.3$$

where γ_1 = elastic component = τ/G
γ_2 = anelastic component
γ_3 = viscous component

and where τ = shear stress
G = shear modulus

Clearly erosion resistant polymers, in general, will have large, recoverable elastic and anelastic components and a low irrecoverable viscous component. However, the polymers tested in this study were all crystalline polymers for which the elastic term, y_i is the major term in equation 7.3 (viscosities are high therefore 12 and y3 are small). Hence y2 and y3 can be ignored and total displacement is given by:

$$\gamma_{total} = \tau/G$$

One would anticipate a relationship between erosion resistance and yield strength for these materials. But the high strain rates of cavitation and the effect of absorbed water modify the expected relationship.

Clearly the response of polymers to cavitation is complex and,on the basis of the findings of this limited study, it is impossible to state which specific material parameters control erosion resistance. However, in general, it would appear that a high yield strength and a high strain to fracture are necessary for resistance. On the other hand, sensitivity to strain rates and absorbed water,as in the case of the nylons,are a distinct disadvantage.

The various materials investigated in this project together with the explanations for their performances are summarized in Table 7.14.

TABLE 7.14

Stellites	High σ_y. High WHR and ε_f due to twinning and $\alpha \rightarrow \varepsilon$ transformation in cobalt rich phase (low SFE)
Cemented Carbides (Nickel based)	High σ_y of binder due to plastic constraint
NiTi	High WHR and ε_f due to phase transformation
Polyethylene	High ε_f and moderate σ_y
Nylons	High σ_y . Absorbed water detrimental to polymer.
Cobalt-based cemented carbides, martensitic steels, etc.	Controlled primarily by σ_y of cobalt matrix or martensite phase ($\alpha \rightarrow \varepsilon$ transformation in WC-Co samples also influences erosion resistance of low cobalt content composites)
Polyacetal	Low ε_f
Hadfield's steel and AISI 304	Low SFE, high WHR and ε_f due to $\gamma \rightarrow \alpha'$ transition or dynamic strain ageing.
AISI 316 and Nickel based alloys.	High SFE, low σ_y and WHR $\therefore$ low resistance
Ferritic Stainless Steels	High notch and strain rate sensitivity
PTFE	Low σ_y

7.3 CONCLUSIONS - SPECIFICATIONS FOR THE OPTIMUM MATERIAL

This study has revealed a number of material properties which control resistance to erosion and these are specified below. Although practical constraints determine ultimately what material is most suitable for a particular application, these specifications are guides for material selection and erosion resistant material design. An alloy to be used in an erosive environment should have as many of the following properties as possible :

I. A high yield stress.

2. A high work hardening rate and resultant high $_{cu}$ (induced by phase transformation, twinning,dynamic strain ageing).

3. A low stacking fault energy to ensure phase transformation and twinning.

4. A ductile erosion mechanism.

5. A low notch/strain rate sensitivity

6. No second phase particles or erosion initiating sites in surfaces exposed to cavitation.

A polymer (crystalline) with a high erosion resistance will have :

I. A high yield stress (high resilience)

2. A high c_f.

3. No filler particles.

The material science, structure-property approach adopted in this work confirms once again that the general selection of materials for applications involving wear or erosion cannot be based on a bulk property without a simultaneous appreciation of the influence of microstructure on erosion mechanisms.

CHAPTER EIGHT

SUMMARY OF FINDINGS AND GENERAL CONCLUSIONS

The main objectives of this study were (i) to establish whether oil-in-water emulsions suppressed cavitation erosion and if so to determine which emulsion type or group of emulsions reduced erosion the most, and (ii) to determine which materials or group of materials have the highest resistance to erosion.

The investigations into the effect of temperature of the medium and the effect of separation distance on cavitation erosion were of secondary importance. In addition efforts were made to elucidate the modes of erosion and the mechanisms of erosion resistance of the various materials. Explanations have been proposed for the performances of materials and also for the influence of oil-in-water emulsions on cavitation erosion. The findings of this work are as follows:-

1. A separation distance of 0,35mm between test piece and drill tip results in maximum erosion of pure iron.

2. The erosion of Are iron in distilled water and in 5:95 oil-in-water emulsions shows a broad maximum for medium temperatures of -40 C.

3. In general erosion rates in oil-in-water emulsions are lower than those in water, but higher than those in mineral oil. In addition emulsions with a high mineral oil content suppress cavitation more than do low oil content and synthetic emulsions. The effect of oil content may be due to either the formation of a thin oil film on the metal surface which prevents nucleation of surface cavities or to the cushioning of cavity collapse as a result of a high dissolved air content or possibly a combined effect of the two mechanisms.

4. Nickel based cemented carbides and the shape memory alloy NiTi are as erosion resistant as the Stellite alloys which, as a group, were the most erosion resistant materials tested in this work.

5. Flurodur or ultra high density polyethylene has a very high erosion resistance - equivalent to that of hardened and lightly tempered low and high alloy steels which, in turn, follow the Stellite alloys in order of erosion resistance.

6. Nylons are also highly resistant to cavitation but deteriorate rapidly on absorbing a small amount of water. The critical contents are -2,0% for Nylon 6,6 and -1,0% for a commercial, MoS_2 filled nylon - Nylatron GSM.

7. High stacking fault energy and notch or strain rate sensitive alloys have very poor resistance to cavitation. Also polymers having a low tensile strength perform very poorly when exposed to cavitation.

8. Second phase particles in alloys and fillers in polymers provide initiating sites for erosion (at the interface). Furthermore elastic modulus differences assist cracking at the interface.

9. Stress induced phase transformations improve alloy performance by causing rapid increases in mechanical properties such as flow stress, work hardening rate and strain to fracture. The best example of the influence of a shear transformation is in the shape memory alloy NiTi which has a hardness of HV200 but an erosion resistance equal to that of the Stellites.

10. Materials for use in erosive environments should have as many of the following properties as possible:-

<u>(i) Alloys</u>

(a) A high flow stress
(b) A high work hardening rate
(c) High strain to fracture
(d) A low stacking fault energy
(e) A ductile erosion mechanism
(f) A low notch and/or strain rate sensitivity
(g) No second phase particles

<u>(ii) Polymers</u>

(a) A high yield stress
(b) A high elongation to fracture
(c) No filler particles.

The findings of this work must apply, not only to erosion by cavitation, but also to degradation of materials by other high strain rate wear mechanisms, such as,liquid droplet and solid particle impact erosion.

APPENDIX 4.1

ADDITIONAL INFORMATION ON POWER ULTRASONICS (Ref. 83,84)

1. AMPLIFICATION FACTOR OF DRILL HORNS

The amplitude transformation of exponential couplers (horns) is given by the ratio of the end diameters (D/d). In the case of the KLN Ultrasonic drills used in this project D 38mm and d 11mm; therefore the transformation ratio is 3,45. Providing the ratio is approximately three, the exponential shape can be approximated to a linear form which simplifies fabrication of the component.

2. MATCHING THE WORKING TIP TO THE DRILL HORN

The length of a drill horn can be calculated, if the ratio of the end diameters is known, from the equation :

$$L = C/2f \ \{1 + (\log_e n^2)/\pi\}^{\frac{1}{2}}$$

where L = total length of the exponential horn
C = sound speed in the horn material
f = operating frequency of drill
n = transformation ratio (D/d)

The theoretical length of a horn for the KLN equipment is 11,556cm. However, the horn is cut back to allow for the attachment of a working tip and the actual length of the exponential horn of the KLN drill is 11,0cm. This means the allowed working tip length is about 0,6cm.

The suitability of an alloy as a tip material depends on its sound velocity. The optimum sound speed of a working tip material is, in turn, a function of the sound speed of the horn material and of the dimensions of the working tip and can be calculated from the following equation :

$$C_2 = C_1/L_1 \times L_2$$

where C_2 = sound speed in tip material
C_1 = sound speed in horn material
L_1 = Length of horn removed for tip
L_2 = Length of tip

Appendix 4.1 Con't ...

For the values

$C_1 = 4{,}3 \times 10^5$cm/sec
$L_1 = 0{,}556$cm
$L_2 = 0{,}65$cm

the optimum sound speed, $C_2 = 5{,}0 \times 10^5$cm/sec

A material with a C value close to this is Ti318 ($C = 4{,}9 \times 10^5$ cm/sec) and it is thus a suitable material for the working tips. Furthermore Ti318 transmits high energy vibrations very efficiently, the transmitting efficiency of a material being a function of its fatigue strength, F, density, p, and sound velocity, C. The efficiency is represented by the ratio :

$$E = F/\rho c$$

The ratio for Ti318 is E = 3408 compared with E = 465 for Monel 400. In fact Ti318 has one of the highest ratios and therefore has a high energy transmitting efficiency. This is a further incentive for using this material for the working tips.

APPENDIX 7.1

TABLE A GENERAL ALLOYS

MATERIAL	COMPOSITION (% by wt.)											CONDITION OR HEAT TREATMENT
	C	Mn	Si	Cr	Ni	Mo.	Fe	W	Cu	Ti	Nb	
817 M40	0,43	-	-	1,05	1,48	0,29	Bal	-	-	-	-	Oil quench from 840°C; tempered
835 M30	0,32	-	-	1,12	3.96	0,26	Bal	-	-	-	-	Oil quench from 830°C; tempered
DIN 4112	0,91	-	-	18,5	0,25	1,15	Bal	-	-	-	-	Oil quench from 1040°C; tempered
431 S 29	0,11	-	-	15,6	2,34	-	Bal	-	-	-	-	Oil quench from 1040°C; tempered
AISI 430	0,14	0,72	0,43	16,35	-	-	Bal	-	-	-	-	Hot rolled
AISI 409	0,03	0,84	0,51	11,42	0,31	-	Bal	-	-	0,17	-	Hot rolled
AISI 304	0,08	0,87	-	18,2	8,4	-	Bal	-	-	-	-	Wrought and annealed
AISI 316	0,06	-	-	16,5	10,4	2,02	Bal	-	-	-	-	Wrought and annealed
3 CR 12	0,02	0,97	0,56	11,14	0,42	-	Bal	-	-	0,24	-	As cast; wrough and annealed
3CR 12 Ni	0,03	0,78	0,54	11,49	1,31	-	Bal	-	-	0,30	-	Wrought and annealed
NiTi	-	-	-	-	53,5	-	-	-	-	45,3	-	Annealed at 900°C
Incalloy 825	-	0,74	-	20,8	41	2,77	31,8	-	2,13	0,75	-	Annealed
Monel 400	-	-	-	-	66,6	-	-	-	31,9	-	-	Annealed
Hadfield's Steel	0,84	13,9	-	-	-	-	Bal	-	-	-	-	Water quench from 1040°C
SG 80	3,48	-	2,62	-	-	-	Bal	-	-	-	-	As received
TB 18	2,21	-	-	12,8	-	1,34	Bal	-	-	-	-	As cast
CB 24	3,0	-	-	23,2	-	-	Bal	-	-	-	-	As cast
Alloy C	0,10	-	1,0*	17,0*	Bal	17,0*	6,0*	5,0*	-	-	-	As cast
Alloy 3040	1,28	-	1,0*	34,0*	Bal	10,0*	3,0*	-	-	-	3*	As cast

* *Nominal Values*

APPENDIX 7.1 con't ....

TABLE B STELLITE ALLOYS

MATERIAL	COMPOSITION							CONDITION OR HEAT TREATMENT
	C	Si	Cr	W	Fe	Ni	Mo	
Stellite 3	2.61	-	30,2	11,9	-	-	-	As Cast
Stellite 4[†]	1,17	1,22	31,30	13,98	1,06	0,16	-	"
Stellite 6[†]	1,15	1,15	24,30	5,11	3,32	1,43	0,27	"
Stellite 8[†]	0,27	0,25	27,00	-	0,78	2,86	5,25	"
Stellite 20[†]	2,35	0,76	33,10	16,26	2,22	1,38	-	"
Stellite 2006[†]	1,40	1,60	30,25	-	19,82	7,68	6,25	"

[†] *Deloro Stellite Product*

TABLE C CEMENTED CARBIDES[*]

GRADE	COMPOSITION (% by wt.)		GRAIN SIZE (µm)
	CARBIDE TYPE & CONTENT	MATRIX	
8 LC	95 WC	5 (Ni,Cr,Mo)	2
8 MC	91 WC	9 Ni	2
CN02	90 $(W,Ti,Cr,Mo)_x C_y$	10 (Ni,Co)	2
CG 20	94 WC	6 Co	2
CT 30	94 WC	6 Co	5
CG 35	90,5 WC	9,5 Co	2
4 DC	90,5 WC	9,5 Co	5
CG 60	85 WC	15 Co	2
CT 65	85 WC	15 Co	5
Lab grd. A	80 WC	20 Co	2
Lab Grd. C	75 WC	25 Co	2

[*] *Sandvik (Sweden) product*

APPENDIX 7.1 con't ....

TABLE D POLYMERS

MATERIAL	BASE POLYMER	TYPE AND CONTENT OF FILLER	CONDITION
Nylon 6,6	Nylon 6,6	-	Annealed 1 hour at 110°C
Nylatron GSM	Nylon (6,6?)	MoS_2	"
Polyacetal (Delrin)	Polyacetal Homopolymer	-	"
Flurodur	Ultra High molec. wt. Polyethylene	-	"
PTFE (pure)	PTFE	-	"
PTFE + 15% Glass	PTFE	15% Glass fibres	"
PTFE + 25% Glass	PTFE	25% Glass fibres	"
PTFE + Carbon	PTFE	25% Carbon	"
PTFE + Carbon + Graphite	PTFE	Carbon, Graphite	"
PTFE + Bronze	PTFE	60% Bronze	"

APPENDIX 7.2 THE EROSION CURVES OF THE MATERIALS (VOLUME LOSS vs. TIME)

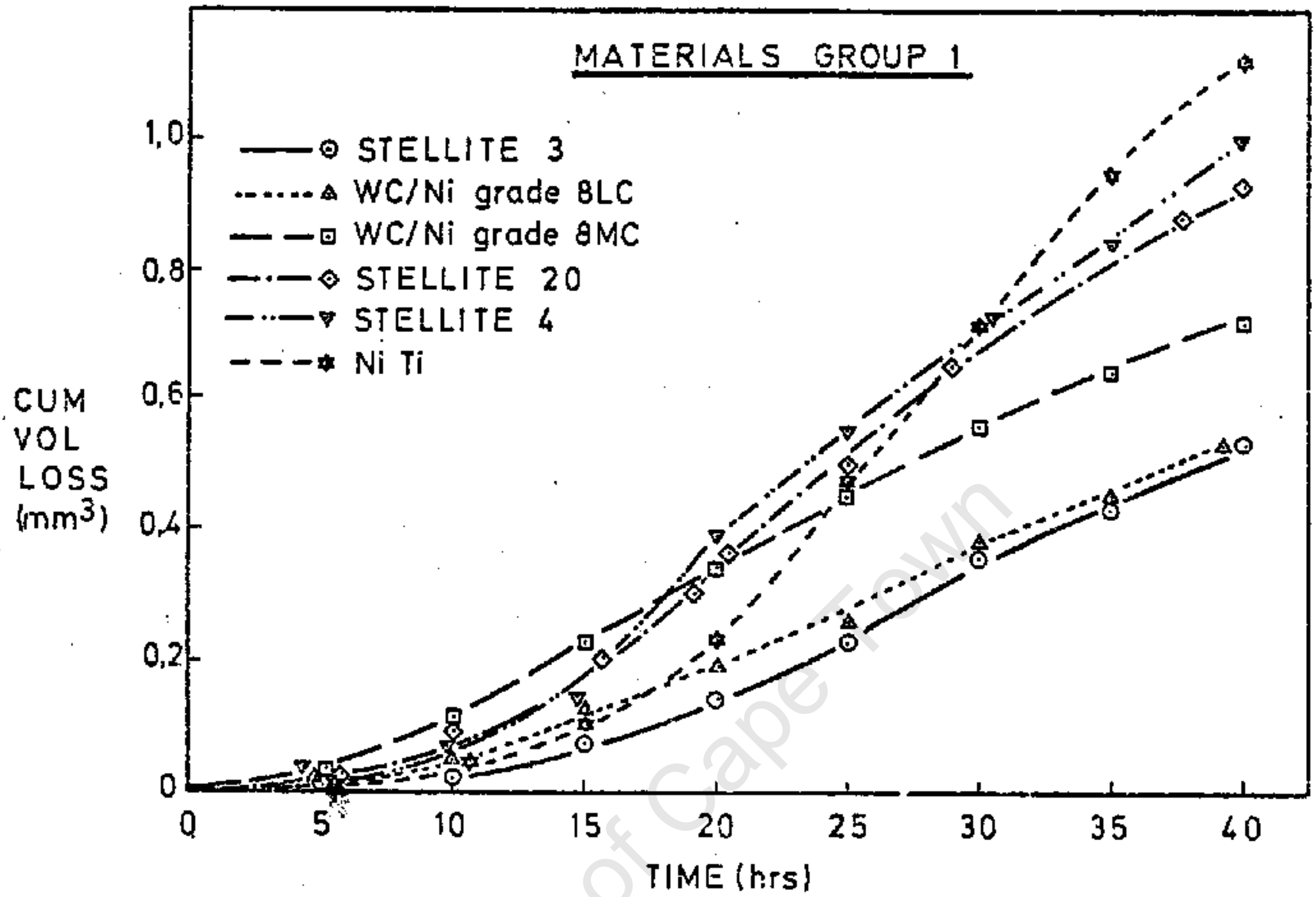

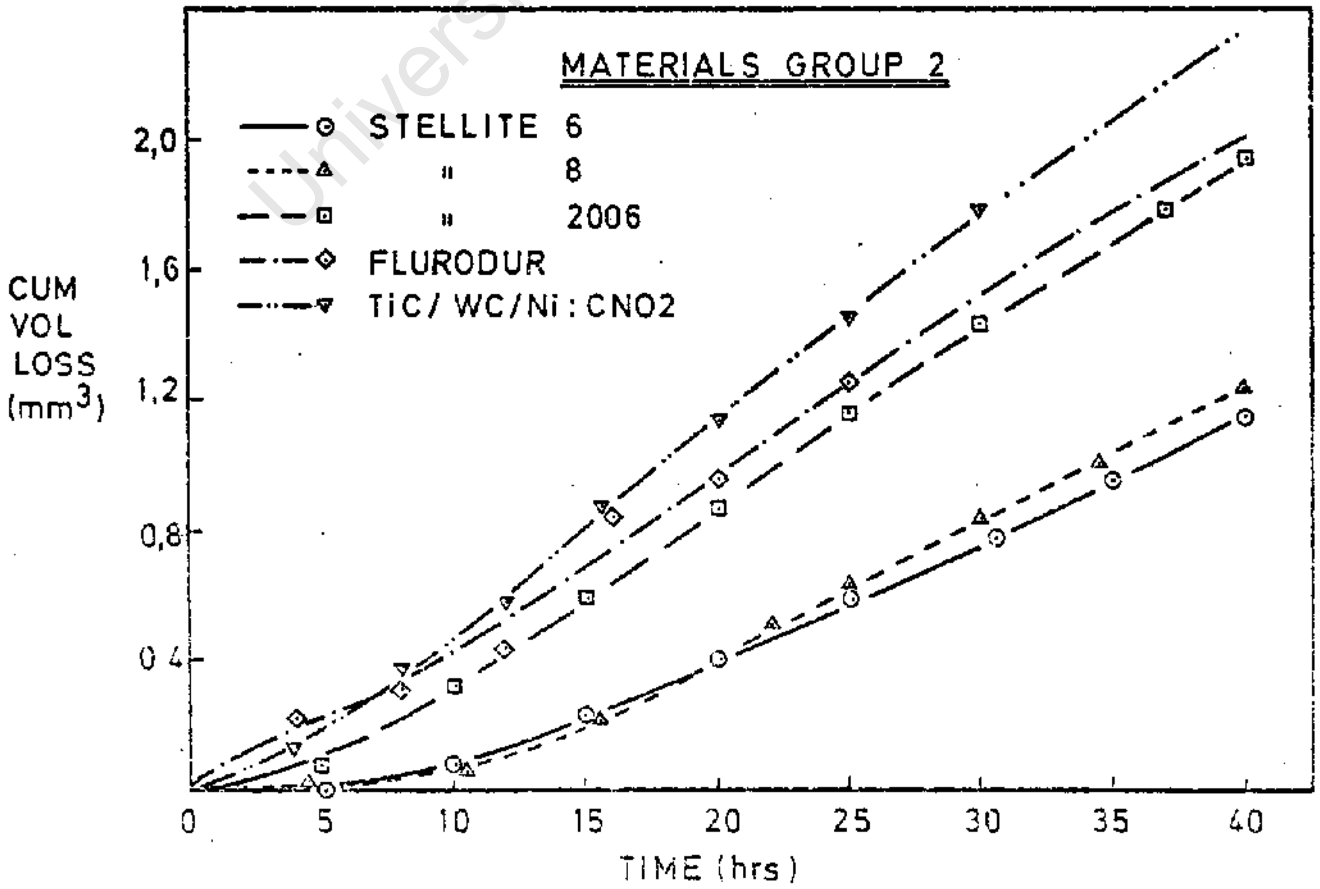

APPENDIX 7.2 contd.

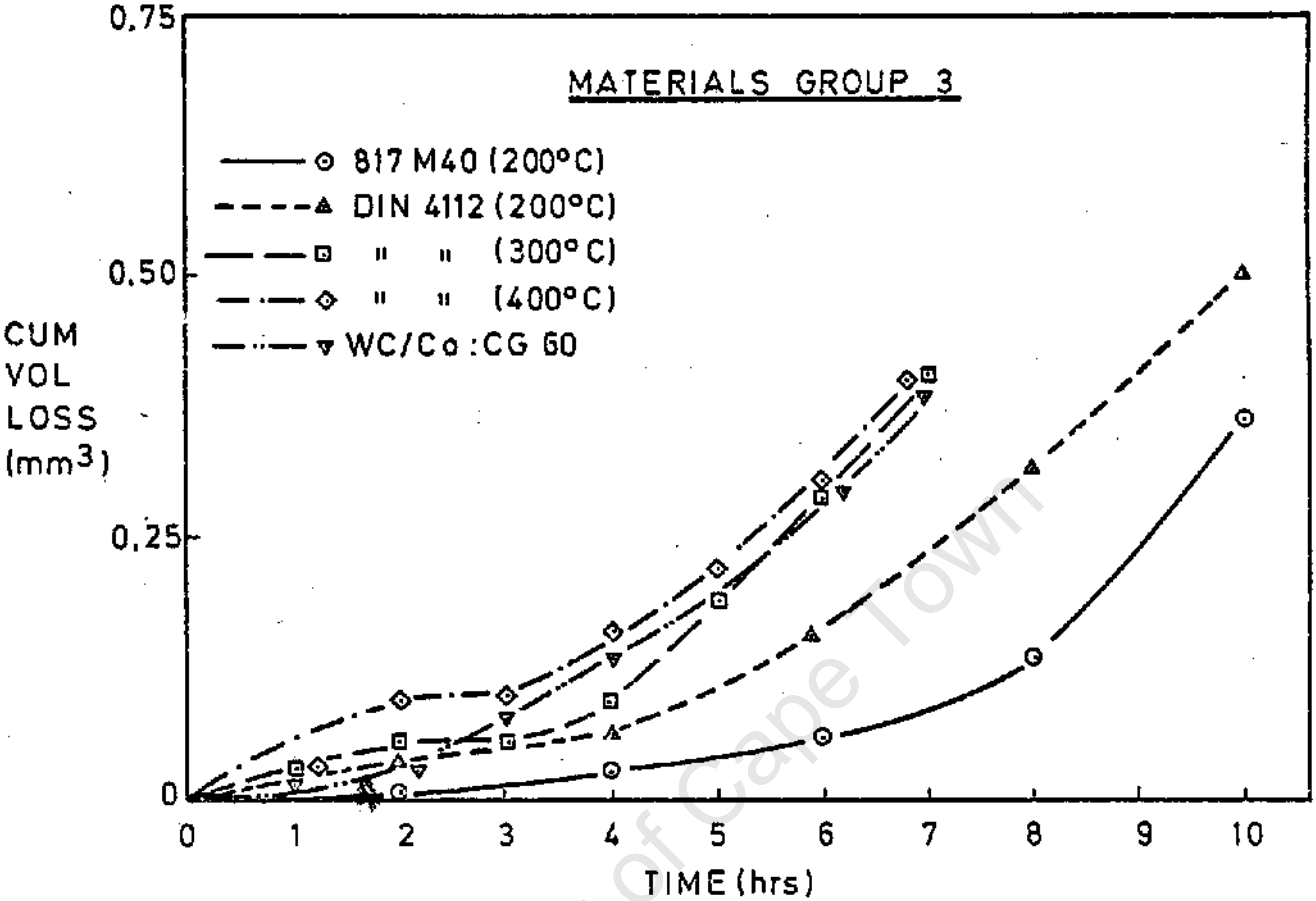

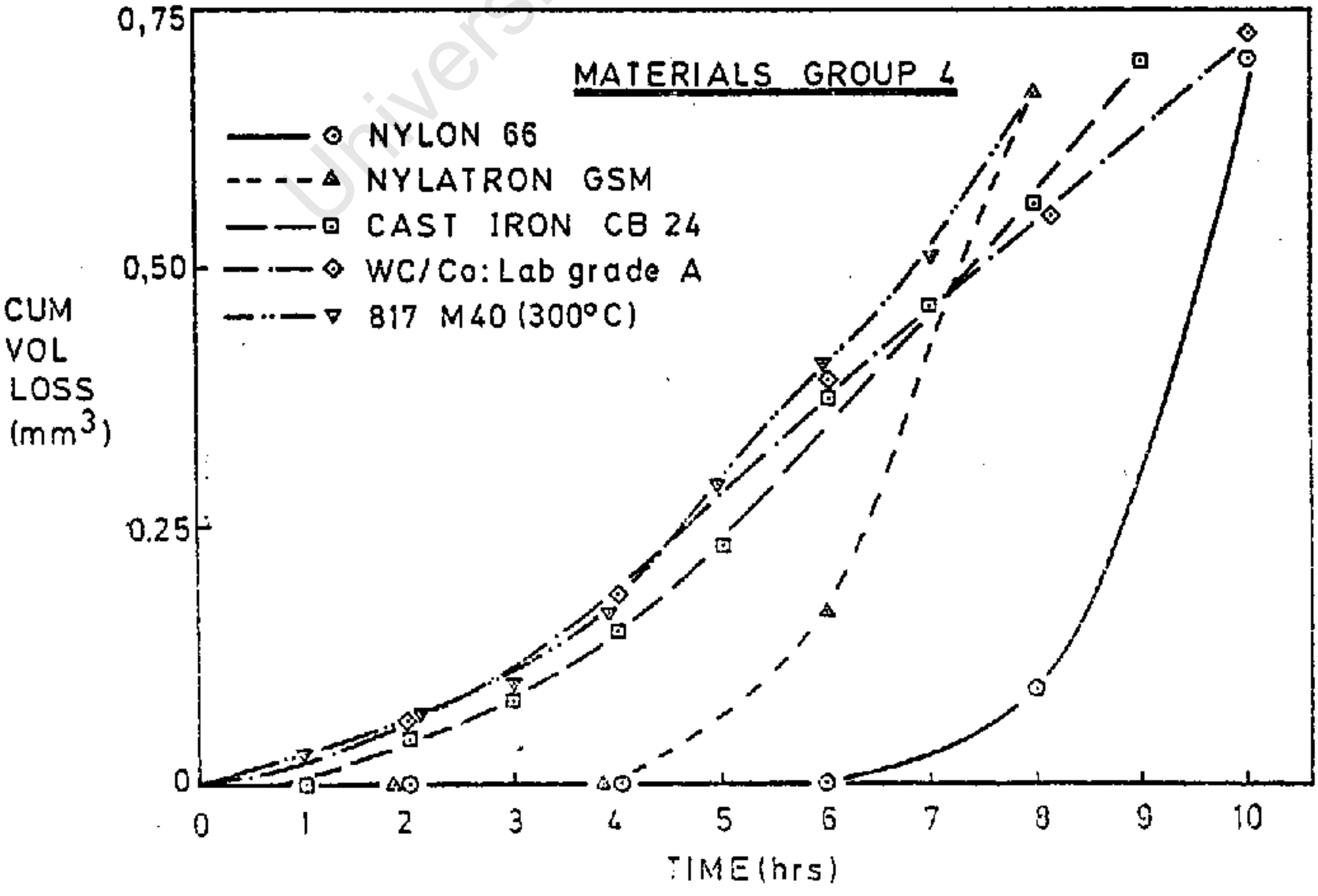

APPENDIX 7.2 contd.

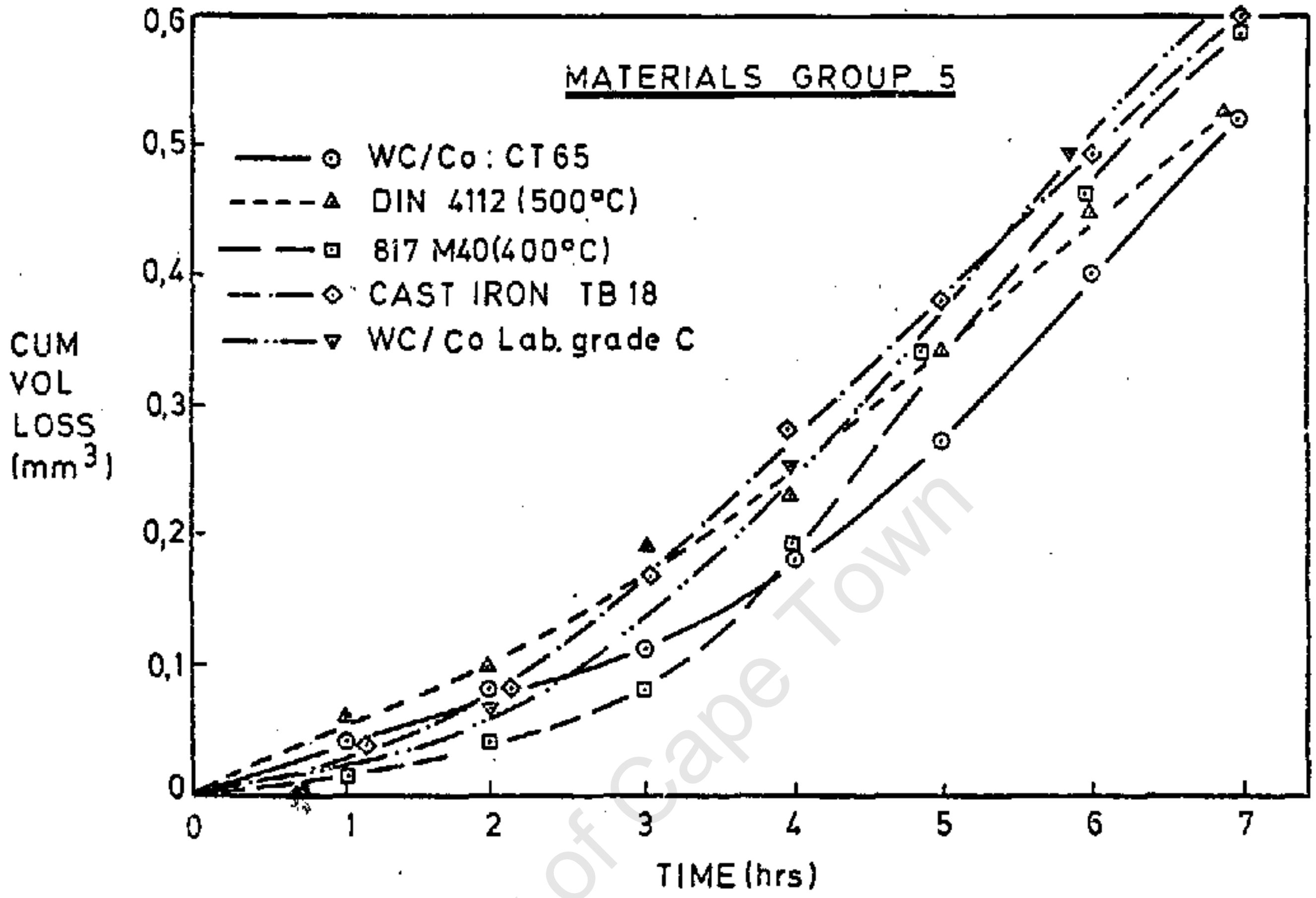

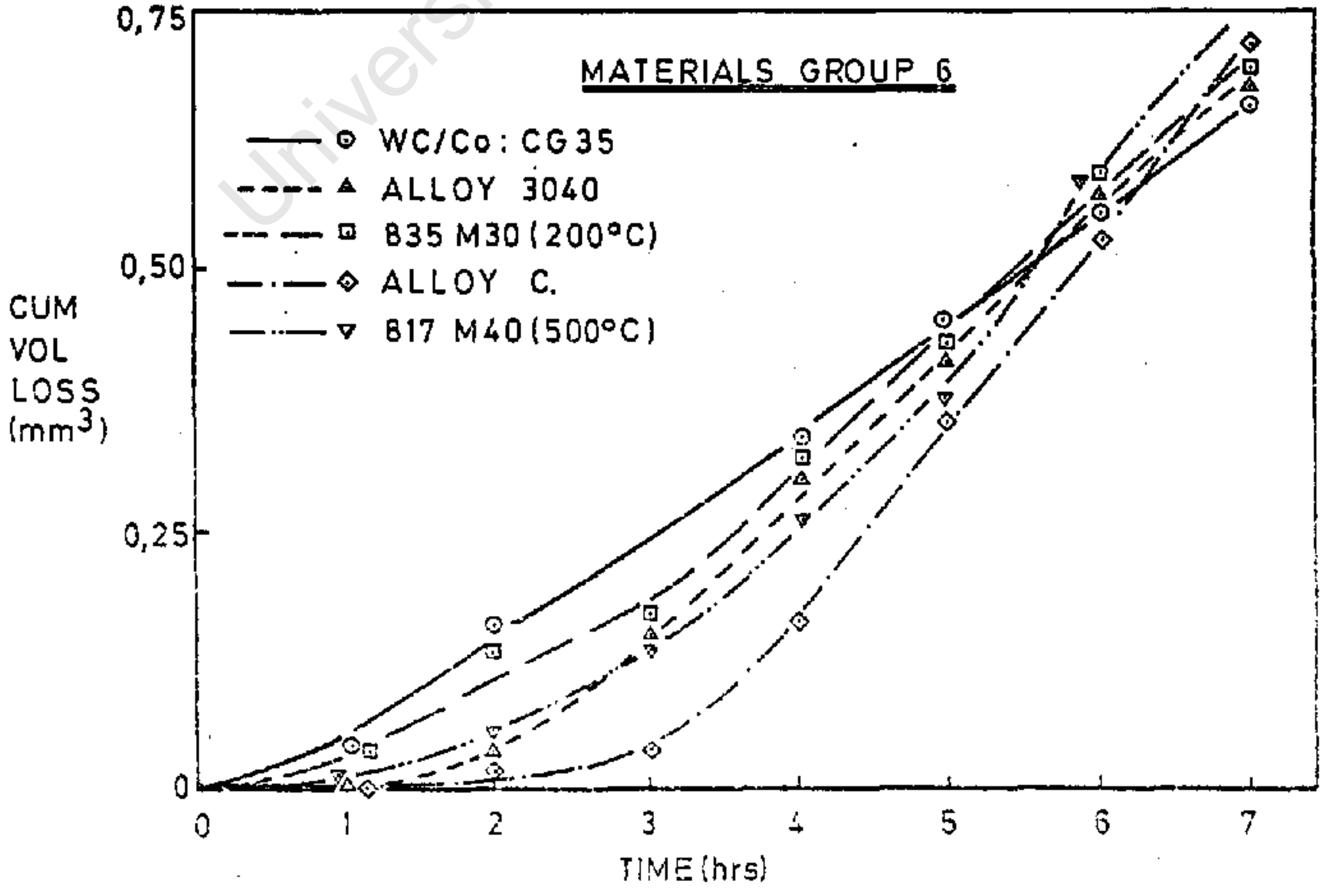

APPENDIX 7.2 contd.

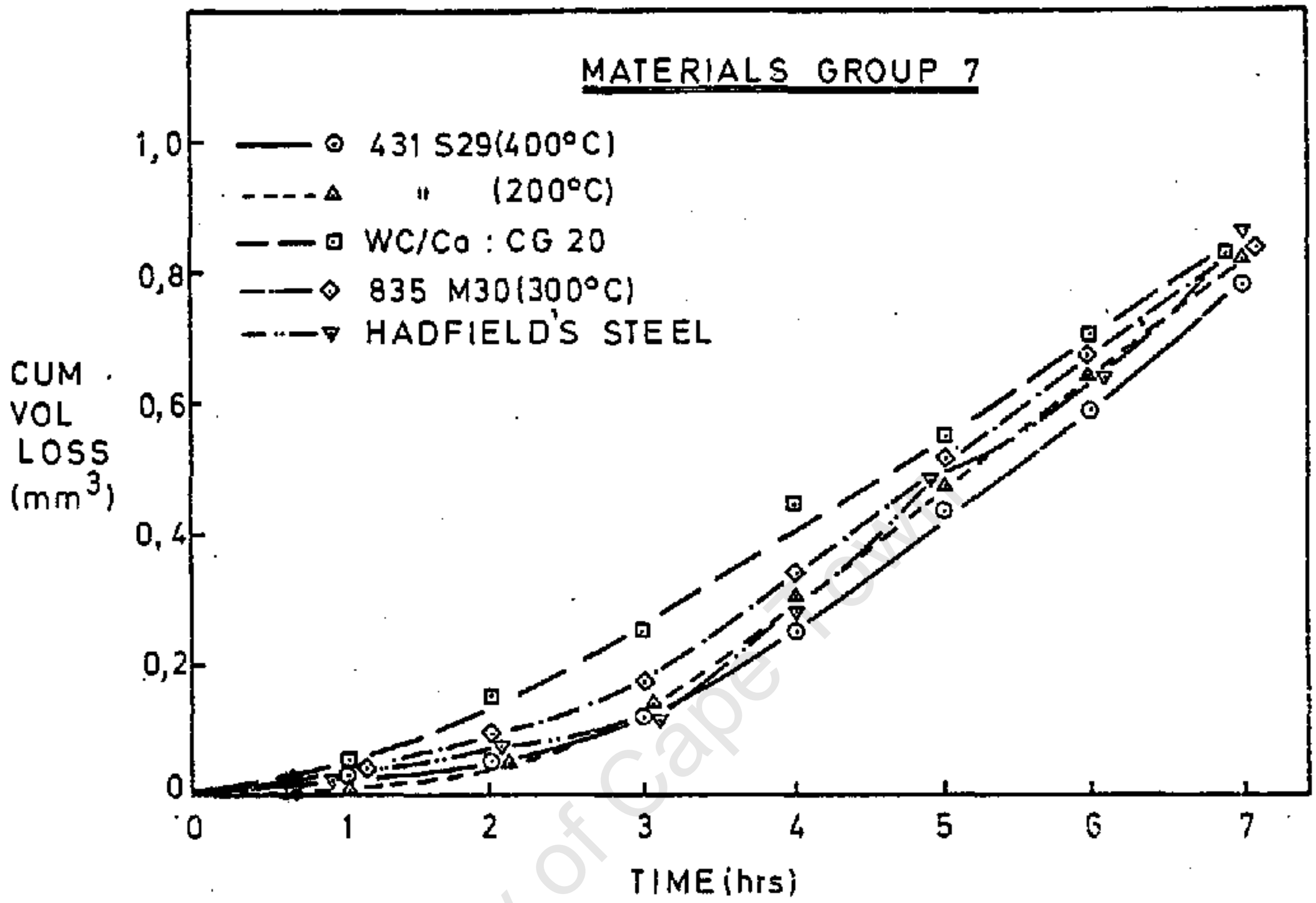

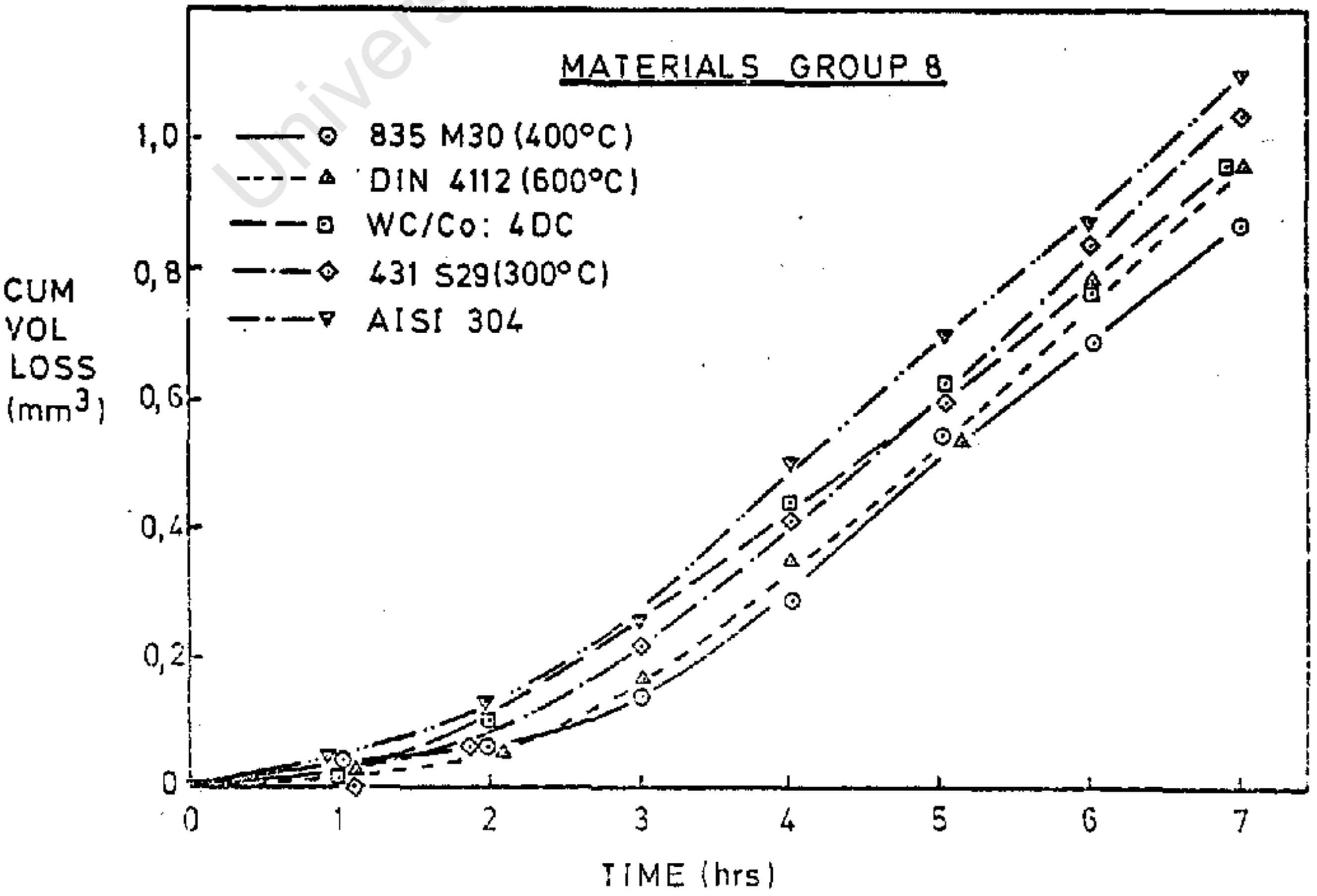

APPENDIX 7.2 contd.

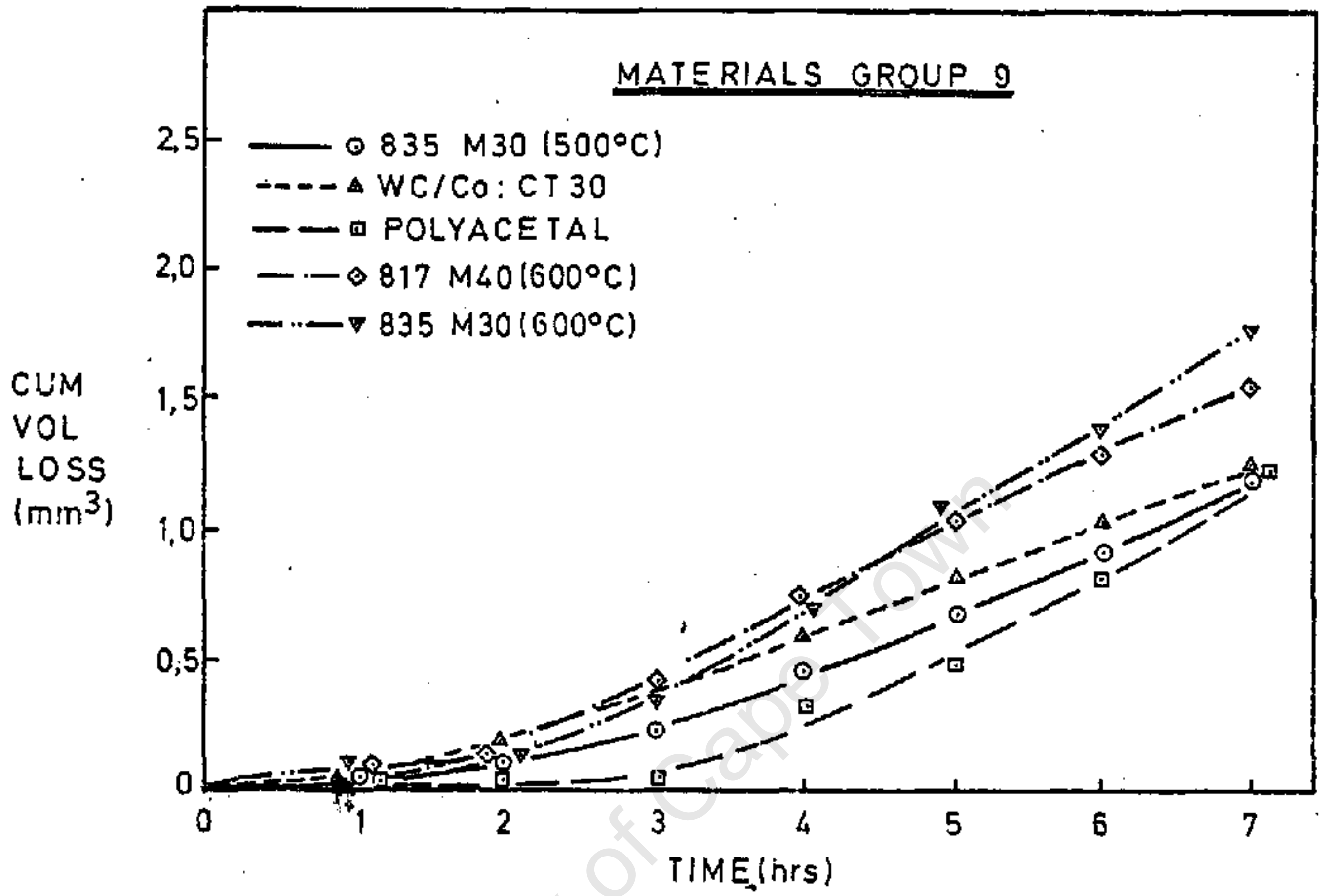

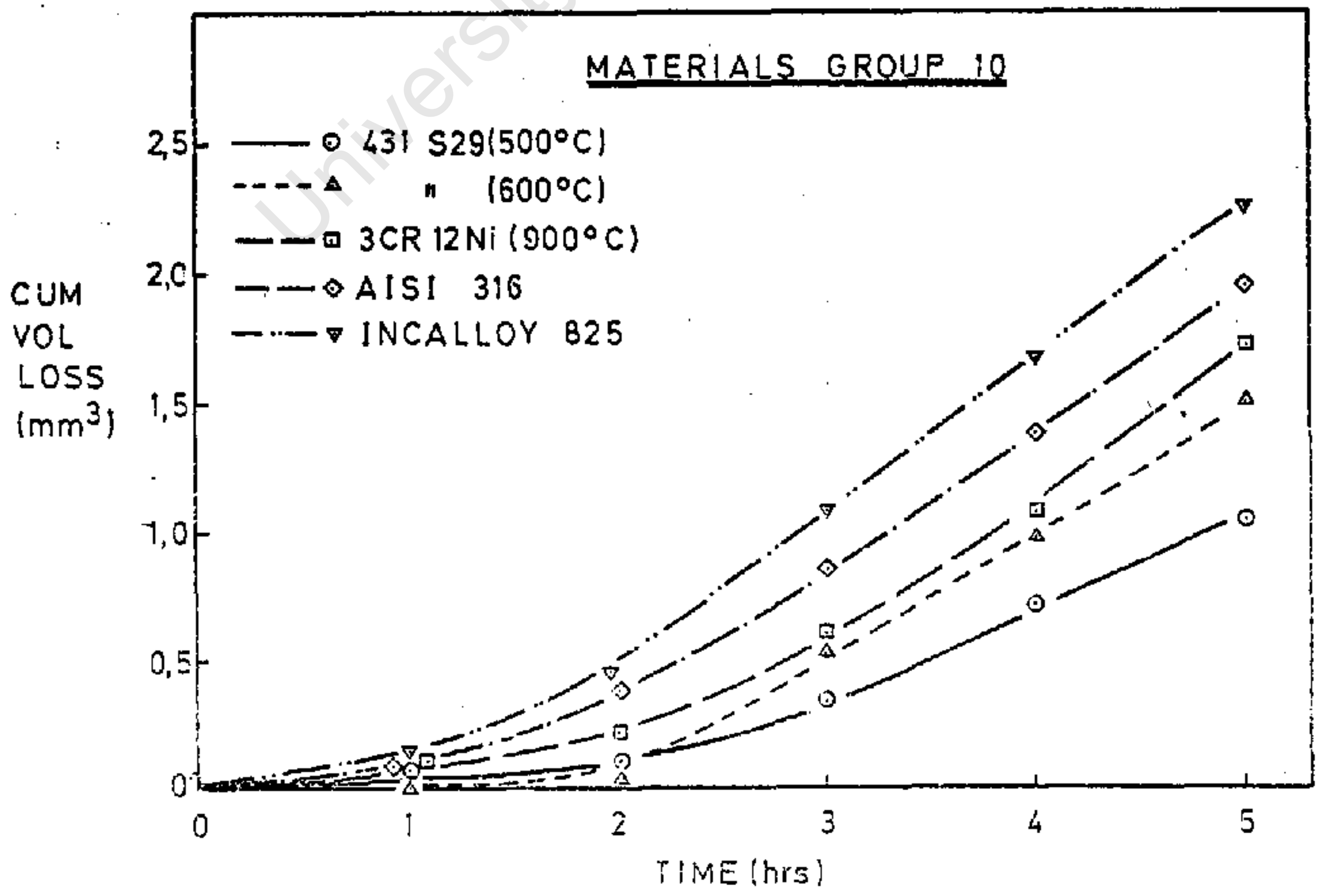

APPENDIX 7.2 contd.

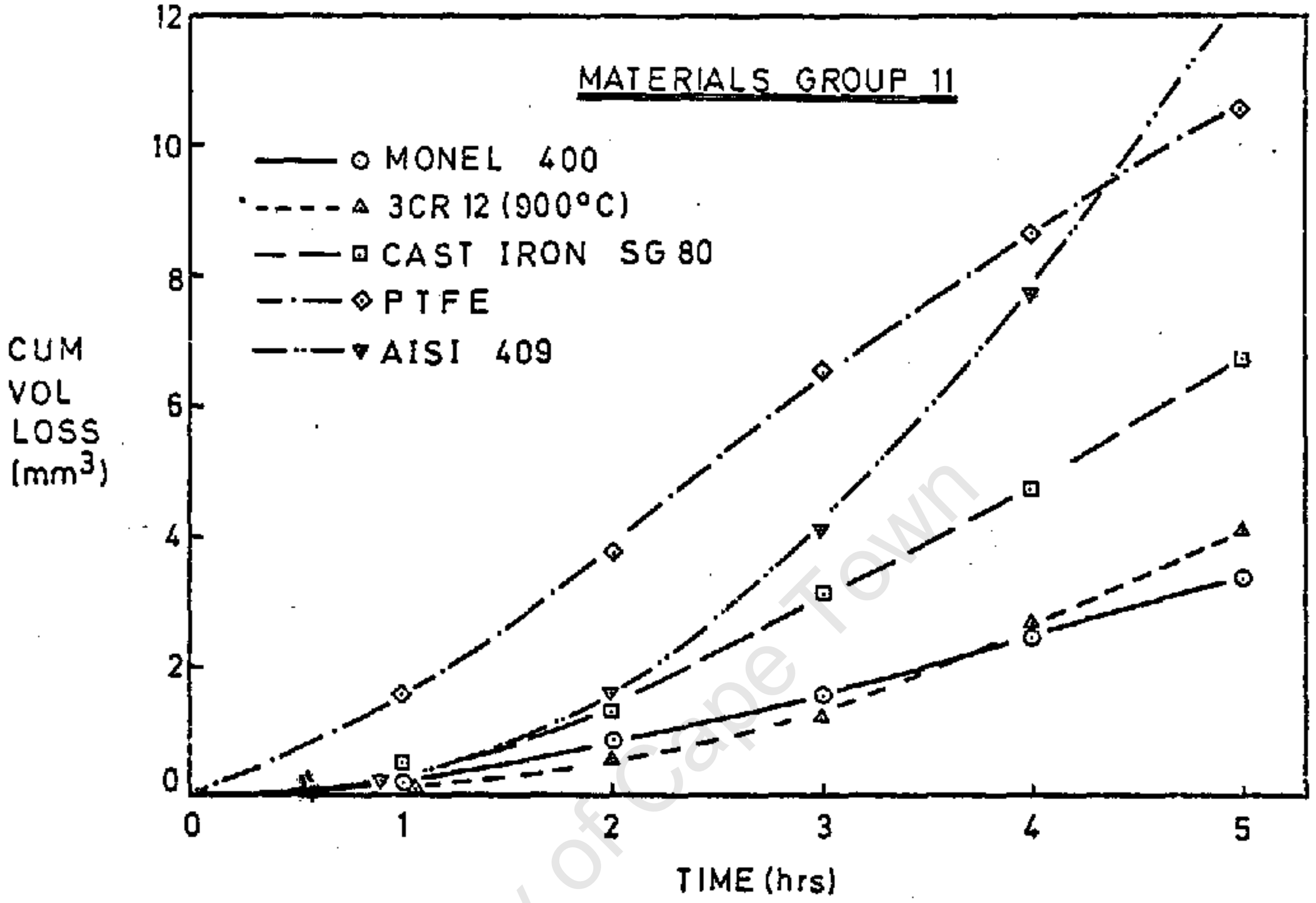

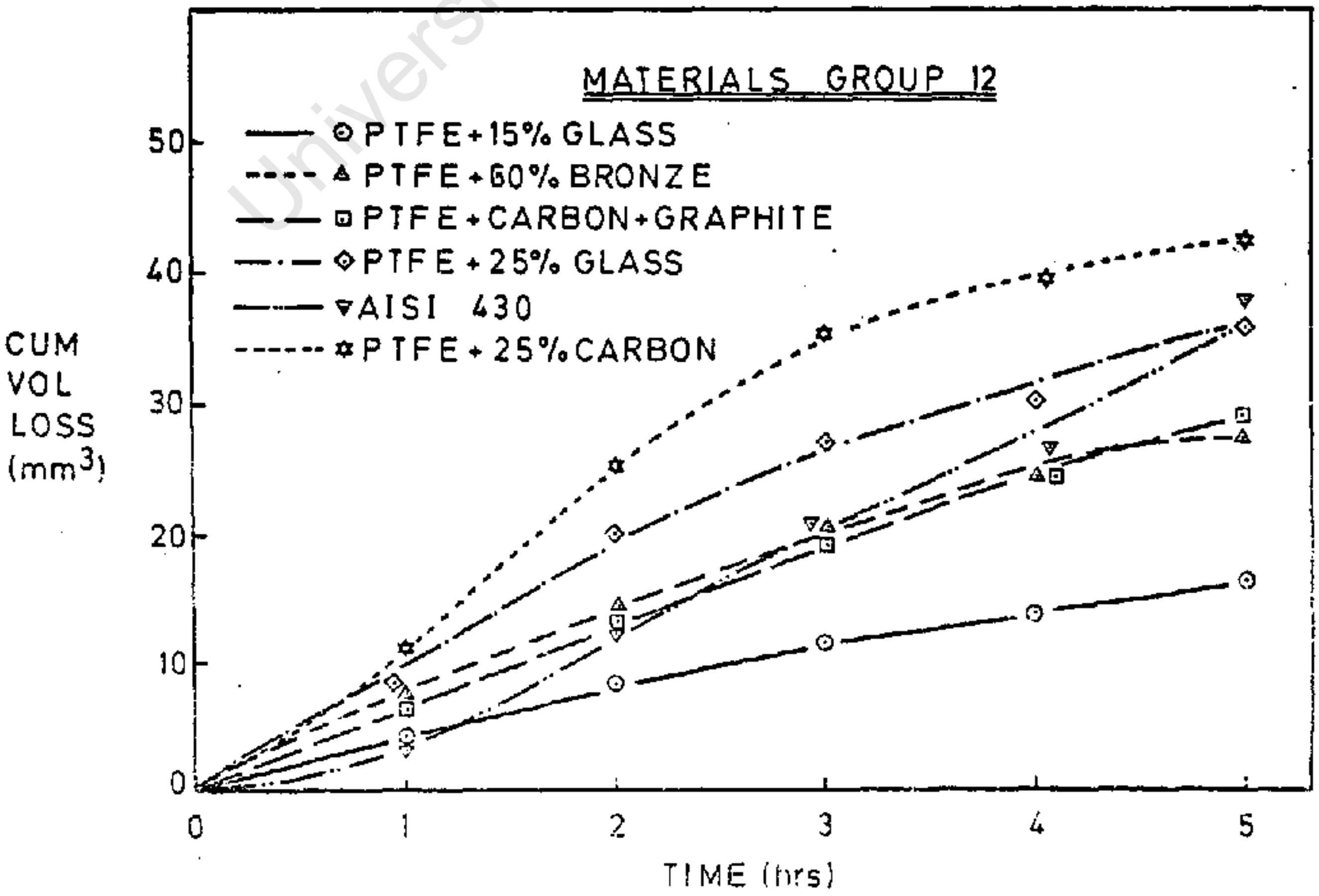

APPENDIX 7.3

CALCULATION OF THE STRESSES IN THE COBALT BINDER PHASE OF THE WC-CO CERMETS

Using equation 7.2

$$\sigma_{Co} = \varepsilon_{Co}E/1-2\nu \qquad \ldots\ldots\ldots\ldots\ldots \qquad 1$$

and the values $E_{Co} = 215\text{GPa}$

$\nu_{Co} = 0,32$

$\varepsilon_{Co} \sim 0,002$ (see below)

thus $\sigma_{Co} = 0,002 \times 215 \times 10^3/1-2(0,36)$

$= 1194$ MPa

Estimation of ε_{Co}

$$\varepsilon_{Co} = a_{o(Co)} - a_{o(Co\text{-}WC)}/a_{o(Co)} \qquad \ldots\ldots\ldots\ldots\ldots \qquad 2$$

where $a_{o(Co)}$ = Lattice parameter of pure α-Co

= 3.554 Å

$a_{o(Co\text{-}WC)}$ = Lattice parameter of Co in cermet

Calculation of $a_{o(Co\text{-}WC)}$

From the Bragg equation

$$a_o = \lambda/2\sqrt{(h^2 + k^2 + l^2)}/\sin\theta$$

and using $(h,k,l) = (111)$, $\lambda = 1,5418$ and $\theta = 22,15^*$

$$a_o = 1,5418\sqrt{3}\ /\ 2(\sin 22,15)$$

$$= 3,539\ \text{Å}$$

Similarly for $(h,k,l) = (200)$, $\theta = 25,7^*$

$$a_o = 3,555\ \text{Å}$$

Thus $a_{o(Co\text{-}WC)}$ average ~ 3,547 Å.

Substituting this value of $a_{o(Co\text{-}WC)}$ in equation 2 one obtains an approximate value of ε_{Co}, namely:

$$\varepsilon_{Co} \sim 0,002$$

---

* *Values taken from XRD trace of uneroded WC-Co grade CT65*

APPENDIX 7.4 (Taken from Ref. 126)

It is required to find a relation for the strain to plastic instability (necking) in terms of the work hardening exponent.

Since necking occurs at maximum load the condition for plastic instability is:

$$dP = 0 \qquad \ldots\ldots\ldots\ldots \quad 1$$

and since $P = \sigma A$

$$dP = \sigma dA + A d\sigma = 0$$

or

$$-dA/A = d\sigma/\sigma \qquad \ldots\ldots\ldots\ldots \quad 2$$

For a ductile metal, necking occurs at large strains where the constant volume condition holds:

$$dV = Adl + ldA = 0$$

or

$$-dA/A = dl/l \qquad \ldots\ldots\ldots\ldots \quad 3$$

substituting for dA/A from equation 2

$$d\sigma/\sigma = d\varepsilon$$
$$d\sigma/d\varepsilon = \sigma \qquad \ldots\ldots\ldots\ldots \quad 4$$

In other words plastic instability occurs in uniaxial tension at the strain when the slope of the true stress - true strain curve equals the true stress at that strain. The conditions for necking can also be expressed in terms of the strain hardening exponent when the power law $(\sigma=k\varepsilon^n)^*$ fits the stress - strain curve. The strain hardening exponent is:

$$n = d(\log\sigma)/d(\log\varepsilon)$$
$$= d(\ln\sigma)/d(\ln\varepsilon)$$
$$= \varepsilon/\sigma\,(d\sigma/d\varepsilon) \qquad \ldots\ldots\ldots\ldots \quad 5$$

on substituting for dσ/dε from eqn. 4 we get:

$$\varepsilon_{\text{unstable}} = n \qquad \ldots\ldots\ldots\ldots \quad 6$$

That is, necking occurs when the true strain equals the strain hardening exponent.

---

* *If this equation describes the σ→ε curve then a log - log plot of true stress and plastic strain from yield to maximum load will be a straight line of slope n.*

REFERENCES

1 A.Thiruvengadam, ASME, Applied Mechanics Reviews, March 1971, p. 245 - 253.

2 A.Thiruvengadam, Proc. 3rd Int. Conf. on Rain Erosion, Royal Aircraft Establishment, Elvetham Hall, U.K., 1970, p. 565.

3 P.Eisenberg, H.S.Preiser and A.Thiruvengadam, Trans. Society of Naval Architects and Marine Engineers, 73, 1965, p. 241 - 286.

4 E.Webster, Ultrasonics, Jan - Mar.1963, p. 39.

5 A.Thiruvengadam, Proc. 19th Meeting of Mechanical Failures Prevention Group, Boulder, Colorado. Edited by T.R.Shives and W.A.Willard, Metallurgy Division, Institute for Materials Research, National Bureau of Standards, Washington D.C., Nov. 1973, p. 13.

6 C.M.Preece and N.H.Macmillan, Annual Review of Materials Science, 7, 1977, p. 95 - 121.

7 F.G.Hammit, Applied Mechanics Reviews, 32, No. 6, June 1979, p. 665 - 675.

8 C.M.Preece (Ed.), Treatise on Materials Science and Technology (Erosion), 16, Academic Press, 1979.

9 N.C.Joughin, Journal of S.A. Institute of Mining and Metallurgy, 78 (8), March 1978, p. 207 - 217.

10 D.G.Wymer, S.A. Chamber of Mines 14th Annual Research Review, 1976 - 1977.

11 B.E.Protheroe, Proc. 5th Int. Conf. on Erosion by Solid and Liquid Impact, Cambridge, England, Sept. 1979, p. 64 - l.

12 F.Erdmann - Jesnitzer and H.Louis, ASTM STP 567, 1973, p. 171.

13 J.W.Holl, Trans ASME, Journal of Basic Eng., Dec. 1970, p. 681.

14 E.Harvey et al, Journal of Cellular and Comparative Physiology, 24, No. l, Aug. 1944; cited in Ref. 13.

15 F.E.Fox and K.F.Herzfeld, Journal of the Acoustical Society of America, 26, No. 6, Nov. 1954; cited in Ref. 13.

16 D.C.Pearse and L.R.Blinks, Journal of Physical and Colloidal Chemistry, 51, 1947, p. 556: cited in Ref. 13.

17 Lord Rayleigh, Phil. Mag., 34, Aug. 1917, p. 94.

18 R.T.Knapp, J.W.Daily and F.G.Hammit, 'Cavitation', McGraw-Hill Book Co., New York, 1970.

19 H.G.Flynn, Physical Acoustics, 1, Part B, (Ed. W.P.Mason), Academic Press, New York, 1964.

20 G.W.Sutton, Journal of Applied Mechanics, 24, p. 340; cited in Ref. 19.

21 B.Vyas and C.M.Preece, Journal of Applied Physics, 47, No. 12, Dec. 1976, p. 5133.

22 I.R.Jones and D.H.Edwards, Journal of Fluid Mechanics, 7, 1960, p. 596.

23 R.Hickling and M.S.Plesset, Physics of Fluids, 7, p. 7, 1964.

24 H.Poritsky, Proc. 1st U.S.National Congress of Applied Mechanics (ASME), p. 813, 1952; cited in Ref. 18.

25 J.M.Hobbs and A.Laird, Report No. 438, National Engineering Laboratory, East Kilbride, Glasgow, Oct. 1969.

26 F.G.Hammit and D.O.Rogers, Journal of Mechanical Engineering Science, 12, No. 6, 1970, p. 432.

27 M.S.Plesset, Trans ASME, Journal of Basic Eng., Sept. 1972, p. 559.

28 B.G.Singer and S.J.Harvey, Wear, 52, 1979, p. 147.

29 W.Wagenbach, Zeitschrift fur das Gesante Turbinenwesen, 4, 1907, p. 273; cited by W.J.Rheingans, ref. 32.

30 J.M.Mousson, Trans. ASME, 59, 1937, P. 399.

31 S.Logan Kerr, Trans. ASME, 59, 1937, p. 373.

32 W.J.Rheingans, Trans. ASME, 72, 1950, p. 705.

33 R.Garcia and F.G.Hammit, Trans. ASME, 89, Series D, 1967, p. 753.

34 S.G.Young and J.R.Johnston, ASTM STP 408, 1967, p. 186.

35 J.Z.Lichtman, Journal of Materials, 2, No. 3, Sept. 1967, p. 638.

36 G.C.Gould, ASTM STP 474, 1970, p. 182.

37 J.M.Hobbs and A.Laird, Report No. 495, National Engineering Laboratory, East Kilbride, Glasgow, Dec. 1971.

38 A.Laird and J.M.Hobbs, Report No. 496, National Engineering Laboratory, East Kilbride, Glasglow, Dec. 1971.

39 S.Vaidya and C.M.Preece, Met. Trans., 9A, Mar. 1978, p. 299.

40 E.Wade and C.M.Rreece, Met. Trans., Series A, 9, 1978, p. 1299.

41 J.M.Hobbs, ASTM STP No. 408, 1966, p. 159.

42 A.Thiruvengadam, Trans. ASME, 85, Series D, 1963, p. 365.

43 F.G.Hammit et al, Trans. ASME, Series D, 87, 1965, p. 453.

44 G.M.Wood, L.K.Knudsen and F.G.Hammit, Trans. ASME, 89, Series D, Mar. 1967, p. 98.

45 F.J.Heymann, ASTM STP 474, 1970, p. 212.

46 F.G.Hammit et al, ASTM STP 474, 1970, p. 288.

47 J.W.Tichler, A.W.J. de Gee and H.C. van Elst, ASTM STP 567, 1973, p. 56.

48 B.C.S.Rao et al, Trans. ASME, Series D, 92, 1970, p. 563.

49 J.Z.Lichtman et al,Corrosion, 17, No. 10, Oct. 1961, p. 119.

50 F.G.Hammit et al, ASTM STP 567, 1973, p. 197.

51 H.Busch, G.Hoff and G.Lanbein, Phil. Trans. Roy.Soc., 260A, 1966, p. 168.

52 M.S.Plesset and A.T.Ellis, Trans. ASME, 77, p. 1055.

53 M.S.Plesset and R.Divine, Trans. ASME, Series D, Dec. 1966, p. 691.

54 B.Vyas and C.M.Preece, ASTM STP 567, 1973, p. 77.

55 W.C.Leith and A.L.Thompson, Trans. ASME, Journalof Basic Eng., Dec. 1960, p. 795.

56 J.C.Grosskreutz and P.Waldow, Acta Metallurgica, 11, 1963, p. 717.

57 C.E.Feltner, Acta Metallurgica, 11, 1963, p. 817.

58 M.F.Rose and T.L.Berger, Phil. Mag., 17, 1968, p. 1121.

59 M.De Vries and A.Mastenbroek, Met. Trans. A, 8, Sept. 1977, p. 1497.

60 J.Awatani and T. Shiraishi , Met. Trans.A, 7, Oct. 1976, p. 1599.

61 E.Moin and L.E.Murr, Journal of Materials Science and Engineering, 37(3), 1979, p. 249.

62 C.M.Preece et al, Proc. 4th Int. Conf. on Strength of Metals and Alloys, Nancy, France, Aug./Sept. 1976, p. 1397.

63 C.J.Heathcock, B.Protheroe and A.Ball, Proc. 5th Int. Conf. on Erosion by Liquid and Solid Impact, Cambridge, England, Sept. 1979, p. 63 - 1.

64 B.Vyas and C.M.Preece, Met. Trans. A, 8, June 1977, p. 915.

65 W.Lauterborn, Proc. 5th Int. Conf. on Erosion by Liquid and Solid Impact, Cambridge, England, Sept. 1979, p. 58 - 1.

66 J.H.Brunton, same proceedings as Ref. 65.

67 C.M.Preece, S.Vaidya and S.Dakshinamoorthy, ASTM STP 664, 1978, p. 409.

68 F.Erdmann-Jesnitzer, F.Louis and J.Petersen, Metallwiss Tech., 31, p. 59, 1977; cited in Ref. 8, p. 283.

69 I.N.Bogachev and R.I.Mints, Oldbourne Press, London, 1966; cited in Ref. 8, p. 287.

70 J.V.Hackworth and W.F.Adler, M.F.P.G., U.S. National Bureau of Standards, Special Publ. 394, 1974, p. 54; cited in Ref. 8, p. 287.

71 J.W.Tichler and A.W.J. de Gee, Proc. 3rd Int.Conf.on Rain Erosion, (A.A. Fyall and R.B.King, Editors), Royal Aircraft Establishment, U.K., 1974, p. 847; cited in Ref. 8, p. 287.

72 D.A.Woodford, Met. Trans., 3, 1972, p. 1137.

73 W.L.Silence, Proc. The Int. Conf. on Wear of Materials, (W.A.Glaeser, K.C.Ludema and S.K.Rhee - Editors), ASME, St. Louis, Missouri, 1977, p. 77.

74 J.B.Marriott and G.Rowden, Phil. Trans. Roy. Soc., 260 A, 1966, p. 144.

75 S.G.Young and J.R.Johnston, ASTM STP 474, 1969, p. 67.

76 G.C.Gould, Proc. 3rd Int. Conf. on Rain Erosion, (A.A.Fyall and R.B.King - Editors), Royal Aircraft Establishment, Farnborough, U.K., 1970, p. 881; cited in Ref. 8, p. 289.

77 K.C.Antony and W.L.Silence, Proc. 5th Int. Conf. on Erosion by Liquid and Solid Impact, Cambridge, England, Sept. 1979, p. 67 - 1.

78 F.P.Bowden and J.H.Brunton, Proc. Roy. Soc. London, Series A, 263, 1961, p. 433.

79 J.H.Brunton and M.C.Rochester, Treatise on Materials Science and Technology, (Erosion) (C.M.Preece Ed.), 16, p. 185.

80 W.F.Adler, Proc.5th Int. Conf. on Erosion by Liquid and Solid Impact, Cambridge, England, Sept. 1979, P.9 - 1.

81 C.K.Chatten and A.Thiruvengadam in "Testing of Polymers", (J.V.Schmidz and W.E.Brown, Eds.), Vol. III, Wiley Interscience, New York, 1967, p. 245; cited in Ref. 8, p. 296.

82 C.M.Preece, Communication with S.A.Chamber of Mines, 1978.

83 J.Perkins, Kerry Ultrasonics, "An Outline of Power Ultrasonics", reprinted by W.S.Caines Ltd., London, El38AB.

84 "Titanium Probes for Ultrasonics", Dawe Instruments Limited, 1978.

85 M.Sketch, Private Communication, Central Acoustics Laboratory, University of Cape Town, 1980.

86 W.C.Brunton, J.M.Hobbs and A.Laird, Report No. 431, National Engineering Laboratory, East Kilbride, Glasgow, Sept. 1969.

87 J.M.Hobbs, Private Communication, National Engineering Laboratory, East Kilbride, Glasgow, 1980.

B8 R.Hickling, see discussion of Ref. 27.

89 W.C.Leith, Proc. Amer. Soc. Test. Materials, 65, 1965, p. 789; cited in Ref. 8, p.

90 P.Kenny et al, The Mining Engineer, Sept. 1979, p. 235.

91 J.M.Hobbs, Proc. Int. Conf. arranged by Fluid Machinery Group of the Institution of Mechanical Engineers, Heriot-Watt University, Edinburgh, Sept. 1974, p. 269.

92 R.Buhrmann, Private Communication, Mining Technology Laboratory, South African Chamber of Mines, 1980.

93 P.Becher, Emulsions: Theory and Practice, 2nd Edition, Robert E.Krieger Publishing Company, New York, 1977, p. 386.

93a J.H.Brunton, Proc. 2nd Int. Conf. on Rain Erosion, 1967, p. 291; cited in Ref. 8.

93b J.A.Halat and G.O.Ellis, 19th meeting MFPG, Boulder, Colorado, Edited by T.R.Shives and W.A.Willard, Metallurgy Division, National Bureau of Standards, Washington D.C..

94 P.S.Epstein and M.S.Plesset, Journal of Chemical Physics, 18, 1950, p. 1505.

95 Transistor Automation Corporation, "A Simple Instrument Measures Physical Properties of Polymers", Chem. Eng., 71, Mar., 1964, p. 62.

96 A.G.Guy, Elements of Physical Metallurgy, 2nd Edition, Addison-Wesley Publishing Company, Reading, Massachusetts, 1959, p. 351.

97 F.B.Pickering, Physical Metallurgy and Design of Steels, Applied Science Publishers Limited, London, 1978, p. 229.

98 F.Lecroisey and A.Pineau, Met. Trans., 3, Feb. 1972, p. 387.

99 D.Hennessey, G.Steckel and C.Altstetter, Met. Trans., 7A, March 1976, p. 415.

100 W.N.Roberts, Trans. Metallurgical Society of AIME, 230, April 1964, p. 372.

101 K.S.Raghaven et al, Trans. AIME, 245, 1969, p. 1569; cited in Ref. 102.

102 Y.N.Dastur and W.C.Leslie, Proc. 5th Int. Conf. on Strength of Metals and Alloys, Aachen,. W.Germany, Aug. 1979, p. 619.

103 W.O.Binder and H.R.Spendelow, Trans. ASM, 43, 1951, p. 759; cited by J.J.Demo, ASTM STP 619, 1971, p. 48.

104 A.Ball and J.Hoffmann, to be published in Metals Technology.

105 D.Bard, U.S.Naval Applied Science Lab., Technical Memo., No. 16, Lab. Project 9300-41, 1966.

106 K.N.Melton and O.Mercier, Acta Metallurgica, 27, 1979, p. 137.

107 D.J.Beckwith and J.B.Marriott, ASTM STP 408, 1966, p. 111.

108 H.W.Newkirk and H.H.Sisler, Journal of Amer. Ceram. Soc., 41, No. 3, March 1958, p. 93.

109 S.Timoshenko and J.N.Goodier, Theory of Elasticity, 2nd Edition, McGraw-Hill Book Company, Inc., New York, 1951, p. 524; cited in Ref. 108.

110 H.E.Exner, International Metals Reviews, Review No. 243, No. 4, 1979, p. 149.

111 V.K.Sarin and T.Johannesson, Metal Science, 9, 1975, p. 472.

112 H.C.Lee and J.Gurland, Materials Science and Engineering, 33, 1978, p. 125.

113 W.Dawihl and B.Frisch, Cobalt, 22, March 1964, p. 22.

114 D.W.Baker, K.H.Jolliffe and D.Pearson, Phil. Trans. Roy. Soc., 260A, 1966, p. 24.

115 Cobalt Monograph, Centre D'information du Cobalt (Ed), Brussels, 1960, p. 375.

116 D.A.Woodford and J.H.Beattie, Met. Trans., 2, 1971, p. 3223.

117 A.Giamei, J.Burma and E.J.Freise, Cobalt, 39, June 1968, p. 88.

118 L.Remy and A.Pineau, Materials Science and Engineering, 26, 1976, p. 123.

119 A.H.Graham and J.L.Youngblood, Met. Trans., l, Feb. 1970, p. 423.

120 J.Z.Lichtman et al, Corrosion, 17, No. 10, Oct. 1961, p. 119.

121 J.W.S. Hearle, Proc. Textile Inst./Inst. Text. de France Conf., Paris, 1975, p. 60; cited by J.J.Kausch, Polymers: Properties and Applications 2, Polymer Fracture, Spinger Verlag, Berlin, 1978, p. 203.

122 P.Meares, Polymers: Structure and Bulk Properties, D. van Nostrand Co., London, 1965, p. 107.

123 P.E.Bretz, R.W. Hertzberg and J.A.Manson, Journal of Materials Science, 14, 1979, p. 2482.

124 Y.S.Papir et al, Journal of Polymer Science, 10, Part A2, 1972, p. 1305.

125 J.A.Brydson, Plastics Materials, 2nd Edition, Iliffe Books, London, 1969, p. 108.

126 W.J.McGregor Tegart, Elements of Mechanical Metallurgy, The Macmillan Co., New York, 1966, p. 19.

PUBLICATIONS

Proc.5th Int.Conf on Erosion by Solid and liquid Impact

THE INFLUENCE OF EXTERNAL VARIABLES AND MICROSTRUCTURE ON THE CAVITATION EROSION OF MATERIALS

C.J. Heathcock*, B.E. Protheroe**, and A. Ball*

*Dept. of Metallurgy 8 Materials Science,
University of Cape Town, Rondebosch, 7700, R.S.A.

**Mining Technology Laboratory, Chamber of Mines of South Africa,
Johannesburg, 2000, R.S.A.

Parameters affecting acoustic cavitation have been studied by eroding pure iron by means of a laboratory apparatus. A separation distance of 0,35 mm between the test piece and source of cavitation and also a liquid medium temperature of 35 C give rise of maximum erosion rates. Aeration of, and the addition of suspended solids, to the test medium, do not affect the intensity of cavitation, However, the presence of certain water soluble oils in the test liquid reduces the rate of erosion.

A range of materials has been tested under 'standard' conditions and optical and electron microscopy (S.E.M.) of the damaged surfaces has revealed several distinct erosion mechanisms. These are used as a basis for classification of materials. Erosion resistance can be correlated with certain mechanical properties for materials with a common mechanism of erosion.

INTRODUCTION

Cavitation is prevalent in hydraulic systems and causes rapid loss of material from pump components and valves. In recent years users of hydraulic systems have changed to water based hydraulic fluids (57, oil/water emulsions), due to rising costs, and also to eliminate the hazards associated with pipe bursts when using mineral hydraulic oils. These low viscosity water based fluids are less resistant to cavity formation, and severe erosion of hydraulic components is frequently experienced. The present work, has been undertaken with a view to alleviating these problems.

The vibratory cavitation apparatus is a well established laboratory method of studying the effects of various parameters on cavitation. In most reported studies the test piece has had the form of a tip, which is attached to the end of the vibrating horn but more recently (1,2), in order to eliminate fatigue damage, the specimen is located below thehorn tip. The rate of erosion has been found to be a function of the separation distance between specimen and drill tip. This parameter was therefore investigated initially in order to obtain standard conditions. The characteristics of the liquid medium which pertain to practical conditions such as temperature, degree of aeration and suspended solids were researched systematically, with a view to determining any beneficial effects which could be incorporated into an industrial system.

The selection of material, as a cost-effective method of avoiding cavitation erosion, requires the establishment of a correlation between erosion rate, and a conventional mechanical property such as hardness. This has been the objective of numerous projects. Reliable relationships have not been obtained, and our work (3) on materials of widely varying properties, microstructure, and chemical composition, has given some insight into the controlling properties. It will be seen that material loss occurs by several mechanisms and correlotions between erosion properties and macromechanical properties will only be expected for materials undergoing a given type of erosion. It should now be possible to design an erosion resistant microstructure.

EQUIPMENT AND EXPERIMENTAL PROCEDURES

Industrial ultrasonic drills have been used to generate controlled cavitation damage. These drills operate at a frequency of 20kHz while the high frequency current outputs were adjusted to give vibratory amplitudes of 71pm and 75pm respectively. The amplitude was determined optically and an electrical transducer was used for continuous monitoring. The vibratory cavitation apparatus (Fig.1) allows for the easy removal and accurate replacement of the test piece and the setting

(±0,01) of the distance between specimen and drill tip. It is imperative to allow the system to attain thermal equilibrium (over a period of 90 mins.) at the working amplitude prior to the commencement of a test. This ensures that no subsequent change occurs in the separation distance between specimen and drill tip due to expansion of the horn. Replaceable screw-in tips were manufactured from a titanium alloy (318A) which has good erosion and corrosion resistance, good acoustical properties and low density. The low density permits reasonable tip dimensions while maintaining the acoustical balance of the horn.

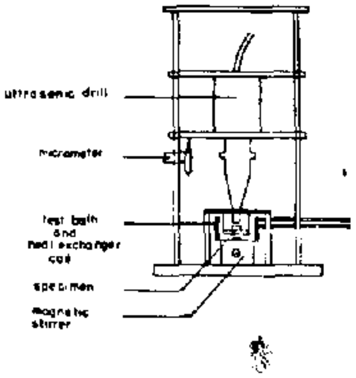

Fig. 1. Cavitation erosion apparatus.

It is necessary to maintain the test medium at a constant temperature during a test. A twelve litre tank of water is held at the required temperature, through the complimentary action of a thermoregulator and cooling coil. This water is then circulated through a heat exchanger coil, immersed in the test bath, while satisfactory heat exchange and uniform bath temperatures are achieved by means of a magnetic stirrer.

Distilled water was used in the test baths for all tests and the emulsions (5% strength volume to volume) were always made up immediately prior to testing. A temperature of 25°C was taken as standard in all tests except in the case of the emulsions which were held at 45°C (the approximate operating temperature of hydraulic mining machinery).

Pure iron (<15ppm impurities) was used as the material for the investigation into the influence of the various parameters on cavitation erosion. The test pieces in the form of 14 x 5,5 x 2,2mm thick coupons were prepared from 5mm diameter rods by rolling. Subsequent annealing produced a standard 90μm grain size. All specimens were polished to a 1μm grit finish. The experiments were conducted over a period of five hours and erosion was monitored by hourly weight measurements on a balance accurate to ± 0,1mg. The specimens were washed and handled carefully prior to weight checks in order to eliminate any extraneous weight changes.

RESULTS AND DISCUSSION

1. Separation distance

Maximum cavitation erosion of pure iron occurs when the distance between the horn tip and specimen is approximately 0,35mm (Fig.2.). This same effect had been observed by Preece (1) and Singer and Harvey(2) with aluminium and copper specimens respectively.

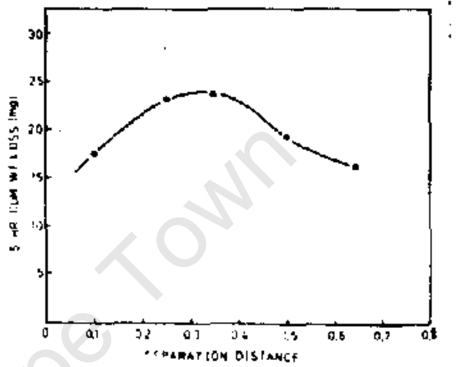

Fig. 2. Five hour weight loss of pure iron as a function of separation distance between horn tip and specimen.

There are two possible explanations for this maximum erosion rate, viz, (i) the stress which creates the cavities within a liquid is attenuated with increasing distance from the horn tip and therefore the number of cavitation events would be expected to decrease in a similar manner. However, the numbers of cavities formed, assuming a uniform nuclei distribution, will depend upon the volume of liquid between specimen and horn tip. Thus for a small separation distance, the number of nuclei in the volume of liquid between horn tip and specimen will restrict the total number of cavitation events and hence the rate of erosion. It will be expected, therefore, that maximum material removal will occur at a critical separation distance. (ii) For cavitation to occur, the liquid must re-enter the region between the horn tip and specimen during each tension stroke of a vibration cycle. As the distance between tip and specimen is reduced, the extent to which this occurs will decrease and thus cavitation damage, as measured by weight loss of the specimen, will be reduced. This effect, when combined with the attenuation of the stress cavitating the liquid with distance from the horn tip, will result in the observed maximum in erosion with separation distance. This optimum distance was used for all subsequent liquid and material investigations reported herein (0,35mm).

2. The effect of medium temperature

A medium temperature of 35°C results in a maximum in erosion rate in both distilled water and 5% oil/water emulsions (fig.3). Singer and Harvey (2) obtained a similar result in water using copper as the test material while Hobbs and Laird (4) and Plesset (5) found maxima at approximately 50°C for a range of metals.

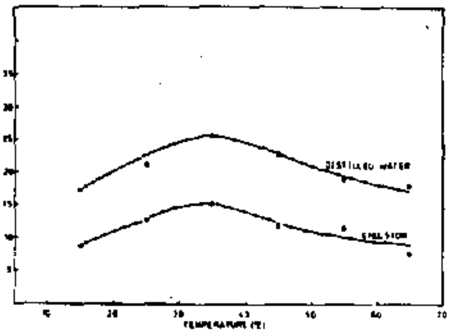

Fig. 3. Five hour weight loss of pure iron as a function of the temperature of the liquid medium.

The effect at temperature has been ascribed (4,5,6) to the combined effects of increased gas solubility at low temperatures and increased vapour pressure at high temperatures. At low temperatures (less than 35°C) the increased dissolved gas content leads to a higher rate of diffusion of gases across cavity boundaries. The pressures gradient across the boundary is therefore reduced, the result being a decrease in the stress produced by bubble collapse. As the temperature is increased, the solubility of gases in water decreases and erosion rates increase correspondingly. At still higher temperatures, the vapour pressure within the cavities in the liquid increases and again their collapse is dampened due to smaller pressure differences.

The presence of 5% of a soluble oil does not apparently affect the processes involved in the temperature effect; the oil droplets in the emulsion do not interfere with the diffusion of gases across the walls of the cavities within the water phase.

3. The effect of suspended solids

The influence of suspended solid material in the cavitating medium was investigated by adding either the residue from a mine service water or pure kaolin to the test medium. It was suspected that the suspended particles would act as nuclei for cavity formation, but no increase in the rate of erosion was observed. One can conclude, therefore, that there are more than sufficient nuclei in the distilled water prior to provision of additional nuclei. Also, since it is probable that the nucleation of the most damaging cavities occurs at the very numerous irregularities and imperfections on the specimen surface, then the provision of additional nuclei in the liquid has a negligible effect on erosion.

4. The effect of aerating the liquid medium

Aerating the distilled water medium during the course of a cavitation test does not affect the rate of erosion of pure iron. The dissolved oxygen content (assumed to be proportional to the total dissolved gas content at room temperature and pressure), was monitored during these tests. The concentration of oxygen was found to decrease from 7,7 ppm to 7,2 ppm during the course of a test run under equilibrium conditions, while for the tests in which the medium was aerated, the dissolved oxygen content remained constant at the saturation value of 8,7 ppm.

The change in dissolved gas content due to aeration is clearly not sufficient to influence cavity collapse processes in the manner outlined in Section 2. Also, any increase in nuclei density due to aeration does not seem to affect cavitation. It appears, as in the case of the suspended solids, that an excessive number of nuclei already exist in the liquid or at the specimen surface.

5. Cavitation tests in oil-water emulsions

The influence of various oil-water emulsions of constant 5:95 volume ratio on cavitation erosion has been determined. Fig. 4 shows typical erosion curves of pure iron in water, three emulsions and a mineral oil and Fig. 5 illustrates the relationship between emulsion 'performance' and oil droplet size.

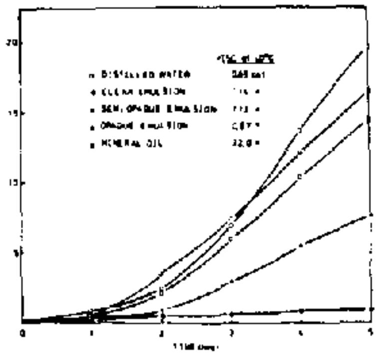

Fig. 4. Cumulative weight loss of pure iron as function of time in distilled water, mineral oil and 5 percent volume oil-water emulsions of various droplet sizes.

It will be noted from Fig. 4 that the viscosities of the emulsions are little different from that of distilled water and that the decrease in erosion loss does not show a correlation with any increase in

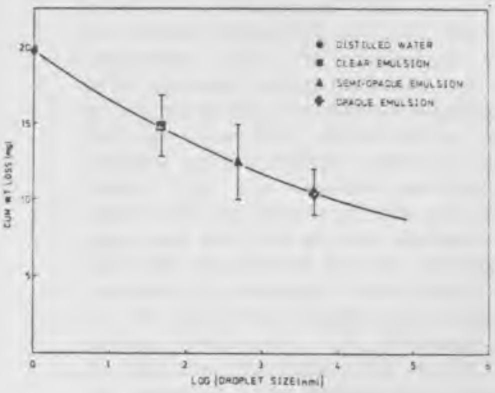

Fig. 5. Five hour weight loss of pure iron as a function of the droplet size of the 5 percent volume oil-water emulsions.

viscosity. Furthermore, moderate increases of up to 10 percent in concentration of the oil in water does not improve the erosion rate significantly. It is only when the concentration is very high that erosion is substantially reduced. These results therefore do not indicate that the viscosity of dilute emulsions is an important parameter. However, a distinct correlation does exist between oil droplet size and erosion. Erosion is reduced by an increase in droplet size (Fig. 5) and the occurrence of brittle removal of material, as determined by scanning electron microscopy, (Fig. 6.) is diminished. Since water has a surfeit of nuclei, it is unlikely that the presence of small oil droplets affects the erosion rate through the provision of extra nuclei within the liquid volume. A more tenable explanation follows from the relationship between the amount of emulsifier and oil droplet size. A decrease in the amount of emulsifying agent will result in an increase in the surface tension γ_{ow} at the oil-water interface and hence an increase in droplet size. The ability of the oil to 'wet' the specimen metal surface will also increase since the adhesion of the wetting liquid is measured by the work W per unit area to break the interface. The work is given by

$$W = \gamma_{mw} + \gamma_{ow} - \gamma_{mo}$$

$$\text{or} \quad W = \gamma_{ow}(1 + \cos\theta)$$

where the surface tensions γ_{mo}, γ_{ow} and γ_{mo} refer to metal-water, oil-water and metal-oil interfaces respectively and are related by the equilibrium of tensions,

$$\text{viz.:} \quad \gamma_{mw} = \gamma_{mo} + \gamma_{ow}\cos\theta$$

at the triple point with contact angle θ. A large value of γ_{ow} and the corresponding large droplet size will thus favour a large W and good wetting. (θ small). It can be postulated, therefore, that the decreased erosion rate is due to the formation of a persistent oil film on the specimen surface. Since it is considered (1,7) that the cavities which cause the most erosion lie within a radius (<100μm) of the specimen surface, then the

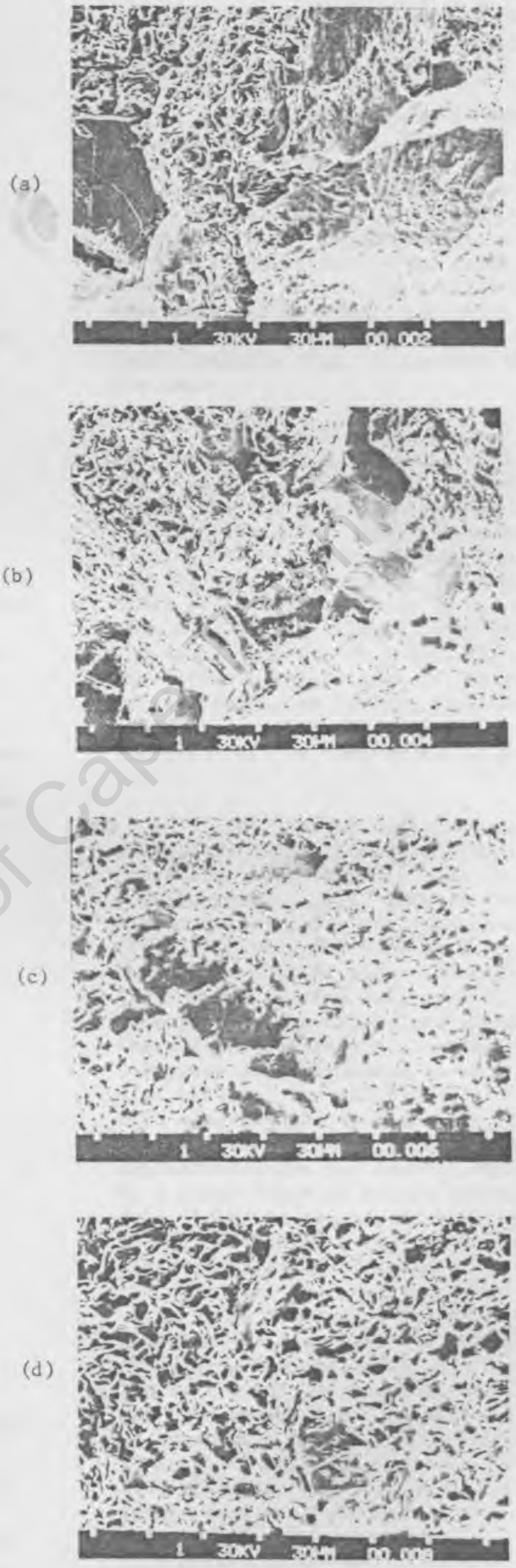

Fig. 6. Scanning electron micrographs of pure iron specimens after cavitation erosion for five hours in (a) distilled water (b)clear emulsion, droplet size 50 nm. (c) semi-opaque emulsion, droplet size 500 nm. (d) opaque emulsion, droplet size 5000 nm.

beneficial effect of this oil film will result from either or both of the following reasons:- (i) the surface of the specimen will possess irregularities and imperfections which nucleate the most damaging cavities. The oil film will effectively 'smooth' this surface and eliminate near surface nucleation. (ii) The nearest cavities will be at least the thickness of the oil film from the specimen and the stress created on collapse will be attenuated by the viscous layer. Evidence to support this theory is provided by the scanning electron micrographs of the eroded specimens. The decrease in the amount of brittle fracture with an increase in the oil droplet size indicates a decrease in the rate of shock loading of the iron test piece surface. The oil film would also inhibit any corrosion component of the erosion process.

6. Materials

A large number of engineering materials has been tested for cavitation erosion resistance. These materials include low and high alloy steels, cobalt and nickel alloys, sintered carbides and various polymers including polytetrafluoro-ethylene (PTFE), nylons, polyacetal copolymer and polyethylene. The duration of tests and material volume losses varied greatly and for this reason the perfomances of the materials have been divided into six ranges. Fig. 7 shows the relative positions of these ranges and also the materials in each of these categories.

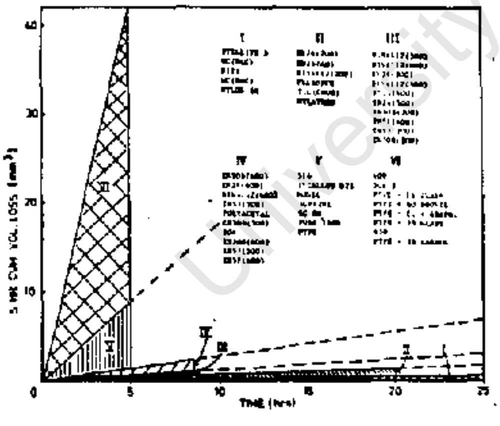

Fig. 7. Erosion behaviour of materials divided into six regions of performance. The volume loss versus time curve for a given material lies within the appropriate region as listed.

Examination of the eroded surfaces by optical stereomicroscopy and scanning electron microscopy has revealed several mechanisms of material removal and this information, together with values of elastic resilience, has indicated the various material parameters which determine erosion resistance. The methods of material removal have been identified as (i) low energy transgranular cleavage and/or intergranular grain removal, (ii) high energy ductile extrusion and rupture, (iii) the fibrous tearing of resilient polymers and (iv) 'plastic' deformation of PTFE.

The first of these is typified by the transgranular cleavage, Fig. 8(a) which occurs in the strain rate sensitive ferritic steels and in particular in those such as 409 and 430 type stainless steels which contain chromium. Pure iron loses material partly by a brittle intergranular and partly by the ductile mode. Since the brittle mechanisms dissipate little energy extensive erosion is anticipated for these metals and the experimental results, Fig. 7, confirm this prediction.

Material loss by ductile extrusion and rupture occurs in metals such as Monel 400, Incalloy 825, SG 80, austenitic stainless steels and the heat treated high and low alloy steels. Fig. 8(b) shows the cavitated surface of Monel 400 which is typical of ductile material removal. This mode of material failure also occurs in the more resistant metals, for example, Fig, 8(c) shows the damage surface of a sintered carbide. The softer matrix erodes preferentially by a ductile mechanism leaving the hard carbide particles exposed. These are subsequently 'knocked out' or removed by cavitation action.

The erosion resistant polymers such as nylons, high density polyethylene and polyacetal copolymer all lose material by fibrous tearing (Fig. 8(d)). Pure PTFE and PTFE containing fillers such as graphite, carbon, glass and bronze have poor erosion resistance and the mode of material loss (Fig. 8(e)) is very different to that of the more resilient polymers mentioned above. There is no evidence of tearing of the polymer structure and the damage is more of a 'plastic' nature. The addition of fillers to PTFE enhances the erosion rate considerably. The presence of these particles provide initiation sites for erosion while removal of a glass fibre or bronze particle results in a 'hole' in the material surface exposed to the cavitation cloud which assists the rapid progression of damage.

In discussing these results it is important to note that the volume loss versus time curve for most materials has two distinct linear regimes below and above a time t_o which has been termed the 'incubation time'. It is reasonable to make the hypothesis that up to t_o, a material is accumulating fatigue-like damage in the form of plastic flow and/or the nucleation and growth of sub-critical microcracks. Volume loss is minimal. Beyond t_o the rate of volume loss increases to another constant value. It appears that a steady state condition has been attained such that the material undergoes ductile or brittle fracture via the propagation of existing flaws and simultaneously accumulates 'fatigue' damage and microcracks. The rate of volume loss in the steady state period is, in general, inversely related to the incubation period.

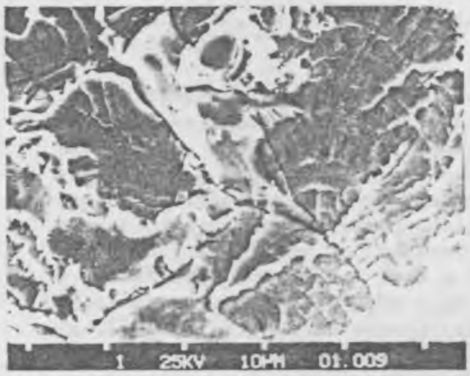

Fig. 8(a). Brittle erosion mode as typified by a 409 type stainless steel.

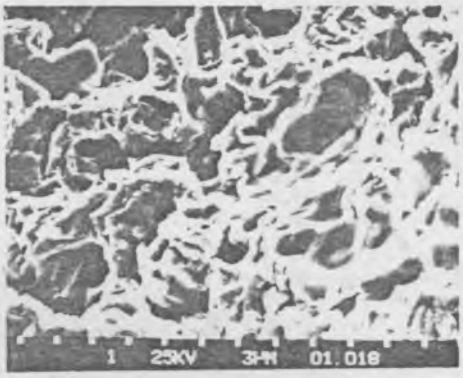

Fig. 8(b). Ductile erosion mode as typified by Monel 400.

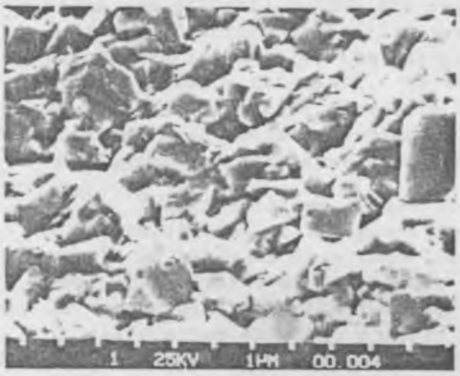

Fig. 8(c). Erosion damage of a sintered carbide. The matrix has been removed by a ductile mode of erosion leaving the carbide particles.

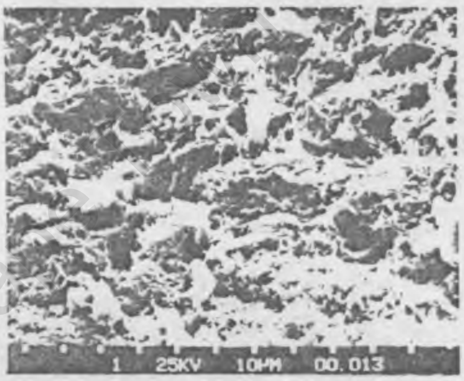

Fig. 8(d). Erosion damage of Nylatron. The fibrous character of the surface is typical of the polymers which have good erosion resistance.

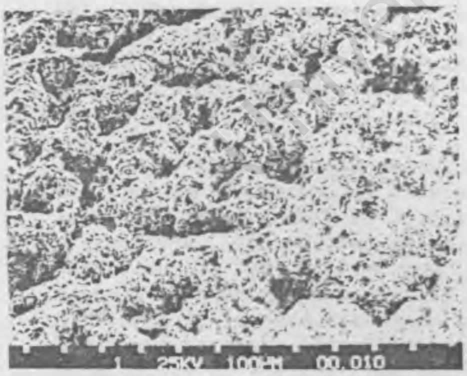

Fig. 8(e). Erosion damage of polytetrafluoroethylene.

Fig. 8. Scanning electron micrographs of eroded surfaces which are typical of the various material removal modes.

Since erosion damage is caused by the high frequency (20kHz) collapse of bubble clouds close to the specimen surface the material will experience shock-impact and tension during each cycle. This will result in any of the following deformations: (i) reversible elastic distortion of the surface with no accumulation of damage, (ii) the nucleation and propagation of cracks, (iii) irreversible plastic deformation with the accumulation of 'fatigue' damage, (iv) reversible plastic distortion with little or no accumulation of damage. For constant testing conditions their occurence will be

SS, the as-quenched or lightly tempered carbon steels, and the compound NiTi are capable of undergoing strain via shear-type transformations. The cobalt-rich matrix in Stellite and WC-Co metals will transform from f.c.c. to c.p.h., retained austenite in 304 type and the carbon steels will transform to martensite, while NiTi is known to undergo a reversible transformation at temperatures close to ambient. In Fig. 9. the values for the alloys which may undergo phase transformation are indicated with 0 symbols. They lie below the curve which relates volume loss after 5 hours to Shore hardness. This indicates that the transformations have a beneficial effect on the erosion properties and transmission electron microscopy of specimens taken from close to the surface of 304 type stainless steel indicates that a transformation has indeed been induced by erosion (3).

CONCLUSIONS

The findings of our work on the various parameters affecting cavitation intensity are summarized below:

(i) A separation distance of 0,35mm has been found to give rise to a maximum in the erosion rate of pure iron. This effect is thought to be a result of a combination of the attenuation of cavitation stress with distance and either the physical restriction of nucleation and cavity growth processes, or simply the inability of the liquid to re-enter the cavitation zone.

(ii) A medium temperature of 35°C gives rise to maximum erosion rate. High gas solubility at low temperatures and increased vapour pressure at high temperatures are considered to be the cause of this phenomenon.

(iii) The lack of an increase in erosion rate with addition of suspended material is thought to be due to the adequate number of nuclei present in the medium or at the specimen surface prior to provision of additional nuclei.

(iv) Aeration of the medium during cavitation tests has no influence on the erosion rates. The small increase in gas content is not sufficient to affect cavity collapse stresses and again the provision of extra nuclei in the form of gas bubbles, has no affect on cavitation.

(v) Oil/water emulsions have a beneficial effect on erosion rates. There is a correlation between oil droplet size and oil performance, and this can be understood in terms of the corresponding increase in the ability of the oil to 'wet' the specimen surface. The resulting oil film eliminates near surface cavity nuclei and also provides a shock absorbant layer.

(vi) The study of the cavitation erosion properties of a wide range of materials with different microstructures has enabled us to establish that several mechanisms of material loss and resistance occur and improved performance can be achieved by using materials with one or more of the following properties.

(i) a high elastic resilience,

(ii) a high resistance to the accumulation of 'fatigue' damage under repeated shock loading conditions. This requires either a high yield strength or the occurrence of a stress induced phase transformation.

(iii) a microstructure which is tough with respect to the propagation of microcracks.

ACKNOWLEDGMENTS

The Chamber of Mines of South Africa and the University of Cape Town are acknowledged for their generous provision of financial support and laboratory facilities. The valuable discussions of the results with Mr. R. Bührman and the kind cooperation of the Electron Microscopy Unit of the University of Cape Town are appreciated. Mrs. G. Perez and Mrs. J. Sharland are gratefully thanked for their assistance with the collation of the laboratory results and the preparation of the manuscript.

REFERENCES

1. Vyas B. and Preece C.M. 1976, J. of Appl. Phys. 47, 5133.
2. Singer B.G. and Harvey S.J. 1979, Wear 52, 147-160.
3. Heathcock C.J., Protheroe B. and Ball A. to be published in Proc. 5th Int. Conf. on Strength of Metals and Alloys, Aachen, 1979.
4. Hobbs J.M. and Laird A. 1969, National Engineering Laboratory Report No. 438, East Killbride, Glasgow.
5. Plesset M.S. 1972, J. of Basic Eng. Trans. ASME 94, 559.
6. Logan Kerr S. 1937, Trans. ASME 59, 373.
7. Knapp R.T., Daily J.W. and Hammit F.G. 1970, Cavitation. McGraw-Hill.
8. Preece C.M., Vaidya S. and Dakshinamoorthy S. 1977, presented at ASTM Symposium 'Erosion: Prevention and Useful Applications' Colorado, U.S.A.
9. Gould G.C. 1970, presented at Third Int. Conf. on Rain, Erosion and Associated Phenomena, England.
10. Woodford, D.A. and Beattie H.J. 1971, Met. Trans. 2, 3223.
11. Woodford D.A. 1972, Met. Trans. 3, 1137.
12. Zackay, V.F., Parker E.R., Fahr D. and Busch R. 1967, Trans A.S.M., 60, 252.
13. Pineau A.G. and Pelloux R.M. 1974, Met. Trans. 5, 1103.

determined by the properties of the material and these will, in turn, be controlled by microstructure.

Reversible elastic response will be favoured by those materials with high elastic resilience. Resilience is a measure of the ability of a body to absorb the energy of an impact elastically, without failure, and therefore depends on either a high failure (by plastic yielding or fracture) stress or a low elastic constant. Thus a hardened steel or a rubber will have high elastic resilience. Figure 9. demonstrates the experimental relationship between resilience and erosion loss. As predicted, both hard steels and pure polymers have high resilience and good ersoion properties. The presence of impurities or filler materials not only increases the elastic moduli of the polymers but also provides regions of elastic mismatch and suitable nuclei for rupture. Purity and surface perfection are thus important parameters for the performance of high resilience materials. Ceramics, such as alumina which have extremely high yield stresses have inherent surface flaws and thus have low resilience in practice.

The oscillating stress will promote the accumulation of fatigue-like damage in metals at stresses less than the measured macroscopic yield stress. This 'fatigue' hardening will take the form of an increase in dislocation density, and, as the hardening continues with each cycle, the local internal stress may become sufficient to initiate brittle or ductile failure. Brittle failure is inherent to the b.c.c. metals (particularly those containing chromium) at low temperatures or at high strain rates and the very high erosion losses for the ferritic SS of the types 409 and 430 are evidence for this. The fractures may be of the transgranular cleavage type (Fig. 8(a)) or intergranular. The latter is favoured when trace impurity atoms have segregated on grain boundaries.

The f.c.c. metals do not become embrittled at high rates of strain and volume loss (Fig.8(b)) occurs by ductile extrusion and rupture. The rate of volume loss will depend on the rate of 'fatigue' damage accumulation which in turn will depend on the level of imposed stress as compared with the yield stress. Soft materials will suffer more damage in a given time period and material loss will be more rapid. The rupture will be discouraged by an increase in the toughness of a microstructure. Small grains or second phases with strong interfaces will increase the yield strength and its resistance to crack propagation. The beneficial effect of reducing the grain size or microstructural dimensions of ductile materials has been established both in the present study and by Preece, Vaidya and Dakshinamoorthy (8).

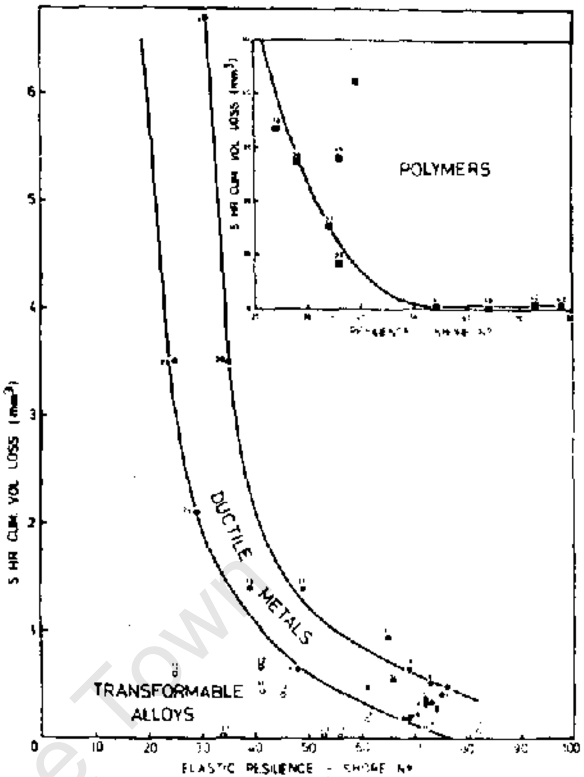

1. EN24	200	22. 304 SS
2.	300	23. S.G. 80
3.	400	24. Incalloy 825
4.	500	25. Stellite 3
5.	600	26. Monel 400
6. EN30B	200	27. WC - 8MC
7.	300	28. WC - 8LC
8.	400	29. WC - CNO2
9.	500	30. 3Cr12Ni
10.	600	31. EN24 - A.Q.
11. EN57	200	32. NiTi
12.	300	33. PTFE
13.	400	34. PTFE - 60 Bronze
14.	500	35. PTFE - 25 Carbon
15.	600	36. PTFE - C + Graph
16. DIN4112	200	37. PTFE - 15 Glass
17.	300	38. PTFE - 25 Glass
18.	400	39. Nylatron
19.	500	40. Nylon 66.
20.	600	41. Flurodur
21. 316 SS		42. Polyacetal

Fig. 9. Relationship between erosion loss and elastic resilience as measured by a Shore Scheroscope.

The occurrence of a stress-induced phase transformation at the surface of cobalt containing alloys during cavitation erosion has been reported (9,10,11). Since it has been established that similar phase transformations in TRIP and stainless steels enhance both their ductility (12) and fatigue properties(13), it is reasonable to assume that cavitation erosion resistance will be similarly improved. This would arise from improved 'fatigue' lifetime due to the reduced build-up of internal strain (dislocation density) afforded by the phase transformation. The refinement of the microstructure due to the presence of laths of the new phase would also improve the micro-toughness. Stellite, the tungsten carbide 'hard' metals, the 304 type

ELECTRON METALLOGRAPHY OF MATERIAL WEAR

C.J. Heathcock, C. Allen and A. Ball

Department of Metallurgy and Materials Science, University of Cape Town

The wear of engineering materials in industrial situations can occur under a wide variety of conditions and many mechanisms of damage may be responsible for material loss. Electron microscopy is a most powerful technique for the elucidation of these mechanisms and for the assessment of the influence of the particular conditions of stress and environment. Processes involved in the wear by cavitation (the growth and collapse of cavities in a liquid) and by solid particle abrasion have been studied using both scanning and transmission electron microscopy.

Four distinct modes of material removal from surfaces subjected to a cavitating environment have been identified in a range of engineering materials, viz: (a) ductile fracture in nickel and cobalt alloys, austenitic stainless steel and high and low alloy carbon steels, (b) brittle transgranular and intergranular failure in ferritic stainless steels, (c) fibrous tearing in resilient polymers such a nylon and polyacetal copolymer and (d) 'plastic flow' like deformation of polytetrafluorethylene. Transmission electron microscopy has revealed evidence of structural changes which occur in some alloys as a result of cavitation action. These transformations absorb, in part, the energy of the impacting blows from bubble collapse.

The mechanisms of material removal during abrasive wear are different to those occurring in cavitation erosion due mainly to the difference in locally applied strain rates. In general the abrading particle causes severe local plastic deformation followed by crack nucleation and propagation. Parameters such as yield stress, work hardening and microstructure are being investigated in relation to abrasive wear resistance. To date the following features have been observed; the surface of 'soft' metals is ploughed and ductile fracture is responsible for metal loss, the surface of harder steels shows evidence of microcracking occurring in conjunction with plastic deformation while polymers show fibrial stretching and tearing.

The accompanying scanning electron micrographs illustrate the nature of surfaces damaged by cavitation erosion and sliding abrasion.

Fig.1: Ductile failure of the matrix in a sintered carbide and the exposed carbide particles; Fig.2: Brittle transgranular and intergranular failure in type A.I.S.I. 409 stainless steel; Fig.3: 'Plastic flow' deformation in polytetrafluorethylene +25% glass fibre mixture showing the exposed fibres; Fig.4: Abrasive wear of copper showing surface ploughing and extrusion of material to form ridges; Fig.5: General surface deformation and evidence of microcracking in high carbon steel following abrasion with quartzite rock; Fig.6: Showing the drawing and tearing of fibrils in Nylon 66 following surface abrasion.

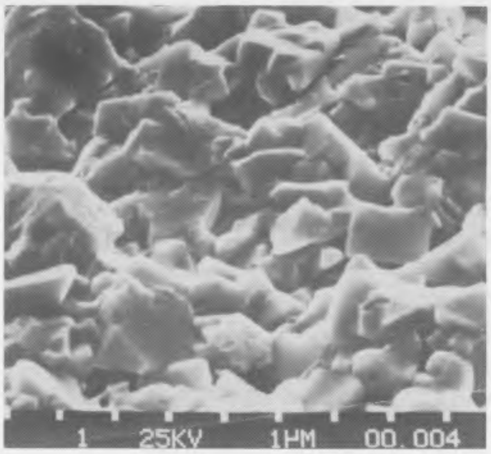

Fig. 1

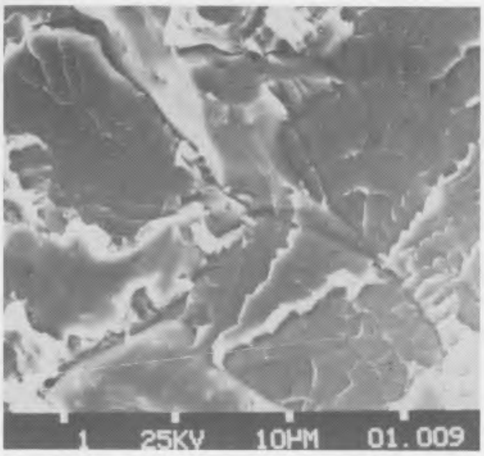

Fig. 2

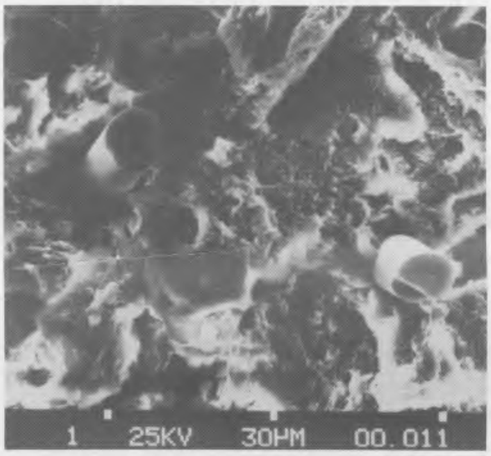

Fig. 3

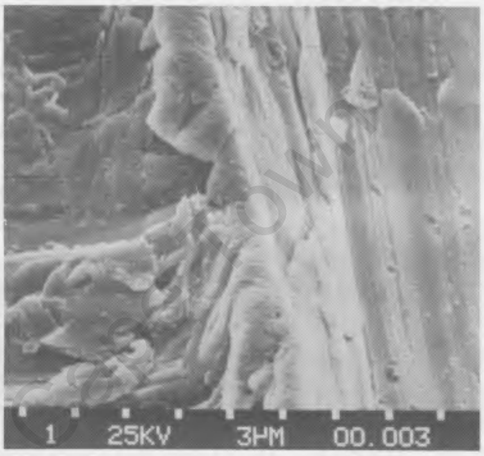

Fig. 4

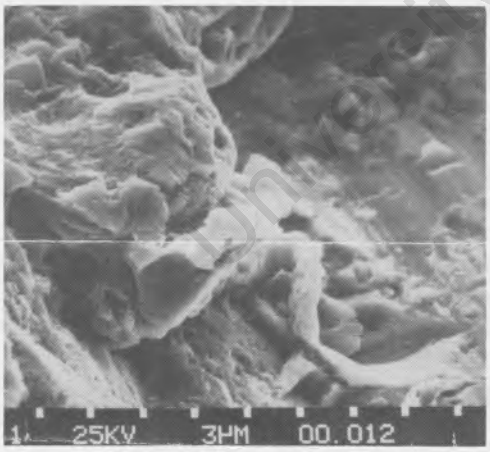

Fig. 5

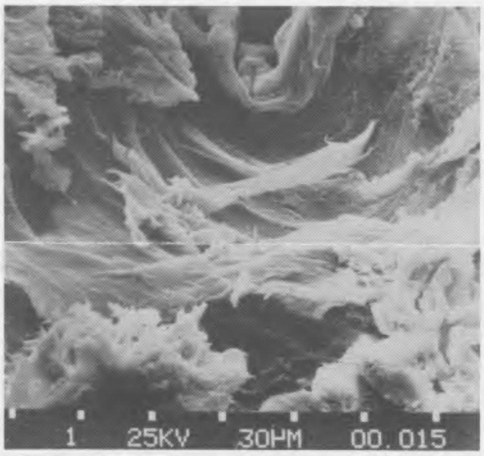

Fig. 6